Regulation of cAMP Signalling to Phospholemman by Phosphodiesterases

Mak, Jason

Awarding institution:
King's College London

Title: Regulation of cAMP Signalling to Phospholemman by Phosphodiesterases

Author: Jason Mak

Regulation of cAMP Signalling to Phospholemman by Phosphodiesterases

Jason KC Mak

Sponsored by a 4-year PhD studentship from the
British Heart Foundation

Thesis undertaken for the degree of
Doctor of Philosophy in Cardiovascular Medicine

Department of Cardiac Physiology
Cardiovascular Division
The Rayne Institute
St Thomas' Hospital
London SE1 7EH
United Kingdom

Submitted July 2013

ABSTRACT

The ubiquitous second messenger molecule, cyclic adenosine monophosphate (cAMP), regulates a multitude of cellular functions, with Protein Kinase (PK)A being the major effector of its actions. There is increasing evidence to suggest that phosphodiesterases (PDEs), a class of enzymes that selectively hydrolyses cyclic nucleotides, play a key role in determining cAMP signalling specificity to a number of PKA substrates in the heart. Phospholemman (PLM) is a phosphoprotein that is physically and functionally coupled to the cardiac Na/K-ATPase (NKA). The latter provides the primary route of Na extrusion from mammalian cardiac myocytes, thereby contributing to the maintenance of transmembrane ion gradients and the indirect control of myocardial contractility.

The work described in this thesis investigated whether individual cardiac PDE subtype(s) are responsible for modulating cAMP signalling to PLM and the NKA in adult rat ventricular myocytes (ARVMs). The use of selective inhibitors for PDE subtypes 2-4 in biochemical assays identified PDE4 as the predominant PDE involved in modulating PLM phosphorylation at Ser68, the consensus PKA site, in the presence of the β-AR agonist isoprenaline hydrochloride (ISO). The augmentation of PLM-Ser68 phosphorylation was accompanied by a corresponding increase in intracellular cAMP accumulation, indicating that PDE4 selectively modulates downstream PKA activity via cAMP hydrolysis. In contrast, ISO-mediated PDE2 inhibition was found to induce the greatest increase in NKA activity, suggesting that upon neurohormonal stimulation, PDE2 may modulate NKA function via a mechanism independent of PKA phosphorylation of PLM.

As PDE2 activity comprises a relatively low proportion of total cardiac PDE activity in the rat heart, our findings suggest that the actions of PDE2 may be compartmentalised. A recombinant adenovirus encoding a novel fluorescence resonance energy transfer (FRET)-based cAMP sensor, PLM-Epac1-camps, was generated to enable direct monitoring of cAMP levels in the vicinity of PLM/NKA in ARVMs. Using fluorescence confocal microscopy, PLM-Epac1-camps was observed to be predominantly targeted to the perinuclear regions of the myocytes. However, preliminary ratiometric FRET measurements using a dual-photometer setup demonstrated a robust response to intracellular cAMP elevation with forskolin. Collectively, our findings suggest that further characterisation of this methodology could provide insights into whether PDE2 activity locally regulates cAMP signalling to the NKA in a compartmentalised manner during β-AR stimulation.

ACKNOWLEDGMENTS

First of all, I would like to express my sincerest gratitude to my principal supervisor, Professor Michael Shattock, for his endless enthusiasm and invaluable support and guidance throughout my PhD. It has been a real pleasure to be part of your group and I will always remember my time here. Thank you also to my second supervisor, Professor Philip Eaton, for his advice and guidance.

I am extremely grateful to the other members of Cardiac Physiology for spending time and effort to assist me with my project and for answering my many questions. Specifically, I would like to thank Dr Andrii Boguslavskyi for his help with Western blotting, Dr Davor Pavlovic for the many insightful discussions, and Mrs Karen Aughton for being a constant source of support and encouragement both in and out of the laboratory. Thank you and I wish you all every success in the future.

I count myself very fortunate to have undertaken my PhD at the Rayne Institute, within a cluster of principal investigators, postdoctoral researchers, research assistants and fellow PhD students, all of whom have helped me in some way or another during my time here. The members of staff that I am particularly indebted to are Dr Shiney Reji for numerous myocyte isolations, Dr Elizabeth Kemp for adenoviral vector generation, Dr Peter Stevenson for his assistance with confocal microscopy, Dr Rebecca Charles for her guidance with the cAMP enzymeimmunoassay, Dr James Clark for his help with computer-related issues, in addition to Dr Fiona Sutherland and Dr Robert Haworth for their general assistance. Additionally, I would like to thank Dr Andrew Hall for helping me with voltage-patch-clamp experiments during the first year of my PhD.

A special thank you also goes to my project collaborators, Dr George Baillie at the University of Glasgow, who kindly permitted me to use the cAMP sensor and other tools from his laboratory, and Dr William Fuller at the University of Dundee, for his help with co-immunoprecipitation experiments. Additionally, I am extremely grateful to the British Heart Foundation for sponsoring my PhD.

Last but not least, I would like to thank all the animals that have been sacrificed for my experiments, and also my family – my wonderful parents and sister – for their unending support, encouragement and love. It is to you that I dedicate this thesis.

LIST OF PUBLICATIONS

Abstracts

Mak JK, Watkinson O, Baillie GS, Shattock MJ (2010) Phosphodiesterase Isoforms 2-4 Modulate cAMP Signalling to Phospholemman During β-Adrenergic Stimulation. *Circulation* 122: A15858

TABLE OF CONTENTS

LIST OF FIGURES

LIST OF TABLES

LIST OF ABBREVIATIONS

%	percent
aa	amino acid
AC	adenylyl cyclase
AKAP	A-kinase anchoring protein
5'-AMP	5'-adenosine monophosphate
ANOVA	analysis of variance
AP	action potential
APS	ammonium persulphate
AR	adrenergic receptor
ARVM	adult rat ventricular myocyte
ATP	5'-adenosine triphosphate
AV	atrioventricular
Ba	barium ion
$BaCl_2$	barium chloride
β-AR	beta-adrenergic receptor
BIS	bisindolylmaleimide
^oC	Celsius
Ca	calcium ion
$CaCl_2$	calcium chloride
cAMP	3'-5'-cyclic adenosine monophosphate
CFP	cyan fluorescent protein
cGMP	cyclic guanosine monophosphate
Cil	cilostamide
C_m	cell membrane capacitance

cMyBP-C	myosin binding protein C
CMV	cytomegalovirus
CNG	hyperpolarisation-activated cyclic nucleotide-gated channel
co-IP	coimmunoprecipitation
Cs	caesium ion
$C_sCH_3O_3S$	caesium methanesulfonate
$CsCl_2$	caesium chloride
C-terminal	carboxyl terminal
cTnI	cardiac troponin I
ddH_2O	double distilled H_2O, resistance 18 Ω
DNA	deoxyribonucleic acid
EC_{50}	half-maximal effective concentration
ECC	excitation-contraction coupling
ECL	enhanced chemiluminescence
E. coli BJ5183	*Escherichia coli* BJ5183 cells
E. coli DH5α	*Escherichia coli* DH5α cells
EGTA	ethylene glycol tetraacetic acid
EHNA	erythro-9-(2-hydroxy-3-nonyl)adenine
EIA	enzymeimmunoassay
E_m	membrane potential
Epac	exchange protein directly activated by cAMP
Epac1-camps	Epac1-based cAMP sensor
ERK5	extracellular signal-regulated kinase 5
FRET	fluorescence-resonance energy transfer
FRSK	forskolin
FXYD	family of proteins expressing the consensus motif proline-phenylalanine-x-Tyrosine-Aspartic acid

g	gram
g	acceleration of 9.8 m/s^2
GΩ	gigaohm
GFP	green fluorescent protein
Gly	glycine residue
GOI	gene of interest
G_SPCR	G_S protein-coupled membrane receptor
GTP	guanosine triphosphate
H-89	N-(2-[bromocinnamylamino]-ethyl)-5-isoquinoline-sulphonamide
H/K ATPase	hydrogen potassium ATPase
HEK293	human embryonic kidney 293 cells
HEPES	N-[2-hydroxyethyl]piperazine-N'-[2-ethamesulphonic acid]
HF	heart failure
hr	hour(s)
HR	heart rate
HRP	horseradish peroxide
IBMX	3-isobutyl-1-methylxanthine
$I_{Ca,L}$	L-type Ca current
I_{CNG}	hyperpolarisation-activated cyclic nucleotide-gated channel current
IgG	Immunoglobulin G
IgY	Immunoglobulin Y
I_p	Na/K-ATPase current
ISO	isoprenaline hydrochloride
IU	international unit
K	potassium ion

Kan^R	Kanamycin resistance
KCl	potassium chloride
kDa	kilodalton
kg	kilogram
K_i	inhibition constant
K_m	Michaelis-Menten constant (measure of half maximal effective concentration)
KI	knockin
KO	knockout
LB	lysogeny broth
LTTC	L-type calcium channel
MΩ	megaohm
mA	milliamp
MCS	multiple cloning site
mg	milligram
Mg	magnesium ion
$MgCl_2$	magnesium chloride
MI	myocardial infarction
min	minute
ml	millilitre
mm	millimetre
mmol/L	millimolar
MOI	multiplicity of infection
ms	millisecond
mV	millivolt
n	number of samples
Na	sodium ion

NA	noradrenaline
Na_2HPO_4	Disodium hydrogen phosphate
$NaCH_3O_3S$	Sodium methanesulfonate
NaCl	sodium chloride
NCX	sodium/calcium exchanger
$NiCl_2$	nickel(II) chloride
NKA	sodium/potassium adenosine triphosphatase
nmol/L	nanomolar
NMR	nuclear magnetic resonance spectroscopy
NO	nitric oxide
N-terminal	amino terminal
pA	picoamp
PBS	phosphate buffered saline
PBS-T	phosphate buffered saline with Tween
PCR	polymerase chain reaction
PDBu	phorbol 12,13-dibutyrate
PDE	3’-5’-cyclic nucleotide phosphodiesterase
pF	picofarad
PFA	paraformaldehyde
PFU	plaque-forming unit
PGE_1	prostaglandin E_1
PKA	protein kinase A
PKAI	protein kinase A holoenzyme type I
PKAII	protein kinase A holoenzyme type II
PKC	protein kinase C
PLB	phospholamban

PLM	phospholemman
PLM-Epac1-camps	Epac1-based cAMP sensor with PLM sequence attached
PLM-KO	phospholemman knock-out
PLM-KI	phospholemman knock-in
PLMS	phospholemman-like protein from shark
PLM-WT	phospholemman wildtype
PMA	phorbol-12-myristate-13-acetate
PVDF	polyvinylidene difluoride
R_{acc}	access resistance
RIA	radioimmunoassay
RNA	ribonucleic acid
Rol	rolipram
R_{pip}	open pipette resistance
rpm	revolutions per minute
R_s	seal resistance
R_{tip}	electrode tip and cell membrane resistance
RyR	ryanodine receptor
s	second
SDS	sodium dodecyl sulphate
SDS-PAGE	sodium dodecyl sulphate polyacrylamide gel electrophoresis
SEM	standard error of the mean
Ser	serine residue
SERCA	sarco/endoplasmic reticulum calcium ATPase
siRNA	small interfering RNA
SR	sarcoplasmic reticulum
TEMED	tetramethylethylenediamine

temp.	temperature
Thr	threonine residue
T-tubule	transverse tubule
Tris	tris(hydroxymethyl)aminomethane
U	amount of enzyme that catalyses the transformation of 1 micromole of substrate per minute under standard conditions
UCR	upstream conserved region
µg	microgram
µl	microlitre
µmol/L	micromolar
UV	ultraviolet
[x]	concentration of x
$[x]_i$	intracellular concentration of x
V	Volt
V_{max}	maximal enzyme reaction rate
VPC	voltage-patch-clamping
v/v	volume per 100 ml
w/v	weight per 100 ml
YFP	yellow fluorescent protein
WB	Western blotting
WT	wildtype

1 GENERAL INTRODUCTION

1.1 β-adrenergic receptor stimulation and the cardiac cAMP signalling pathway

The 3'-5'-cyclic adenosine monophosphate (cAMP) signalling pathway is involved in the regulation of a multitude of cellular functions in virtually all mammalian tissues, and is widely regarded as the 'classical' messenger pathway. In the heart, this signalling cascade is responsible for regulating cardiac contractility, relaxation, automaticity, metabolism and gene expression; as such, it is potentially the most important sympathetic modulator of heart function.[1] Specifically, the activation of cardiac β_1- and β_2-adrenergic receptors (-ARs) by noradrenaline (NA), a catecholamine released from intracardiac nerve terminals, triggers G_s protein-coupled activation of adenylyl cyclases (ACs), a family of largely plasma membrane-bound enzymes that catalyse the conversion of 5'-adenosine triphosphate (ATP) to cAMP [Figure 1.1].[2] This results in an increased intracellular concentration of this ubiquitous second messenger.

cAMP exerts its functions through the activation of three effectors; the primary and most-studied one is protein kinase A (PKA), the others being exchange protein directly activated by cAMP (Epac) and hyperpolarisation-activated cyclic nucleotide-gated (CNG) channels. PKA is a broad spectrum Ser/Thr kinase that can phosphorylate a multiplicity of cytoplasmic and nuclear targets, thus mediating a wide variety of functional effects. Specifically with regards to the catecholaminergic control of contractile function, PKA phosphorylates a number of key proteins involved in the excitation-contraction coupling (ECC) system upon sympathetic stimulation [Figure 1.1]. These include L-type calcium (Ca) channels (LTCCs), ryanodine receptors (RyRs), cardiac troponin I (cTnI), cardiac myosin binding protein C (cMyBP-C), phospholamban (PLB) and of particular relevance to this thesis, phospholemman (PLM). Phosphorylation of these PKA targets exerts an intricately coordinated combination of positively inotropic, lusitropic and chronotropic effects on the intact heart that contribute to the characteristic '*fight-or-flight*' response, namely an increased force and frequency of cardiac contractions.[3,4] Functionally, the activation of the cAMP-PKA signalling cascade upon β-AR stimulation could be regarded as a major

compensatory mechanism that serves to maintain or augment cardiac performance during physiologically stressful conditions, enabling the necessary adjustments to confront imminent danger or to prevent precipitous drops in blood pressure. At the same time, inappropriate or excessive activation of the adrenergic signalling pathway can potentially contribute to a number of disease states including heart failure (HF).[5]

1.1.1 cAMP – one messenger for multiple messages

The molecular basis for the cAMP-PKA signalling pathway was the subject of much speculation during the late 1970s and early 1980s. This was borne out of the numerous examples of cAMP-dependent signalling that could not be satisfactorily explained by the notion of random diffusion of cascade components and contemporary models of 'collision coupling' between receptors and effectors. Additionally, it gradually became apparent that the interior of most cells is not an aqueous 'sac' of protein and solutes, but constructed of highly ordered lattices of various cytoskeletal networks continuous with intracellular organelles and the plasma membrane. In particular, a series of studies in isolated rat hearts provided the first conclusive evidence that distinct responses result from different external stimuli converging on the cAMP-PKA signalling cascade. Specifically, both the non-selective β-AR agonist isoprenaline hydrochloride (ISO) and prostaglandin E_1 (PGE_1) were shown to trigger cAMP synthesis and PKA activation, yet different functional responses were elicited by the two agonists; β-AR stimulation was found to augment contractility and promote glycogen metabolism, while PGE-1 stimulation produced neither of these effects.[6] This observation raised the question of how the cell is able to distinguish between different stimuli acting via the same second messenger.

A first clue to this paradoxical observation was the identification of two isoforms of the PKA holoenzyme (PKAI and PKAII) in the myocardium, differing by the nature of their regulatory subunits (RI and RII) and by their distribution. Whereas PKAI is mostly soluble, PKAII is associated with the particulate fraction.[7,8] In rabbit heart homogenates, it has been shown that up to 50% of the PKA could be localised to the sarcolemma.[7] Interestingly, ISO was found to activate both the soluble and particulate fractions of PKA and increase the activity of phosphorylase kinase[6], glycogen phosphorylase,[6] and cTnI,[9] whereas PGE_1 activated only the soluble fraction of PKA

without affecting the phosphorylation states of these substrates.[6,9] This suggested that β-AR effects specifically correlate with the action of particulate but not cytosolic PKA, in contrast to PGE1 stimulation. On the basis of these findings, Hayes and Brunton postulated in 1982 that the cAMP-PKA signalling cascade is confined into distinct intracellular compartments, which allows signalling specificity to be conferred upon activation of individual G_s protein-coupled membrane receptors (G_sPCR).[10]

Importantly, this functional dichotomy of ISO and PGE_1 in isolated hearts was reproduced in isolated myocytes, indicating that the differences observed had a subcellular basis and were not due to the different cell types present in the whole heart.[11] This distinction in cAMP/PKA-dependent functional responses has subsequently been extended to several other G_sPCRs present in the heart, including glucagon receptors[12,13] and glucagon-like peptide-1 receptors.[14] While activation of these receptors results in intracellular cAMP elevation, the resulting functional responses are markedly different from those induced by β-AR stimulation.[12-14] Interestingly, the level of specificity is sophisticated; even β_1- and β_2-ARs have subsequently been observed to elicit qualitatively different responses in isolated myocytes, with activation of β_2-ARs appearing more restricted and unable to phosphorylate the entire spectrum of PKA substrates observed for β_1-AR stimulation.[15-17] On the whole, these data support the notion that in addition to β_1- and β_2-ARs, cardiac myocytes express a multitude of G_sPCRs that share the cAMP-PKA signalling pathway yet exert distinct downstream effects.[18]

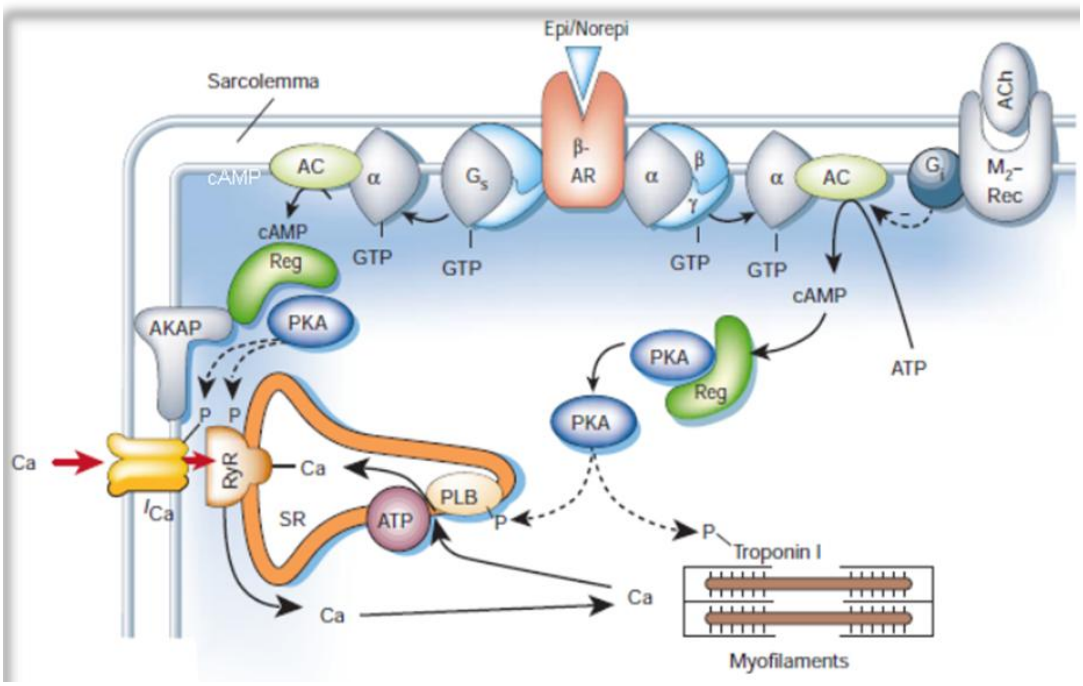

Figure 1.1 β-Adrenergic receptor activation, the cAMP signalling pathway and PKA phosphorylation targets relevant to excitation contraction coupling.

AC, adenylyl cyclase; ACh, acetycholine; AKAP, A kinase anchoring protein; β-AR, β-adrenergic receptor; M2-Rec, M2-muscarinic receptor; PLB, phospholamban; Reg, PKA regulatory subunit; SR, sarcoplasmic reticulum [taken from 3].

1.1.2 Intracellular compartmentalisation of cAMP signals

The finding that the functional outcome is dependent upon the activation of the particulate or the cytosolic fraction of PKA indicated that selective localisation of PKA activity may be an important mechanism for achieving a specificity of response. This notion was highly consistent with the functional promiscuity of PKA. Further studies and the development of biochemical techniques for investigating protein-protein interactions[19] led to the discovery of A-kinase anchoring proteins (AKAPs) in the early 1990s.[20-24] AKAPs are a large (≥50 members) and diverse family of scaffolding proteins that sequester PKA to distinct intracellular domains in proximity of its substrates, thereby allowing for their preferential phosphorylation and ensuring that the specificity of parallel signalling pathways is maintained [Figure 1.2].[24-26] The identification of AKAPs has further substantiated the concept that PKA is physically constrained in defined intracellular compartments.

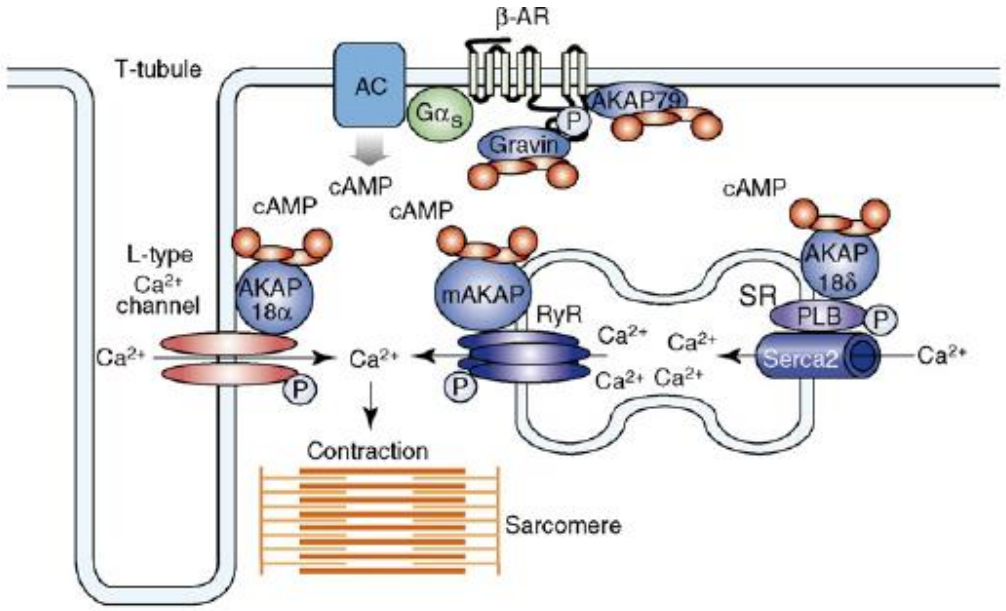

Figure 1.2 Schematic representation of the AKAPs involved in the control of Ca handling in cardiac myocytes.

The relative localisation of the different AKAP complexes is shown. AKAP18a is found in association with the L-type Ca channel, mAKAP forms a complex with the ryanodine receptor (RyR) at the SR, whereas the AKAP18δ complex consists of phospholamban (PLB) and SERCA2. Finally the b-adrenergic receptors (β-ARs) have been shown to interact with both AKAP79 and AKPA250 [taken from 27].

Considering the diversity of the components constituting the pathway, the tight functional coupling of PKA and cAMP, in addition to the complex interconnectivity of the cAMP pathway with other signalling pathways,[1] it became clear that in order for stimuli-specific responses to be generated, spatial control not only involves PKA, but also cAMP itself.[28,29] cAMP is a small, hydrophilic molecule that is highly diffusible;[30] on the basis of its molecular weight and cell viscosity, the second messenger has been estimated to have a diffusion constant of up to 700 $\mu m^2/s$[30,31] and a diffusion distance of ~220 μm.[32] If unchecked, it is envisaged that cAMP generated by ACs at the plasma membrane would uniformly saturate the entire cell within a fraction of a second, leading to non-selective phosphorylation of all PKA substrates irrespective of what they are coupled to.

There is substantial evidence of cAMP compartmentalisation in cardiac myocytes.[18] Studies comparing the effects of ISO and forskolin (FRSK; a direct, non-selective AC activator) found that achieving equal post-PKA responses generally requires a smaller

elevation of cAMP with ISO than that with FRSK.[33] Conversely, if cellular or tissue cAMP were elevated to similar levels by these two agonists, the downstream effects are more pronounced with ISO.[33] Indeed, it has been demonstrated that ISO results in a proportionally greater accumulation of cAMP in the particulate fraction than with FRSK in isolated canine ventricular myocytes, with this increase in particulate cAMP corresponding to an increase in Ca transient amplitude and decay kinetics.[29] In contrast, FRSK was found to mainly increase cAMP in a compartment not accessible to PKA and not coupled to the measured responses in the isolated perfused rat heart.[33]

Extending from these findings, subsequent studies in live myocytes provided further evidence for a spatial restriction of cAMP signals upon β-AR stimulation. In 1996, a study using a double microperfusion system enabled $I_{Ca,L}$ to be simultaneously measured on two physically isolated portions of frog ventricular myocytes using whole-cell patch-clamping.[34] The authors found that application of ISO induced a local activation of the current while FRSK resulted in a more uniform activation, suggesting the existence of a local pool of cAMP in the vicinity of the LTCC that is activated upon β-AR stimulation.[34] In line with this idea, measurement of whole cell CNG current (I_{CNG}) as an index of subsarcolemmal $[cAMP]_i$ in ARVMs over-expressing a recombinant rat olfactory CNG channel demonstrated that only a limited number of CNG channels are activated near-maximally upon β-AR stimulation.[35] An important advancement in the field was the development of real-time imaging techniques that enabled the quantitative monitoring of changes in cAMP concentration within distinct intracellular compartments in single living cardiac myocytes [Figure 1.3],[36,37] in particular those based on fluorescence resonance energy transfer (FRET).[38] The approach used in one such study made use of a ratiometric FRET-based biosensor[39] to demonstrate for the first time the generation of multiple, localised microdomains with increased [cAMP] in response to β-AR stimulation in neonatal mouse myocytes [Figure 1.4].[40]

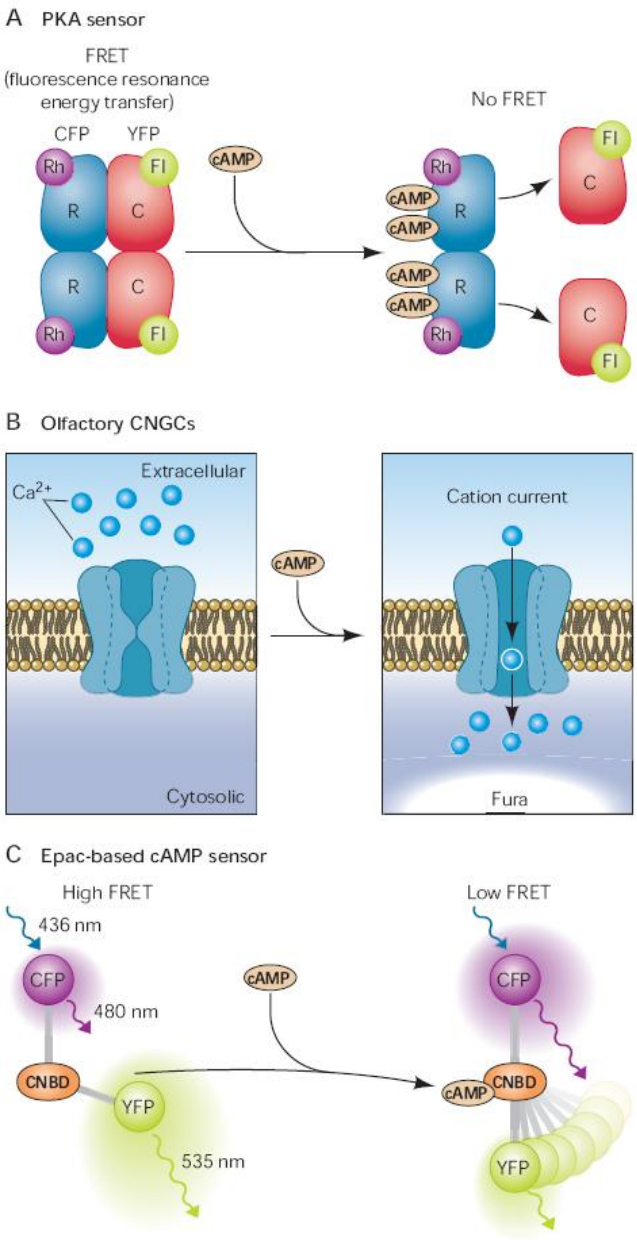

Figure 1.3 Principles of cAMP sensors constructed using PKA, CNGCs and Epac.

A: in absence of cAMP, PKA sensor is a complex of two regulatory (R) and two catalytic (C) subunits tagged with rhodamine (Rh)/CFP and fluorescein (FI)/YFP, respectively, and high FRET is observed. After cAMP binding to the two sites in each regulatory subunit, catalytic subunits are released from the complex that results in the loss of FRET. **B**: olfactory CNGCs are gated by subsarcolemmal pools of cAMP. Increases in cAMP result in a current, which can be measured electrophysiologically for monovalent cations and calcium. Calcium influx can also be visualized in cells by imaging of a calcium-sensitive dye, e.g., Fura. **C**: Epac-based cAMP sensors (camps) are comprised of a single cyclic nucleotide binding domains (CNBD) fused between CFP and YFP. cAMP induces a conformational change leading to an increase in distance between the fluorophores, which is measured as a decrease in FRET [taken from 41].

Recent work using real-time detection of cAMP signals in intact cells showed that the β-AR and the PGE_1 receptor generate spatially distinct pools of cAMP which in turn preferentially activate different subsets of AKAP-anchored PKA enzymes, leading to the phosphorylation of distinct downstream targets.[42] The finding that catecholamines, but not PGE_1, raise the phosphorylation level of key components of the ECC machinery and increase myocyte contractility via generation of a spatially confined pool of cAMP, is entirely consistent with their distinct effects on cardiac inotropism, as aforementioned.[6,9] Similarly, in accordance with the functional effects associated with

the two β-AR subtypes,[15] live imaging using a cAMP-FRET sensor in adult rat cardiac myocytes (ARVMs) has revealed that β_1-ARs induce far-reaching cAMP signals, whereas β_2-AR-induced cAMP remains locally confined.[43] Again, such differences have been shown to translate to distinct PKA activities.[44] These findings underline the spatial confinement of the multiple elements of the cAMP-PKA signalling pathway, with cAMP compartmentalisation playing a central role in this scheme.

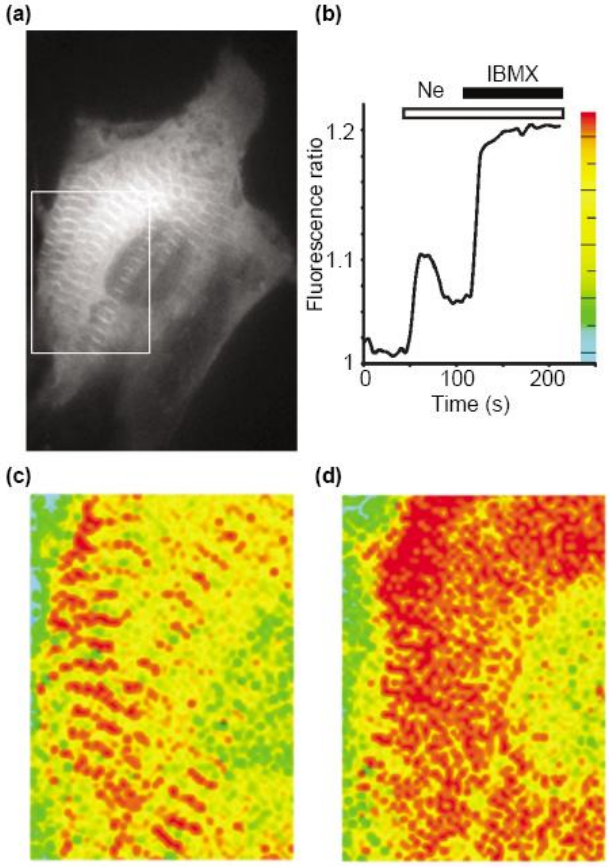

Figure 1.4 Microdomains of cAMP monitored in live cardiac myocytes using a cAMP sensor based on FRET and PKA.

(a) A cardiac myocyte transfected with C–YFP (C, the catalytic subunit of PKA) and R–CFP (R, the regulatory subunit of PKA) shows a localisation of the probe in thin parallel striations in correspondence of the sarcomeric Z line. **(b)** The effect of the β-adrenergic agonist norepinephrine (Ne, white bar) and of the broad range PDE inhibitor IBMX (black bar) on the concentration of cAMP is monitored by measuring FRET changes. The cell is excited at 440 nm (the CFP excitation wavelength). Fluorescence emission of both CFP (at 480 nm) and YFP (at 545 nm) is collected and the 480 nm : 545 nm fluorescence ratio value is plotted against time. The values shown in **(b)** are the mean ratio values calculated over the entire area of the cell. **(c)** & **(d)** The detail delimited by the box in Panel **(a)** is shown in pseudocolour. Different colours correspond to different fluorescence ratio values, according to the colour bar indicated in Panel **(b)**. **(c)** The cell was imaged at the peak of the response to norepinephrine (time = 60 s) and red, corresponding to the sarcomeric Z lines, indicates localised regions of high cAMP levels. Addition of IBMX abolishes this subcellular heterogeneity, and the level of cAMP rises uniformly in the cytosol, as indicated in **(d)**, which illustrates the same cell imaged at the plateau of its response to IBMX (time = 200 s) [taken from 45].

1.2 Phosphodiesterases

The tight local regulation of cAMP hydrolysis helps explain the observation that stimulation of β-ARs leads to highly restricted elevations of the second messenger, despite its effects on global myocardial contractile function. In the identification of the mechanisms responsible for restricting cAMP diffusion, it was initially thought that physical barriers created by specialised membrane structures exist within the cytosol, with such a scenario proposed to explain the limited diffusion of cAMP from the plasma membrane to the deep cytosol in HEK293 cells upon PGE_1-R stimulation.[46] However, although cardiac myocytes are rich in physical submembrane microdomains, an experimental proof for this hypothesis remains lacking. In contrast, there is an increasing body of evidence suggesting that the degradation of cAMP by 3', 5'-cyclic nucleotide phosphodiesterases (PDEs) is critical for the formation of dynamic cAMP microdomains. PDEs consist of a superfamily of evolutionarily conserved phosphohydrolases that are the only enzymes currently known to degrade cAMP and other cyclic nucleotides [Figure 1.5: Panel (a)].[47-52] cAMP is converted into the inactive metabolite 5'-adenosine monophosphate (5'-AMP) when the hydrolysis of its phosphodiester bond is catalysed by PDE activity. As such, the amplitude and duration of the cAMP signal is dependent on the activity of the cAMP-degrading PDEs.

1.2.1 General characteristics

Mammalian PDEs are encoded by 21 different genes and are subdivided into 11 families (PDE1-11) based on primary amino acid sequence homology, enzymatic properties and sensitivity to inhibitors.[51,52] Cardiac myocytes express several PDE families: PDEs 1, 2, 3, 4, 5, 8 and 9, with PDEs 1 – 4 thought to be primarily responsible for cAMP degradation in the heart.[51] While PDE4 is selective for cAMP (K_m = 2 – 4 μmol/L) , PDEs 1-3 can hydrolyse both cAMP and cGMP, albeit with different affinities and catalytic rates. In particular, PDE2 and PDE3 induce a crosstalk between these two cyclic nucleotide pathways, providing a means by which cGMP signals can modulate cAMP signals (see Section 1.2.4).

Each PDE family encompasses 1 to 4 distinct genes; specifically, PDE2 consists of 1 gene (PDE2A), PDE3 has 2 genes (PDE3A & B), while 4 genes are present in the PDE4

family (PDE4A – D). It is currently thought that cardiac myocytes express 2 forms of PDE2A,[53] 3 forms of PDE3A[54] (and possibly PDE3B) and more than 5 forms of PDE4 encoded by PDE4A, B and D.[55-57] Specifically, a number of studies have provided direct or indirect evidence for the presence of these PDE gene products in rat cardiac tissues.[56,58-61]

Importantly, the individual genes encode for multiple isoforms within each PDE family, either as products of alternative splicing or transcription from distinct promoters.[51] The individual isoforms, of which ≥80 have been identified to date, are thought to generally exist as dimers and exert specific, non-redundant functional roles as a consequence of a unique combination of intracellular localisation, tissue-expression patterns, substrate specificity, regulatory mechanisms and enzyme kinetics.[51,52] Despite this, the monomeric structure of these PDE isoforms has common features with three distinct domains. The N-terminal regulatory domain characterises each family and their variants. The catalytic domain is relatively conserved, sharing 25% to 52% homology with other mammalian PDE catalytic domains, and contains a zinc ion binding site. The C-terminal domain can be prenylated[62] or phosphorylated by mitogen-activated protein kinase.[63] A number of these PDE isoforms will be described in more detail in Sections 1.2.3 – 1.2.5.

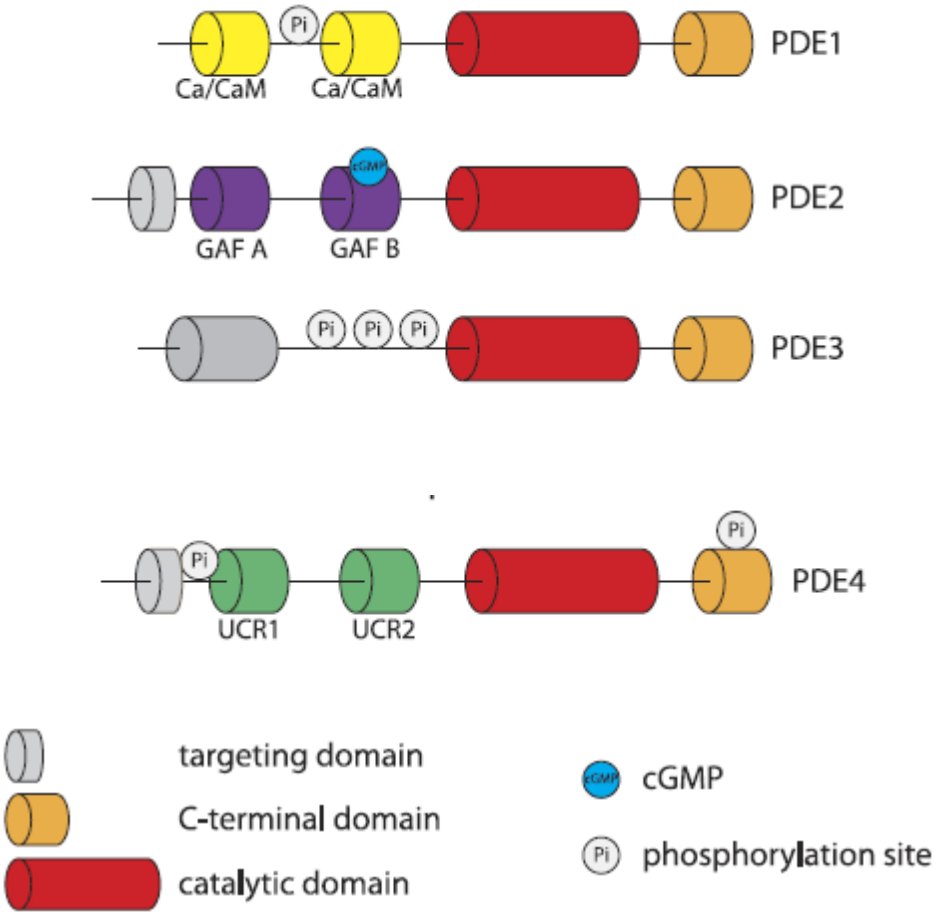

Figure 1.5 Schematic representation of the main PDE families expressed in the cardiovascular system.

The N-terminal targeting domain characterises each family and its isoforms, while the C-terminal domain is relatively conserved. The activity of PDEs can be regulated by a number of mechanisms; for example, binding of cGMP to the GAF-B domain of PDE2 results in the latter's stimulation, while cGMP is a competitive inhibitor of PDE3 activity. Additionally, PKA phosphorylation has been shown to increase the activity of both PDE3 and PDE4 isoforms, the latter via binding to the UCR1 domain present on long isoforms of the enzyme.

UCR: upstream conserved region; GAF: cGMP-binding PDEs; Ca/CaM: Ca calmodulin binding domains; Pi: inorganic phosphate (taken from 50).

1.2.2 Contribution to intracellular cAMP compartmentalisation

Investigation of the functional roles of PDEs has been made possible by the development of pharmacological agents that selectively inhibit their activities; indeed, the effects of PDE inhibition have been studied extensively in cardiac myocytes. Among the earliest indications of a potential contribution of PDEs to modulation of

cAMP signalling stemmed from a comparison of the effects of ISO, the broad-spectrum PDE inhibitor 3-isobutyl-1-methylxanthine (IBMX) and the PDE3 inhibitor milrinone in guinea pig perfused hearts. Although each of these pharmacological agents increased intracellular cAMP and produced positive inotropic and lusitropic effects, they were found to induce different patterns of PLB, cTnI and cMyBP-C phosphorylation.[64] Moreover, it was demonstrated that approximately 45% of the total cAMP in canine ventricular myocytes is found in the particulate fraction in response to ISO, with this fraction declining to <20% on the addition of the non-selective PDE inhibitor IBMX in combination with ISO, although total cAMP still increased 3-4 fold.[29] Similarly, while local application of ISO to half of a cell was found to increase $I_{Ca,L}$ half maximally, corresponding to activation of the channels located in the same part of the cell as the β-AR agonist, addition of IBMX activated LTCCs in the distant part of the cell in response to ISO, implicating a role of PDEs in defining local cAMP pools involved in the β-AR stimulation of LTCCs.[34] These and subsequent findings suggest a differential expression of PDEs at the membrane and in the cytosol, establishing a model whereby PDEs prevent excessive cAMP accumulation upon β-AR stimulation by limiting the diffusion of the second messenger from the membrane into the cytosol.[65]

The contribution of PDEs to cAMP compartmentalisation has become more intricately characterised with the more recent imaging approaches.[41,66] As aforementioned, the stimulation of β-ARs in NRVMs was shown to generate localised increases in cAMP levels in correspondence of Z lines that could be directly imaged using a FRET reporter.[40] These cAMP gradients were dissipated by application of the PDE inhibitor IBMX, demonstrating that PDEs play a key role in the formation of these restricted cAMP microdomains [Figure 1.4].[40]

1.2.3 Functional roles of PDE2-4

Interestingly, the relative activity of the different PDE subtypes seem to be highly dependent on the species investigated; in mouse and rat cardiac myocytes, PDE4 represents the major cAMP-PDE, contributing to up to 60% of total cAMP-hydrolytic activity, whereas PDE3 accounts for 20-30%, and PDE1 and PDE2 representing the remaining activity.[65,67-69] In contrast, PDE4 activity represents only 10% of the total

PDE activity in the human heart,[69-72] while PDEs1-3 represent the vast majority of the hydrolytic cAMP activity.[69,73,74]

Despite representing merely around 1% of the total PDE activity in the neonatal rat heart, PDE2 was found to be responsible for the degradation of a large proportion of the cAMP generated by β-AR stimulation.[75] Moreover, it has been shown using a genetically encoded, fluorescent cAMP sensor that activation of PDE2 results in a rapid decrease of intracellular cAMP from high micromolar to the sub-micromolar range within a few seconds; indeed, the rate of cAMP hydrolysis by PDE2 was found to be greater than hormone-stimulated synthesis of the second messenger.[76] Consistent with this, PDE2 has been found to tightly control the activity of LTCCs in a number of species [77-80]. For example, in frog cardiomyocytes, where it is the most abundant PDE subtype,[81] PDE2 activation has been shown to decrease a local pool of cAMP in the vicinity of LTCCs and only a slight decrease in cAMP in the rest of the cell, implying the existence of a microdomain between the β-AR, LTCC and PDE2,[77] consistent with observations in human atrial myocytes.[82]

Similarly, selective inhibition of approximately 10% of the total PDE4 activity in neonatal mouse myocytes was demonstrated to result in a dramatic increase in cAMP.[83] The profound effect of PDE4 inhibition on the catecholamine-induced cAMP response suggests a tight functional coupling of PDE4 with the β-AR, consistent with a number of studies in adult ventricular myocytes from rats and mice indicating that while PDE4 exerts little effect on basal cAMP levels, it becomes crucial for hydrolysing cAMP generated during β-AR stimulation and for the control of PKA phosphorylation of key proteins in ECC such as the LTTC,[59,65] RyR2[84] and PLB.[85-87] It was shown in a PDE4D-KO model that some of these changes in protein phosphorylation correlate with increases in cardiomyocyte shortening, Ca transients, Ca transient relaxation rates and SR Ca loads, corresponding with an enhanced both *in vivo* and *ex vivo* myocardial contractility.[87] As a consequence, PDE4 inhibition strongly potentiates the inotropic effects of β-AR stimulation in these species.[88-91]

On the contrary, despite PDE3 representing approximately 30% of the total PDE activity in the rodent heart, its role in cAMP compartmentalisation during β-AR stimulation remains less clearly understood. In neonatal mouse myocytes, PDE3

inhibition seems to exert only a marginal effect on the cAMP response to β-AR stimulation, and appears to be comparable to the contribution of PDE4 only when all ACs are non-selectively activated by FRSK.[83] However, it has been reported that PDE3 as well as PDE4 activities are specifically coupled to the β-AR, with their inhibition augmenting both subsarcolemmal [cAMP] and $I_{Ca,L}$, [92] while PDE3 has been shown to play a major role in modulating Ca entry consecutively to cAMP-dependent phosphorylation of the LTTC.[93] Furthermore, PDE3 inhibition has been reported to mediate cardiac contractility and Ca cycling in mouse myocytes, with elevated levels of both PLB and RyR2.[86] Interestingly, the role of PDE3 appears to supersede that of PDE4 in larger mammals; for example, β-AR inotropic responses in human atrium are predominantly regulated by PDE3,[94] while PDE3 inhibitors have been found to exert a potent positive inotropic effect in the dog heart.[86]

1.2.4 cGMP-cAMP crosstalk

Under basal conditions, PDE2 has similar affinity for cAMP and cGMP (K_m cAMP = 15 μmol/L, K_m cGMP = 15 μmol/L) but its enzymatic activity is allosterically regulated by cGMP with positive cooperative kinetics. Specifically, binding of cGMP to the regulatory GAF-B domain at the N-terminus of PDE2 increases the rate of cAMP hydrolysis by up to10-fold (GAF domains are found in mammalian cGMP-specific phosphodiesterases, cyanobacterial adenylate cyclases and *Escherichia coli* formate hydrogen lyase transcription activator FhlA).[95-97] For this reason, PDE2 was first named cGMP-stimulated PDE (cGS-PDE). Therefore, via the activation of PDE2, stimuli that elevate cGMP may attenuate cAMP signals, for example, following NO production.[75,98]

In contrast, PDE3 has a similarly high affinity for cAMP and cGMP (K_m cAMP = 0.2 μmol/L, K_m cGMP = 0.1 μmol/L) but a much higher catalytic rate for cAMP than for cGMP; cGMP therefore behaves as a competitive inhibitor of PDE3 [Figure 1.5]. As a consequence, PDE3 provides a means by which an increase in cGMP may lead to an increase in cAMP within the cell.

Interestingly, the functional impact of cGMP signals on cAMP seems to be dependent on the intracellular concentrations of cGMP. At low concentrations (<50 nmol/L),

cGMP exclusively inhibits PDE3, whereas at higher concentrations (200-500 nmol/L), cGMP also activates PDE2.[99]

1.2.5 Intracellular localisation of PDE isoforms

The inter-species differences in expression levels of the different PDE families could potentially complicate comparison of different studies. However, a clear trend has emerged whereby the divergent effects of the different PDEs on the catecholamine-induced cAMP increase could be attributed to the specific localisation of individual PDE subtypes, rather than the total expression level of the enzymes. In support of this idea, immunostaining experiments have shown that individual PDE isoforms belonging to the different PDE subtypes are localised in distinct compartments within the cardiac myocyte, in accordance with their differential functional effects. Interestingly, this scheme often seems to be species-dependent. Specifically, PDE2 isoforms in rat and frog myocytes are found preferentially in microsomal fractions[75,81] in association with functional membrane structures – plasma membrane, sarcoplasmic reticulum (SR), Golgi apparatus and nuclear envelope.[52] Similarly, PDE3 isoforms can be either present in the cytosol or anchored to the aforementioned intracellular structures depending on the species[52,100]. In the guinea pig and rat, PDE3 is mainly found in the soluble fraction;[101-103] in contrast, PDE3 activity in the dog heart is found in the membrane fraction and associated with the SR membrane, where PDE3 inhibitors exert a potent inotropic effect.[101,104,105] The multiplicity of the different PDE4 isoforms seems to favour a highly intricate differential expression within the rodent heart, which will be outlined in more detail in the next section [Section 1.2.4]. These findings indicate that different PDE isoforms are sequestered into defined intracellular locations and functionally coupled with the distinct pools of cAMP that are selectively activated in response to β-AR stimulation.

The ability of PDE isoforms to be targeted to distinct intracellular regions is underlined by their structural features. The enzymes possess a highly conservative (20-25% homology in isoforms belonging to different subtypes) C-terminal catalytic domain of approximately 270 aa that harbours the cyclic nucleotide binding site [Figure 1.5]. In contrast, the less-conserved N-terminal domain has a unique amino acid sequence within each PDE subfamily and contains domains responsible for targeting the

individual isozymes to discrete intracellular compartments, through either direct binding to membrane lipids or selective protein-protein interactions.[106] Indeed, the partition of PDE2 and PDE3 isoforms between membrane structures and the cytosol in general seems to be highly dependent on the specificities of their N-terminal domains.[52] Also located on the N-terminal are dimerisation domains, binding sites for specific regulators of PDE activity as well as phosphorylation sites targeted by protein kinases [Figure 1.5].[106] For example, it has been found that the two GAF domains, GAF-A and GAF-B, present on the N-terminal domain of the PDE2A subunit have distinct roles in dimerisation and cGMP binding,[107] while PKA phosphorylation sites (in addition to those for a number of other kinases) have been identified on the long isoforms belonging to the PDE3 and PDE4 families.[108,109]

1.2.5.1 Intracellular targeting of PDE4 isoforms

Of all the currently identified PDE isoforms, those belonging to the PDE4 family seem to exhibit the most sophisticated control of cAMP signals, and studies on these variants have significantly enhanced our understanding of how individual PDE isoforms are physically constrained within defined intracellular locales. PDE4 comprises the largest PDE family and consists of more than 20 distinct isoforms that are encoded by 4 highly similar subfamily genes (PDE4A-D) through alternative mRNA splicing coupled to the use of different promoters, although only PDE4A, PDE4B and PDE4D are expressed in cardiac tissue.[56]

A constantly growing body of literature concerns the roles of PDE4D isoforms expressed in the heart, while less is known about PDE4A and PDE4B isoforms, yet they have been detected as active proteins in both rodent and human myocardium.[69] These enzymes have a highly conserved catalytic core but each is characterised by a unique N-terminal region.[110,111] PDE4 isoforms are categorised into long, short, super-short or dead-short forms based on the presence or absence of the unique upstream conserved regions (UCR) 1 and 2 close to the N-terminus [Figure 1.5].[111-113] The latter has a major functional role in regulating the maximal reaction rate (V_{max}) of the PDE4 catalytic unit, particularly in integrating the effect of phosphorylation. For instance, upon PKA phosphorylation, PDE4 activity can be increased by approximately 60% for a variety of long isoforms.[109] It is thought that this scheme provides an important negative feedback

loop by which PKA limits excessive cAMP accumulation during β-AR stimulation.[35,65,114] Intriguingly, dimerisation has been shown to be a requisite for the activation of long PDE4 isoforms by PKA phosphorylation [115]

The use of a dominant negative approach, which exploits the overexpression of a catalytically inactive PDE isoform to displace its endogenous cognate and allows for the compartment- and subtype-specific blockade of PDE enzymatic activity,[116,117] RNA silencing,[118] in addition to the development of mice with ablation of PDE4A,[87] B[119] and D[84] have facilitated dissection of the functional roles of the individual PDE4 isoforms. The picture that has gradually emerged is that individual PDE4 variants are localised to discreet cAMP microdomains to exert control on the activity of individual ECC proteins, with PDE4D5, PDE4D8 and PDE4D9 having been shown to interact directly or indirectly via β-arrestin with β-AR receptors in neonatal rat cardiomyocytes [Figure 1.6].[116,120,121] PDE4D could also coassemble with SERCA2a;[86,87] similarly, both PDE4B and PDE4D have been found to associate with the LTCC in the mouse heart, although PDE4B seems to be predominantly responsible for mediating Ca current in this experimental model.[119]

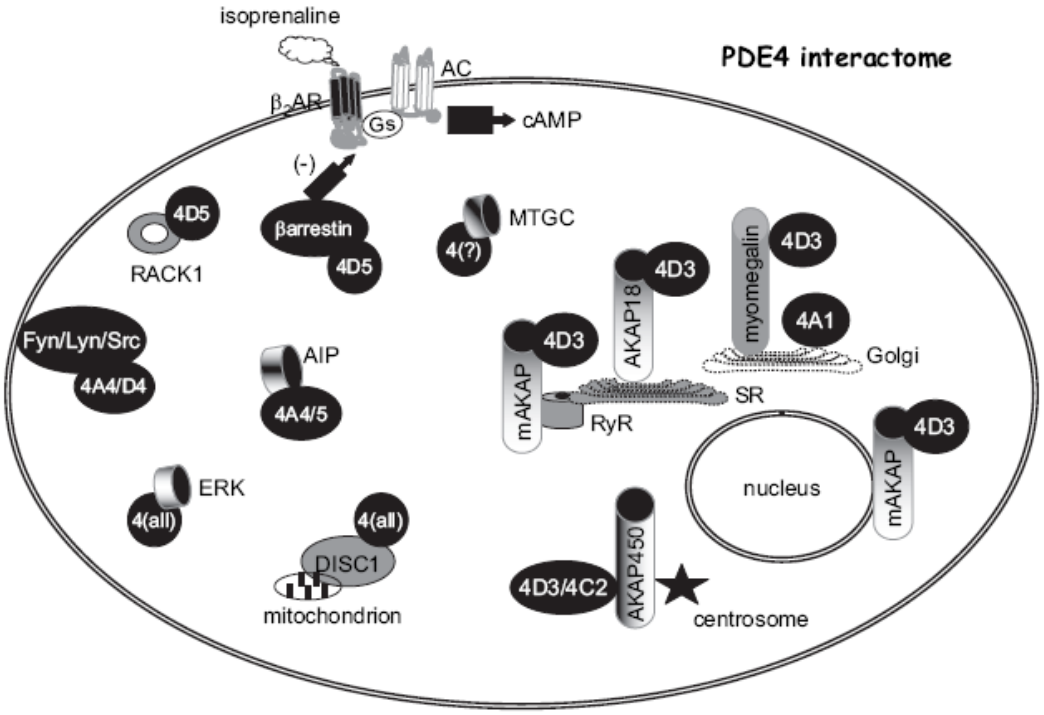

Figure 1.6 The PDE4 'interactome'.

Some of the proteins and AKAPs currently known to interact with PDE4 isoforms to form signaling-specific signalling scaffold complexes that in certain instances are targeted to specific cellular regions. Such complexes underpin 'sink' formation and the compartmentalisation of cAMP signalling [taken from 112].

Particularly intriguing is the ability of PDE4 isoforms to interact with AKAPs [Figure 1.6]. Through binding of other components of the cAMP signalling pathways, including ACs,[122,123] PDEs[124,125] and phosphatases,[126] AKAPs organise macromolecular signalling complexes where the signal is generated, modulated and relayed to the appropriate target. Specifically, PDE4D3 has been demonstrated to interact directly with the mAKAP (which also binds PKA, Epac and the extracellular signal-regulated kinase 5 (ERK5)) via its unique 18 amino acid N-terminal domain.[114] A sophisticated and multilayered control of local [cAMP] and PKA activation has been demonstrated to take place at the mAKAP signalling complex [Figure 1.7]. The basal activity of mAKAP-anchored PKA is kept under control by the anchored PDE4D3.[114] Upon β-AR stimulation, cAMP concentration increases and the resulting PKA-mediated phosphorylation of PDE4D3 at Ser54 and Ser13 strengthens the interaction between mAKAP and PDE4D3 and increases PDE4D3 enzymatic activity to achieve more rapid

termination of the cAMP signal.[127,128] Conversely, ERK5-mediated phosphorylation of PDE4D3 at Ser579 inhibits the enzyme, resulting in an increase in cAMP and triggers a signalling cascade initiated by Epac.[63,109,129] The integration of the two signalling pathways allows the generation of local fluctuations of cAMP and pulses of PKA activity, as directly confirmed by imaging studies in live cells.[130] Interestingly, the RyR2 has been found in a signalling complex with PDE4D3, PKA and mAKAP,[131] with PDE4D3 potentially involved in regulating the function of the latter [Figure 1.6].[84]

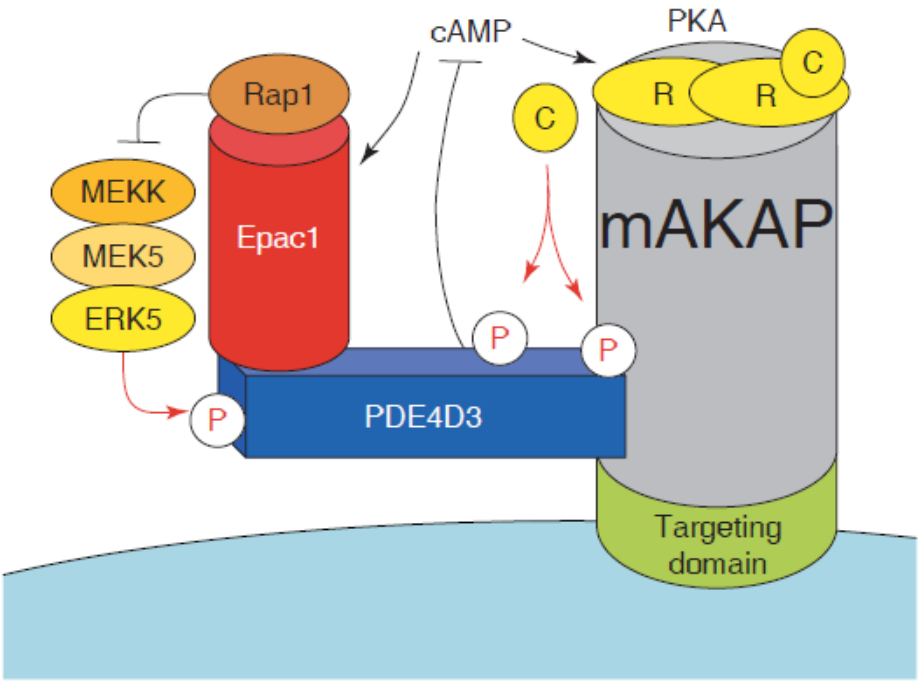

Figure 1.7 The mAKAP complex at the nuclear membrane of cardiomyocytes brings together three cAMP effectors: PKA, PDE4D3 and Epac1.

Each of these enzymes is activated at different concentrations of cAMP and there is interaction between them. As cAMP levels rise, activated PKA phosphorylates PDE4D3 in the complex at two distinct sites (double red arrow). Phosphorylation of Ser 13 enhances the PDE affinity for mAKAP and phosphorylation of Ser54 increases the activity of the PDE. This increase in activity depletes the local concentrations of cAMP and enables reformation of the inactive PKA holoenzyme. As cAMP levels fall, the EPac1-mediated inhibition of ERK5 pathway is blocked and the consequent ERK phosphorylation (red arrow) of PDE4D3 decreases the PDE activity, enabling accumulation of more cAMP (taken from 25).

1.2.6 An evolving model of intracellular cAMP compartmentalisation

Such a model of spatially confined PDE4 isoforms in determining local cAMP signals was further confirmed in a study in HEK293 cells using dominant-negative mutants to displace cognate endogenous active PDE isoforms,[132] which disrupted the cAMP gradients generated by PGE_1 activation. Intriguingly, the investigators found cAMP levels to be higher in the membrane and nuclear compartments when compared to the cytosol,[132] indicating that the cAMP gradient between the point of cAMP synthesis and the bulk cytosol was not uniform and therefore could not be attributed to an enzymatic PDE barrier, as postulated previously. Rather, it was found that the specific spatial arrangement of PDE4B and PDE4D generates a pattern of local 'sinks' that drain cAMP in defined locales, thus resulting in the generation of multiple gradients of cAMP.[132]

Such a model implies that multiple cAMP gradients could be generated simultaneously in different cellular locations irrespective of their distance from the AC that generated the cAMP response, dependent instead on their proximity to the nearest PDE4 sink. It is now thought that microdomains ensure that a range of $[cAMP]_i$ are made available to modulate the activity of high-affinity effectors such as PKA.[133] In this way, cAMP concentrations can be increased sufficiently above the threshold of activation for cAMP effectors such as PKA or EPAC, except in localised PDE4 'hotspots', which presumably serve to protect against inappropriate activation.[132] This notion has been supported by the most recent advance, which uses PDE isoforms themselves as cAMP reporters. One approach to show that cAMP gradients form around PDE molecules involved monitoring the PKA phosphorylation of catalytically inactivated PDE4 isoforms as an indicator of 'localised' PKA activity[117] while the other used FRET reporters fused to individual PDEs.[134] Computational approaches, using existing theoretical and experimental data on the kinetics of cAMP production, have also concluded that compartmentalised signalling intermediates, including PDE4, shape the cAMP response of the β_1-AR.[133,135]

1.2.7 Selective targeting of PDE isoforms: a novel therapeutic approach?

It is now recognised that the cAMP pathway transduces signals in a compartmentalised manner such that individual stimuli only engage a subset of the pathway components

that are physically constrained within defined intracellular locales, thus resulting in a precise functional outcome. The evidence outlined above provides a glimpse into the incredibly complex spatial organisation of this pathway in response to β-AR stimulation. To add to this complexity, there is now evidence to suggest that cGMP signals may also be compartmentalised[136] and can selectively modulate local pools of cAMP by regulating the activities of PDE2 and PDE3 in a differential manner, thus giving rise to a crosstalk between the two signalling pathways[99,137]. Furthermore, it is now appreciated that signal propagation is not only limited to undergo regulation in space, but could also be controlled temporally.[138]

Finally, it must be emphasised that the compartmentalisation of PKA and cAMP signals is complemented by a number of other mechanisms that critically contribute to such spatial control. These include the intracellular confinement of AC isoforms associated with β-AR stimulation[139] and the β-AR itself[140] into specialised membrane microdomains, including caveolae.[141] In addition, the precise regulation of protein kinases and phosphatases is essential for the control of the phosphorylation state of PKA substrates. In the heart, >90% of total phosphatase activity is contributed by the types 1 and 2A Ser/Thr PP-1 and PP-2A. Specifically, PP-1 has been implicated in the regulation of cardiac β-AR responses and as a negative regulator of cardiac contractility,[142-144] while PP-2A has been identified as an integral component of the mAKAP complex[145] (see Section 1.2.5.1).

Disturbance of such intricately organised compartmentalisation of cAMP signals is likely to contribute to pathological states if disturbed, as exemplified by the redistribution of β_2-ARs in HF[5] and the altered expression and activity of PDEs observed in both HF[5,55] and arrhythmia[119] models. Indeed, in many pathologies including inflammation, cardiovascular diseases, neurodegenerescence and cancer, alterations of intracellular signalling related to PDE isozyme deregulation might contribute in explaining the difficulties observed in the prevention and treatment of these pathologies. The multiplicity of biochemical and structural properties of PDEs, their specific subcellular compartments, their transcriptional and post-transcriptional regulation raises the possibility that only the altered PDE isozymes are targeted, thus avoiding and/or decreasing the adverse effects induced by non-selective treatments. This spatial and temporal control of local signalling to phosphorylation substrates is thus critical for the

contractile response to β-AR stimulation. ECC substrates introduced earlier include the sarcolemmal protein PLM, which is the main focus of this thesis.

1.3 Phospholemman

1.3.1 Expression and structure

PLM is a sarcolemmal protein that is abundantly expressed in cardiac[146-148] and skeletal muscle,[149] and to a lesser extent in regions within the brain,[150] kidney[151] and smooth muscle.[152] PLM is synthesised as a 92 amino acid peptide, with the 20 aa signal sequence at the N-terminus cleaved off during processing to form the mature protein containing 72 amino acid residues.[153] Despite being initially characterised as a 15 kDa protein, the molecular weight of PLM is actually 8409Da,[153] with the discrepancy between the two values reflecting the slow migration of PLM on SDS-PAGE, specifically by the transmembrane domain.[154]

The amino acid sequence of mouse PLM (also known as FXYD1; see Section 1.3.3) as determined by Edman degradation is shown in Figure 1.8 and illustrates the amino, transmembrane and carboxyl regions of the mature protein, which are comprised of 17, 20 and 35 amino acids respectively.[153] The extracellular N-terminal domain is made up of amino acids 1-17, including the FXYD consensus sequence (see Section 1.3.3 for definition of FXYD proteins), has overall negative charge and is highly resistant to protease degradation. The transmembrane domain comprises amino acids 18-37, which are uncharged and hydrophobic, and the cytosolic C-terminal domain is composed of amino acids 38-72, with an overall positive charge. Sequence homology has been observed between PLM and the γ-subunit of the NKA (see Section 1.4.1) and PLB. The region of similarity in the latter (RSSIRRLST in PLM[155] and RSAIRRAST in PLB[156]) contains serines and threnonines that are potential phosphorylation sites (see Section 1.3.2).

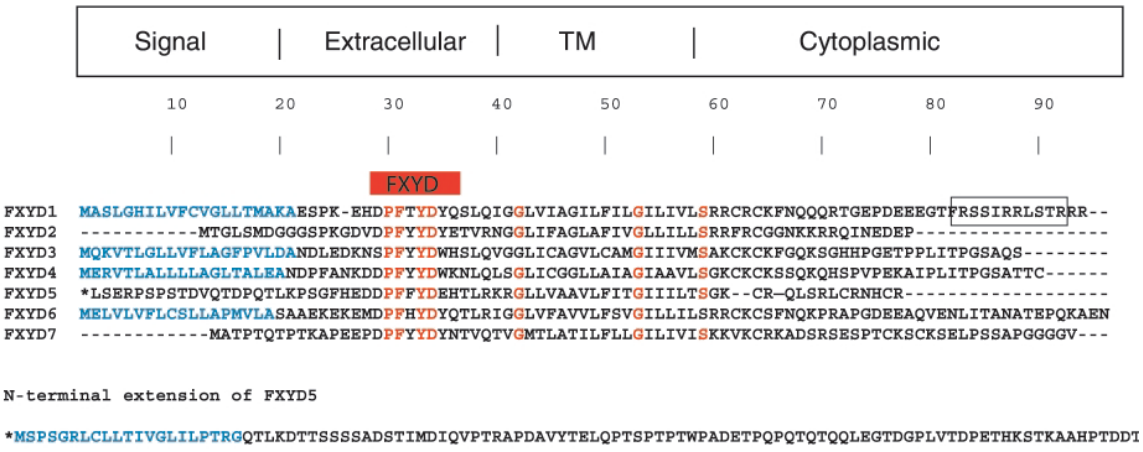

Figure 1.8 Amino acid sequence alignment of the seven currently known mammalian FXYD proteins.

Conserved residues are in red. All except FXYD2 and FXYD7 contain a candidate cleavable N-terminal signal (in blue). The PKA/PKC multisite phosphorylation domain of phospholemman (PLM) is framed. All sequences are from human (taken from 157).

Figure 1.9 shows the structure of PLM. Infrared[158] and nuclear magnetic resonance spectroscopy[159,160] has revealed that the transmembrane domain of PLM reconstituted in liposomes is alpha-helical, with a maximum tilt of 15-17^{o}. Additionally, NMR spectroscopic studies of highly purified PLM in model micelles has shown that Helices 1 (residues 12-17), 2 (residues 22-38) and 3 (residues 39-45) are rigidly connected and their relative orientations determined, with Helix 1 located in the extracellular N-terminus and Helix 2 being the main transmembrane helix.[159] Helix 4 (residues 60-68), located in the cytoplasmic region, is connected to Helix 3 by a long flexible loop and its relative orientation has not been pre-determined. While PLM does not express splice variants, the PLM gene is alternatively spliced in the 5' untranslated region, which could potentially add another level of regulation to PLM expression.[161] Human PLM appears to be a unique gene localised on chromosome 19q13.1.[162]).[154,161]

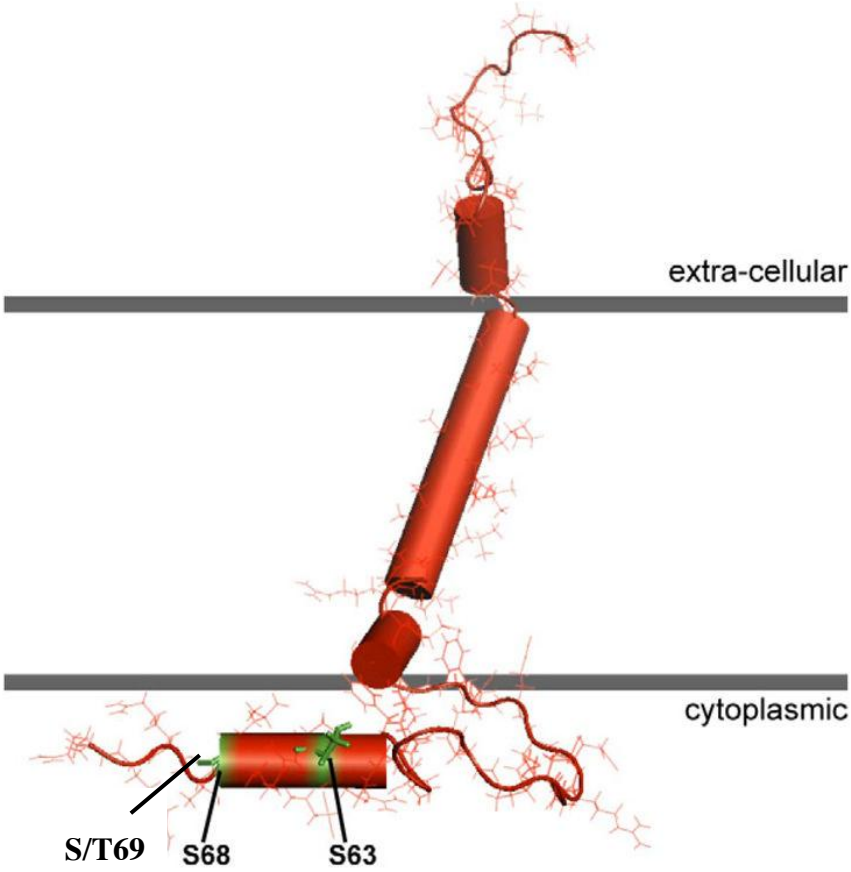

Figure 1.9 Structure of PLM determined by combining the NMR constraints obtained in micelles with those obtained in lipid bilayers.

The consensus phosphorylation sites, Ser63, Ser68 and Ser/Thr69 in the cytoplasmic helix of PLM are highlighted (adapted from 159).

1.3.2 Kinase phosphorylation of PLM

It was first demonstrated in 1985 that PLM phosphorylation occurs in response to both PKA[163] and PKC,[164] although the target residues were not identified at the time. Amino acid sequence determination of PLM revealed four consensus phosphorylation sites located on its cytosolic C-terminal domain; Ser62, Ser63, Ser68 and Thr69 (Ser69 in mouse).[153] PLM is unique within the FXYD family in that it possesses phosphorylation sites in the C-terminal domain that are conserved across all vertebrate sequences cloned to date. It is interesting to note that Ser16 on PLB constitutes another key PKA phosphorylation target during β-AR stimulation,[165] consistent with the aforementioned region of sequence similarity present on the two proteins. There is now a large body of

evidence generated from studies using synthetic peptides mimicking the cytoplasmic C-terminal region of PLM,[166,167] or in FRSK-[146,168] or ISO-treated myocytes[169,170] from a variety of species, that PKA phosphorylates PLM at Ser68. It has been suggested that PLM as a PKA phosphorylation target is quantitatively comparable to cTnI and PLB, making it potentially one of the most important cardiac PKA phosphorylation targets upon β-AR stimulation.[153,163]

Peptide studies have also shown that PKC can phosphorylate PLM at both Ser63 and Ser68,[166,167] which was later confirmed with PDBu-treated *Xenopus* oocytes[168] and mouse ventricular myocytes.[169,170] Although the peptide studies suggested that prior phosphorylation of Ser68 by PKA was able to hinder subsequent Ser63 phosphorylation by PKC,[166,167] subsequent studies with native PLM demonstrated no difference in Ser63 phosphorylation following sequential PKA and PKC stimulation in either order.[168,170] Similarly, an additive effect of sequential PKA and PKC stimulation on Ser68 phosphorylation was observed, again independent of treatment order.[168,170]

Furthermore, PLM has been shown to be phosphorylated at Ser63 and Ser68 *in vivo* in the absence of exogenous PKA and PKC stimulation, and this has been quantitatively estimated in cardiac tissue. The basal phosphorylation levels of Ser63 and Ser68 have been estimated to be 16-30%,[171,172] and 20-46%[146,163,172,173] respectively in mouse and rat myocytes by a number of independent laboratories. The variation in these values may be attributed to different methods of estimation used and the various assumptions made in each case, in addition to possible discrepancies between the basal adrenergic state of the animals used in each study immediately prior to tissue isolation.[174] However, it is likely to be predominantly due to the Ca content within the myocytes post-isolation, which is determined by how much basal PKC phosphorylation is present; indeed, variations in basal phosphorylation can been modulated by either using a low Ca incubation or with PKC inhibitors such as bisindolylmaleimide.[171] In practice, the relatively high basal phosphorylation of PLM often poses a significant complication in the investigations into the relationship between PLM and the NKA. This will be discussed in more detail in Chapter 3 (Section 3.4).

More recently, it was demonstrated in ARVMs that while Ser/Thr69 is barely phosphorylated under basal conditions; it is transiently phosphorylated in response to receptor-mediated PKC activation, in contrast to the sustained phosphorylation at Ser63 and Ser68.[171] In contrast, it is now appreciated that Ser62 is unlikely to be a target for phosphorylation. Additionally, while PLM-Ser63 has been reported to be a substrate for NIMA kinase,[166] there is no known functional connection between this kinase and the pump.

1.3.3 PLM as FXYD1

Based on electrical measurements on *Xenopus* oocytes in which PLM is over-expressed in artificial lipid bilayers, the function of PLM was initially proposed to facilitate the membrane flux of ions[154] and/or serve as a hyperpolarisation-activated channel for taurine transport,[156] ultimately contributing to the regulation of cell volume.[175,176]

The role of PLM as a modulator of NKA function became clear once it was recognised as the first sequenced member of the FXYD family (FXYD1) in 2000.[177] The FXYD family (named after a conserved Pro-Phe-X-Tyr-Asp motif in the extracellular N-terminus domain) is comprised of single-span transmembrane proteins involved in tissue-specific regulation of the NKA [Figure 1.8].[177] These small proteins are widely distributed in mammalian tissues, with predominant expression in tissues that carry out fluid and solute transport or that are electrically excitable, i.e. where the movement of Na across membrane has an important functional role.[178] Importantly, FXYD proteins display a high level of tissue specificity [Figure 1.8], and it is now accepted that such exclusivity of expression allows most FXYD proteins to function as a tissue-specific regulatory subunit of the NKA, allowing the pump to meet the exact requirements of Na transport in the individual tissues.[178]

1.4 The Na/K-ATPase

Discovered in 1957 by Jens Christian Skou (who received a share of the Nobel Prize in Chemistry in 1997),[179] the NKA is a highly conserved, heterodimeric membrane protein and is a member of the ubiquitous P-type ATPase family of cation pumps. It is an extremely high capacity system that couples the hydrolysis of ATP to the movement of

Na and K ions across the plasma membrane of mammalian cells.[180] The energy derived from the hydrolysis of one ATP molecule is used by the NKA to extrude three Na in exchange for two K against their electrochemical gradients, resulting in a net flux of one positive charge from the cell per cycle that generates a small outward membrane current (I_P).[181] The latter forms a significant part of the total net current during the cardiac action potential plateau phase.[181] The NKA provides an indispensable means of active membrane transport in essentially every eukaryotic single and multi-cellular organism, and is the molecular target of the foxglove extracts digitalis and digoxin, having been in clinical use for treating HF since the eighteenth century.

1.4.1 Structure

The crystal structure of the NKA was solved in 1997 [Figure 1.10],[182] with the pump comprising of two essential subunits, α and β. The α-subunit is approximately 1000 amino acid long and has a molecular weight of 112kDa.[183] It is a multi-spanning membrane protein with intracellular amino and carboxyl termini, consisting of ten transmembrane domains.[184] The α-subunit is the catalytic core of the enzyme and contains binding sites for Na, K, ATP, Mg, inorganic phosphate and cardiac glycosides (a class of compounds that act as specific NKA inhibitors, including ouabain and digoxin).[185] Currently, four isozymes of the α-subunit have been identified (α_1, α_2, α_3 and α_4), which display a tissue-specific pattern of expression that may be important in the maintenance and regulation of NKA activity.

Specifically, α_1 and α_2 are expressed in mouse[186] rat and guinea pig[187] hearts while α_1, α_2 and α_3 are expressed in human heart.[188] In practice, only α_1 and α_2 have been reported to be expressed at significant levels in cardiac myocytes. Both the α_1[189] and α_2[186] subunits of the NKA have been found to be functionally linked to the NCX in ventricular myocytes, although the subcellular distribution of the two isoforms seems to be different, with the α_2 subunit more concentrated in transverse (T)-tubular membranes.[190] This has led to some proposing different physiological roles for these two subunits;[186,191] the current paradigm is that while both subunits are involved in the regulation of ECC, α2-containing pumps are principally concerned with regulation of contractility, while α1-containing pumps control both contractility and bulk intracellular Na.[192]

The latter is approximately 370 amino acids long and has a core molecular weight of around 35 kDa.[193] This subunit is highly glycosylated and its actual molecular weights varies between 42 and 55 kDa depending on the extent of glycosylation.[194] It is a single-spanning transmembrane protein with its amino terminal in the cytoplasm, and it interacts with the α-subunit at the amino acid linker region between transmembrane domains 7 and 8 to form the functional pump unit.[195] This obligatory association with the β-subunit is required for the assembly, trafficking and insertion of the pump in the plasma membrane, preventing its degradation close to the endoplasmic reticulum and therefore making the pump functionally active.[196-198] Although the β-subunit is not necessary for specificity as it does not bind the substrates,[199] it has previously been suggested to have a contribution to catalytic activity.[200] Indeed, the affinity of the NKA for K has been shown to be β isozyme-dependent.[200] There are strong bonds between the α- and β-subunits, and altering the conformation of either subunit will alter the affinity of the substrates and therefore pump activity.[201] Three β isozymes (β_1, β_2 and β_3) have been identified to date, and these are expressed in mouse, rat and human hearts.[193,202] The principal β-subunit found in cardiac muscle is β1. On the whole, the existence of the multiple isoforms of the α- and β-subunits, and 7 FXYD proteins (see Section 1.3.3) in mammalian genomes can theoretically support the assembly of over 100 functionally different NKAs to fulfil different physiological requirements.

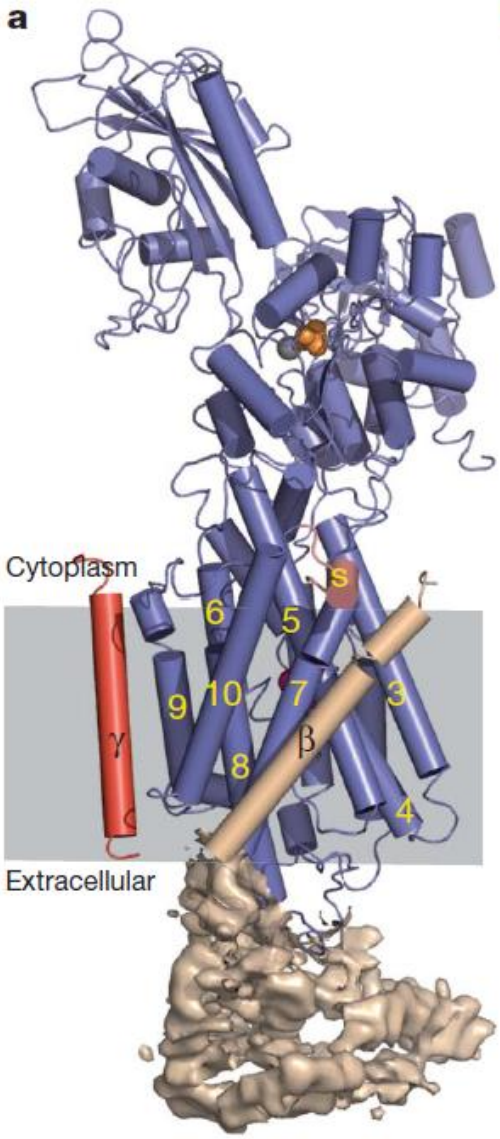

Figure 1.10 Structure of the Na/K-ATPase.

The α-, β-subunits are coloured blue and wheat respectively. Also shown is the γ-subunit (FXYD2; coloured red), which is associated with the NKA in the kidney. The β-ectodomain is shown by surface representation of the experimental electron density. The transmembrane segments of the α-subunit are numbered (in yellow) starting with the most N-terminal. The small C-terminal helix (S, for switch) is light red. (taken from 182).

1.4.2 Function

The NKA provides the major route for cellular Na extrusion in mammalian cells and the activity of the NKA under normal conditions matches the cumulative activity of all the plasmalemmal transporters that lead to Na influx.[203] It has been suggested that approximately 40% of the resting ATP consumption in cardiac myocytes could be attributed to NKA turnover,[204] giving an indication of the pump's importance for the normal functioning of the heart.

Specifically, since $[Na]_i$ in cardiac myocytes is determined by a fine balance between Na influx and efflux, the NKA plays a crucial role in maintaining a low steady-state $[Na]_i$ (4 - 14 mmol/L compared with extracellular [Na] at approximately 140 mmol/L) at the expense of metabolic energy.[203] The transmembrane Na gradient established by NKA activity is essential not only for generating the rapid upstroke of the action potential, but also for driving a number of ion exchange and transport processes critical for normal cellular function, ion homeostasis, and the control of cell volume.[203] Specifically, the steep electrochemical gradient provides the electromotive energy for a number of energetically unfavourable transmembrane transport processes involved in the movement of ions, substrates and amino acids (secondary active transport).

Of particular relevance to the physiological functioning of the heart is the coupling of the sarcolemmal Na/Ca exchanger (NCX) to Na transport; by controlling steady-state $[Na]_i$, the NKA determines the set-point for intracellular Ca via NCX, which in turn determines the SR Ca content. NKA activity could therefore be regarded as an indirect regulatory mechanism of myocardial contractility.[205] Functionally, this may have important consequences as the precise control of cytosolic and SR Ca concentrations is essential for maintaining cardiac output, with derangement of Ca handling being a primary cellular cause of contraction abnormalities and HF.[203,206] Consequently, interventions that influence either the set-point of the NKA, or indirectly the transarcolemmal Na gradient, could profoundly affect myocardial function.

1.4.3 Physical interaction between PLM and the NKA

In addition to its regulation by a number of factors within the cellular environment (including intracellular [ATP], $[Na]_i$, subsarcolemmal Na gradients and membrane potential (E_m)),[207] NKA activity is also functionally coupled to the β-adrenergic signalling system. Specifically, there is considerable evidence indicating that PLM is an integral component of the cardiac NKA complex that serves to modulate the function of the pump upon kinase activation. A physical association between PLM and NKA was first observed in *Xenopus* oocytes co-expressing rat NKA subunits and dog PLM cDNAs,[208] and this interaction has also been observed with recombinant PLM in native heart (bovine) and skeletal (rat) muscle.[208] Moreover, native PLM has been co-immunoprecipitated with the NKA α_1 in the heart.[148] More recently, PLM has been

shown to be in close proximity to the α-subunit in detergent-solubilised membranes from HeLa cells expressing both proteins.[209]

The specific association of PLM with the α_1 subunit of cardiac NKA has been supported by immunofluorescence studies in isolated guinea-pig myocytes, which illustrate that PLM primarily localises with the NKA α_1-subunit but not the α_2.[146,148] As mentioned in Section 1.4.1, the distinct intracellular distribution of the α1 and α2 isoforms has led to the suggestion that the two α isoforms possess distinct physiological roles.[192]While such observations initially led to the suggestion that PLM may exert isoform-specific regulation,[146] it is now generally accepted that during when phosphorylated by either PKA or PKC, PLM interacts with and regulates both the α1 and α2 isoforms to a similar extent.[210]

Despite much speculation on the nature of any potential interactions between PLM residues and the α-subunit of the NKA,[211] along with mechanisms for how the proteins interact to form the PLM-NKA complex,[212]the precise sites of interaction between PLM and pump α subunits remain to be defined.

1.4.4 PLM as regulator of kinase-mediated NKA activity

It is now generally accepted that PKA phosphorylation of PLM, rather than direct phosphorylation of the NKA α subunit, is responsible for regulating activity of the pump. The only well-characterised phosphorylation within the NKA α1 subunit is Ser943, present in a short helical segment between TM 8 and 9, and is thought to be a PKA site. The consensus recognition sequence for PKA is Arg-Arg-X Ser/Thr-Phe, where X is any residue and Phe is a hydrophobic residue. PKA has been shown to phosphorylate the residue, but only after SDS extraction.[213,214] The expected localisation of the residue close to the cytoplasmic membrane interface and the detergent dependence led to scepticism of whether the observed phosphorylation is physiologically relevant. The distinct lack of evidence for PKA-mediated phosphorylation of the intact NKA protein suggests that direct phosphorylation of Ser ^{938} on the NKA α subunit occurs only when the protein is unfolded or at least partially denatured by detergents, as shown by later studies confirming the necessity of Triton X-100 for PKA-mediated Ser^{938} phosphorylation to take place.[215,216]

1.4.4.1 Under basal conditions

1.4.4.1.1 Measurements of pump current in single cells

Despite the general agreement over the necessary role of PLM in regulating NKA function, some disagreement remains over the exact functional effect of PLM on the cardiac NKA under resting conditions, in part due to the variety of experimental models and approaches employed.

Single-cell studies using cardiac myocytes from PLM-KO mice have revealed that maximal NKA rate is 20-30% higher in PLM-KO myocytes compared to their WT counterparts, despite NKA α-subunit expression being reduced in the former.[169,170,217-219] These studies demonstrate that unphosphorylated PLM inhibits NKA activity via a reduction in Na affinity[169,219] and possibly also in V_{max},[173,217,220] although this reduction in pump current is thought to be partially compensated for by a decreased membrane expression of the pump α subunit. In general, observations from our laboratory suggest that basal pump current is consistently higher in KO myocytes compared with WT, and therefore pump current per pump protein molecule is likely to be substantially increased. Specifically, normalising the rate for equal subunit expression has demonstrated that the presence of PLM approximately halves the unitary NKA current rate in comparison to that observed in PLM-KO myocytes under basal conditions.[218]

1.4.4.1.2 Measurements of in vivo contractility

In contrast, the role of PLM in modulating cardiac contractility *in vivo* remains somewhat less clear, possibly due to the effects of autonomic regulation which are absent *in vitro*. *In vivo* conductance catheter measurements carried out by our laboratory revealed a mildly depressed cardiac contractile function in PLM-KO mice with congenic background (C57BL/6), which was associated with a mild cardiac hypertrophy[218]. Biochemical analysis showed a significantly increased NKA activity in the crude ventricular homogenates from PLM-KO hearts, in agreement with the pump current measurements made on single cells mentioned above.[218] The expression of the NKA α1-subunit was found to be decreased by ~25% in the PLM-KO hearts compared to the WT controls, although this difference was not statistically significant.[218]

The depressed cardiac contractility observed *in vivo* was exacerbated when hearts were isolated and Langendorff-perfused, and is consistent with the expectation that with relief of inhibition of the NKA, PLM-KO hearts should exhibit a lower (and unregulated) contractility (due to the presence a lower $[Na]_i$) when compared with WT hearts. The cardiac hypertrophy was not complemented by significant changes in action potential morphology in paced Langendorff-perfused hearts, suggesting that at 11 weeks, the hypertrophy remained a physiological adaptation to compensate for the depressed contractility.

Similarly, a separate group has identified a mild cardiac hypertrophy in PLM-KO mice with mixed genetic background (C57BL/6 and 129/SvJ), but with an increased ejection fraction and a reduction in NKA activity.[218,220] To complicate matters further, more recent observations in closed-chest catheterised mice show slightly increased baseline +dP/dt in congenic PLM-KO hearts.[221]

Overall, these findings point to an important role of PLM in regulating cardiac contractility. However, the evidence outlined above suggests that PLM-KO hearts may contract at least as well as WT hearts under basal conditions, and the disparity within these findings may well reflect the different experimental conditions in the studies, including different genetic backgrounds, imaging/catheterisation procedures, anaesthesia and blood loss. On the other hand, these observations may support a scenario whereby PLM is functionally quiescent at rest, as supported by similar $[Na]_i$ values observed between WT and PLM-KO myocytes,[169,221] but becomes important under stressful conditions.

1.4.4.2 During β-adrenergic receptor stimulation

There is now considerable evidence indicating the functional importance of PLM in regulating NKA activity upon β-AR stimulation. While treatment of guinea-pig myocytes with FRSK was shown to result in an increased α_1-subunit NKA current, Western blotting (WB) analysis did not reveal a simultaneous change in α_1-subunit phosphorylation but rather an increased phosphorylation at Ser68 on PLM.[146,148] This observation is consistent with the concurrent increase in NKA activity in PLM-WT myocytes treated with ISO observed in a number of studies, although this effect seems

to be also dependent on$[Ca]_i$ (See Chapter 4; Section 4.4 for reasoning).[169,170,221] Of particular importance, there was an absence of ISO-mediated stimulation of the NKA in PLM-KO mice, with $[Na]_i$ remaining elevated in these animals,[169,170,221] indicating that PKA-dependent phosphorylation of PLM, rather than the direct phosphorylation of the NKA α-subunit, is responsible for mediating the β-AR effects on NKA function. Similarly, PDBu-induced PKC activation increased NKA activity in PLM-WT myocytes, via an increase in maximal turnover rate but with no change in Na affinity, with this effect being absent in PLM-KO cells.[170] This indicated that PKC-dependent regulation of NKA function is also modulated by PLM, as confirmed by an increased phosphorylation at Ser63 and Ser68 on the protein.[170] Investigation into how PLM mechanistically inhibits the NKA and relieves this inhibition remains ongoing. It has been demonstrated that only the intracellular (19 C-terminal residues) region of PLM is required to regulate the NKA.[217] Co-immunoprecipitation (co-IP) experiments have shown that complete dissociation of the two proteins does not occur upon PKA and PKC phosphorylation,[147,148] although FRET analysis suggests that the interaction between the α-subunit of NKA and PLM is altered upon Ser63 or Ser68 phosphorylation.[222] This functional scheme has been proposed to be analogous to the loss of inhibition seen in the sarcoplasmic/endoplasmic reticulum Ca ATPase (SERCA) following PLB phosphorylation.[223] Recently, it has been shown that PLM could potentially regulate NKA activity via other mechanisms that are independent of phosphorylation, including palmitoylation and glutathionylation.[207,224] These pathways will be discussed in more detail in Chapter 4 (Section 4.4).

1.4.4.3 Functional consequences

The most important functional consequence of PLM-modulated NKA activity may be the precise control of cytosolic and sarcoplasmic reticulum (SR) Ca content, which is essential for the maintenance of normal systolic and diastolic function.[225,226] During β-AR stimulation, the increased Ca transients drive greater Ca extrusion via the NCX, which leads to increased Na influx at each beat, along with a more frequent and larger Na current via Na channels, thus resulting in a significant increase in $[Na]_i$.[3,226] The elevated [Na] contributes to the inotropic response of β-AR stimulation by favouring

more Ca influx and less Ca efflux through the NCX, and is likely to be compensated for by an enhanced Na extrusion via the NKA.[227-229]

A general hypothesis based on the above findings is that the association of PLM with the NKA provides the link between kinase activity and NKA modulation in a manner analogous to how PLB modulates SERCA, a P-type pump closely related to the NKA. That is, while unphosphorylated PLM inhibits NKA by primarily reducing its affinity for $[Na]_i$,[146,168,169,208] phosphorylation of PLM at Ser68 by PKA or Ser63 and Ser68 by PKC relieves this tonic inhibition and stimulates NKA activity by increasing its affinity for $[Na]_i$, and perhaps V_{max}.[146,169,208] Figure 1.11 denotes a hypothetical relationship between PLM and NKA and suggests how NKA function could be altered by PLM phosphorylation during cardiac sympathetic stimulation.

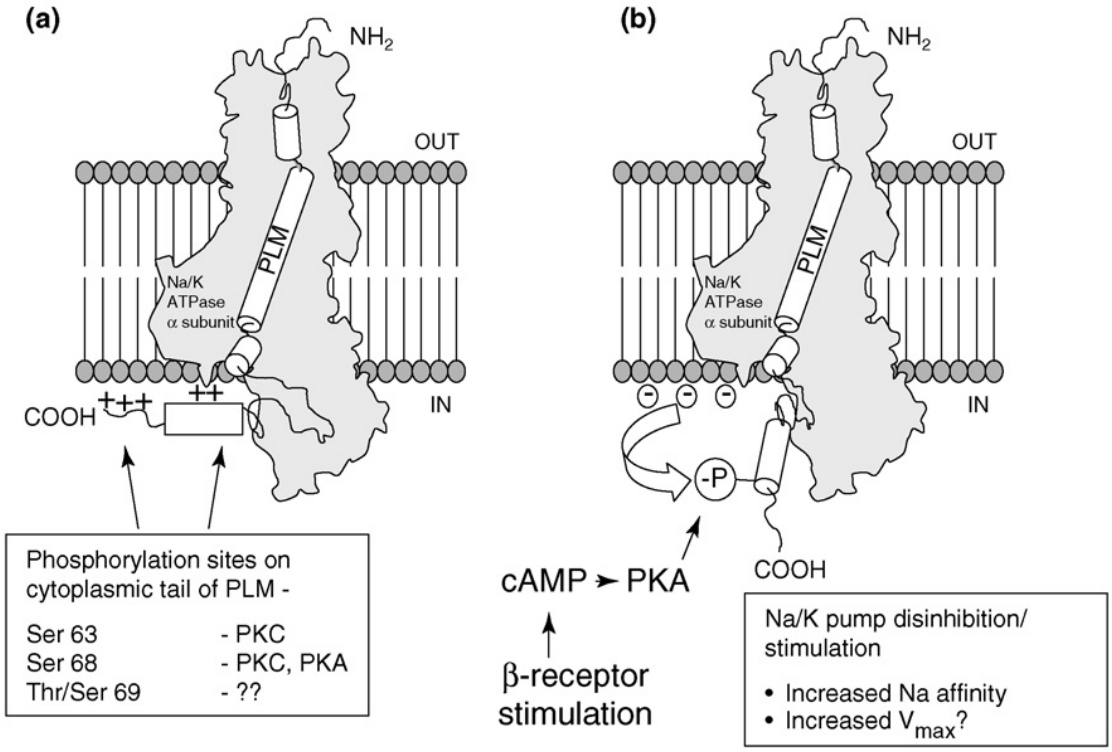

Figure 1.11 The hypothetical relationship between phospholemman (PLM) and the Na/K ATPase a-subunit and alterations induced by PLM phosphorylation.

(a) PLM is a single transmembrane spanning protein that inserts into the sarcolemma with its carboxy terminus on the cytoplasmic side of the membrane. The cytoplasmic tail of PLM contains three known phosphorylation sites at Ser63, Ser68 and Thr69 (Ser69 in mouse). **(b)** The helical structure of PLM [taken from [159]] normally orientates with the cytoplasmic a-helix (H4) close to, or inserted into, the membrane [230]. The basic nature of this region (+) means that it associates with the negatively charged phospholipids of the membrane. However, when PLM is phosphorylated at any or all of the phosphorylation sites indicated in Panel A (for example, by PKA: Panel B) the orientation of the cytoplasmic tail may shift altering its interaction with the Na/K ATPase a subunit and disinhibiting/stimulating ion transport [taken from 203].

Interestingly, it has been proposed more recently that PLM may physically associate with and directly modify the function of the NCX, with phosphorylation at Ser68 on PLM inhibiting NCX activity.[172,231,232] However, much of the evidence supporting NCX modulation by PLM has not been reproduced by other groups and may merely be reflecting a secondary effect of PLM's regulation of the NKA (PLM-mediated inhibition of the NKA results in reduced Na extrusion from myocytes, which will in turn reduce forward Na/Ca exchange). Similarly, it has been demonstrated more recently in heterologous expression systems that PLM cooimmunoprecipitates with $Ca_v1.2$ channels from guinea pig myocytes, and may act as an endogenous regulator of

$Ca_v1.2$ channel gating.[233] Collectively, these findings suggest that PLM is potentially a central player in the sympathetic response, playing a major role in the regulation of cardiac contractility under stressful conditions.[206,234] Indeed, from a physiological perspective, limiting the rise in $[Na]_i$ at the expense of reduced inotropy has been suggested to prevent Ca overload in response to β-stimulation, prevent diastolic dysfunction and protect against arrhythmias.[203,206,234,235] This model is consistent with the number of pathophysiological states found to be associated with altered cardiac NKA function, including HF,[147,236] cardiac ischemia[148] and post-MI.[173]

1.5 Rationale, general hypothesis and aim of project

It is now largely accepted that PDE activity is critical for spatial and temporal regulation of cAMP signal propagation. PDEs are strategically distributed within the cell and selectively regulate cAMP signals triggered by individual G_SPCRs, including the β-AR. Specifically, the evidence outlined above suggests the existence of multiple PDE variants with different catalytic and regulatory properties that permit the generation of tailored cAMP signals within distinct intracellular compartments in proximity to individual PKA substrates. Since PLM is a major cardiac PKA phosphorylation target and resides in close proximity to the LTCC in the sarcolemma, we hypothesised that PDE activity is involved in modulating cAMP signalling signalling to PLM during β-AR stimulation. Indeed, prior to the start of the PhD project, we have generated some preliminary data indicating the presence of an AKAP in the vicinity of PLM. In voltage-patch-clamp (VPC) experiments, FRSK-induced NKA activation was shown to be blocked by Ht31 (a peptide that competes with endogenous AKAPs for binding to the R subunits of PKA) dissolved in the pipette solution, suggesting that AKAP binding of PKA is a requisite for PLM phosphorylation (unpublished data). In support of this AKAP-based model, we have pilot data showing that PLM interacts with other membrane-bound and cytosolic proteins, suggesting that PLM may be a nodal point in signalling to cardiac transporters and integrates signalling from multiple pathways (unpublished data). Interestingly, our group has shown that NKA activity and primarily the Ser68 phosphorylation residue on PLM are negatively modulated by the aforementioned PP-1 in resting cardiomyocytes, with this mechanism being sensitive to Inhibitor-1 (I-1).[237] Moreover PLM-Ser68 phosphorylation was found to be markedly

diminished in failing human hearts, which is consistent with hyperactivated PP-1 and I-1 deactivation previously observed in HF and may be involved in the pathogenesis of HF and arrhythmogenesis.

Therefore, identifying the PDE subtype(s) involved in the regulation of cAMP signalling to PLM is a logical step that will shed light onto the functional link between β-AR stimulation and NKA activity. Considering the importance of NKA in indirectly regulating myocardial contractility and the crucial role of PDEs in upholding normal cAMP signalling, in addition to the potential therapeutic use of PDE inhibitors as pharmacological agents, our findings may bear therapeutic potential for treating HF and other pathological conditions potentially involving PDE and NKA dysfunction.

General hypothesis

That one or more PDE subtypes contribute to the regulation of cAMP signalling to PLM and the NKA during β-AR stimulation.

Aim of project

To identify the PDE subtype involved in regulating cAMP signalling to the PLM-NKA complex during β-AR stimulation and characterise its physical and functional associations with the complex using electrophysiological, biochemical and imaging approaches.

2 GENERAL METHODS

Details of methodology relevant to more than one chapter are provided here. Details of specific methodology and experimental groups are provided within the *Specific Methods* section of each chapter.

2.1 Reagents

All analytical-grade chemicals and consumables used were purchased from Sigma-Aldrich or VWR unless otherwise indicated. Purified water (Elgastat UHP, Elga Ltd.) at resistivity >18.2 MΩ was used to make up all solutions.

2.2 Animals

2.2.1 Principles

The vast majority experiments described in the following chapters were carried out using ventricular myocytes from the adult rat. Rat myocytes are generally more robust than mouse myocytes, which makes them more conducive to VPC studies. Additionally, due to the greater size of the heart in rat in comparison to the mouse, isolations generally yield a higher number of live cells, which facilitates WB studies by providing a strong protein signal, in addition to enabling multiple conditions to be tested using cells from a single heart. This serves to reduce the number of animals culled for each experiment.

2.2.2 Animal housing and handling

Adult male Wistar rats (250 – 300 g; B & K Universal Ltd) were maintained on site (Biological Services Animal Care Facility, King's College London). Animals were maintained humanely in compliance with the 'Principles of Laboratory Animal Care' prepared by the National Society for Medical Research, and the 'Guide for Care and Use of Laboratory Animals' from the National Academy of Sciences, published by the National Institutes of Health (NIH Pub. No. 85-23, revised 1985). All animals were kept in containment rooms maintained at 25^{o}C with a 12-hour light-dark cycle; between

4 and 6 rats were housed in each cage, allowing free access to food and water. All animal protocols were approved by both the local King's College London Ethical Review Process Committee and performed in accordance with the Home Office Guidelines on the Operation of the Animal Scientific Procedures Act (1986) published by Her Majesty's Stationary Office, London.

2.3 ARVM isolation

2.3.1 Isolation procedure

ARVMs were isolated using a standard collagenase-based digestion protocol, yielding Ca-tolerant rod-shaped cells. All the work described in Section 2.3.1 was undertaken by our 'in-house' research technician Dr Shiney Reji.

Animals were anaesthetised by an intraperitoneal injection of sodium pentobarbitone (50 mg/kg; Sagatal, Rhone Merieux), followed by an injection of heparin (150 I.U; Leo Laboratories Ltd) into the femoral vein to prevent blood coagulation and clot formation in the excised heart. Once the animal was unconscious, as determined by an absence of pedal and corneal reflexes, the abdominal cavity was opened just below the sternum and the heart exposed by removing the diaphragm and cutting laterally either side of the ribcage. The chest wall was reflected and the heart gently lifted and rapidly excised with the proximal aorta and pulmonary trunk intact, and immersed in ice cold Ca-free modified Tyrode's Solution (see Table 2.1 for composition). After removal of excess thymus and fatty tissue, the aorta was cut just below the aortic arch and tied to a custom-made blunt stainless steel cannula and the aorta using 4/0 surgical silk (Johnson and Johnson). Perfusion was commenced within 60 s of excision.

Hearts were perfused at 37^{o}C in the retrograde fashion though a modified Langendorff preparation for three sequential periods as follows: with (1) modified Tyrode's solution containing 0.75 mmol/L $CaCl_2$ (Solution A) for 4 min to clear the heart of blood and allow healthy stable contractions to be established; (2) Ca-free modified Tyrode's solution containing 0.2 mmol/L EGTA (Solution B) for 4 min to arrest the heart; (3) modified Tyrode's solution containing 0.1 mmol/L $CaCl_2$ and 125 U/ml collagenase (Type II; Worthington Biochemical Corporation) for 7 min for enzymatic digestion of the heart tissue. The coronary flow rate was maintained at 10 ml/min using a Gilson

Minipuls peristaltic pump, and all solutions were maintained at 37^{o}C and gassed with 100% O_2 throughout the procedure. The compositions of Solutions A-E are displayed in Table 2.2.

After the perfusion protocol, the heart was removed from the cannula and the aorta, atrial and non-ventricular tissue carefully removed. The right ventricle was then removed before the left ventricle was cut into fragments, first with sterile scissors and then using a sharp scalpel blade, before re-suspended in 20 ml of digestion buffer (Solution C). The tissue fragments were then gently bubbled with 100% O_2 for between 15 and 20 min, and were subsequently carefully triturated using a 2 ml plastic dropping pipette to facilitate cell dispersion (<2min). Digested cells were then filtered through a nylon mesh (200 μmol/L pore size). The suspension was left to settle for 8 min to allow the cardiac myocytes to pellet. The supernatant was then removed and the remaining live myocytes washed and re-suspended in warmed modified Tyrode's solution containing 0.5 mmol/L $CaCl_2$ (Solution D). After a further settling step lasting 8 min, the supernatant was removed and the myocytes washed and re-suspended in warmed modified Tyrode's solution containing 1 mmol/L $CaCl_2$ (Solution E), in order for the $CaCl_2$ concentration to be increased to 1 mmol/L. The cell suspension (>70% rod-shaped as estimated by light microscopy) was maintained in Solution E in a water bath set at 35^{o}C for approximately 2 hr prior to use in VPC experiments or maintained in culture at 37^{o}C/5% CO_2 for at least 2 hr prior to use in biochemical/adenoviral infection experiments.

Table 2.1 Composition of modified Tyrode's Solution used in isolation of ARVMs.

1x stock of the solution was prepared without glucose, which was added on the day of use. The solution was then filtered through a cellulose acetate filter (0.2 µm pore).

Compound	Concentration (mmol/L)
NaCl	130
KCl	5.4
$MgCl_2$	1.4
Na_2HPO_4	0.4
HEPES	4.2
Glucose*	10
Taurine	20
Creatine	10

*Added on day of use

pH 7.3 at 37^{o}C with NaOH

Table 2.2 Composition of Solutions A – E used in isolation of ARVMs

Solution	Additions
A	750 µmol/L $CaCl_2$
B	100 µmol/L EGTA
C	100 $CaCl_2$ & 0.5 mg/ml collagenase
D	0.5 mmol/L$CaCl_2$
E	1 mmol/L$CaCl_2$

2.3.2 Cell viability

Viable ARVMs were recognised as rod-shaped rectangular cells. Healthy myocytes were identified by their defined edges and square ends. Only isolations with viable cells equal to or in excess of 70% were used in experiments/maintained in culture.

2.3.3 Post-isolation treatment of ARVMs

As aforementioned, ARVMs were incubated/cultured for approximately 2 hr prior to experimentation to allow recovery from the isolation procedure. Unpublished observations by our group suggest that the isolation procedure activates a number of stress kinases, which results in the hyper-phosphorylation of PLM. Experimentally, this could potentially be problematic since a large proportion of our experiments are dependent upon agonists being able to stimulate PLM phosphorylation to a significant degree so that it is detectable by WB, and the corresponding changes in NKA current measured by electrophysiological means.

If PLM is already maximally or close to being maximally phosphorylated, then any potential changes in PLM phosphorylation mediated by agonists and/or other pharmacological agents may remain undetected. Therefore, with the aim of maximising the 'window' for detecting increases in PLM phosphorylation and NKA activity, our group has investigated the 'recovery window' (i.e. the time required for PLM phosphorylation to significantly decrease and stabilise post-isolation). Unpublished data generated by our group indicate that ARVM recovery and the decrease in PLM phosphorylation become stable after approximately 2 hr post-isolation. By this time-point, PLM phosphorylation is reduced by approximately 60% compared to freshly-isolated ARVMs. Further unpublished observations show that culturing ARVMs for 24 hr significantly potentially reduces basal PLM phosphorylation by 80%. However, a comparison of PLM phosphorylation responses to a range of ISO concentrations made between ARVMs left for 2 hr post-isolation and those cultured for 24 hr revealed similar results, with both experimental setups generating the same IC_{50} values.

2.3.3.1 Freshly-isolated ARVMs

As outlined earlier, freshly isolated ARVMs were placed in a water bath heated to 35^{o}C for 2 hr post isolation to allow recovery from the isolation procedure. Myocytes were washed and re-suspended in an appropriate volume of modified Tyrode's solution (Table 2.1) after 2 hr to remove any dead cells prior to use in electrophysiological experiments.

2.3.3.2 Short-term culture of ARVMs

Laminin (2 ml of a 15 μg/ml solution) was added to 6- or 12-well plates, which were incubated at room temperature for 1.5 to 2 hr. The laminin was then removed (and stored at -20^{o}C for re-use up to 3 times) and the wells washed with 1-2 ml of sterile modified Hank's M199 culture medium (containing Hanks salts, 25 mmol/LHEPES, L-glutamic acid and L-amino acids; Invitrogen; 500 ml bottle supplemented with 2 mmol/L L-carnitine, 5 mmol/L creatine, 5 mmol/L taurine and 1% penicillin (100 units/ml) and streptomycin (100 μg/ml)). The medium was aspirated from the wells prior to myocyte plating.

After settling for approximately 1 hr post-isolation, modified Tyrode's solution was aspirated from ARVMs isolated from a whole/half heart and the cells were washed at room temperature with approximately 30 ml M199 culture medium. Cells were pelleted by centrifugation in a Heraeus Sepatech Megafuge 1.0R centrifuge at 300 rpm for 1 min at room temperature, the supernatant removed by aspiration and the cell pellet re-suspended in an appropriate volume of pre-warmed M199 medium. The myocytes were gently agitated to ensure equal suspension, before getting plated down in a volume of 1 or 2 ml/well on pre-laminated 12- or 6-well culture plates respectively. Throughout the culture process, the plated cells were kept in a humidified tissue culture incubator (37^{o}C/5% CO_2). After 1.5 to 2 hr, the culture medium was exchanged for fresh media, in the process removing any dead myocytes that have not adhered prior to conduction of any biochemical/adenoviral infection experiments and/or further incubation of the cells overnight. At the start of each experiment, the culture medium in each well was aspirated and 1 ml fresh medium added.

2.4 Pharmacological agents

2.4.1 PDE inhibitors

IBMX is a widely used non-selective inhibitor of all PDE subtypes, while EHNA, Cil and Rol are selective inhibitors of PDE2, PDE3 and PDE4 respectively. IBMX was used at 100 μmol/L while the subtype-selective inhibitors were used at 10 μmol/L (See Chapter 3; Section 3.4 for reasoning). All PDE inhibitors were prepared as 1000x stocks in 100% DMSO. In WB experiments, these stocks were diluted 1:10 in M199 culture media to facilitate accurate loading into the wells. See Table 2.3 for details of these compounds.

2.4.1.1 IBMX

Theophylline was the first PDE inhibitor to be described in the literature, in 1962.[238] A decade later, a new xanthine analogue, IBMX, was shown to be 100-fold more potent than theophylline.[239] Both IBMX[240] and theophyline[241] inhibit the PDEs belonging to the different families. In the last decade, a large number of PDE inhibitors have been developed; some of them inhibit PDE activity very potently, in the nanomolar range, and are very specific for a single PDE family. Therefore, in the span of several decades, the potency of PDE inhibitors has increased by 10^6 and the selectivity of some of them has increased by 10^4.

2.4.1.2 EHNA

There are many compounds which significantly interfere with PDE2, although many of them also inhibit other PDE subtypes. EHNA (previously known as cGS-PDE or MEP 1), has a very particular mechanism, and remains the only compound so far described that is able to inhibit PDE2 both basally (IC_{50} = 38 μmol/L) and when activated by cGMP[242,243] (IC_{50} = 2 μmol/L).[244] The precise mechanism of this inhibition is not entirely elucidated, since ENHA does not appear to displace cGMP from the regulatory site on PDE2.[79] However, it is important to note that EHNA is also a potent adenosine deaminase inhibitor at lower concentrations[245] (K_i = 10 nmol/L) and must therefore be used with caution as a PDE inhibitor.

2.4.1.3 Cilostamide

Cil (also known as OPC-3689[246]) was the first potent and selective inhibitor of PDE3 described. It was the initially described as a platelet anti-aggregant. PDE3 was considered as a cardiotonic target, with medicinal chemistry focusing on PDE3 inhibitors, giving rise to amrinone, milrinone and enoximone.

2.4.1.4 Rolipram

PDE4 is characterised by its selective sensitivity to Rol (K_i value = 0.8 μmol/L), an antidepressant compound[247] that was found to specifically bind with high affinity to membrane brain fractions and was shown to be a potent inhibitor of cAMP hydrolysis in brain homogenates.[248] Accordingly, Rol became an archetype for the synthesis of new potent and selective PDE4 inhibitors.[249] Importantly, there is now extensive evidence indicating a highly selective binding of Rol to PDE4 in a number of cell types[250,251], including the myocardium.[252-254] Rol binds to PDE4 at two sites, termed low-affinity rolipram binding site and high-affinity binding site.[248,255]

2.4.2 Kinase agonists

Further details of the kinase agonists used in our experiments are listed in Table 2.3.

2.4.2.1 Isoprenaline hydrochloride

Based on the chemical structure of noradrenaline, ISO is a potent, non-selective β-AR agonist that increases $[cAMP]_i$ and induces PKA activation. ISO was prepared fresh in distilled water before each experiment and stored away from light to prevent oxidation. The desired concentrations were obtained using serial dilutions.

2.4.2.2 Phorbol-12-myristate-13-acetate

PMA is a potent PKC agonist which directly activates the kinase due to the structural similarities between PMA and diacylglycerol (DAG, the endogenous PKC agonist). PMA was prepared in 100% DMSO as a 1000x stock. In some of our experiments,

PMA was used as a positive control to maximally stimulate PLM phosphorylation at Ser63, Ser68 and Thr69. This allowed us to access the approximate magnitude of maximal PLM phosphorylation at this site, which provides an insight into how reactive the myocytes are to an external agonist.

Table 2.3 Details of pharmacological agents used in experiments.

Names, stock concentrations, appropriate vehicles used, suppliers and catalogue numbers.

Compound	Use	Stock concentration	Vehicle	Supplier	Catalogue number
ISO	β-AR agonist	5 mmol/L	H_2O	Sigma Aldrich	I5627
FRSK	AC activator	50 mmol/L	DMSO	Sigma Aldrich	F6886
PMA	PKC activator	300 µmol/L	DMSO	Sigma Aldrich	P8139
EHNA	PDE2 inhibitor	10 mmol/L	DMSO	Sigma Aldrich	E114
Cil	PDE3 inhibitor	10 mmol/L	DMSO	Sigma Aldrich	C7971
Rol	PDE4 inhibitor	10 mmol/L	DMSO	Sigma Aldrich	R6520
IBMX	Non-selective PDE inhibitor	100 mmol/L	DMSO	Sigma Aldrich	I5879

2.4.3 Storage of compounds and experimental conditions

After desiccation, all compounds (apart from ISO, which was prepared immediately prior to experimental use) were stored in aliquots at -20^{o}C. As the majority of compounds were prepared in 100% DMSO, which may non-selectively activate several signalling pathways within the cardiac myocyte, care was taken during experiments to ensure that myocytes were exposed to no more than 0.1% DMSO during all treatment conditions, and that all treated wells were exposed to an equal amount of DMSO. Any samples that have been treated with a maximal concentration of PMA but did not show the expected response were excluded from subsequent statistical analysis.

2.5 SDS-PAGE/Western blotting

2.5.1 Principles

SDS-PAGE and WB represent two of the most widely-used biochemical techniques and when employed together allow quantification of the amount of one specific protein from within a cell/tissue sample. SDS-PAGE separates all the proteins in a sample though a gel matrix according to their molecular weights. Once separated the proteins can be transferred onto a supporting membrane and probed for binding to a specific antibody.

2.5.2 Pharmacological treatment of ARVMs and sample preparation for SDS-PAGE

Cultured ARVMs were treated with various pharmacological agents including PDE inhibitors and kinase agonists. The supernatant was subsequently removed and the cells lysed in 100 µl or 150 µl 2x sample buffer for 12-well or 6-well culture plates respectively. The wells were scraped with a disposable cell scraper to ensure full cell lysis and maximise protein harvesting for biochemical analysis. Samples were pipetted into 1.5 or 2ml Eppendorf tubes and stored at -20^{o}C. Prior to loading on a gel, samples were boiled at 95^{o}C for 5 min (only if probing with anti-phospho Ser16 antibody; see *Specific Methods* of the relevant results chapters) and spun at 13,000 rpm for 5 min. Details of the compounds used are provided in Table 2.3, while the concentrations at

which they were used and durations of treatment are described in the *Specific Methods* of the relevant results chapters.

2.5.3 SDS-PAGE

Proteins were separated by SDS Polyacrylamide Gel Electrophoresis (SDS-PAGE) according to their molecular weight. The gel matrix constituted of a lower resolving gel and a stacking gel into which wells were set for sample loading. The 0.75 mm-thick resolving gels (see Table 2.4 for composition) were prepared first; 15% (v/v) acrylamide (Protogel, National Diagnostics; 37.5:1 acrylamide to bisacrylamide) gels were used to investigate PLM and PLB phosphorylation status and 10% (v/v) for that of larger proteins. Water-saturated butanol was overlaid whilst the resolving gel polymerised to prevent drying; the butanol was then washed off and the 1.5 ml layer of stacking gel was prepared (see Table 2.4 for composition). Toothed combs with 10-15 wells were inserted into the stacking gel and removed after polymerisation to leave rectangular wells.

Table 2.4 Composition of stacking and running gels used in SDS-PAGE.

	Resolving gel		Stacking gel
	10%	**15%**	
Tris HCL (mol/L)			
pH 8.8	0.38	0.38	-
pH 6.8	-	-	0.12
Acrylamide (w/v, %)	10	15	4.5
SDS (w/v, %)	0.1	0.1	0.1
TEMED (v/v, %)	0.1	0.1	0.17
APS (w/v, %)	0.09	0.09	0.11

Samples and Precision Plus Protein ™ Dual-Colour Standards (Bio-Rad; containing proteins ranging between 8 and 180 kDa in molecular weight) were loaded onto the stacking gel and immersed in running buffer (0.025M Tris-base, 0.19M glycine, 0.1% w/v SDS). The markers were run in parallel to the samples on every gel to aid determination of transfer efficiency and to enable protein identification by molecular weight. SDS-PAGE was carried out using the Mini protean III Tetra Cell system (Bio-Rad) at 80 V (approximately 15 min) for protein migration through the stacking gel, and at 150-200 V until the bromophenol blue dye front reached the bottom of the resolving gel (approximately 45–60 min).

2.5.4 Semi-dry electrophoretic transfer

Polyvinylidene fluoride (PVDF) membranes (GE Healthcare) were cut to size and pre-soaked in methanol, followed by transfer buffer (0.025 mol/L Tris-base, 0.19 mol/L glycine, 20% (v/v) methanol, 0.1% (w/v) SDS). The membranes and resolving gels were sandwiched between six pieces of electrode paper, also pre-soaked in transfer buffer, and placed in a Hoeffer TE77 semi-dry transfer unit. Transfer was carried out at 10V for 35 min with the current limited to 250 mA per gel.

2.5.5 Western blotting

Following transfer, membranes were blocked against non-specific binding of antibodies by incubating in phosphate-buffered-saline-Tween (PBST) (5% (w/v) dried skimmed

milk powder (Marvel), 0.1% (v/v) Tween-20, in PBS) for ≥1 hr on an orbital shaker at room temperature. Following a brief wash in PBST, membranes were incubated with the relevant primary antibodies (diluted in 5% (w/v) milk) in PBST). The specific conditions for primary antibody incubations are detailed in Table 2.5. Following antibody binding, membranes were washed repeatedly in PBST (4 – 6 times, 10 – 15 min each) and then incubated with horseradish peroxidise (HRP)-conjugated secondary antibody (diluted in 5% (w/v) milk in PBST). The specific conditions for secondary antibody incubations are detailed in Table 2.6. The membranes subsequently underwent 4 – 6 washes in PBST for 10 – 15 min each before being prepared for enhanced chemiluminescence (ECL) analysis.

Table 2.5 Details of primary antibodies used in Western blotting experiments.

Antibody	ID no.	Dilution	Origin	Source	Incubation conditions
Anti-phospho PLM-Ser68*#	Cp68	1:10,000	Rabbit	J Randall Moorman, University of Virginia	60 min; room temp.
Anti-phospho PLM-Ser63	Cp63	1:10,000	Rabbit	J Randall Moorman, University of Virginia	60 min; room temp.
Anti-phospho PLM-Ser/Thr69	T69	1:100	Sheep	Raised 'in house' King's College London	30 min; room temp.
Anti-phospho PLB-Ser16#	A010-12	1:5000	Rabbit	Badrilla	Overnight; 4^{o}C
Anti-phospho cTnI-Ser22/23	4004	1:5000	Rabbit	Cell Signalling	Overnight; 4^{o}C
Anti-total PLM (N-terminal domain)	N1	1:100	Chicken	Raised 'in house' King's College London	60 min; room temp.
Anti-total PLB	A1	1:1000	Mouse	Badrilla	60 min; room temp.
Anti-total cTnI	4002	1:1000	Rabbit	Cell Signalling	Overnight; 4^{o}C
Anti-total actin	JLA20	1:1000	Mouse	Developmental Studies Hybridoma Bank	60 min; room temp.
Anti-GFP	A11121	1:1000	Mouse	Invitrogen	Overnight; 4^{o}C

*This antibody has been shown to cross-react with PLB-Ser16.

#Requires pre-boiling of samples at 95^{o}C for 10 min to remove pentameric PLB.

Table 2.6 Details of secondary antibodies used in Western blotting experiments.

Antibody	ID no.	Dilution	Origin	Source	Incubation conditions
Anti-Rabbit IgG HRP-linked	NA934V	1:1000	Donkey	GE Healthcare	60 min; room temp.
Anti-mouse IgG HRP-linked	NA931V	1:1000	Sheep	GE Healthcare	60 min; room temp.
Anti-chicken IgY HRP-linked	G135A	1:1000	Rabbit	Promega	60 min; room temp.
Anti-Sheep IgG HRP-linked	31840	1:1000	Rabbit	ThermoScientific	60 min; room temp.

2.5.6 Enhanced chemiluminescence and quantification of Western blots

The ECL system (GE Healthcare) is a light emitting, non-radioactive technique used to detect an immune complex on a WB membrane through the binding of an HRP-conjugated antibody. Equal volumes of ECL Reagents A & B were mixed and membranes incubated in the resulting solution for up to 60 s. Excess ECL was removed and the membranes placed within a plastic wallet inside a developing cassette. Hyperfilm ECL high performance X-ray film (GE Healthcare) was exposed to the membranes for approximately 30 s and developed using a Fuji RGII automatic processor (Fuji). Exposed films were scanned into a computer using a flatbed scanner, and the intensity of protein bands quantified using a Bio-Rad GS800 densitometer and Quantity One software (Bio-Rad). PVDF membranes were subsequently stained with Coomassie blue (2.4 mmol/L Coomassie Brilliant Blue R, 10% (v/v) acetic acid, 50% (v/v) methanol) for 30-60 min to stain the membrane for total protein, to confirm equal protein loading across samples and that protein transfer from the gel to the membrane had been successful.

2.6 Statistical analysis

Data are expressed as means ± SEM from at least six individual experiments performed. Statistical comparisons and curve-fitting were carried out using GraphPad Prism software; the Student's *t*-test was used for comparing two groups (paired if both groups were from the same population) and one-way ANOVA followed by Bonferroni's post-test was used for comparing three or more groups. A value of $p<0.05$ was considered to be statistically significant.

3 EFFECTS OF PDE INHIBITION ON PLM PHOSPHORYLATION

3.1 Introduction

3.1.1 Background

As outlined in Chapter 1 (Section 1.2), PDEs restrict intracellular cAMP diffusion by degrading the second messenger to 5'-AMP, and there is increasing evidence to suggest that such a scheme plays a key role in the spatial and temporal control of cAMP signals within the cell. The investigation into the functional roles of PDEs has been made possible by the introduction of broad-spectrum inhibitors that non-selectively inhibit all the known PDE families, such as IBMX, and selective inhibitors for individual PDE families, including EHNA for PDE2, Cil for PDE3 and Rol for PDE4. Specifically, the use of family-selective inhibitors has allowed the functional roles of a particular PDE subtype to be assessed in combination with electrophysiological, biochemical and imaging techniques. This has greatly enhanced our understanding of how individual PDEs contribute to modulating cAMP signalling.

One drawback to the use of PDE inhibitors is the inherent difficulty in accurately assessing their pharmacological selectivity within an experimental system. Although they are designed to be selective for each PDE subtype, it is thought that if used at too high a concentration, they may act to inhibit other PDE subtypes, while at too low a concentration, they may not be optimally effective for the targeted PDE subtype. As such, using the inhibitors at an appropriate concentration constitutes an important experimental factor for consideration. Another disadvantage is the fact that all the commercial PDE inhibitors available currently do not have the capability to distinguish between individual isoforms within a given PDE family. Considering the emerging picture that individual PDE variants have differential, non-redundant functions, as delineated by methods such as PDE isoform ablation and RNA silencing, data generated from PDE inhibitors may not reflect the full complexity of the manner in which PDEs contribute to the intracellular regulation of cAMP signalling, and therefore more intricate delineation is often necessary.

Nonetheless, it must be emphasised that the use of PDE inhibitors has without any doubt provided some of the most important insights into the functional effects of several of the major cardiac PDE subtypes. In this study, we therefore decided to use the inhibitors as tools for identifying the PDE subtype(s) that have a functional contribution to cAMP signalling to PLM during β-AR stimulation. As the basal phosphorylation level of PLM is relatively high, this set of experiments involved using a submaximal [ISO] so that any effects induced by PDE inhibition in the presence of ISO could be observed.

The primary aim of the experiments presented in this chapter was to characterise the effects of PDE inhibition on the phosphorylation status of PLM . We hypothesised that inhibition of PDE2, PDE3 or PDE4 in the absence of ISO would induce no significant effect on the phosphorylation of PLM by either PKA or PKC. In contrast, in light of the considerable evidence suggesting a key role of PDE4 isoforms in regulating cAMP signalling to a number of cardiac substrates during β-AR stimulation, including PLB and SERCA, we hypothesised that selective inactivation of PDE4 in the presence of ISO would significantly increase the amplitude of cAMP signals to PLM and therefore the phosphorylation status of PLM specifically at Ser68, the PKA consensus site. As PDE4 selectively degrades cAMP, we hypothesised that PDE4 inhibition would induce significant intracellular cAMP accumulation in both the absence and presence of ISO. The specific hypotheses and objectives of the studies described in this chapter are outlined below.

3.1.2 Specific hypotheses

- That pharmacological inhibition of PDE2, PDE3 or PDE4 in the absence of ISO would induce no effect on PLM phosphorylation at Ser68, Ser63 or Thr69 as basal phosphorylation appears predominantly mediated via PKC phosphorylation.

- That pharmacological inhibition of PDE4 in the presence of a submaximal concentration of ISO would selectively induce a significantly increase in the phosphorylation level of PLM-Ser68.

- That pharmacological inhibition of PDE4 also influences PLB-Ser16 and cTnI-Ser23/24 in the absence and/or presence of ISO.

- That pharmacological inhibition of PDE4 in both the absence and presence of ISO results in significant intracellular cAMP accumulation.

3.1.3 Specific objectives

1. To generate a concentration response curve to a range of ISO concentrations in order to identify a suitable submaximal [ISO].

2. To investigate the effects of PDE2, PDE3 and PDE4 inhibition on the phosphorylation status of PLM-Ser68, PLM-Ser63 and PLM-Thr69 in the absence and presence of ISO.

3. To investigate the effects of PDE4 inhibition on the phosphorylation status of PLB-Ser16 and cTnI-Ser23/24 in the absence and presence of ISO.

4. To investigate the effects of PDE4 inhibition on total intracellular cAMP concentration in the absence and presence of ISO.

3.2 Methods

3.2.1 Isolation and culture of ARVMs

The experiments in this chapter were performed using ARVMs isolated from the hearts of adult (250 – 300 g body weight) male Wistar rats (B & K Universal), as described in Chapter 2 (Section 2.3.1). Cells were maintained in culture at 37°C/5% CO_2 for 2 hr prior to use in biochemical experiments, as described in Section 2.3.3.2.

3.2.2 Pharmacological treatment of ARVMs and sample preparation for SDS-PAGE

For generation of an individual ISO concentration-response curve for PLM phosphorylation using SDS-PAGE/WB, 10 concentrations of ISO were tested (1 nmol/L, 3 nmol/L, 10 nmol/L, 30 nmol/L, 100 nmol/L, 300 nmol/L, 1 μmol/L, 3 μmol/L, 10 μmol/L and 30 μmol/L). For assessment of PDE2-4 inhibition on the phosphorylation levels of PLM, PLB and cTnI, 100 μmol/L IBMX, 10 μmol/L EHNA, 10 μmol/L Cil and 10 μmol/L Rol alone or in combination with ISO, DMSO (vehicle control), 10 nmol/L ISO alone in addition to PMA (positive control) were added to individual wells. Treated myocytes were incubated for 10 min at 37°C/5% CO_2; the reactions were stopped by addition of 2x SDS sample buffer to the myocytes and the proteins subsequently scraped off the wells as described in Section 2.5.2. All wells contained 0.1% DMSO.

3.2.3 SDS-PAGE/Western blotting

SDS-PAGE/WB was used to probe for phosphorylation levels of PLM-Ser68, PLM-Ser63, PLM-Thr69, PLB-Ser16 and cTnI-Ser23/24, in addition to total actin levels, as described in Chapter 2 (Section 2.5). In addition, total levels of PLM, PLB and cTnI were probed for to ensure equal protein loading between samples, but only total actin levels were used for data normalisation. The incubation times for each of the primary and secondary antibodies used are listed in Tables 2.5 and 2.6 respectively.

3.2.4 Total intracellular cAMP enzymeimmunoassay

3.2.4.1 Principles

The cAMP Biotrak™ competitive enzymeimmunoassay (EIA) system (GE Healthcare; catalogue number: RPN2251) enables a simple, direct measurement of total $[cAMP]_i$ to be made using novel lysis reagents to facilitate simple and rapid extraction of cAMP from cell cultures. The requirement for traditional, time-consuming extraction procedures and the need for removal of extraction reagents prior to measurement are therefore obviated. The assay combines the use of a peroxidase-labelled cAMP conjugate, a specific antiserum which can be immobilised on to pre-coated microplates, and a one-pot stabilised substrate solution.

3.2.4.2 Pharmacological treatment of ARVMs and sample preparation for total $[cAMP]_i$ measurements

Sample preparation for the cAMP EIA was carried out according to the manufacturer's instructions. The 96-well microplate provided (coated with donkey anti-rabbit IgG) was set up to enable the running of all blanks, standards and samples in duplicates as required. ARVMs that have been cultured for 24 hr as described in Chapter 2 (Section 2.3.3.2) were treated with 10 μmol/L Rol in the absence and presence of 10 nmol/L ISO for 10 min. Reactions were quenched through the aspiration of the culture medium followed by the rapid lysis/agitation and scraping of the myocytes in 100 μl lysis buffer. Samples were subsequently stored on ice prior to evaluation using the cAMP EIA kit.

3.2.4.3 Assessment of total $[cAMP]_i$

The cAMP EIA was carried out according to the manufacturer's instructions. Briefly, all reagents were equilibrated to room temperature prior to use and the temperature was maintained at 4^{o}C by incubation on crushed ice/ in refrigerator throughout the duration of the assay. 100 μl of antiserum was subsequently added to each well of the microplate and the plate was incubated at 4^{o}C for 2 hr. This was followed by addition of 50 μl cAMP-peroxidase conjugate to the wells and 1 hr incubation at 4^{o}C. The solutions were then aspirated and the wells thoroughly washed (6 x with wash buffer) and dried prior to the addition of 150 μl enzyme substrate into all wells. The plate was left on a

microplate shaker for 30 min at room temperature before the reaction was halted by pipetting 100 µl of 1.0 M sulphuric acid into each well. The optical density was immediately determined in a microplate reader at 450 nm.

For data processing, the mean optical density for each set of replicate wells was first calculated, followed by the percent bound for each standard and sample using the following equation:

$\%B/B_0$ = [(standard or sample OD-NSB OD) x 100]/(zero standard OD-NSB OD)

An 8-point standard curve was subsequently generated by plotting the% B/B_0 as a function of the log[cAMP], which allowed the fmol/well values for each sample to be determined.

3.2.5 Post-statistical analysis issues

For a number of data sets, large increases in phosphorylation level were observed in response to PDE inhibitors that were nevertheless found to be not statistically significant. Therefore, it was decided that changes that had a statistical significance of $p>0.05$ but < 0.1 or with a magnitude of 3-fold or greater would be referred to as having 'a trend for a change' in the Results and Discussion sections of this chapter. In addition, for several of these data sets, a power calculation was carried out to determine how many samples would theoretically be required for a change of the observed magnitude to be statistically significant.

3.3 Results

3.3.1 Identification of a suitable submaximal [ISO]

To identify a suitable submaximal [ISO] for investigating the functional effects of PDE inhibition on PLM phosphorylation, an individual concentration response curve for PLM-Ser68 to a range of [ISO] was constructed. Our decision to investigate the effects of ISO on PLM-Ser68 was based on the fact that it represents to date the only known PKA phosphorylation site on PLM,[146] and our hypothesis was based on the notion that PDE inhibition is likely to mediate its effects on PLM phosphorylation through cAMP and PKA signalling. The curve demonstrated that the relationship between [ISO] and the phosphorylation status at PLM-Ser68 in ARVMs is sigmoidal, with the phosphorylation level reaching a peak of approximately 2.5-fold increase in response to 100 nmol/L ISO, and subsequently reaching a plateau in response to the higher ISO concentrations tested [Figure 3.1]. This is wholly consistent with published studies establishing that agonist-induced phosphorylation of PLM in rat ventricular muscle generally elicits only a two- to three-fold increase in phosphorylation at Ser68, corresponding to the relatively high basal phosphorylation of PLM in rat ventricular myocytes (~40%) in comparison with other classical cardiac proteins such as PLB. It has been shown that this basal phosphorylation is mostly contributed to by PKC activity, consisting of a rapid turnover of phosphorylation and dephosphorylation,[171] which could pose a significant complication into the investigations into PLM phosphorylation.

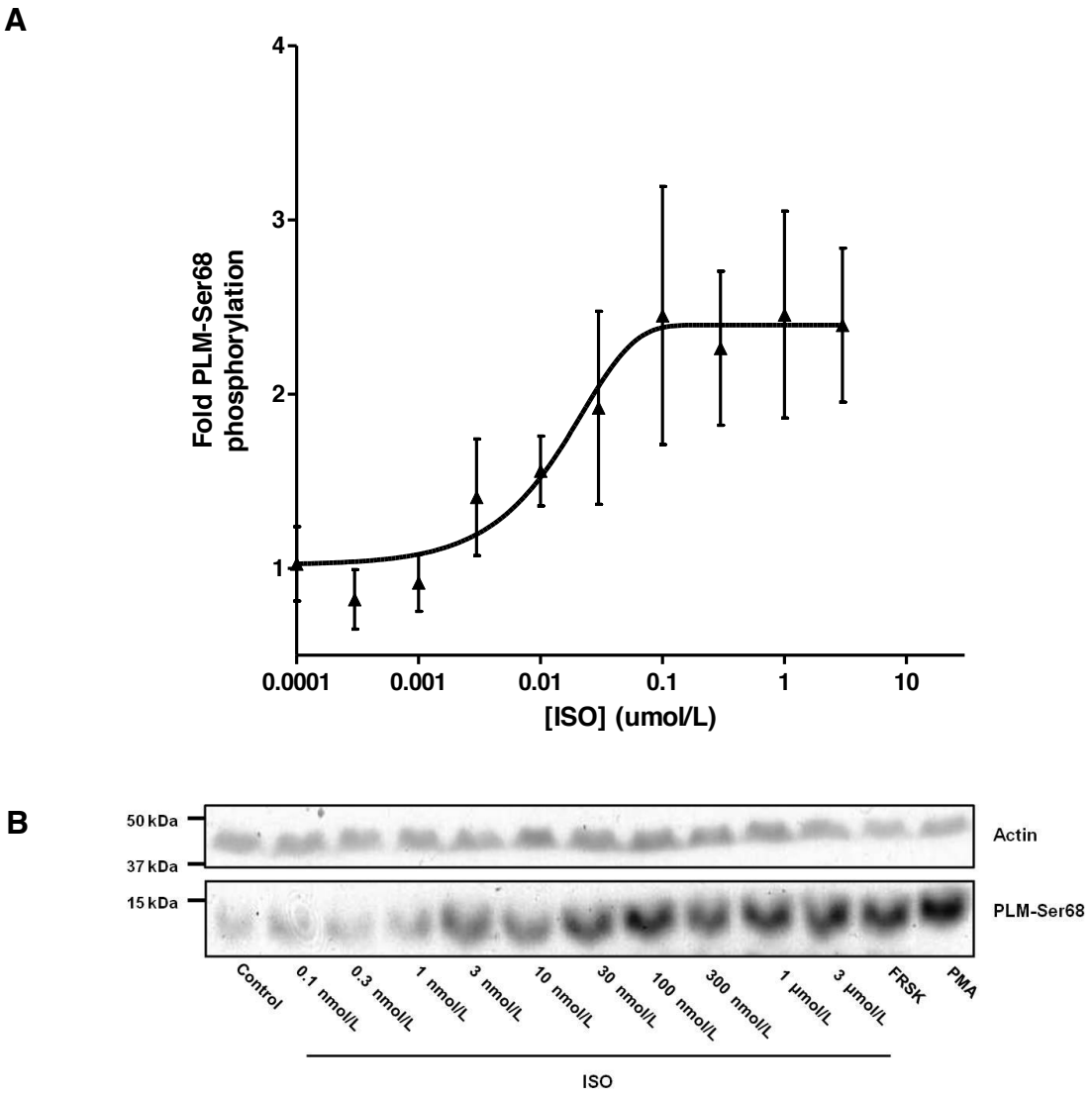

Figure 3.1 PLM-Ser68 phosphorylation levels in response to treatment with a range of [ISO].

(A) ISO concentration-response curve for PLM-Ser68 phosphorylation levels. ARVMs were treated with a range of [ISO] (0.1 nmol/L, 0.3 nmol/L, 1 nmol/L, 3 nmol/L, 1 nmol/L, 30 nmol/L, 100 nmol/L, 300 nmol/L, 1 µmol/L & 3 µmol/L) for 10 min and PLM-Ser68 phosphorylation levels were analysed by SDS-PAGE (15% gel) and WB analysis using an anti-phospho PLM-Ser68 antibody. Addition of 0.1% DMSO only was used as a negative control while positive controls comprised of ARVMs challenged with 50 µmol/L FRSK or 300 nmol PMA (not shown). ARVMs in all treatment groups were exposed to 0.1% DMSO. Samples were subjected to complementary WB analysis using anti-total actin and anti-total PLM antibodies, to demonstrate equal protein loading between samples. Membranes were subsequently stained with Coomassie Blue to demonstrate equal protein loading and transfer. Densitometry values for PLM-Ser68 were normalised to those for total actin and subsequently normalised to the control to generate fold values. Data are expressed as means ± SEM. (n=6) Mean data were fitted with a sigmoidal concentration response curve (variable slope). **(B)** Representative blot of PLM-Ser68 phosphorylation levels in response to pharmacological treatment.

A suitable submaximal [ISO] was defined as a concentration of the agonist that resulted in an increase in PLM-Ser68 phosphorylation quantitatively large enough to be detected by SDS-PAGE/WB, but small enough as to provide a sufficiently large window for any subsequent increases induced by PDE inhibition to be detected. After careful consideration, 10 nmol/L ISO was selected as the ideal submaximal concentration. At this concentration, the corresponding increase in PLM-Ser68 phosphorylation was found to be situated at the bottom of the steep part of the curve [Figure 3.1], indicating that while the response was relatively small, it was quantifiable, with a 0.5-fold increase in PLM-Ser68 phosphorylation compared with the control that was found to be statistically significant [Figure 3.2; Panel A]. This helped to confirm 10 nmol/L ISO as a submaximal concentration with a small but 'real' effect on PLM-Ser68 phosphorylation rather than a subthreshold concentration.

As discussed above, 10 nmol/L ISO was subsequently used in all biochemical PDE inhibition experiments; in contrast to our previous observations, we found that in these experiments, 10 nmol/L ISO exerted no apparent effect on the phosphorylation level of PLM-Ser68 [Figure 3.2; Panel B]. This discrepancy may be attributed to the presence of a mixture of phosphorylated and unphosphorylated PLM in the rat heart under basal conditions, with the phosphorylated portion being critically influenced by the adrenergic state of the heart when myocytes are prepared predominantly through PKC activation (See Chapter 1, Section 1.3.2 for reasoning). Indeed, 'resting' PLM phosphorylation is likely to vary between laboratories, and as may be the case here, even from day to day within the same laboratory. In some ways, this finding was unexpected because previous unpublished observations from our laboratory suggested that in comparison to freshly-isolated myocytes, basal PLM-Ser68 phosphorylation is reduced to normal levels (~40%) when cultured myocytes have been allowed to recover from the stresses of isolation via incubation at 37^{o}C/5% CO_2 for approximately two hours (see Chapter 2; Section 2.3.3.2). One would therefore have expected these cells to be accordingly more responsive in terms of fold changes in phosphorylation following agonist application. Our finding highlights how using a submaximal concentration of ISO carries with it an inherent danger of its relatively small effect on PLM-Ser68 phosphorylation (previously determined to be an approximately 50% increase) being undetectable on top of the

primarily PKC-driven phosphorylation 'window', as is likely the case here [Figure 3.2; Panel B].

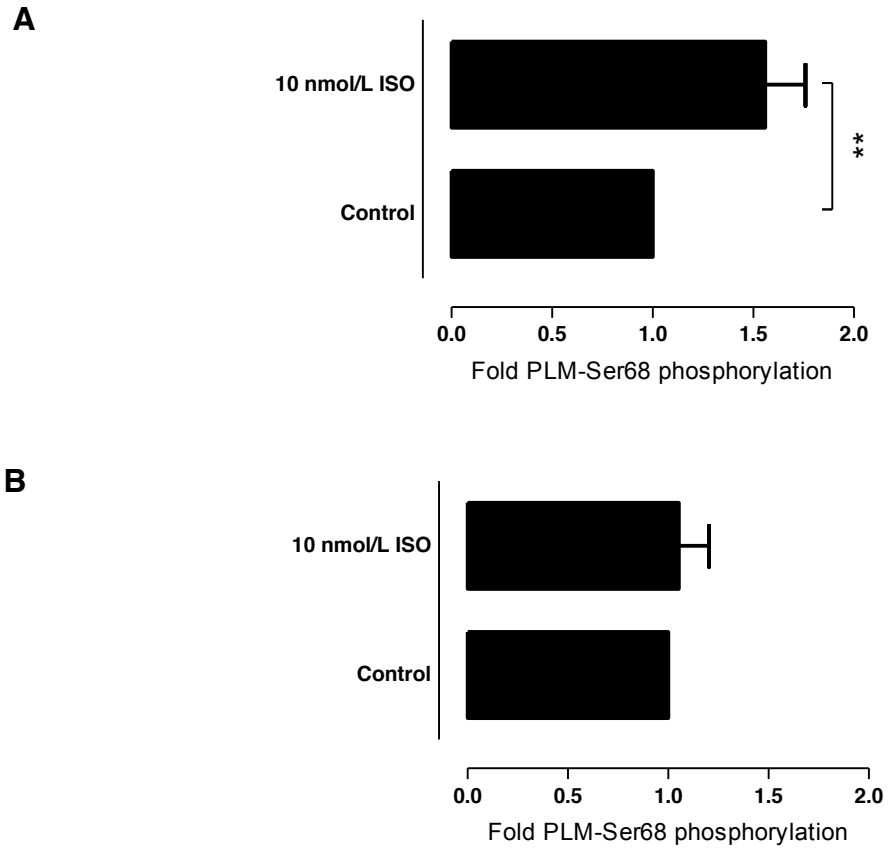

Figure 3.2 Changes in PLM-Ser68 phosphorylation level in response to treatment with 10 nmol/L ISO

ARVMs were treated with 10 nmol/L ISO for 10 min in **(A)** individual concentration-response curve or **(B)** PDE inhibition experiments and PLM-Ser68 phosphorylation levels were analysed by SDS-PAGE (15% gel) and WB analysis using an anti-phospho PLM-Ser68 antibody. Addition of 0.1% DMSO only was used as a negative control while positive controls comprised of ARVMs challenged with 50 μmol/L FRSK or 300 nmol PMA. ARVMs in both treatment groups were exposed to 0.1% DMSO. Samples were subjected to complementary WB analysis using anti-total actin and anti-total PLM antibodies, to demonstrate equal protein loading between samples. Membranes were subsequently stained with Coomassie Blue to demonstrate equal protein loading and transfer. Densitometry values for PLM-Ser68 were normalised to those for total actin and subsequently normalised to the control to generate fold values. Statistical comparisons were made using paired Student's t-test and data are expressed as means ± SEM. (n=6) **$p \leq 0.01$

3.3.2 Effects of PDE2-4 inhibition on PLM-Ser68 phosphorylation in the absence and presence of a submaximal [ISO]

In order to assess the functional roles of PDE2-4 in regulating PKA phosphorylation of PLM, ARVMs were challenged with the broad-spectrum PDE inhibitor IBMX and selective inhibitors for the individual PDE subtypes. Upon treatment with the broad-spectrum PDE inhibitor IBMX, we observed an approximately 3-fold increase in PLM-Ser68 phosphorylation compared with control myocytes [Figure 3.3; Panel A]. Similarly, exposure to IBMX in the presence of 10 nmol/L ISO resulted in an approximately 3-fold increase in phosphorylation level at this site compared with myocytes treated with ISO alone [Figure 3.3; Panel A]. However, these changes were found to be not statistically significant.

On the other hand, treatment with the PDE2 inhibitor EHNA or PDE3 inhibitor Cil was found to exert no effect on PLM-Ser68 phosphorylation in both the absence and presence of 10 nmol/L ISO [Figure 3.3; Panels B & C]. However, selective inhibition of PDE4 with Rol, whilst exerting no apparent effect on PLM-Ser68 phosphorylation under basal conditions, was found to induce an approximately 5-fold increase in PLM-Ser68 phosphorylation in the presence of 10 nmol/L ISO [Figure 3.3; Panel D]. This difference did not reach statistical significance, but did show a trend for a change ($p = 0.0899$).

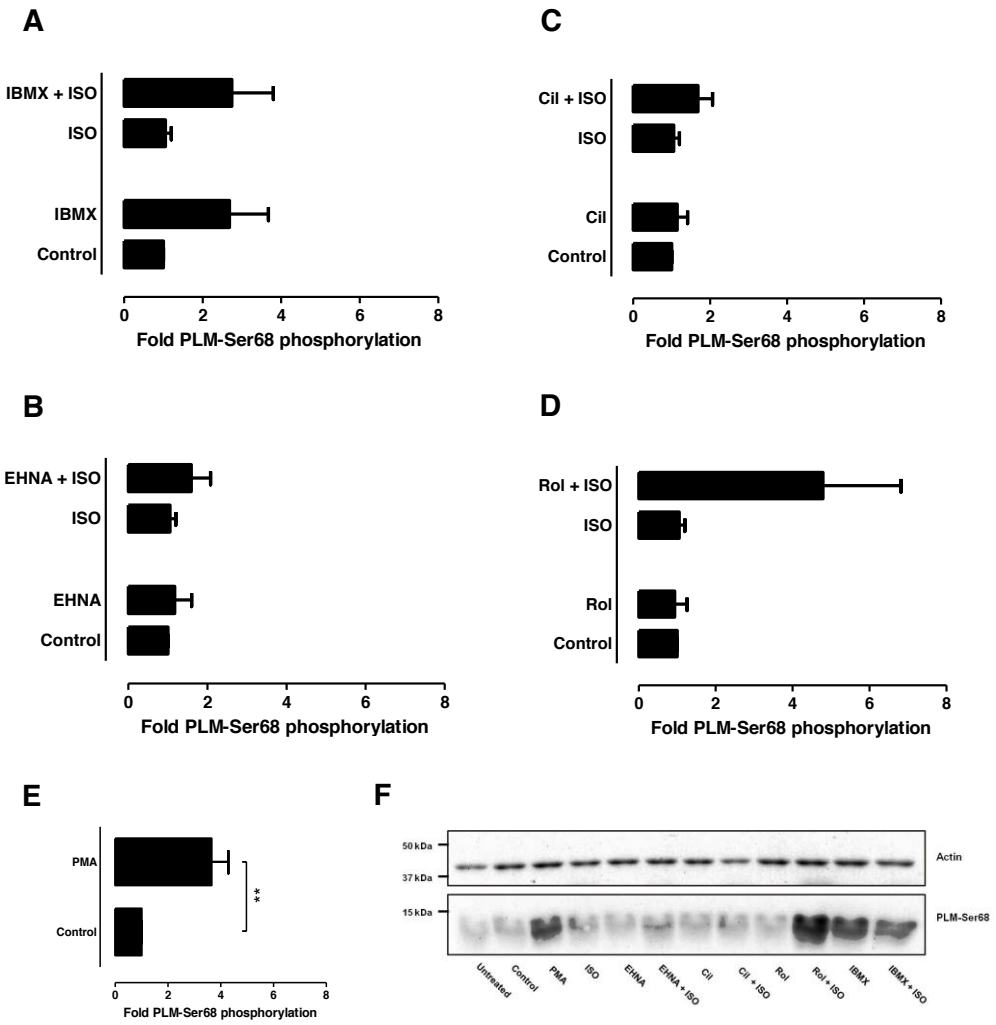

Figure 3.3 PLM-Ser68 phosphorylation levels in response to PDE inhibition in the absence and presence of a submaximal [ISO].

ARVMs were treated with **(A)** 100 µmol/L IBMX; **(B)** 10 µmol/L EHNA; **(C)** 10 µmol/L cilostamide or **(D)** 10 µmol/L rolipram alone or in combination with 10 nmol/L ISO. Negative and positive controls comprised of ARVMS challenged with 0.1% DMSO and **(E)** 300 nmol/L PMA respectively. ARVMs in all treatment groups were exposed to 0.1% DMSO. SDS-PAGE (15% gel) and WB analysis was used to analyse PLM-Ser68 phosphorylation levels using an anti-phospho PLM-Ser68 antibody. All samples were subjected to complementary WB analysis using anti-total actin and anti-total PLM antibodies, to demonstrate equal protein loading between samples. Membranes were subsequently stained with Coomassie Blue to demonstrate equal protein loading and transfer. Densitometry values for PLM-Ser68 were normalised to those for total actin and subsequently normalised to the DMSO control to generate fold values. Statistical comparisons were made using paired Student's t-test and data are expressed as means ± SEM (n=8).
p ≤ 0.01 **(F) Representative blot of PLM-Ser68 phosphorylation levels in response to pharmacological treatment.

3.3.3 Effects of PDE2-4 inhibition on PLM-Ser68 phosphorylation under Ca-free conditions

The discrepancy observed between the effects of 10 nmol/L ISO on PLM-Ser68 phosphorylation in the two sets of experiments mentioned above indicates that the mean basal phosphorylation of PLM in the myocytes used in the PDE inhibition experiments could have been higher than normal. Since basal phosphorylation is extremely sensitive to the resting cellular Ca load, this carried the possibility that the discrepancy could be attributed to the Ca content within the cells. Basal PLM phosphorylation can be substantially reduced either by lower extracellular Ca or by treating cells with bisindolylmaleimide (BIS) implicating the Ca-activated PKCs in this basal tone.

This prompted us to assess the effects of PDE inhibition on PLM-Ser68 phosphorylation in myocytes that have been cultured using a Ca-free protocol, in which myocytes were cultured in Ca-free Tyrode's Solution instead of standard M199 media. Unexpectedly, usage of this protocol did not result in an augmented response upon treatment with the individual PDE inhibitors. Rather, the reduction in extracellular Ca seemed to have negated the effects observed in myocytes that had undergone the standard culturing protocol [Figure 3.4: Panels A-D]. Specifically, none of the inhibitors were found to induce differences in PLM-Ser68 phosphorylation under basal conditions; in the presence of 10 nmol/L ISO, inhibition of PDE2-4 had no effect on the phosphorylation level at this site. Although inhibition of total PDEs with IBMX was found to exert a 2-fold increase in phosphorylation, (in contrast to the 3-fold increase in the previous experiment), this was found to be not statistically significant [Figure 3.4; Panel A].

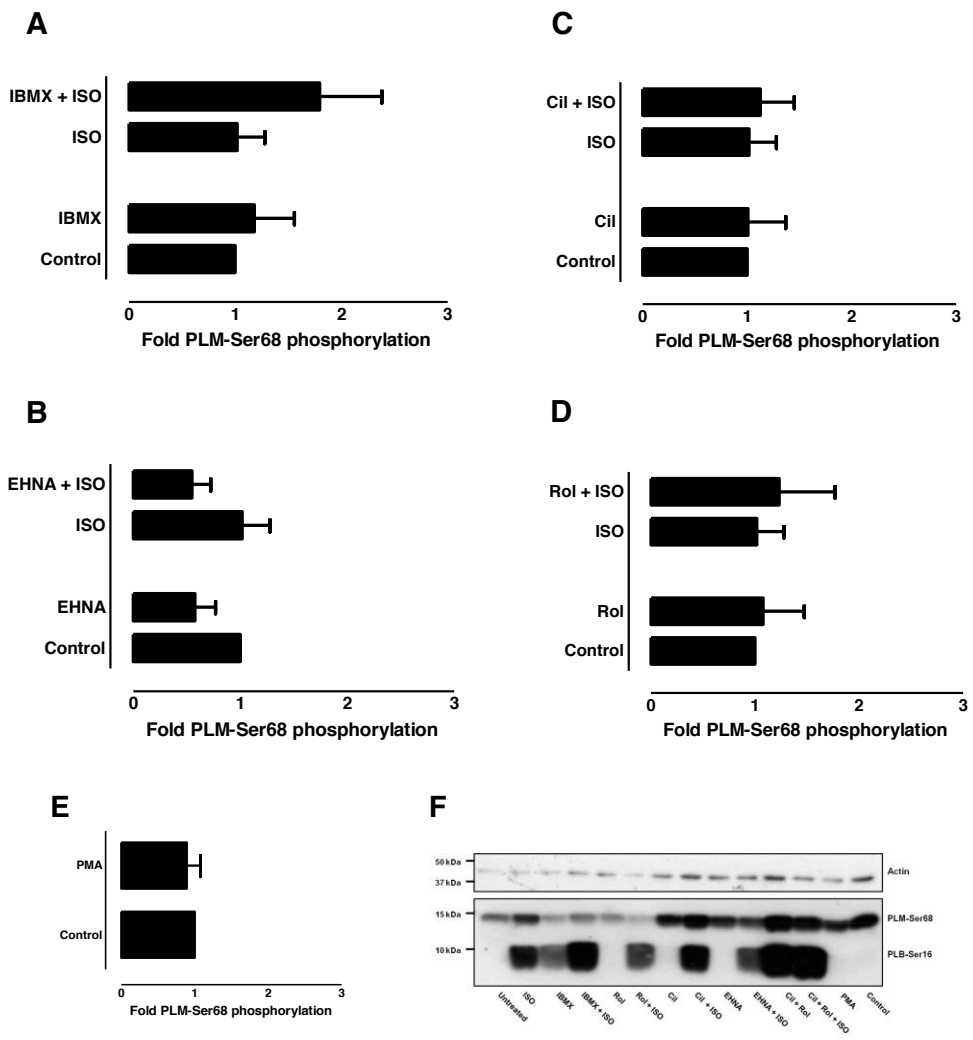

Figure 3.4 PLM-Ser68 phosphorylation levels in response to PDE inhibition in the absence and presence of a submaximal [ISO] under Ca-free conditions.

ARVMs cultured in Ca-free Tyrode's Solution were treated with **(A)** 100 µmol/L IBMX; **(B)** 10 µmol/L EHNA; **(C)** 10 µmol/L cilostamide or **(D)** 10 µmol/L rolipram alone or in combination with 10 nmol/L ISO. Negative and positive controls comprised of ARVMS challenged with 0.1% DMSO and 300 nmol/L **(E)** PMA respectively. ARVMs in all treatment groups were exposed to 0.1% DMSO. SDS-PAGE (15% gel) and WB analysis was used to analyse PLM-Ser68 and PLB-Ser16 phosphorylation levels using an anti-phospho PLM-Ser68 antibody (samples were pre-boiled at 95^{o}C for 10 min to remove pentameric PLB). All samples were subjected to complementary WB analysis using anti-total actin and anti-total PLM antibodies, to demonstrate equal protein loading between samples. Membranes were subsequently stained with Coomassie Blue to demonstrate equal protein loading and transfer. Densitometry values for PLM-Ser68 were normalised to those for total actin and subsequently normalised to the DMSO control to generate fold values. Statistical comparisons were made using paired Student's t-test and data are expressed as means ± SEM (n=6).
(F) Representative blot of PLM-Ser68 phosphorylation levels in response to pharmacological treatment.

3.3.4 Effects of PDE2-4 inhibition on PLM-Ser63 phosphorylation in the absence and presence of a submaximal [ISO]

Challenge with IBMX under either basal conditions or β-AR stimulation had no effect on PLM-Ser63 phosphorylation, even though an approximately 2-fold increase in phosphorylation was observed in the presence of 10 nmol/L ISO [Figure 3.5; Panel A]. Treatment with EHNA, Cil or Rol was found to exert no effect on phosphorylation at this site in both the absence and presence of ISO [Figure 3.5; Panels B-D].

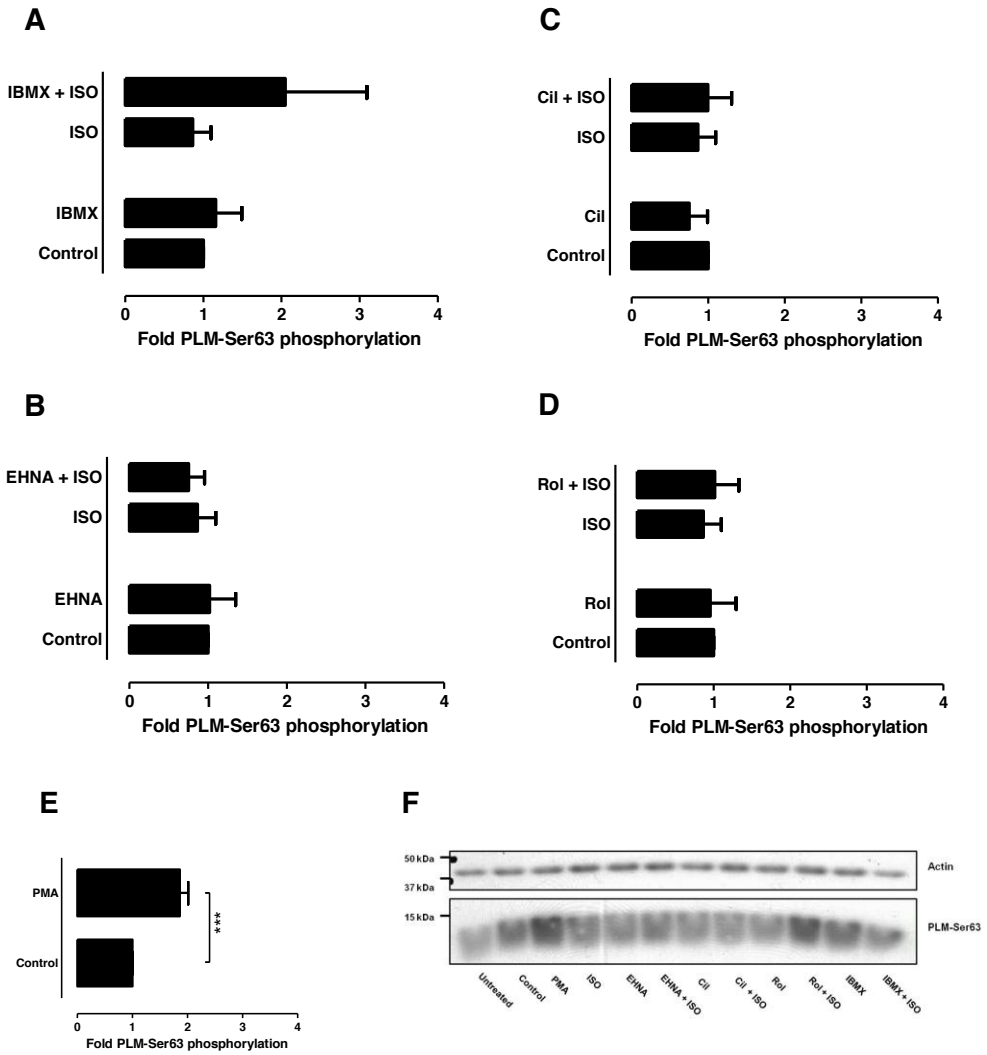

Figure 3.5 PLM-Ser63 phosphorylation levels in response to PDE inhibition in the absence and presence a submaximal [ISO].

ARVMs were treated with **(A)** 100 µmol/L IBMX; **(B)** 10 µmol/L EHNA; **(C)** 10 µmol/L cilostamide or **(D)** 10 µmol/L rolipram alone or in combination with 10 nmol/L ISO. Negative and positive controls comprised of ARVMS challenged with 0.1% DMSO and **(E)** 300 nmol/L PMA respectively. ARVMs in all treatment groups were exposed to 0.1% DMSO. SDS-PAGE (15% gel) and WB analysis was used to analyse PLM-Ser63 phosphorylation levels using an anti-phospho PLM-Ser63 antibody. All samples were subjected to complementary WB analysis using anti-total actin and anti-total PLM antibodies, to demonstrate equal protein loading between samples. Membranes were subsequently stained with Coomassie Blue to demonstrate equal protein loading and transfer. Densitometry values for PLM-Ser63 were normalised to those for total actin and subsequently normalised to the DMSO control to generate fold values. Statistical comparisons were made using paired Student's t-test and data are expressed as means ± SEM (n=8). ***$p \leq 0.001$ **(F)** Representative blot of PLM-Ser63 phosphorylation levels in response to pharmacological treatment.

3.3.5 Effects of PDE2-4 inhibition on PLM-Thr69 phosphorylation in the absence and presence of a submaximal [ISO]

None of the PDE inhibitors tested exerted any statistically significant changes in PLM-Thr69 phosphorylation in both the presence and absence of 10 nmol/L ISO [Figure 3.6; Panels A-D]. Interestingly, while the addition of IBMX induced an approximately 1.5-fold increase in PLM-Thr69 phosphorylation under basal conditions, the phosphorylation level at this site was found to be reduced in the presence of 10 nmol/L ISO [Figure 3.6; Panel A].

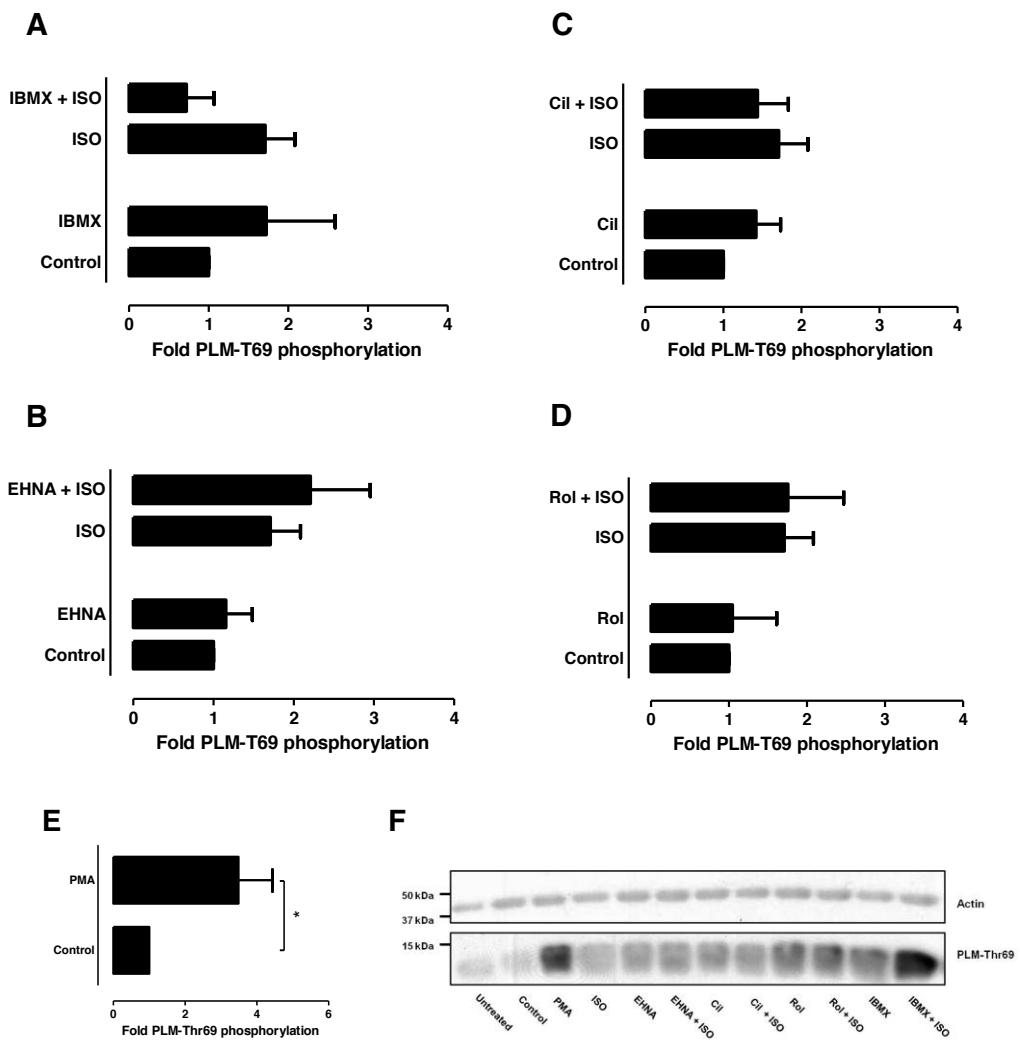

Figure 3.6 PLM-Thr69 phosphorylation levels in response to PDE inhibition in the absence and presence of a submaximal [ISO].

ARVMs were treated with **(A)** 100 µmol/L IBMX; **(B)** 10 µmol/L EHNA; **(C)** 10 µmol/L cilostamide or **(D)** 10 µmol/L rolipram alone or in combination with 10 nmol/L ISO. Negative and positive controls comprised of ARVMS challenged with 0.1% DMSO and **(E)** 300 nmol/L PMA respectively. ARVMs in all treatment groups were exposed to 0.1% DMSO. SDS-PAGE (15% gel) and WB analysis was used to analyse PLM-Thr68 phosphorylation levels using an anti-phospho PLM-Thr69 antibody. All samples were subjected to complementary WB analysis using anti-total actin and anti-total PLM antibodies, to demonstrate equal protein loading between samples. Membranes were subsequently stained with Coomassie Blue to demonstrate equal protein loading and transfer. Densitometry values for PLM-Thr69 were normalised to those for total actin and subsequently normalised to the DMSO control to generate fold values. Statistical comparisons were made using paired Student's t-test and data are expressed as means ± SEM (n=8). *$p \leq 0.05$ **(F)** Representative blot of PLM-Thr69 phosphorylation levels in response to pharmacological treatment.

3.3.6 Effects of PDE2-4 inhibition on PLB phosphorylation

Since PDE4 activity influences PKA phosphorylation of a number of ECC components in the heart, including PLB and cTnI, we decided to investigate the effect of PDE4 inhibition on the phosphorylation status of PLB-Ser16, as well as that of cTnI-Ser22/23. As mentioned in Chapter 1 (Section 1.3.2), Ser16 represents the primary PKA phosphorylation site on PLB and has been reported to be sufficient in mediating the latter's maximal cardiac responses to β-agonists.[165] Similarly, cTnI-Ser22/23 represents another established PKA phosphorylation target in the rodent heart, and phosphorylation of these serine residues leads to a reduction of myofilament Ca sensitivity and shifts the force-pCa relationship rightwards.[256,257]

PLB-Ser16 phosphorylation was augmented by a statistically significant margin (approximately 40-fold compared with control mycoytes) in response to treatment with IBMX [Figure 3.7; Panel A], while also exerting a 2-fold increase in the presence of 10 nmol/L ISO [Figure 3.7; Panel A]. Treatment with EHNA or Rol also significantly increased PLB-Ser16 phosphorylation (approximately 2-3-fold compared with control myocytes) [Figure 3.7; Panels B & D], but quantitatively comparable responses were observed when the inhibitors were added in the presence of 10 nmol/L ISO [Figure 3.7; Panels B & D]. The effect of Cil on PLB-Ser16 phosphorylation was augmented in the presence of ISO but the inhibitor did not significantly increase phosphorylation at this site in both the absence and presence of ISO [Figure 3.7; Panel C].

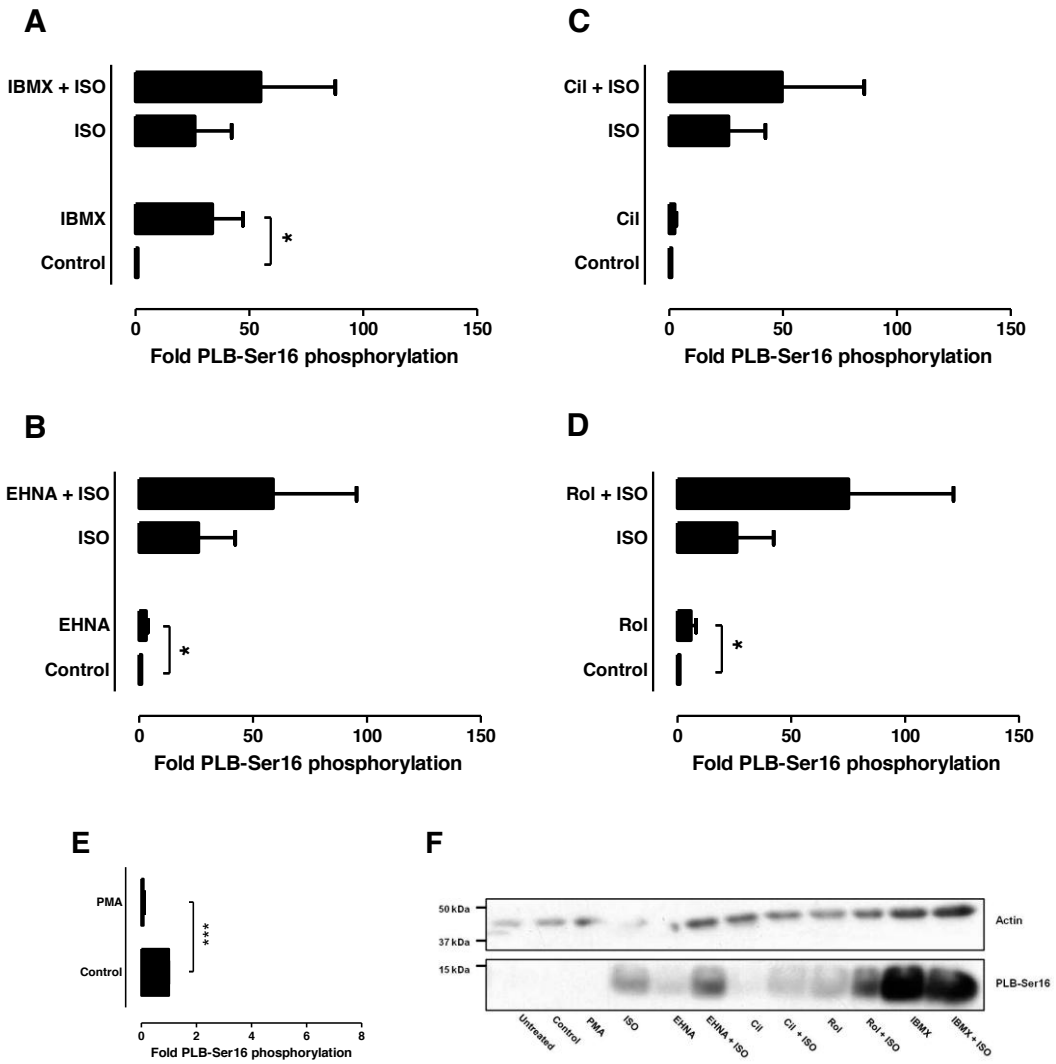

Figure 3.7 PLB-Ser16 phosphorylation levels in response to PDE inhibition in the absence and presence of a submaximal [ISO].

ARVMs were treated with **(A)** 100 µmol/L IBMX; **(B)** 10 µmol/L EHNA; **(C)** 10 µmol/L cilostamide or **(D)** 10 µmol/L rolipram alone or in combination with 10 nmol/L ISO. Negative and positive controls comprised of ARVMS challenged with 0.1% DMSO and **(E)** 300 nmol/L PMA respectively. ARVMs in all treatment groups were exposed to 0.1% DMSO. SDS-PAGE (15% gel) and WB analysis was used to analyse PLB-Ser16 phosphorylation levels using an anti-phospho PLB-Ser16 antibody. All samples were subjected to complementary WB analysis using anti-total actin and anti-total PLB antibodies, to demonstrate equal protein loading between samples. Membranes were subsequently stained with Coomassie Blue to demonstrate equal protein loading and transfer. Densitometry values for PLB-Ser16 were normalised to those for total actin and subsequently normalised to the DMSO control to generate fold values. Statistical comparisons were made using paired Student's t-test and data are expressed as means ± SEM (n=7).
*p ≤ 0.05; ***p ≤ 0.001 **(F)** Representative blot of PLB-Ser16 phosphorylation levels in response to pharmacological treatment.

3.3.7 Effects of PDE2-4 inhibition on PLB-Ser16 phosphorylation under Ca-free conditions

In contrast to PLM-Ser68 phosphorylation, it was found that the effects of IBMX treatment on PLB-Ser16 phosphorylation under Ca-free conditions was augmented, with profound increases at this site in both the absence and presence of 10 nmol/L ISO (approximately 500- and 5-fold increases) [Figure 3.8; Panel A]. Similarly, addition of Rol significantly increased basal PLB-Ser16 phosphorylation (approximately 100-fold increase) but in this case, also led to a statistically significant effect under β-AR stimulations (approximately 5-fold increase) [Figure 3.8; Panel D]. On the other hand, challenge with EHNA did not result in a statistically significant change in basal PLB-Ser16 phosphorylation, in contrast to our observations under Ca-containing conditions [Figure 3.8; Panel B]. Indeed, both EHNA and Cil did not significantly alter PLB-Ser16 in both the absence and presence of ISO [Figure 3.8; Panels B & C].

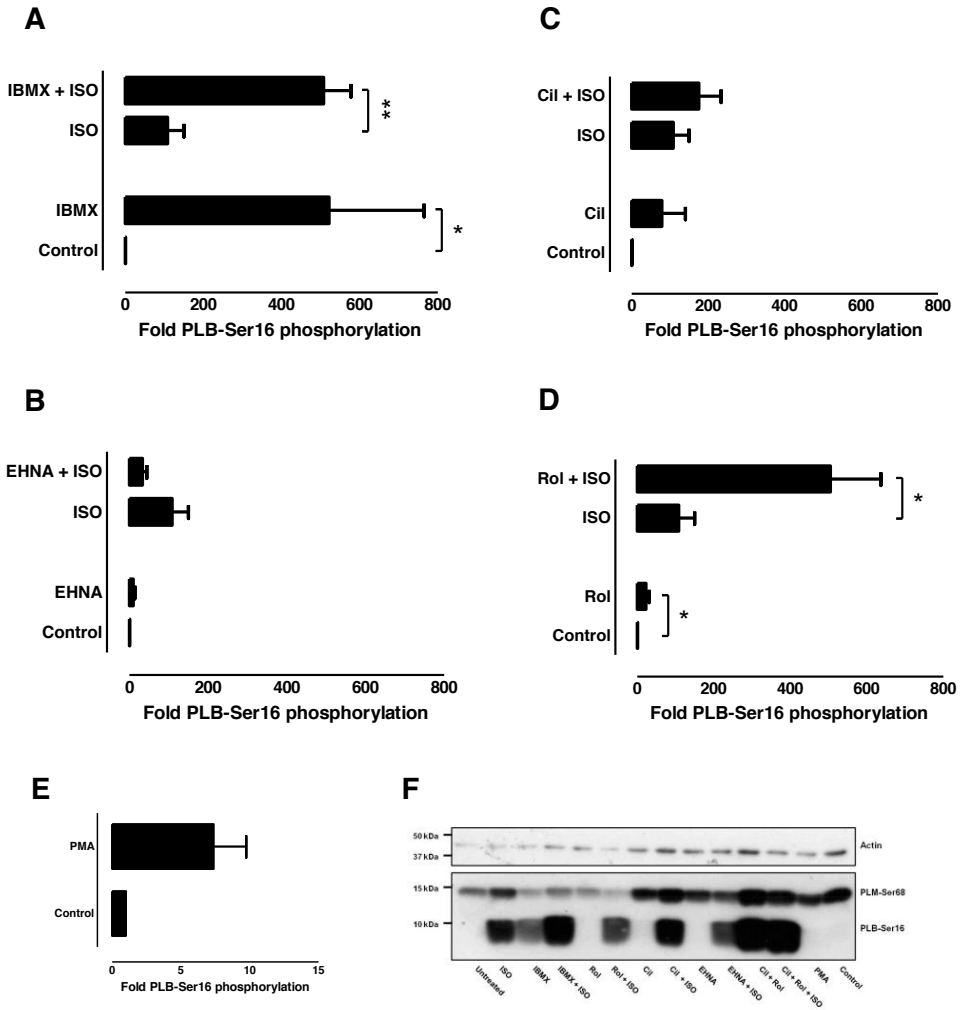

Figure 3.8 PLB-Ser16 phosphorylation levels in response to PDE inhibition in the absence and presence of a submaximal [ISO] under Ca-free conditions.

ARVMs cultured in Ca-free Tyrode's Solution were treated with **(A)** 100 µmol/L IBMX; **(B)** 10 µmol/L EHNA; **(C)** 10 µmol/L cilostamide or **(D)** 10 µmol/L rolipram alone or in combination with 10 nmol/L ISO. Negative and positive controls comprised of ARVMS challenged with 0.1% DMSO and 300 nmol/L PMA **(E)** respectively. ARVMs in all treatment groups were exposed to 0.1% DMSO. SDS-PAGE (15% gel) and WB analysis was used to analyse PLM-Ser68 and PLB-Ser16 phosphorylation levels using an anti-phospho PLM-Ser68 antibody (samples were pre-boiled at 95^{o}C for 10 min to remove pentameric PLB). All samples were subjected to complementary WB analysis using an anti-total actin and anti-total PLB antibodies, to demonstrate equal protein loading between samples. Membranes were subsequently stained with Coomassie Blue to demonstrate equal protein loading and transfer. Densitometry values for PLM-Ser68 were normalised to those for total actin and subsequently normalised to the DMSO control to generate fold values. Statistical comparisons were made using paired Student's t-test and data are expressed as means ± SEM (n=6).
*p ≤ 0.05; **p ≤ 0.01 **(F)** Representative blot of PLM-Ser68 phosphorylation levels in response to pharmacological treatment.

3.3.8 Effects of PDE2-4 inhibition on cTnI-Ser22/23 phosphorylation

cTnI-Ser22/23 phosphorylation was found to be increased in response to addition of IBMX in the absence of ISO (approximately 75- fold increase), although this was not observed in the presence of ISO[Figure 3.9; Panel A]. Challenge with EHNA did not exert any effect on basal cTnI-Ser 22/23 phosphorylation, although the effect of ISO was found to be decreased in the presence of EHNA. This difference was found to be not statistically significant, although there was a trend for a change ($p = 0.0873$) [Figure 3.9; Panel B].

Treatment with Cil was found to exert an increase in cTnI-Ser22/23 phosphorylation level under both basal conditions and β-AR stimulation (approximately 30- and 270-fold increases respectively) [Figure 3.9; Panel C], while addition of Rol resulted in similarly increased phosphorylation levels at this site under both basal and ISO-stimulated conditions (approximately 40- and 60-fold increases respectively)

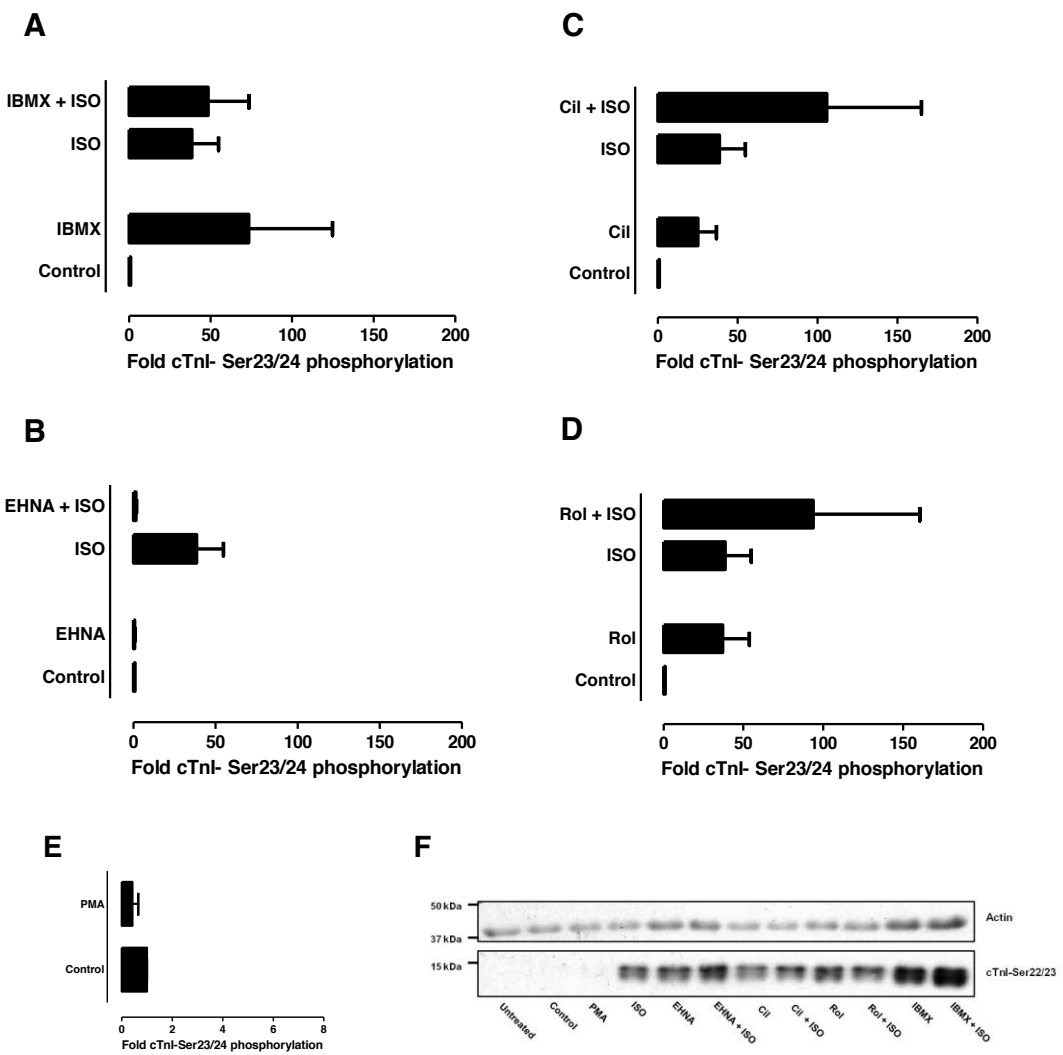

Figure 3.9 cTnI-Ser22/23 phosphorylation levels in response to PDE inhibition in the absence and presence of a submaximal [ISO].

ARVMs were treated with **(A)** 100 µmol/L IBMX; **(B)** 10 µmol/L EHNA; **(C)** 10 µmol/L cilostamide or **(D)** 10 µmol/L rolipram alone or in combination with 10 nmol/L ISO. Negative and positive controls comprised of ARVMS challenged with 0.1% DMSO and 300 nmol/L PMA **(E)** respectively. ARVMs in all treatment groups were exposed to 0.1% DMSO. SDS-PAGE (15% gel) and WB analysis was used to analyse cTnI-Ser22/23 phosphorylation levels using an anti-phospho cTnI-Ser22/23 antibody. All samples were subjected to complementary WB analysis using anti-total actin and anti-total cTnI antibodies, to demonstrate equal protein loading between samples. Membranes were subsequently stained with Coomassie Blue to demonstrate equal protein loading and transfer. Densitometry values for cTnI-Ser22/23 were normalised to those for total actin and subsequently normalised to the DMSO control to generate fold values. Statistical comparisons were made using paired Student's t-test and data are expressed as means ± SEM (n=5).
(F) Representative blot of cTnI-Ser22/23 phosphorylation levels in response to pharmacological treatment.

3.3.9 Generation of standard curve for total $[cAMP]_i$ measurements

To obtain further insights into the mechanism of action underlying PDE4 inhibition, we examined its effect on total $[cAMP]_i$ in ARVMs. The standard curve depicted in Figure 3.10 is illustrative of the cAMP EIA measurements carried out for this chapter. As a result of the complete lysis of the samples prior to measurement with the EIA system, the increase in total $[cAMP]_i$ within the cell could be detected.

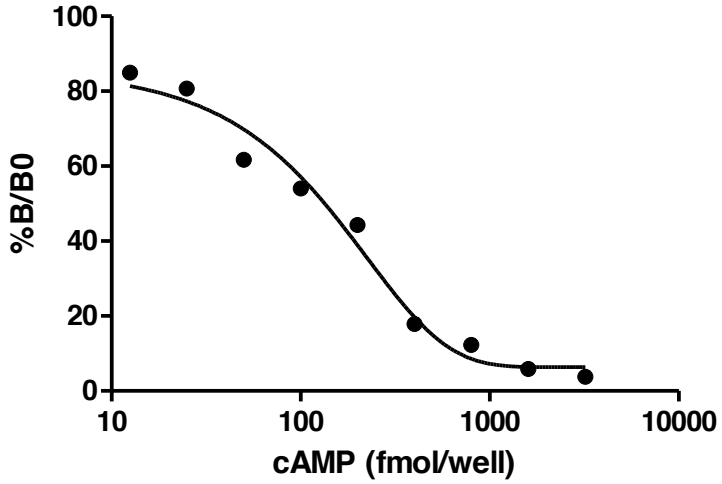

Figure 3.10 Representative standard curve generated for total intracellular [cAMP] measurements.

Identification of total intracellular cAMP levels regulated by PDE4 activity was measured via inhibition using rolipram. Known standards (12.5, 25, 50, 100, 200, 400, 800, 1600 and 3200 fmol) were added to individual wells, and a standard curve was generated by plotting the percent bound for each standard as a function of the log cAMP concentration per well (See Section 3.2.4.3 for equation). Similarly, the percent bound for each sample was calculated and the fmol/well value could subsequently be determined directly from the graph.

3.3.10 Effects of PDE4 inhibition on total [cAMP]i

As depicted in Figure 3.11, the total $[cAMP]_i$ in ARVMs was significantly augmented upon treatment with Rol in both the absence and presence of ISO when compared with the DMSO control and 10 nmol/L ISO respectively.

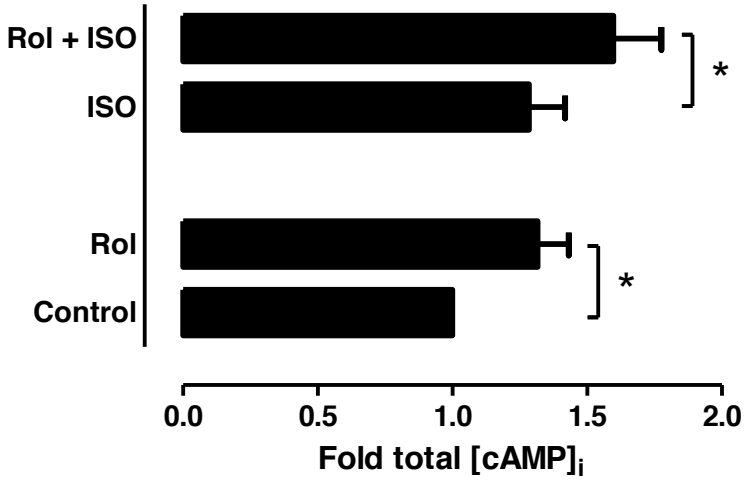

Figure 3.11 Total intracellular cAMP concentration in response to PDE4 inhibition in the absence and presence of a submaximal [ISO].

ARVMs were treated with 0.1% DMSO, 10 nmol/L ISO, 10 µmol/L Rol and 10 µmol/L Rol in combination with 10 nmol/L ISO for 10 min and total [cAMP]i was analysed using the cAMP BiotrakTM Enzymeimmunoassay System according to the manufacturer's instructions. All treated myocytes were exposed to 0.1% DMSO. Measurements were taken in duplicate. Statistical comparisons were made using paired Student's t-test and data are expressed as means ± SEM (n=6). *$p \leq 0.05$ The fmol/well value of samples was determined from the standard curve shown in Figure 3.10.

3.4 Discussion

There is now considerable evidence indicating a key role of PDEs in tailoring specific cAMP signals to control PKA phosphorylation of individual cardiac proteins in response to β-AR stimulation (See Chapter 1; Section 1.2.4). In our study, we used the broad-spectrum PDE inhibitor IBMX as well as the family-selective PDE inhibitors EHNA, Cil and Rol to assess the respective roles of PDE2-4 in the regulation of cAMP signalling to PLM under both basal conditions and during β-AR stimulation. Specifically, we compared the effects of selective PDE inhibition on PLM phosphorylation status at the three consensus sites on the protein: Ser68, Ser63 and Thr69.

The vast majority of studies on PDE function in the heart have been carried out in myocytes isolated from the rat or mouse heart. The PDE-inhibition experiments in our study were carried out exclusively in ARVMs because as described in Chapter 2 (Section 2.2.1), the adult rat heart produces a consistently greater cell yield when compared to the adult mouse heart; additionally, the individual myocytes are generally more resistant to apoptosis in comparison with the latter. These features assist in the generation of a more robust response as detected by WB. Despite the relative activity of individual PDE families being similar between ARVMs and NRVMs, we opted to use myocytes from the adult rat heart as opposed to its neonatal counterpart for practical reasons.

As with any pharmacological inhibitors, the relative selectivity of the commercial PDE inhibitors is highly dependent on the concentrations at which they are used. A possible limitation of the present study is the reliance on pharmacological inhibitors to analyze the mechanisms involved in PDE inhibition-induced consequences. For our experiments, we selected the optimal working concentrations of the PDE inhibitors based on the literature. IBMX, EHNA, Cil and Rol are undoubtedly among the most frequently used agents for inactivating total PDEs, PDE2, PDE3 and PDE4 respectively (see Chapter 2; Section 2.4) . Several internationally-renowned groups within this field, including those led by Manuela Zaccolo and Rudolph Fischmeister, have carried out a large number of comparable PDE inhibition experiments using IBMX at 100 μmol/L, and the family-selective inhibitors at 10 μmol/L.[43,59,65,83] We were aware that Cil and

Rol have been used at a lower concentration (25 nmol/L – 1 μmol/L) in some studies; however, the majority of published data are derived from experiments using these particular family-selective inhibitors at 10 μmol/L. To quantitatively confirm the selectivity of the compounds, we calculated their relative selectivity for the individual PDEs based on their estimated inhibition constant (K_i) values. Therefore, at the concentrations used herein these pharmacological compounds have been widely used and probed to be valid tools; however, as with any pharmacological agents, the possibility of undesired non-selective effects cannot be completely ruled out.

Table 3.1 Relative selectivity of PDE inhibitors for PDEs 2-4 used in experiments.

Inhibitor	Inhibition constant (K_i) (μmol/L)		
	PDE2	**PDE3**	**PDE4**
IBMX	0.50	0.18	1.00
EHNA	≤ 0.01	1.00	1.00
Cilostamide	0.19	5.25×10^{-4}	1.00
Rolipram	1.00	1.00	3.80×10^{-3}

Our hypotheses were based on the assumption that PDEs are involved in the regulation of cAMP signalling to PLM specifically during β-AR stimulation. In order to stimulate the β-AR pathway in ARVMs, we used the classical non-selective β-AR agonist ISO in our experiments. For any effect of PDE inhibition in the presence of ISO on PLM to be observed, the effect of ISO alone must be minimal as to provide as large a 'window' as possible in order for further increases in the level of PLM phosphorylation to be detected. As such, we generated a concentration-response curve to quantify the phosphorylation status at PLM-Ser68 in response to a range of [ISO]. This allowed us to determine the submaximal concentration of the agonist (10 nmol/L) that produced a response situated at the bottom of the steep part of the curve.

In our PDE inhibition experiments, we found that 10 nmol/L ISO selectively induced a small increase in PLM-Ser68 phosphorylation level. This observation is consistent with previous work in our laboratory demonstrating that 10 nmol/L ISO could induce

increases in PLM-Ser68 phosphorylation, although the differences were not statistically significant (unpublished data). This suggests that at 10 nmol/L, ISO is sufficient to increase the activity of AC localised in membrane to bring the cAMP concentration above threshold for cAMP-dependent phosphorylation of PLM at Ser68. The effect of this submaximal concentration of ISO on PLM-Ser68 was more modest in comparison with those on PLB-Ser16 and cTnI-Ser22/23.

There are at least two potential explanations for this. One is that the basal level of PLM-Ser68 of the ARVMs used in our experiments was higher than that of PLB and cTnI, which made it more difficult to augment with a low [ISO], as addressed earlier The other possibility is that PLM, PLB and cTnI are located in distinct compartments within the cell, and therefore are differentially regulated by distinct pools of cAMP and PKA. Hence addition of ISO would not induce an equal effect on the phosphorylation levels of these proteins, as activation of the β-AR system might not have induced identical changes in cAMP-PKA signalling within these compartments. Thus our findings may reflect a compartmentalised model of cAMP/PKA signalling, which would be entirely consistent with data generated with cAMP sensors reported in the literature, and which we have attempted to address in Chapter 5.

As described in Chapter 1 (Section 1.3.2), PLM-Ser68 phosphorylation in ARVMs has been estimated by our group to be ~40% at rest.[146] In practice, this value is likely to be significantly higher immediately after myocyte isolation due to the activation of stress kinases initiated by the isolation procedure, as described in Chapter 2 (Section 2.3). Unpublished findings from our group suggest that culturing myocytes for 2 hr at 35^{o}C consistently decreases PLM-Ser68 phosphorylation to a stable level of approximately 40% compared to freshly-isolated cells by reducing PKC phosphorylation of PLM-Ser68 induced by Ca. We therefore opted to culture ARVMS in Ca-containing medium for at least 2 hr prior to their use in PDE-inhibition experiments. In consideration of these preliminary findings, this duration of culture suggests that basal PLM-Ser68 phosphorylation in our experiments was physiologically 'normal' and comparable to that measured *in vivo*, and therefore sufficiently low for experimentally investigating increases in the phosphorylation level at this site upon treatment of ARVMs, as confirmed by treatment with a maximal concentration of PMA. A 24 hr culturing

period could potentially further reduce PLM-Ser68 phosphorylation, although our group had previously found no significant differences between the two durations of culture on PLM-Ser68 phosphorylation.

It is therefore logical that the PKA phosphorylation of PLM-Ser68 basal PLM-Ser68 phosphorylation could theoretically be further reduced by incubation in Ca-free media, and this has been previously by our laboratory to be the case, even if this may be unrepresentative of the normal physiological situation. However, in these experiments, the Ca-free protocol did not seem to enhance the phosphorylation 'window' for PLM-Ser68. We found that this lack of Ca-driven effect on basal PLM-Ser68 phosphorylation surprising, since the removal of Ca and the resulting decrease in PKC phosphorylation under basal conditions imply that any PKA-mediated effects would be more readily observed. We considered the possibility that the Ca removal protocol failed to work, although the augmented effects of IBMX and rolipram on PLB-Ser16 phosphorylation in the presence of ISO under Ca-free conditions as compared to Ca-containing conditions point to a possible reduction of basal PLB-Ser16 phosphorylation. Thus it remains unclear as to why this reduction in Ca concentration within the culture medium did not also result in a reduced PLM-Ser68 phosphorylation under basal conditions. The most likely explanation is that the removal of Ca was not sufficient to adequately reduce basal PKC phosphorylation of PLM-Ser68, and theoretically, also at Ser63 and Thr69. One can only assume that the basal PKC phosphorylation of these sites was higher than ideal under our experimental conditions.

Investigating the effects of PDE inhibition on top of a submaximal concentration of ISO has been attempted previously.[59,83] As mentioned in Section 3.2.5, a recurring feature of my findings in this chapter is that many observed effects of the PDE inhibitors in the presence of ISO stimulation, in particular those with IBMX and rolipram, are large ($\geq$ 3x) and/or close to statistical significance ($p > 0.05$ but < 0.1) but found to be not statistically significant. As such, I have referred to such differences as 'displaying a trend towards an increase' throughout this chapter. A potential explanation for this is the large discrepancy between responses across the sample group. Therefore, a power calculation was carried out for these data points to determine the maximum number of samples that would theoretically be required for a difference of this magnitude to be

statistically significant. From this, we estimated that statistical significance should be achieved if the sample number is doubled.

Our finding that treatment with IBMX induced a trend for an in increase in basal PLM-Ser68 phosphorylation suggests that in our preparations, there was a substantial basal activity of AC that determined a basal cAMP synthesis, and that there was a significant basal PDE activity which limits the degree of cAMP-dependent phosphorylation of PLM.

In contrast, treatment of ARVMS with EHNA, Cil or Rol were found to induce no significant effect on basal PLM-Ser68 phosphorylation, suggesting that inhibition of a single cardiac PDE subtype is insufficient to raise intracellular cAMP concentration to the threshold concentration necessary for PLM phosphorylation. The likely explanation for this finding is that other PDE subtypes accounted for cAMP hydrolysis under basal conditions, with the individual PDEs possessing sufficient enzymatic activity to fully hydrolyse the cAMP produced by the basal activity of ACs. This suggests a scenario whereby PLM phosphorylation in quiescent ARVMs is regulated by PDE subtypes 2-4 functioning in tandem, with the rate of cAMP turnover being low enough such that the activity of the individual PDE subtypes becomes functionally redundant.

Interestingly, it has been reported that basal PDE4 activity is not as prominent in adult rodent myocytes (~40%) and is closely matched by that of PDE3 (~30%), while PDE2 activity is significantly lower.[35,69] On addition of EHNA, it could therefore be conjectured that PDE2 activity is easily compensated for by the activities of PDE3 and/or PDE4. On the other hand, our data suggest that upon treatment with Cil, PDE4 activity had to be increased by at least two-fold in order to compensate for the absence of PDE3 activity, and vice versa on the addition of Rol. To test this idea of functional redundancy of different PDE subtypes, there is the possibility in future experiments to inhibit the activity of two PDE subtypes simultaneously using combinations of PDE inhibitors and observe their effects on PLM-S68 phosphorylation. Considering that PDE2 activity is significantly less than that of PDE3 and PDE4 in the rat heart, it is tempting to speculate from the above that the concomitant inhibition of PDE3 and PDE4 would result in a significant increase in the phosphorylation status of PLM-S68, although we currently have no direct evidence to confirm this.

In contrast, inhibition of PDE4 was found to selectively exert a pronounced stimulation of PLM-Ser68 phosphorylation after application of 10 nmol/L ISO, with the effect being very close to being statistically significant. This enhancement was not observed upon treatment with EHNA or Cil, suggesting that PDE4 is the predominant PDE subtype involved in regulating cAMP signalling to PLM during β-AR stimulation. Thus while a functionally redundant hydrolytic system comprised of PDE2-4 may serve to prevent intracellular cAMP from rising immoderately to exert an effect on PLM-Ser68 phosphorylation in the absence of NA, PDE4 becomes determinant in regulating PLM-Ser68 phosphorylation when the cell is challenged by a stimulus activating the β-AR pathway. Importantly, this effect was found to be quantitatively greater than that induced by IBMX in combination with ISO, which is unexpected considering the notion that PDEs 2-4 represent the main PDE subtypes in the heart, and that IBMX should inhibit all the known PDE isoforms. As such, one would expect the effect of IBMX to be quantitatively equal to that induced by the sum of EHNA, cilostamide and rolipram. As addressed earlier, comparing the effects of different pharmacological inhibitors is highly dependent on the concentration at which they are used, and considering the prominent effect of rolipram, it is possible that IBMX might not have been inhibiting PDE4 to an equal degree, and therefore any residual PDE4 activity could have reduced the overall effect of IBMX. Similarly, it is possible that there are PDEs present in the cell whose activities are not affected by IBMX. Admittedly, these two scenarios are highly unlikely given the standard use of IBMX as a non-selective PDE inhibitor and our current understanding of cardiac PDE subtypes. It is also possible that the discrepancies observed may reflect differences in permeability levels of these PDE inhibitors, or could be attributed to different levels of sensitivity of the cells to the inhibitors. However, these would imply that a fair comparison between these PDE inhibitors cannot be made and the multitude of published studies investigating the effects of these inhibitors in cohort refutes this. The most plausible explanation could well be due to intra-sample discrepancy. However, as mentioned earlier, power calculations suggest that the observed effects of IBMX and rolipram are likely to reflect genuine changes, and it is possible that when the number of samples is doubled (i.e. n = 12), the changes induced by these two inhibitors may match each other more closely.

When considering the manner in which cardiac contractility is regulated and maintained upon sympathetic activation, it is interesting to note some of the similarities that PLM shares with PLB and cTnI from both a regulatory and functional viewpoint. The former is underlined by their specific dependency on PKA in determining their phosphorylation status during β-AR activation. Meanwhile, the latter could be attributed to the indirect role of PLM in maintaining optimum $[Ca]_i$ and hence cardiac contractility in synergy with the ECC proteins, a reflection of the interplay between Na and Ca transport within the cardiac myocyte. Intriguingly, while PDE2-4 inhibition was found to exert little effect on basal phosphorylation levels of PLM-Ser68, PLB-Ser16 phosphorylation was found to be significantly increased in response to treatment with IBMX, or with either EHNA or rolipram when under Ca-free conditions. Similarly, a trend for an increase in cTnI-Ser22/23 phosphorylation was observed in response to inhibition of PDE3 or PDE4.

Indeed, selective PDE4D gene deletion in the mouse myocardium was found to result in increased basal PLB phosphorylation,[87] and our findings are also consistent with a previous report concluding that PLB-Ser16 phosphorylation level is augmented upon the combined inhibition of PDE3 and PDE4 (because the authors found that the effect could only be obtained by the addition of Cil and Rol in combination).[258] Likewise, it has been shown that cTnI-Ser22/23 phosphorylation may also be modulated by PDE3 and PDE4,[258] and that these PDE families are responsible for regulating basal $I_{Ca,L}$ in ARVMs, with PDE4 becoming predominantly involved in the control of the LTTC during β-AR stimulation.[59]

Our findings raise the possibility that for proteins with an intrinsically lower basal phosphorylation level, individual PDE subtypes may be determinant in regulating their phosphorylation status as they are able to sufficiently raise intracellular cAMP levels above the threshold. This may also explain why the effects of total PDE inhibition with IBMX is apparently more pronounced than observed with PLM-Ser68 phosphorylation. However, our findings may also reinforce the notion that PDEs may regulate different PKA substrates in distinct ways, reflecting a possible effect of cAMP compartmentalisation. Thus the functional redundancy underlying PLM-Ser68 phosphorylation may reflect the intrinsically high phosphorylation level of the protein

under basal conditions and/or differential regulation of individual PKA substrates by PDEs.

Under ISO-stimulated conditions, the picture is less clear. The pattern of PDE inhibition in the presence of ISO for PLB-Ser16 seems to largely correspond with that for PLM-Ser68. Under Ca-free conditions, addition of IBMX or rolipram in combination with ISO was found to significantly augment PLB-Ser16 phosphorylation, and despite the lack of statistical significance, we obtained a similar pattern of response with PLM-Ser68 phosphorylation under Ca-containing conditions. It must be emphasised that the mechanism underlying the more pronounced increases in PLB-Ser16 phosphorylation upon addition of IBMX or rolipram observed under Ca-free condition remains unclear. While we hypothesised that a removal of Ca would reduce basal PKC phosphorylation of PLM-Ser68, we expected this protocol to induce no effect on PLB-Ser16 phosphorylation, since there are no published reports to date suggesting a regulation of the latter via PKC phosphorylation. Interestingly, PLB is also phosphorylated by CamKII (at Thr17), which is Ca-dependent, and the question remains whether the Ca-free protocol could have altered the basal PLB-Ser16 phosphorylation via a mechanism involving CamKII phosphorylation?

Meanwhile, it is difficult to draw firm conclusions from the effects of PDE inhibition on cTnI-Ser22/23 in the presence of ISO. We observed no changes in phosphorylation at this site upon treatment with IBMX, and while the addition of cilostamide or rolipram resulted in approximately two-fold increases, they could not be regarded as trends towards an increase and may not represent genuine changes. Interestingly, for both PLB-Ser16 and cTnI-Ser22/23, addition of EHNA in the presence of ISO was observed to reduce phosphorylation level at this site, which could potentially be attributed to a cGMP-mediated effect. As aforementioned, besides inhibiting PDE2, EHNA is also a potent inhibitor of adenosine deaminase. It has been suggested that this mechanism could potentially result in an accumulation of intracellular cGMP. As detailed in Chapter 1 (Section 1.2.4), an increase in [cGMP] leads to a greater rate of cAMP hydrolysis by PDE2, and it is therefore possible that inhibition of adenosine deaminase underlies the observed decreased phosphorylation of cTnI-Ser22/23 observed in the presence of EHNA and ISO. Future experiments could directly address the changes in

intracellular [cGMP] in response to addition of EHNA, which may clarify this potential limitation of using the latter as a PDE2 inhibitor.

From the findings discussed so far, it could be envisaged that the distinct effects of ISO and of the individual PDE inhibitors on basal phosphorylation of PLM, PLB and cTnI may not only reflect different levels of basal protein phosphorylation, but also possibly a scenario whereby the PDEs 2-4 are regulating cAMP signalling to these PKA substrates in a differential manner. During β-AR stimulation, PDE4 becomes primarily responsible for regulating cAMP signals to PLM and PLB (and possibly for cTnI, although this remains unclear).

However, there is also the possibility (which happens to constitute the simplest explanation for our findings) that our observed patterns of PLM-Ser68 phosphorylation may simply reflect the total intracellular activity of PDE2-4 in ARVMs rather than compartmentalised cAMP signalling. It has been suggested that PDE4 isoforms may collectively regulate bulk cAMP levels within the rodent heart;[69] since PDE4 activity represents the dominant fraction quantitatively in the rodent heart,[65,69,92] the fact that it induces a prominent effect on the phosphorylation levels of PLM, PLB and cTnI may therefore be simply be reflecting its high levels of abundance. On the other hand, the low relative activity of PDE2 in ARVMs[92] could potentially limit its effects on downstream targets. Such a model is likely to be overly simplistic, however, given our observations that PDE2, PDE3 and PDE4 seem to differentially regulate PLM-Ser68, PLB-Ser16 and cTnI-Ser23/24 phosphorylation levels, as detailed earlier. Our results therefore suggest that the regulation of cAMP signalling to cardiac proteins by PDEs is highly multifaceted and complex, and PDEs may contribute to the regulation of cAMP signalling to a number of cardiac proteins in a differential manner.

Our finding that PDE4 inhibition resulted in an increase in total $[cAMP]_i$ is consistent with our current understanding of how PDE4 regulates cardiac cAMP signalling. Under normal circumstances, cAMP-PDEs continually hydrolyse cAMP; inhibition of their activity should therefore result in an immediate and significant increase in global cAMP levels inside the cell. Since PDE4 activity comprises the predominant cAMP-hydrolytic fraction in the rodent heart, its inactivation is therefore expected to lead to a significantly accumulation of cAMP within the cell. It is interesting to note that this

increase in cAMP did not translate into a significant augmentation of PLM-Ser68 phosphorylation. There remains some controversy surrounding the basal $[cAMP]_i$ in the rodent heart. It has been demonstrated using a cytosolic cAMP sensor that the basal concentration of total cAMP in intact guinea pig ventricular myocytes could be as high as 1.2 μmol/L.[133] On the other hand, traditional radioimmunoassay (RIA) measurements in mouse ventricular myocytes have shown that basal $[cAMP]_i$ is in the fmol range and that 10 μmol/L Rol induced a 2.5-fold increase in total cAMP levels after 10 min.[68] At the same time-point, we observed a comparable increase of approximately 2-fold in cAMP accumulation, in line with the possibility that basal PDE4 activity is often greater in neonatal rodent myocytes (~60%).[68,83]

Our results additionally provide clues into the downstream mechanisms of cAMP. The effect exerted on PLM phosphorylation by PDE4 inhibition seems to be specifically modulated via the actions of PKA, as treatment of Rol in the presence of ISO did not lead to an augmented phosphorylation level of PLM-Ser63 or PLM-Thr69, the consensus PKC sites on PLM. This suggests that PKA plays a key role in the regulation of cAMP signalling to PLM by PDE2-4 under basal conditions as well as during β-AR stimulation . PKA is a major cardiac effector of cAMP and one would therefore expect its inactivation to completely abolish any cAMP-mediated signals. Indeed, our findings are consistent with imaging experiments using the AKAR PKA probe confirming the functional influence of PDE4 inhibition on PKA activity.[44] The role of PKA in regulating the activities of PDEs themselves should also be considered, as PKA phosphorylation has been shown to increase the activities of PDE3A[259]and the long PDE4 isoforms,[57,109] suggesting that PKA activity could serve as a negative feedback regulator on PDE4 to functionally 'match' PDE activity to the intracellular cAMP concentration. Since PDE4 inhibition induced such a dramatic effect on PLM phosphorylation in the presence of ISO, this implies that PDE4 activity is highly pronounced during β-AR stimulation, consistent with the notion that PKA phosphorylation of several long PDE4 isoforms could potentially increase their activity by up to 60%,[109] and therefore cannot be compensated for by the activities of the remaining PDEs. On the whole, our findings are consistent with the notion that PDE4 is cAMP-specific and therefore selectively influences downstream PKA signalling.

In conclusion, the work described in this chapter suggests that in the adult rodent heart, PDE4 becomes functionally important specifically in response to stimulatory hormones. Overall, these findings support our model of PDE4-mediated PKA phosphorylation of PLM; under basal conditions, the combined activities of PDE3 and PDE4 (and possibly PDE2) are required to regulate basal PKA phosphorylation of PLM in a functionally redundant manner, possibly due to the high basal phosphorylation level of PLM. The latter could be further explored in future experiments whereby the effects of combined PDE inhibition are investigated. On the other hand, upon β-AR activation, our findings suggest that PDE4 becomes determinant in regulating cAMP signalling to this protein, as supported by intracellular cAMP measurements. Intriguingly, this pattern of PDE regulation contrasts with those for PLB and cTnI, suggesting that PDE4 plays extensive yet differential roles in the regulation of cAMP signalling in the rodent heart. Together, our data have revealed insights into the regulation of PLM phosphorylation by PDE4 under neurohormonal stimulation.

4 EFFECTS OF PDE INHIBITION ON NA/K-ATPASE ACTIVITY

4.1 Introduction

4.1.1 Background

In the previous chapter, we presented data suggesting a specific role of PDE4 in regulating PKA phosphorylation of PLM-Ser68 during β-AR stimulation. It is now generally accepted that PLM serves as the functional link between kinase activation and NKA activity upon sympathetic stimulation, with PKA phosphorylation at PLM-Ser68 mediating the increase in NKA activity. As mentioned in Chapter 1 (Section1.4.3), such a scheme has been hypothesised to be physiologically important in limiting the detrimental effects of Na (and indirectly Ca) overload upon β-AR stimulation. Given the well-characterised functional association between PLM and NKA, we proceeded to use whole-cell VPC to investigate the functional impact of PDE inhibition on NKA activity.

We hypothesised that changes in NKA activity upon PDE inhibition would correspond to the pattern of PLM phosphorylation, with inactivation of PDE2, PDE3 or PDE4 under basal conditions having little effect on I_p density while in the presence of ISO, pharmacological inhibition of PDE4 would lead to a significant increase in NKA activity. This series of experiments would shed further light onto the functional association between PLM and the NKA, in addition to the role of PDE4 in the regulation of downstream cAMP targets in the heart. The specific hypotheses and aims of the studies described in this chapter are outlined below.

4.1.2 Specific hypotheses

- That pharmacological inhibition of PDE2, PDE3 or PDE4 in the absence of ISO would induce no significant effect on I_p.

- That pharmacological inhibition of PDE4 in the presence of a submaximal concentration of ISO would selectively induce a significant increase in I_p.

4.1.3 Specific objectives

1. To generate a concentration response curve to a range of ISO concentrations in order to identify a suitable submaximal [ISO].

2. To investigate the effects of PDE2, PDE3 and PDE4 inhibition on I_p in the absence and presence of this submaximal [ISO].

4.2 Methods

4.2.1 Isolation and culture of ARVMs

The experiments in this chapter were performed using ARVMs isolated from the hearts of adult (250 – 300 g body weight) male Wistar rats (B & K Universal), as described in Chapter 2 (Section 2.2.1) Cells were maintained in suspension at 35^{o}C for 2 hr prior to use in electrophysiological experiments, as described in Section 2.3.3.2.

4.2.2 Voltage-patch-clamping

4.2.2.1 Principles

In 1952, prior to the discovery of ion channels and ion transport mechanisms, Hodgkin and Huxley used crude glass electrodes to record E_m in squid giant axon.[260-262] The development of voltage-clamp unfolded in an almost contemporary manner,[263] although the application of voltage-clamp in single cells using micropipettes for intracellular recording was not applied for a further 26 years, when voltage-clamp was used in either two-electrode mode[264] or single-electrode mode.[265] The first recording of the single channel activity of native ion channels in biological membranes (muscle nicotinic acetylcholine receptors) were made by Erwin Neher and Bert Sakmann in 1976 using an innovative modification of the voltage-clamp method.[266] This technique, now known as patch-clamp, used blunt-tipped glass pipettes that, when pressed gently against the cell membrane isolated a small membrane area. A further modification of this technique is now widely used and involves measuring whole-cell current by completely 'breaking' the patch of membrane underneath the electrode tip (the ruptured-patch conformation) or perforating the membrane with antibiotics (the perforated-patch conformation).

4.2.2.2 Pulling and filling of pipettes

Pipettes for patch-clamping were made from thin-walled (1.5 mmol/L outer diameter, 1.17 mm inner diameter) borosilicate glass capillaries (Harvard Apparatus Ltd). These were pulled and fire-polished using a 3-stage electrode puller (DMG Universal Puller, Zeitz-Instrumente Vetriebs GMBH). Puller settings were adjusted to give a consistent open pipette resistance (R_{pip}) of 1-2 MΩ when back-filled with pipette solution and a tip shape to encourage successful whole-cell current recording in the perforated-patch configuration.

4.2.2.3 The amplifier circuit

Back-filled pipettes were placed on a stripped and chloride end of Teflon-coated silver wire (Advent Research Materials Ltd) which was connected to the amplifier head-stage (Model CV 201, Axon Instruments Inc). The CV 201 is dedicated to the Axopatch 200 patch-clamp amplifier (Axon Instruments). An integrated Ag/AgCl electrode placed in the superfusing solution downstream of the cells provided the reference electrode.

Voltage protocols were generated and data acquired using pClamp software (Version 10, Axon Instruments) on a Dell personal computer via a 16-bit analogue/digital converter data acquisition system (ModelDigidata 1440A, Axon Instruments). The amplifier was also connected in parallel to an oscilloscope (Gould Instrument Systems Ltd) and a chart recorder (Model RS3200, Gould Instrument Systems).

4.2.2.4 Whole-cell perforated voltage-patch-clamping

A small volume of cell suspension (~0.5 ml) was placed in a purpose-built perfusion bath on an inverted light microscope (Nikon Diaphot, Nikon). The bath was constructed from Perspex with a glass cover-slip base, allowing solution warmed to 35^{o}C to flow over the cells, past the reference electrode and out into a waste reservoir. The flow rate was ~2-3 ml/min and solution height was maintained by a tissue-paper wick drawing solution towards the waste pipette. Cells were viewed from beneath and continuously imaged using a CCD camera (IonOptix Myocam, InoOptix Corporation) and monitor. The microscope, bath, head-stage and micromanipulator were all placed on an anti-vibration air-table (Ealing Electro-Optics Ltd).

Electrophysiological experiments were carried out using the whole-cell perforated-patch technique at 35°C to record whole-cell I_p. The perforated patch-clamp technique is a less invasive method of I_p as the intracellular content is not dialysed by the pipette solution, as occurs in the ruptured method. On the other hand, whilst this may limit the dialysis of small soluble signalling molecules and important cytosolic factors, a disadvantage is poorer control of intracellular and specifically subsarcolemmal $[Na]_i$.

Cells were left to settle on the glass base for 1-2 min before superfusion with Tyrode's solution [Table 4.1] at 2-3 ml/min. The pipette tip was lowered into the superfusing solution using the coarse setting on the micromanipulator (Patchman, Eppendorf). The fine setting was then used to position the pipette tip close to a single, well-isolated myocyte. At this stage any junction potential between the pipette solution and the superfusing solution was compensated at the amplifier. A 20 mV alternating voltage-step protocol was generated (from 0 mV holding potential) and the size of the response was indicative of the open R_{pip}, as described by Ohm's Law. This was generally between 1 and 1.5 MΩ.

Upon initial contact between the pipette tip and the cell membrane, R_{pip} increased slightly and very gentle negative pressure (~5 cm H_2O) was manually applied through the pipette holder from an air-filled syringe. A tight seal between the cell membrane and the microelectrode tip was subsequently established and considered adequate when this reached gigaohm (GΩ) values. After GΩ seal formation, negative pressure in the pipette was allowed to slowly dissipate. At this point, the series resistance of the electrode tip and the cell membrane (R_{tip}) was very large. A voltage protocol which held the cell at -80 mV and stepped to and from -75 mV was then used to track changes in seal resistance (R_s) by Ohm's Law ($R_S = \delta V/\delta I$).

Amphotericin B dissolved in the pipette solution slowly permeabilised the patch of membrane underneath the electrode tip (by forming monovalent cation-selective pores) and induced a progressive reduction in R_{tip}. Hence, access resistance (R_{acc}) progressively decreased and was monitored with repeated 5 mV depolarising steps as described above (sampling frequency of 100 Hz). Typically, R_{acc} fell to ~10 MΩ within 10-15 min. After the establishment of a 1 GΩ seal, the superfusate was switched to 5 mol/L K-Test solution. After the access resistance had fallen to ~2 MΩ and stabilised,

pump current measurements were made. With a typical 400pA current and a 10 MΩ access resistance, the voltage error is 4 mV. With a holding current of 0 mV, this voltage error should not affect the current recorded as the I-V relationship around 0 mV is relatively stable.

4.2.2.5 Recording the whole-cell current

At this stage, a voltage protocol constructed using pClamp software, could be executed in the presence of different extracellular (superfusing) and intracellular (pipette) solutions [Table 4.1]. The electrophysiological equipment was set up to measure and record the current between the recording electrode and reference electrode during the voltage protocol. Under steady state conditions (equilibrium), this current equals the sum of all currents passing through two parallel resistances: (i) the cell membrane and (ii) the pipette seal. Both these resistances were considered to be in series with the resistance afforded by the pipette tip.

During episodic current recordings (square-step protocols), signals were sampled at 5 Hz and filtered at 1 kHz (low-pass filter). For continuous gap-free current recordings, signals were sampled at 10 Hz and filtered at 1 Hz. In all experiments, signals were sampled at a rate at least three times that of the filter setting to avoid signal aliasing.

4.2.2.6 Experimental solutions

For all electrophysiological recording of I_p, experimental solutions were superfused over the myocytes at 35^{o}C. Experimental solutions were similar to those described by Shattock and Masuura[267] and were adapted from the method described by Gadsby and co-workers.[268] In combination with a specific voltage protocol, experimental intracellular and extracellular solutions [Tables 4.1 and 4.2] were designed to block or avoid activation of any current other than the I_p. Inward $I_{Ca,L}$ were avoided by using Ca-free test solutions (in which Ba ions replaced Ca). K current was blocked by replacing intracellular K with pipette Cs (125 mmol/L) and with 1 mmol/L Ba in the extracellular solution. The NCX was inhibited with 2 mmol/L $NiCl_2$ in the extracellular solutions.[269,270] 2 mmol/L $NiCl_2$ also completely blocked L-type current thus

preventing Ba currents through these channels.[267] Na channel currents were eliminated by recording at a holding voltage of 0 mV.

The pipette solution contained 30 mmol/L [Na] to allow changes in NKA activity resulting from either a change in K_m or V_{max} to be observed. For all VPC experiments, amphotericin B was added to the pipette solution on the day of use. A small quantity of amphotericin B was reconstituted in DMSO (Hybri-max, Sigma) in an opaque microcentrifuge tube to a concentration of 30 mg/ml and vortexed thoroughly. The solution was then added to the pipette solution and vortexed to give a final concentration of amphotericin B in the pipette solution of 225 μg/ml, with [DMSO] of 0.74% (v/v). Pipette solution was protected from light and kept on ice.

Table 4.1 Composition of extracellular experimental test solutions used in voltage-patch-clamp experiments.

Compound	Tyrode's (mmol/L)	K-Test (mmol/L)	K-free (mmol/L)
NaCl	137	140	140
KCl	5.4	5	-
$MgCl_2$	0.4	1	1
$CaCl_2$	1	-	-
$NiCl_2$	-	2	2
$BaCl_2$	-	1	1
Glucose	10	10	10
HEPES	10	10	10

pH 7.4 at 35^{o}C with CsOH

Table 4.2 Composition of intracellular (pipette) experimental test solution used in voltage-patch-clamp experiments.

Compound	Perforated patch 30 mmol/L Na (mmol/L)
$CsCH_3O_3S$	110
$NaCH_3O_3S$	15
$CsCl_2$	8
NaCl	15
$MgCl_2$	1
HEPES	10

pH 7.2 at 35^{o}C with CsOH

4.2.2.7 Measuring I_p

The NKA was activated by perfusion with 5 mmol/L K-test solution and inhibited in a reversible manner by perfusion with K-free test solution (0 mmol/L K), which had previously shown to be identical to that sensitive to 10 mmol/L ouabain.[146] The removal of extracellular K was chosen as opposed to the use of ouabain since the washout time for ouabain is relatively long compared to the rapid reversal of K-free pump inhibition (ouabain is reported to still affect inotropy and intracellular Na for more than 30 min after washout in cardiac tissue). The I_p was continuously recorded whilst the myocyte was held at 0 mV using a continuous, gap-free recording protocol. A stable current recording was established in K-test solution before the protocol was stopped, and the cell perfused with K-free solution. I_p was subsequently defined using the reversible inhibition of the NKA by perfusion with K-free solution (see Section 4.2.2.8.2).

4.2.2.8 Pump current analysis

4.2.2.8.1 Calculating cell capacitance and seal resistance

Capacitors have the ability to store electrical charge upon a change of voltage. The most effective capacitors are parallel conducting plates of large surface area separated by a thin sheet of insulator. This is an excellent approximation of the membrane lipid bilayer. The magnitude of this capacitance is proportional to the area of the capacitance 'plates' (the surface area of the cells) and it can therefore be used as an indirect quantitative measure of cell surface area. Multiple capacitors in parallel are electronically equivalent to a single large capacitor, hence membrane capacitance increases with cell size and is usually expressed as a value per unit area ($pF/\mu m^2$). As a rough approximation the capacitance of the membrane is approximately 1 $pF/\mu M^2$. If current is applied to the membrane it first charges the membrane capacitance before changing the E_m.

In order to obtain an approximation of cell size, a standard protocol was used at the beginning and end of each VPC experiment. A step depolarisation from -80 mV to -75 mV lasting 25 ms gave typical recordings (200 kHz sampling frequency), showing a positive deflection at the start of the voltage step, a negative capacitance spike at the end

and a maintained rise in the whole cell current for the duration of the step. The upward and downward spike deflections are associated with the charging and dissipation of membrane capacitance. The area under the capacitance spike is proportional to the capacitance of the cell membrane (C_m).

4.2.2.8.2 Calculation of I_p

I_p was defined as the current sensitive to the removal of extracellular K, and was identical to that sensitive to 10 mmol/L ouabain (unpublished data). Subtraction of traces recorded in the presence and absence of extracellular K was carried out 'offline' using Clampfit software (Version 10, Axon Instruments) analysis functions and further analysis using Microsoft Excel and GraphPad Prism software. Results were collated and normalised to cell capacitance. The use of cell membrane capacitance to represent the membrane area is well documented[271-273] and such normalisation allows study of I_p density, rather than the whole-cell current which would inevitably vary from cell to cell according to cell size.

I_p was defined as the difference between the stable currents measured in the presence and absence of extracellular K, rather than the peak of the overshoot current after the reintroduction of K, as for example, used by Bers and co-workers. The overshoot observed when K is reintroduced is a product of Na accumulation inside the subsarcolemmal during the period of pump inhibition and inadequate control of intracellular Na by pipette dialysis. While the overshoot is related to the activity of the NKA, it is also influenced by several other factors, which make it a less accurate method of quantifying NKA activity. These factors include the access resistance between the pipette solution and the cell, the Na leak into the cell, in addition to the time during which Na can accumulate within the subsarcolemmal space – i.e. the time period during which the cell is perfused with K-free solution.

4.2.2.9 Exclusion criteria

Cells were excluded from further analysis if the capacitance protocol was not carried out successfully both at the beginning and end of the experimental protocol. If R_s was poor, then the cell was also excluded. An experimental protocol was not started until

R_{acc} was <15 MΩ, with most cells stabilising at around 10 MΩ. Cells which failed to maintain a good seal or give adequate R_{acc} were discarded. Furthermore, cells were excluded if the perforated-patch confirmation spontaneously changed to the ruptured-patch conformation which was evident from a significant decrease in R_{acc} (from ~10 to 3-4 MΩ). Failure to complete the full experimental procedure also resulted in experimental exclusion while cells where were found to be spontaneously contracting, had indistinct cross striations or membrane blebs were also excluded.

4.2.3 Pharmacological treatment of ARVMs

For generation of a cumulative ISO concentration-response curve for I_p density using VPC, 10 concentrations of ISO were tested (1 nmol/L, 3 nmol/L, 10 nmol/L, 30 nmol/L, 100 nmol/L, 300 nmol/L, 1 μmol/L, 3 μmol/L, 10 μmol/L and 30 μmol/L). The individual concentrations of ISO were added to the K-test solution and exposed to myocytes for approximately 10 min, when a steady-state effect (plateau) has been established. For assessment of a single submaximal concentration of ISO on I_p, myocytes were treated with 300 nmol/L ISO for 10 min. For assessment of PDE2-4 inhibition on *Ip*, myocytes were treated with 100 μmol/L IBMX, 10 μmol/L EHNA, 10 μmol/L Cil and 10 μmol/L Rol alone or in combination with 300 nmol/L ISO for approximately 10 min, when a steady-state effect has been established. For all treatments, myocytes were exposed to 0.1% DMSO (in both K-test and K-free solutions) throughout the entire experimental procedure.

4.2.4 Experimental protocols

Panel A of Figure 4.1 outlines the VPC protocol used for assessing the effect of PDE inhibition on I_p density in the absence and presence of ISO while Panel B of the same figure outlines a separate protocol used for assessing the effect of ISO on I_p.

We had initially designed a protocol that enabled the measurement of the responses generated upon treatment with PDE inhibitors under basal conditions, ISO alone and PDE inhibition in combination with ISO in sequential order on a single myocyte. However, the inability to 'wash out' the effects of ISO in our system during preliminary experiments meant that it was necessary to divide this protocol into two mini-protocols

[Figure 4.1; Panels A & B]. This lack of a sufficient 'wash-out' meant that it became preferable to analyse the PDE inhibition-induced effects on I_p density under basal conditions and in the presence of ISO using different statistical methods. Another consequence of this is that in contrast to our initial plans, only the amplitude of the I_p response (and not its temporal profile) could be accurately determined, as the transient nature of the responses observed might have been masked (see Section 4.4).

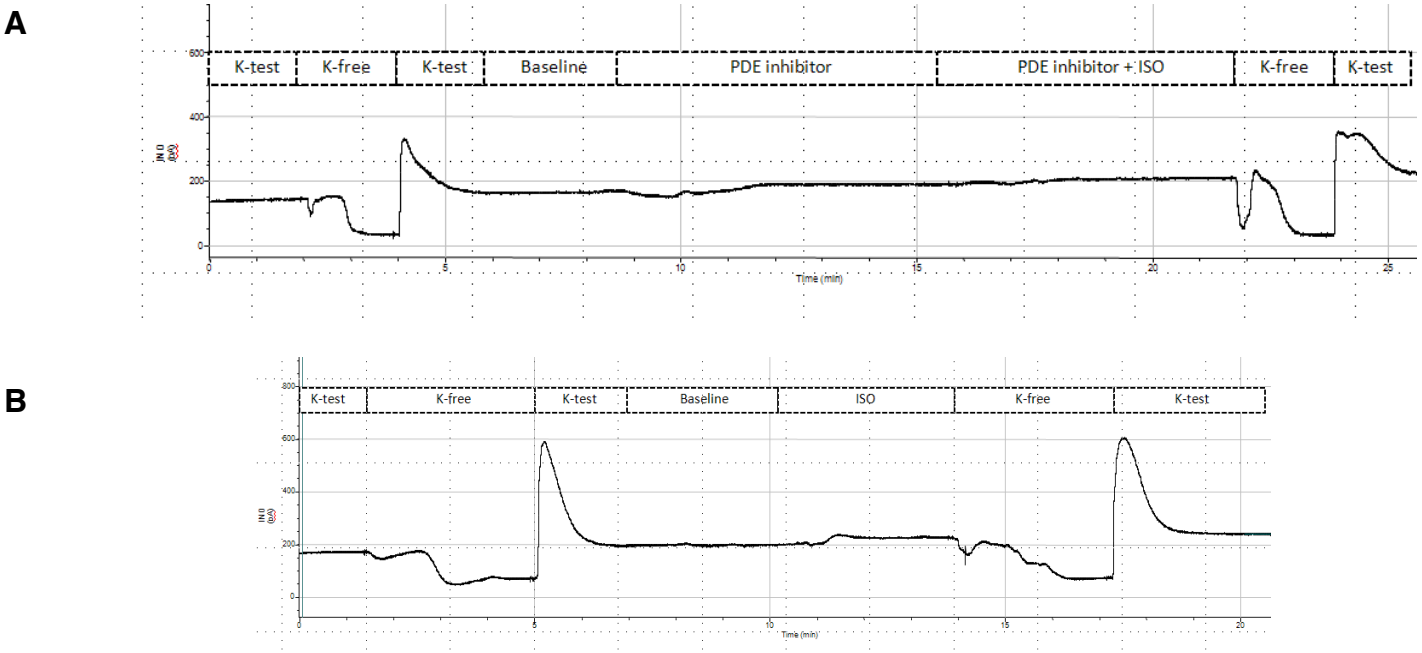

Figure 4.1 Experimental protocols used in voltage-patch-clamp studies.

The cell was initially superfused with K-test solution prior to switching to K-free solution to reversibly inhibit NKA activity. Upon reperfusion with K-test solution, the current was allowed to reach a steady-state level (plateau), defined as the baseline, after which **(A)** PDE inhibitors in the absence and presence of 300 nmol/L ISO were added sequentially to the K-test solution or **(B)** 300 nmol/L ISO alone was added to the K-test solution. Cells were first treated with PDE inhibitors for 10 min, unless a steady-state effect had been attained earlier, followed by treatment with 300 nmol/L ISO for a further period of up to 10 min. The cell was subsequently perfused with K-free solution to ensure R_s had remained stable throughout the experiment. Any alterations in the current recorded in K-free solution resulted in the exclusion of the experiment for data analysis.

Representative trace of a single experiment is shown; all measurements were made using the perforated configuration of VPC (pipette [Na] 30 mmol/L); I_p was defined as the difference between the stable currents measured in the presence and absence of extracellular K. Results were collated and I_p values normalised to cell capacitance to generate I_p density values.

Importantly, in order to ensure that any changes in I_p observed could be directly attributed to the treatments applied and not a result of any inherent 'drifting' of the pump current, which constitutes a major practical complication of any VPC experiments, we carried out time-matched control experiments interspersed in a random manner throughout the series of PDE inhibition experiments to check that I_p typically remained stable throughout the duration of the protocol (typically within 30 – 40 min). In general, we observed that the I_p generated by myocytes remain stable for approximately 60 min, thus eliminating the possibility of the observed changes in response to the different pharmacological treatments arising from alterations in the baseline I_p during the experimental procedure. Additionally, it must be noted that while a 'run-down' of I_p is a recognised complication with the VPC procedures (usually more pronounced with the ruptured patch variation in comparison to the perforated method, due to a greater extent of dialysis of intracellular components and earlier cell death with the former), it is rarer to observe a gradual 'drift-up' of the current, although a gradual decrease in R_s over time could lead to an increase (albeit often a sudden shift) in current that might be unknowingly interpreted to be a genuine effect.

4.3 Results

4.3.1 Identification of a suitable submaximal [ISO]

A cumulative concentration response curve for I_p density to a range of [ISO] was first generated to allow identification of a submaximal [ISO] that was deemed suitable for investigating the functional effects of PDE inhibition on I_p during β-AR stimulation. In contrast to biochemical PDE inhibition experiments, where an individual concentration response curve was generated, a cumulative curve in an electrophysiological setting enabled the measurement of multiple concentrations of ISO on a single myocyte, which eliminated the necessity of testing each concentration on an individual cell. The relationship between [ISO] and I_p density in ARVMs was found to be apparently biphasic, with a two-phase relationship [Figure 4.2], but with a significant amount of variability, consistent with previous observations from our group (unpublished data), and is also in agreement with the relationship between [ISO] and PLM-Ser68 phosphorylation (See Chapter 3, Section 3.3.1). The saturating [ISO], 3 μmol/L induced a peak increase in I_p by approximately 0.5 pA/pF, while the [ISO] needed for half-activation of I_p is approximately 1 μmol/L [Figure 4.2].

A suitable submaximal [ISO] was defined as a concentration of the agonist that produced an increase in I_p density that was quantitatively large enough to be detected by VPC, but sufficiently small as to provide an adequate 'window' for any subsequent increases induced by PDE inhibition to be detected. We therefore selected 300 nmol/L ISO, which was found to induce an I_p response that was situated at the bottom of the slope of the curve [Figure 4.2]. As this effect was extracted from a cumulative concentration response curve, and individual responses have been influenced by preceding treatment, we investigated the effect of an individual treatment with 300 nmol/L ISO on the I_p response. The resulting increase in I_p density was found to be smaller than the effect observed within the concentration-response curve [Figure 4.3; Panel A], as expected, although it did reach statistical significance when analysed using the paired Student's *t*-test [Figure 4.3; Panel B]. Therefore, 300 nmol/L ISO was selected as an appropriate concentration for studying the effects of PDE inhibition on I_p during submaximal β-AR stimulation. Importantly, the inability to 'wash out' the

effects of ISO meant we had to characterise the response of 300 nmol/L ISO alone on I_p (see Section 4.2.4).

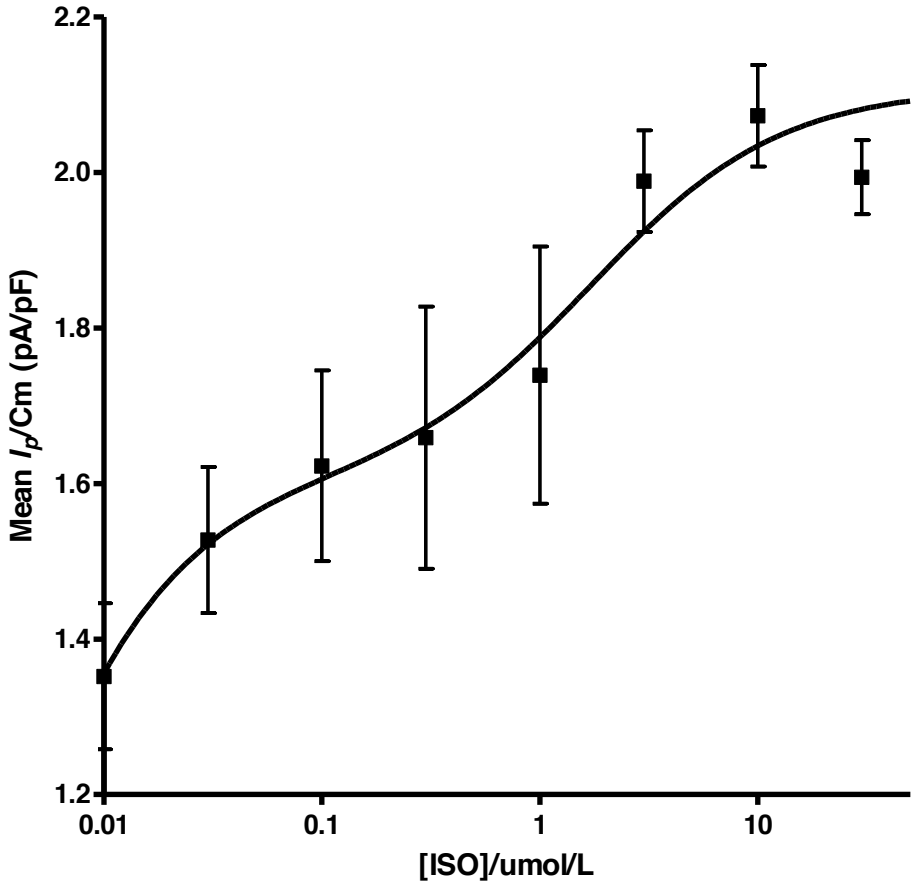

Figure 4.2 Cumulative ISO concentration-response curve for I_p.

ARVMs were superfused with K-test solution and challenged sequentially with 10 nmol/L, 30 nmol/L, 100 nmol/L, 300 nmol/L, 1 µmol/L, 3 µmol/L, 10 µmol/L and 30 µmol/L for 10 min. All treated myocytes were exposed to 0.1% DMSO. Perforated whole-cell VPC was used to determine I_p before and after treatment by switching to K-free solution to reversibly inhibit NKA activity. I_p values were subsequently normalised to cell capacitance to generate I_p density values. Pipette [Na]: 30 mmol/L. Data are expressed as means ± SEM (n=7). Mean data were fitted with a hyperbolic two-site binding function as shown by the solid black line.

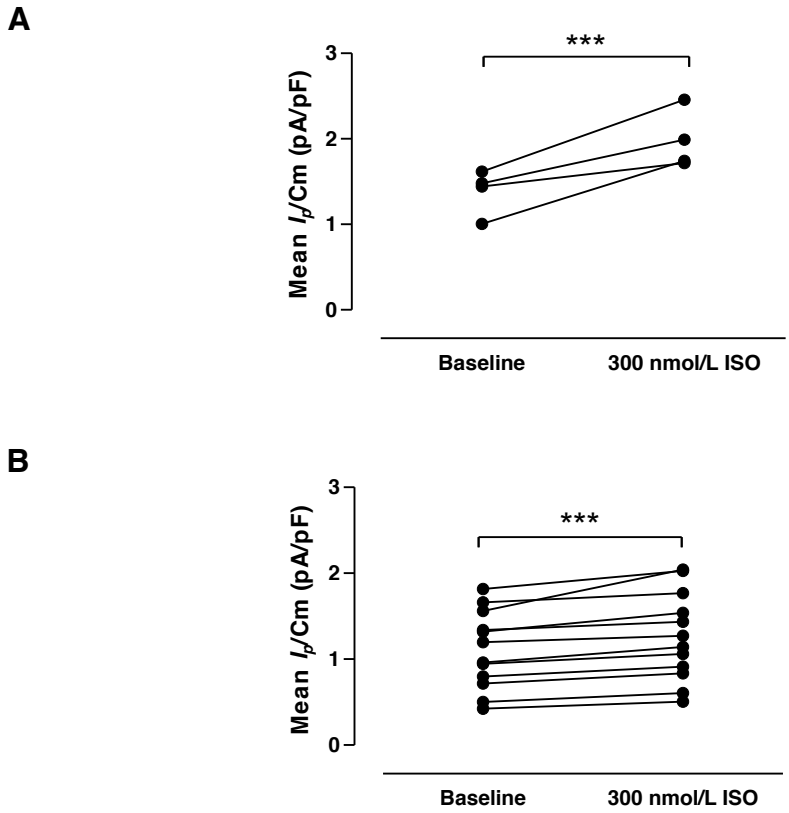

Figure 4.3 Changes in I_p in response to treatment with 300 nmol/L ISO.

ARVMs were superfused with K-test solution and treated with 300 nmol/L ISO for 10 min in **(A)** cumulative concentration-response curve or **(B)** single-concentration experiments. All treated myocytes were exposed to 0.1% DMSO. Perforated whole-cell VPC was used to determine I_p before and after treatment by switching to K-free solution to reversibly inhibit NKA activity. I_p values were subsequently normalised to cell capacitance to generate I_p density values. Pipette [Na]: 30 mmol/L. Data are expressed as means ± SEM (n=12). ***p ≤ 0.001 (paired Student's *t*-test)

4.3.2 Effects of PDE2-4 inhibition on I_p under basal conditions

Due to the nature of the protocols used (see Section 4.2.4), it was deemed most scientifically valid to compare the effects of PDE inhibition on I_p under basal conditions and in the presence of ISO using different statistical methods. It could be observed from Figure 4.4 that steady-state baseline I_p ranges from approximately 0.5 pA/pF to 2 pA/pF. Upon treatment with each of the PDE inhibitors under basal conditions, we observed a significant increase in I_p from the baseline using the paired Student's *t*-test [Figure 4.4; Panels A-D].

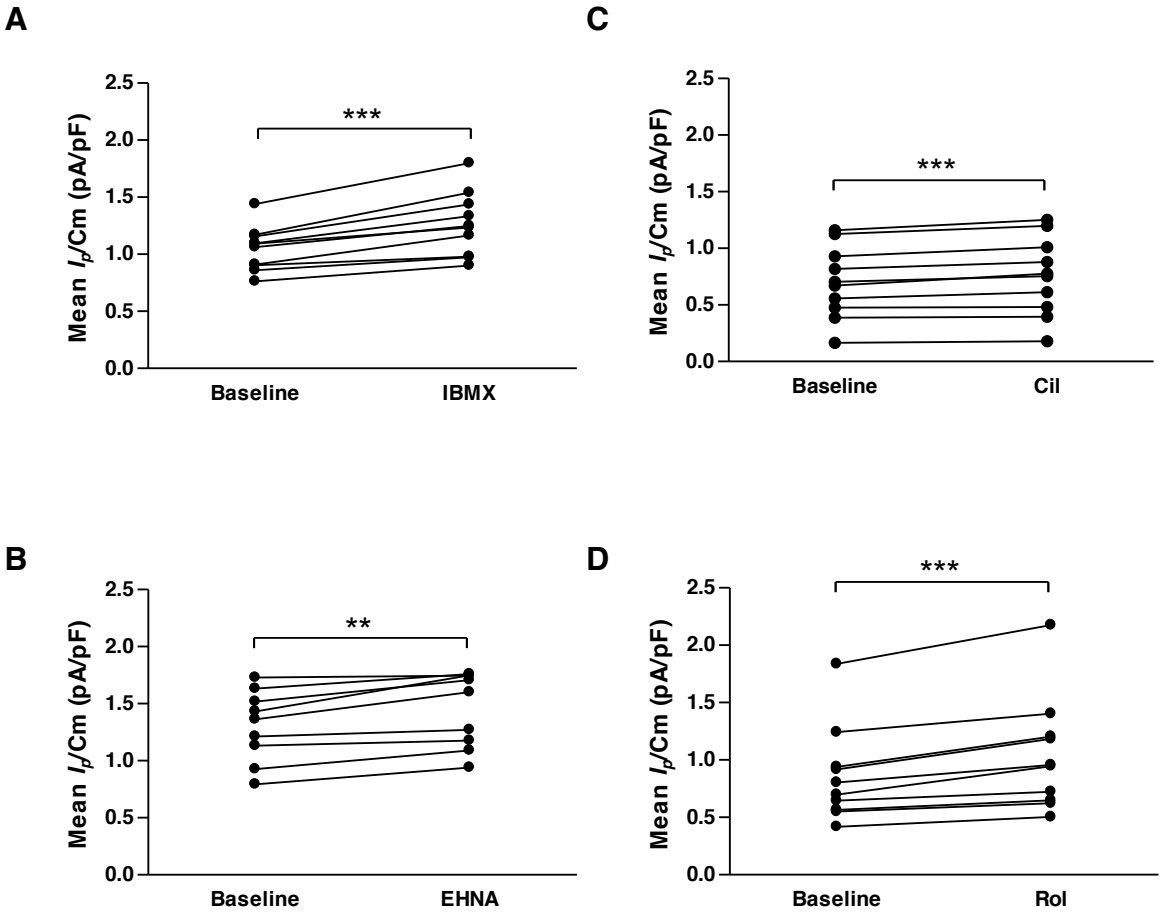

Figure 4.4 Changes in I_p in response to PDE inhibition under basal conditions.

ARVMs were superfused with K-test solution and challenged with **(A)** 100 µmol/L IBMX, **(B)** 10 µmol/L EHNA, **(C)** 10 µmol/L Cil or **(D)** 10 µmol/L Rol for 10 min. All treated myocytes were exposed to 0.1% DMSO. Perforated whole-cell VPC was used to determine I_p before and after treatment by switching to K-free solution to reversibly inhibit NKA activity. I_p values were subsequently normalised to cell capacitance to generate I_p density values. Pipette [Na]: 30 mmol/L. Statistical comparisons were made using paired Student's t-test and data are expressed as means ± SEM (n=10). **p ≤ 0.01; ***p≤0.001

4.3.3 Effects of PDE2-4 inhibition on I_p under ISO-stimulated conditions

As mentioned, since the effects of PDE inhibition on I_p density in the presence of ISO were tested on a separate batch of cells to those that have been treated with ISO alone, the mean changes in I_p density for the two treatment groups were quantitatively compared using the unpaired Student's *t*-test in order for a valid comparison to be made without resolving to plotting fold changes, which artificially removes any variation in the baseline values [Figure 4.5; Panels A-D]. The mean change in I_p density under basal conditions was also plotted, although not used in statistical analysis as they had already been assessed quantitatively using 'before-after' line plots [Figure 4.4; Panels A-D].

As depicted in Figure 4.5, challenge with the non-selective PDE inhibitor IBMX in combination with ISO was found to significantly increase the I_p density by approximately 0.25 pA/pF when compared to treatment with 10 nmol/L ISO alone [Figure 4.5; Panel A]. Similarly, treatment with EHNA or Rol in the presence of ISO resulted in a significant increase of approximately 0.15 pA/pF and 0.1 pA/pF respectively compared to treatment with ISO alone [Figure 4.5; Panels B & D]. In contrast, exposure to either Cil or Rol in combination with ISO did not further augment I_p density [Figure 4.5; Panels C & D].

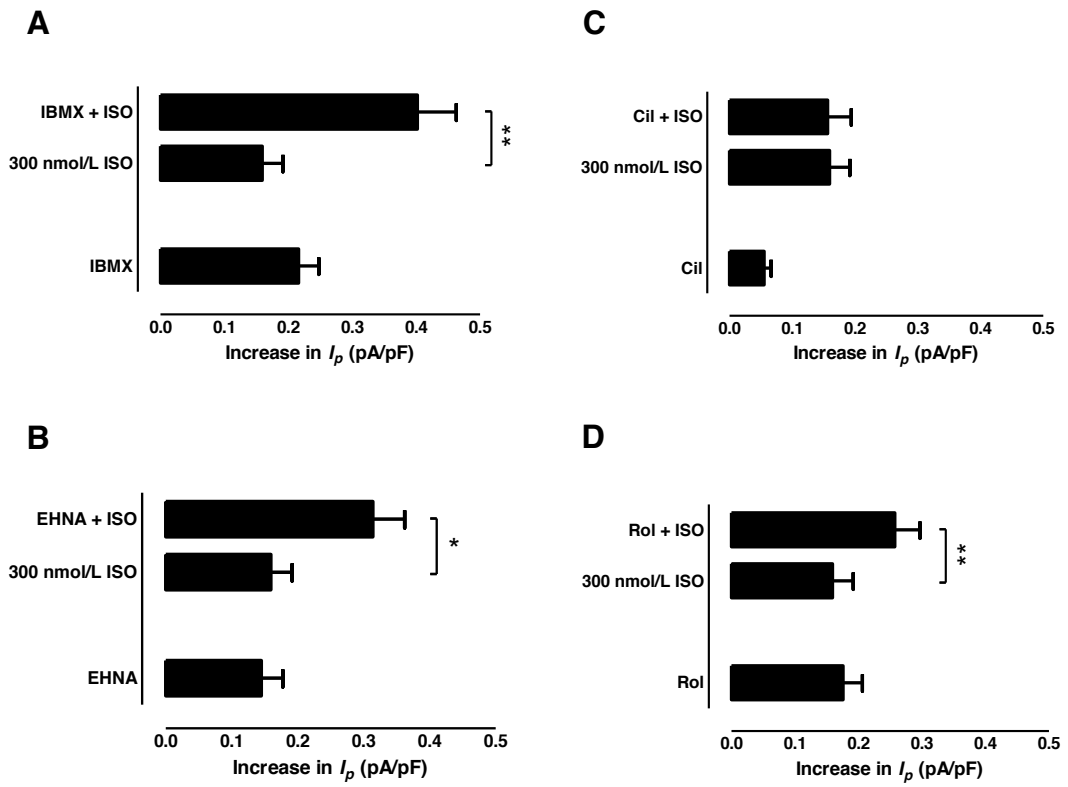

Figure 4.5 Increases in I_p in response to PDE inhibition in the absence and presence of a submaximal [ISO].

ARVMs were superfused with K-test solution and challenged with **(A)** 100 µmol/L IBMX, **(B)** 10 µmol/L EHNA, **(C)** 10 µmol/L Cil or **(D)** 10 µmol/L Rol in the absence and presence of 300 nmol/L ISO for 10 min. All treated myocytes were exposed to 0.1% DMSO. Perforated whole-cell VPC was used to determine I_p before and after treatment by switching to K-free solution to reversibly inhibit NKA activity. I_p values were subsequently normalised to cell capacitance to generate I_p density values. Pipette [Na]: 30 mmol/L. Statistical comparisons were made using paired Student's t-test and data are expressed as means ± SEM (n=10). *p ≤ 0.05

4.4 Discussion

Following on from the experiments outlined in the previous chapter, which primarily focused on the effects of PDE inhibition on the phosphorylation status of PLM-Ser68, the series of experiments described within the present chapter was aimed at characterising the effects of PDE inhibition on NKA activity. The latter was quantitatively assessed by taking advantage of the asymmetrical transport mechanism of the NKA, which governs the outward transport of three Na ions and the inward transport of two K ions for each ATP molecule hydrolysed, up to a hundred times per second, generating a measurable outward current if assayed in millions of pumps (Shattock and colleagues have estimated the presence of approximately ten million pumps per rabbit myocyte[274]).

Specifically, we made use of the perforated-patch version of the VPC technique, in combination with extracellular and intracellular solutions designed to block any contaminating currents, to measure the I_p response to treatment with different PDE inhibitors in the absence and presence of ISO in freshly-isolated ARVMs. We used a relatively low [Na] in the pipette solution at 30 mmol/L, which has previously been shown by our laboratory to be situated at the foot of the Na activation curve for I_p; therefore changes in NKA activity resulting from either a change in K_m or V_{max} of the pump could be detected.

A study by Stimers and Dobretsov in 1997 reported that the myocyte isolation procedure does not impair mechanisms linking β-ARs with the NKA, in guinea pig myocytes maintained in short-term culture.[275] As outlined earlier, the perforated patch method was selected as baseline I_p was found to remain in steady-state for a substantially greater duration than when using the ruptured patch method. This is consistent with the general notion that rupturing a section of the cell membrane results in a greater degree of dialysis of cytosolic components necessary for cell survival in comparison with membranes that are perforated but remain essentially intact. The subsequent reduction in the duration in which the cell remains 'healthy' and viable for experimental use is reflected by the gradual irreversible 'run-down' in I_p after approximately 20 min in ruptured patch mode, as opposed to the steady-state current

lasting for up to 60 min which we found to be typical in untreated cells that have been patched onto using the perforated-patch technique.

The perforated-patch method does have its drawbacks, however, the most significant being a less decisive control of intracellular Ca, and as such, there is the possibility that changes in I_p density may or may not be reflective of genuine underlying physiological changes. Indeed, the addition of ISO was found to elicit an increase in I_p density that was not time-dependent, consistent with their perceived roles in responding to acute stimuli of the pathway. Given the unlikelihood that this inability to 'wash out' the effects of ISO constitutes a genuine physiological phenomenon, the lack of a temporal profile detected may therefore represent an artefact that could be attributed to the inherent nature of the perforated patch method, which somehow prevents the activated β-AR pathway from 'switching off'. Certainly, previous work in our laboratory corroborates with this possibility, with the perforated-patch method generally displaying highly variable time courses, while the ruptured-patch method was shown to clearly demonstrate a differential response to ISO and FRSK. Upon challenging with ISO, I_p returned to baseline levels within 2 min, while exposure to FRSK resulted in an augmentation of I_p that remained for an indefinite period of time (data not shown).

Interestingly, the control of $[Ca]_i$ may effect other important consequences concerning the stimulation of NKA activity by ISO. In isolated cardiac myocytes, ISO has been shown to stimulate the pump by several authors[227,276-278] but having an inhibitory[278-280] or no effect[281] by others in both rat and guinea pig myocytes. In the present study, we found that ISO induced an increase in I_p density in a concentration-dependent manner in ARVMs, consistent with the majority of reports. Importantly, it was determined that while 300 nmol/L ISO is a submaximal concentration in a VPC setting, it represents a maximal concentration as detected by SDS-PAGE/WB (See Chapter 3; Section 3.3.1). This emphasises the inherent characteristics of different experimental techniques and hence the necessity of individually characterising the parameters for each set of experiments.

The reasons underlying the disparate observations on the effects of ISO on I_p remain somewhat controversial, although attempts have been made in recent years to delineate these issues.[275] It is now generally accepted that the most plausible explanation for

these seemingly contradictory findings may at least partially reside in the complexity of the adrenergic stimulation of the NKA, in particular its dependence on $[Ca]_i$. In guinea pig myocytes, it was determined by Gao and colleagues in 1991 that with low $[Ca]_i$ (<150 nmol/L), ISO inhibited I_p, while at high $[Ca]_i$ (>150 nmol/L), ISO stimulated I_p.[277] Subsequent studies reproduced this disparity, with PKA-dependent activation of I_p in the presence of ISO corresponding with a clamping of $[Ca]_i$ to physiological or slightly supraphysiological concentrations,[276,278] while PKA-dependent inhibition corresponding with a subphysiological $[Ca]_i$.[278,279] In general, it seems that laboratories reporting pump inhibition by PKA buffer $[Ca]_i$ below 100 nmol/L[280] while those reporting pump activation by PKA do not buffer $[Ca]_i$.[146,169,171] This effect of Ca buffering on PKA-mediated NKA activation is consistent with the observation that elevated Na affinity of the NKA in PLM-KO myocytes is dependent on pipette [Ca], with this effect being negated when [Ca] is buffered below approximately 10 nmol/L.[282] Indeed, [Ca] has been reported to modify the effect of PKA activation on pump activity in an identical fashion in tissues other than the heart.[283]

Whether this effect of Ca represents merely a biophysical phenomenon or a genuine physiological means to switch the pump from a PKA-inhibitable to a PKA-activatable state remains unclear. Since the average intracellular Ca levels, which are dependent on heart rate and adrenergic tone, would likely exceed the 101-150 nmol/L threshold above which PKA stimulates the pump,[277,278] PKA inhibition of the pump could potentially be of limited biological relevance in cardiac muscle under normal circumstances, but may become important when intracellular Ca levels fall below normal levels in certain pathologies, and also in other cardiac cell types with an intrinsically lower $[Ca]_i$. The potentially high basal phosphorylation level of PLM-Ser68 (discussed in Chapter 3; Section 3.4) is indicative of a high Ca load in the myocytes used in our experiments, which is consistent with PKA activation of the NKA. Indeed, our results are entirely consistent with the extensive evidence suggesting that phosphorylation of PLM-Ser68 by PKA is required for augmenting NKA activity.

Interestingly, Ishizuka and Berlin reported an absence of ISO stimulation on I_p in rat ventricular myocytes, which may be reflective of the particular experimental condition, in which I_p reactivation currents, rather than steady-state currents were measured.[281] As detailed in Section 4.2.2.8.2, we chose to employ a K-removal protocol for I_p

measurement in our VPC experiments, whereby steady-state currents measured in K-test and K-free solutions were subtracted to generate I_p values that were subsequently normalised to cell capacitance to allow a quantitative evaluation of I_p density. In our experience, analysis of steady-state currents surpasses measurement of I_p reactivation currents in both accuracy and reliability, as the overshoot instilled by the reactivation of the NKA by the reintroduction of K is more variable in our hands (See Section 4.2.2.8.2). Thus the disparity between our findings and those by Ishizuka and Berlin may reflect a continuum of NKA transport that is modulated by experimental conditions.

While the ISO-induced increase in NKA activity is matched by a corresponding increase in PLM-Ser68 phosphorylation level, attempts to link the effects of PDE inhibition on NKA activity with those on PLM-Ser68 phosphorylation seem to be more complex. The large body of evidence establishing the functional association between PLM and the NKA during β-AR stimulation has already been outlined in detail in Chapter 1 (Section 1.4.3) and we therefore expected a close correlation between the WB and VPC data sets, as highlighted by our initial hypothesis. As discussed in Chapter 3, treatment of myocytes with PDE inhibitors in a biochemical setting provides evidence for PDE4 being the predominant PDE subtype involved in regulating PKA phosphorylation of PLM during β-AR stimulation. In contrast, exposure to these inhibitors in an electrophysiological setting suggests that PDE2 constitutes the major PDE subtype contributing to the regulation of NKA activity during β-AR stimulation, with PDE4 inhibition also exerting a statistically significant effect.

It is important to emphasise here that the duration of treatment with PDE inhibitors in the biochemical/Western blot experiments differed to that in the VPC study. In the biochemical experiments, cells were exposed to the PDE inhibitors for 10 min simultaneously, while in the electrophysiological experiments, cells were first treated with PDE inhibitors for 10 min, which were left on for a further 10 min in the presence of ISO, and therefore the cell had been exposed to the inhibitor for 20 min in total. We admit that the two protocols do not directly correspond with each other, but this experimental design in the VPC study was unavoidable. Considering the relatively quick onset of action of these inhibitors, and their cell permeability, a difference of 10

min in duration seems unlikely to significantly affect their activities under these experimental conditions.

Since PDE2 appears to play such a prominent role in regulating I_p despite having only a small effect on PLM phosphorylation, this observation raises the possibility that PDE2 may selectively affect NKA activity via a mechanism that is independent of PLM phosphorylation. One such mechanism is *S*-palmitoylation, which is the reversible covalent post-translational attachment of the fatty acid palmitic acid to the thiol group of cysteine via an acyl-thioester linkage.[284] In recent years, protein *S*-palmitoylation has gradually emerged as an important and common post-translational modification in a variety of tissues,[285] and has been found to exert a variety of functions, including the regulation of ion channel/transporter activity, stability, or subcellular localisation.[285,286] Importantly, it was recently shown that PLM can be palmitoylated at two intracellular cysteines, C40 and C42, just beyond the transmembrane domain to exert an overall inhibitory effect on the pump.[287] Interestingly, PLM palmitoylation is directly influenced by its phosphorylation status, such that phosphorylation of PLM-Ser68 by PKA increases PLM palmitoylation.[287] Hence, one post-translational modification of PLM that activates the NKA serves to promote a second that inhibits it.

Another mechanism thought to regulate cardiac NKA activity is glutathionylation of the pump's α subunit.[288] Glutathionylation of the pump occurs in the basal state, and is promoted during cardiac hypoxia, causing profound pump inhibition. Since glutathionylation and palmitoylation may competitively influence the same cysteine residues, it is possible that dynamic regulation of the pump may occur *independently* of PLM phosphorylation. However, it must be emphasised that both of these mechanisms have been shown to result in inhibition rather than stimulation of the NKA; as such, palmitoylation and glutathionylation of PLM is unlikely to explain our findings, which indicate an increase in NKA activity. Therefore, PDE2 would have to selectively reduce PLM palmitoylation or glutathionylation, in order to result in an increase in I_p *without* affecting PLM phosphorylation. Theoretically, this is possible, although it is equally likely that another yet-unidentified mechanism could be involved.

Additionally, as discussed in Chapter 1; (Section 1.4.3), while it is theoretically possible that PKA can directly phosphorylate the NKA (which would provide an alternative

explanation for our findings), the kinase signalling pathways that lead to cardiac NKA activation are now almost universally acknowledged to terminate at PLM. Although it has been suggested that direct phosphorylation of the α subunit of the NKA may be important for regulating the latter's activity in certain cell types, the lack of evidence supporting such a model within the heart suggests that it is highly unlikely to play an important role in specifically regulating cardiac NKA activity.

The PLM phosphorylation-independent regulation of NKA function may be functionally important under basal conditions. Our results suggest that PDE2-4 individually contribute to the regulation of cAMP signalling to the NKA at rest, in contrast to the notion that these PDE subtypes only exert a small effect upon PLM-Ser68 during basal conditions, possibly due to the intrinsically high basal phosphorylation level at this site (See Chapter 3; Section 3.4. What also remains unclear is how the observed effects of PDE inhibition on I_p under basal conditions relate to those during β-AR stimulation. Our findings suggest a scenario whereby PDE2 is primarily important for regulating cAMP signalling to the NKA under both basal conditions and during stimulation of β-ARs. On the other hand, PDE3 seems to be only necessary for modulating NKA activity at rest. In light of previous reports on the effects of PDE inhibition on $I_{Ca,L}$, which demonstrated that selective inhibition of a single PDE subtype was insufficient to significantly raise basal $I_{Ca,L}$, PDE4 becomes predominant in modulating cAMP signalling to the LTTC during β-AR activation.[59] Indeed, it seems logical that a particular PDE becomes functionally important when intracellular cAMP levels are elevated, as supported by augmentation of PDE4 activity via PKA phosphorylation.[109] Our findings are therefore at variance with this model in suggesting a selective 'switching off' of PDE3 function upon sympathetic activation.

On the whole, the potential functional implications of our findings are intriguing. The predominant cAMP-hydrolytic activity of PDE4 in the rodent heart, and its role in the regulation of several key components of ECC is well established in both an *in vitro* and *in vivo* setting. Thus the idea that PDE4 influences cAMP signalling to the NKA by mediating PKA phosphorylation of PLM-Ser68 lies well within the current context in which PDE4 action is thought to unfold. What is perhaps more intriguing is the idea that PDE2 seems to play a role in regulating cAMP signalling to the NKA. As detailed in Chapter 1 (Section 1.2.3), there is evidence for PDE2 regulating cAMP levels in

response to β-AR stimulation.[75] Importantly, as this particular PDE subtype constitutes a much lower percentage of total PDE activity in comparison to PDE3 or PDE4, our findings suggest that the action of PDE2 in relation to the NKA may be compartmentalised, with PDE2 preferentially regulating a local cAMP pool in the vicinity of PLM/NKA. As detailed in Chapter 1 (Section 1.2.5), there is now an extensive body of evidence indicating that individual PDE isoforms are likely to be located in distinct intracellular compartments of the cell, with tethering of the PDE variants directly to cardiac proteins or indirectly via AKAPs to facilitate this local regulation of cAMP signalling. Previous reports have demonstrated a tight control of a local pool of cAMP in the vicinity of LTCCs by PDE2 in a number of species; considering the role of NKA in indirectly regulating $[Ca]_i$,[77,78,80] our findings are therefore in line with this possible scenario of cAMP compartmentalisation involving PDE2.

In conclusion, the effects of pharmacological inhibition of PDE2-4 on NKA activity as assessed by measurement of I_p density using VPC suggests that PDE2 plays a significant role in regulating cAMP signalling to the NKA. This is in addition to our finding that PDE4 seems to be primarily responsible for regulating PKA phosphorylation of PLM-Ser68, indicating a possible scenario whereby PDE2 regulates cAMP signals in the vicinity of PLM/NKA in a compartmentalised manner via a mechanism independent of PLM phosphorylation by PKA.

5 CHARACTERISATION OF A NOVEL FRET-BASED CAMP SENSOR

5.1 Introduction

5.1.1 Background

5.1.1.1 Measurement of intracellular cAMP levels

Despite the notion of intracellular compartmentalisation having been proposed early on in the study of cAMP signalling,[11,289] the lack of high-resolution sensors for monitoring cAMP at the single-cell level has served as a significant obstacle in the experimental – and conceptual – exploration of the spatiotemporal dynamics of intracellular cAMP changes. Measurements of cAMP levels within the cell had traditionally been limited to biochemical antibody-based techniques, such as enzyme immunoassays[290] and RIAs,[291] whereby only total and not free cAMP levels in batches of cells or tissue samples (including those molecules bound to proteins and sequestered in cells) can be measured. Furthermore, the destructive nature of these *in vitro* assays means that cAMP levels cannot be determined with any spatial resolution, in sharp contrast to the concept of cAMP compartmentalisation that has emerged over the past few decades, which suggests that different cAMP concentrations are present in distinct intracellular compartments. A further limitation is that such methods only enable static samples to be taken, thus providing little information on the temporal profile of the responses.

Although such cell population assays are simple, economical and continue to be extremely useful in well-defined situations where spatiotemporal dynamics or individual cellular variation is not a consideration, cAMP compartmentalisation and dynamics are increasingly being recognised as an intrinsic and regulated part of the cellular management of cAMP. As such, there has been a significant development in novel techniques that can resolve the real-time dynamics of cAMP signalling in living cells and tissues with high temporal and spatial resolution to address these issues.

5.1.1.2 Live-cell imaging of cAMP dynamics

The first breakthrough came in the early 1990s with the development of a fluorescent sensor termed 'FICRhr' (pronounced 'flicker') and this advance has been followed by a wave of genetically encoded sensors.[292] The currently available single-cell biosensors for measuring cAMP are all based on downstream targets of the second messenger, including PKA,[40,292,293] CNGCs[294,295] and Epac.[30,296,297] These sensors can be used with microscopic techniques to precisely report physiologically relevant free intracellular cAMP levels that are present in the cytosol and capable of activating effector proteins. Moreover, they are capable of reporting rapid changes in cAMP at a higher temporal resolution and spatially resolve intracellular signalling at the subcellular level.

5.1.1.3 The principle of FRET

The majority of these biosensors are fluorescently tagged molecules that rely on the application of FRET, a quantum mechanical phenomenon first discovered in the late 1940s that occurs between a fluorescence donor and a fluorescence acceptor in molecular proximity of each other if the emission spectrum of the donor overlaps with the excitation spectrum of the acceptor.[298] In this approach, the sensor is attached to a pair of fluorophores with overlapping spectra. Typically, the green fluorescent protein (GFP) variants: cyan fluorescent protein (CFP) and yellow fluorescent proteins (YFP) are used. For these constructs, binding of cAMP to the cAMP-responsive protein generates a conformational change and a consequent decrease in FRET signal as the distance between the CFP and YFP moieties is increased. Specifically, excitation of CFP, which is best achieved with light of a wavelength of 436 nm, normally leads to emission of the typical cyan fluorescence, with a peak at a wavelength of 480 nm. If however, a second fluorophore such as YFP is close by, then – under appropriate circumstances – energy can be transferred to YFP (which has excitation and emission maxima of 514 and 527 nm respectively) and a yellow emission from YFP occurs that has a peak wavelength of 535 nm. In this transfer of energy, CFP acts as the donor and YFP as the acceptor [Figure 5.1].

Figure 5.1 Principle of FRET using CFP and YFP as a donor–acceptor pair.

FRET occurs when the donor (CFP) is close enough (<10 nm) to the acceptor (YFP), so that upon excitation of CFP (with light at a wavelength of 436 nm), energy is transferred to YFP and causes yellow emission (at 535 nm); at the same time, cyan emission (at 480 nm) decreases (adapted from 38).

Importantly, real-time FRET measurements can be made in a number of different cell types, provided that the cells can be efficiently transfected with the CFP- and YFP-tagged cAMP sensor molecules. Further development over the past few years has introduced several modifications to the parent cAMP probes, generating an array of cAMP sensors with improved sensitivity, signal-to-noise ratio, dynamic range and spatiotemporal resolution. Key advances have been driven by the enhanced efficiency of the newer FRET sensors, the targeting of variants of classical cAMP sensors to specific sites within the cell and most recently, the ability to produce transgenic animals expressing genetically encoded FRET-based sensors.

5.1.1.4 FRET-based cAMP sensors derived from Epac

cAMP biosensors based on the exchange protein directly activated by cAMP (Epac) are among the newest additions to the cAMP sensor collection. Figure 1.3 [Panel C] shows how a generic Epac-based cAMP sensor functions according to the principle of FRET mentioned above. Epac represents an important intracellular effector for cAMP and appears to account for many of its effects.[299] Epac consists of a regulatory binding site and a catalytic domain, which has the function of GTP loading of the small G protein Rap1 and maintaining its active state. *In vitro* studies have shown that cAMP is absolutely required for the activation of Epac.[300] In support of the unfolding model,

cAMP binding to the regulatory domain results in a significant conformational change of the protein that leads to a reduction of the FRET signal, compatible with an increased distance between the CFP and YFP moieties [Figure 5.2].[299]

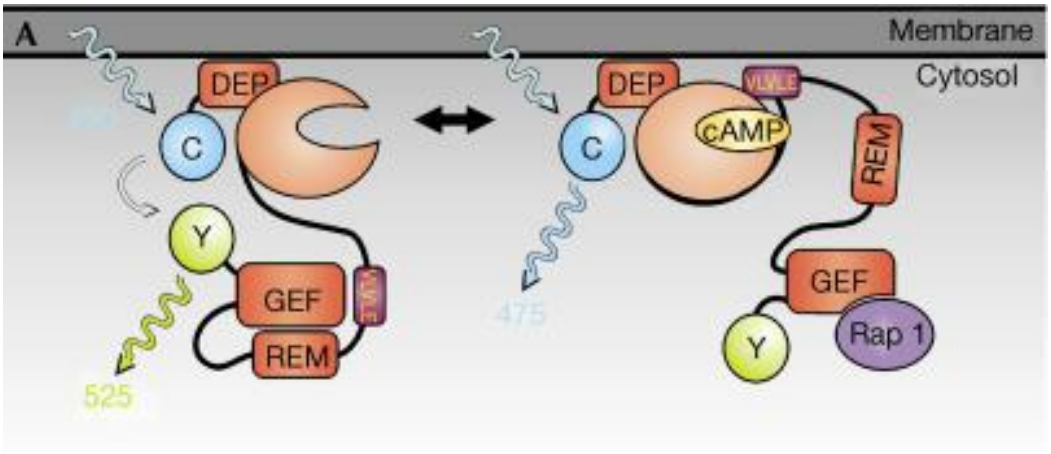

Figure 5.2 Model for the conformational change of Epac following binding of cAMP to the regulatory domain of the protein.

Following cAMP binding, the VLVLE sequence can interact with the regulatory domain, release the inhibition of the GEF domain by the REM domain. FRET between the CFP and YFP tags allows detection of this conformational change (taken from 297).

In 2004, the generation of several FRET-based cAMP sensors containing Epac1 and Epac2 was reported almost simultaneously by three independent groups.[30,296,297] The unimolecular Epac-based probes, in which CFP and YFP are attached to opposite ends of a single effector molecule, increase FRET efficiency and the signal-to-noise ratio compares very favourably with that of the multimolecular PKA-based sensors.[297] PKA has a complex mechanism of activation (cooperative cAMP binding to four interconnected sites of different affinities) and it has been demonstrated that the activation kinetics of several cytosolic Epac-based probes is faster than that of the relatively slowly dissociating PKA-based counterparts.[30] Additionally, Ponsioen and colleagues reported an extended dynamic range for their Epac-based sensor as compared with the PKA-based FRET sensor.[297] More recently, Epac-based constructs have been generated that are selectively localised to the plasma membrane, as well as other variants that are targeted to the nucleus and the mitochondria, thereby enabling cAMP signals in discrete intracellular compartments to be compared.[296]

5.1.1.5 A novel FRET-based cAMP sensor derived from Epac

We generated a variant of the widely-used Epac1-based cAMP sensor Epac1-camps[30] (camps for cAMP sensor) by conjugation with the full-length human PLM sequence in collaboration with Baillie and co-workers (unpublished data). Specifically, this modified sensor comprises human PLM at the N-terminus, and Epac1-camps as the C-terminal tag, thereby producing PLM-Epac1-camps. Due to the presence of PLM, this sensor should in theory be selectively targeted to the plasma membrane of cardiac myocytes, in contrast to Epac1-camps, which has been shown to be distributed within the bulk cytosol of HEK293 cells.[30] As a result of the distinct localisation patterns of the two sensors, we proposed that they will provide novel insights into the spatiotemporal and regulatory patterns of β-AR-mediated response of cAMP signalling to PLM.

Specifically, the potential for delineating whether cAMP signalling to PLM is modulated by PDE4 in a compartmentalised manner, in support of the emerging model of physical association of PDE4 with cardiac substrates in distinct cAMP microdomains, or globally within the bulk cytosol during sympathetic activation is of particular relevance to this project. We had outlined in Chapters 3 and 4 the evidence indicating PDE4 as the predominant PDE subtype in regulating PKA phosphorylation of PLM during β-AR stimulation. Preliminary co-IP experiments suggest that individual PDE4 isoforms could either be tethered to PLM or exist in the immediate vicinity of the protein, giving rise to the possibility that the local regulation of cAMP signals by PDE4 in close proximity to PLM is responsible for our findings [see Appendices I and II]. The use of PLM-Epac1-camps in conjunction with its non-targeted counterpart, Epac1-camps could contribute to delineating between these two potential mechanisms by allowing us to assess whether cAMP levels increase locally in the vicinity of PLM or globally within the bulk cytosol upon pharmacological inhibition of PDE4 in the presence of ISO.

To facilitate effective transfection of these sensors into cultured ARVMs, we first incorporated the sensors into an adenoviral vector. This series of experiments involved characterisation of the sensors in HEK293 cells, incorporation of the constructs into recombinant adenoviruses and subsequent investigation of the functional capabilities of

these sensors in ARVMs. We hypothesised that the presence of the PLM sequence on PLM-Epac1-camps would result in the selective targeting of this sensor to the sarcolemmal membrane of ARVMs (in contrast to Epac1-camps, which remains in the cytosol), with its functional characteristics remaining unaltered. The specific hypotheses and objectives of the studies described in this chapter are outlined below.

5.1.2 Specific hypotheses

- That PLM-Epac1-camps is targeted to the membrane regions of HEK293 cells and ARVMs.
- That Epac1-camps is not specifically localised but rather expressed within the bulk cytosol of both cell types.
- That both PLM-Epac1-camps and Epac1-camps display similar functional characteristics, with both being suitable for use in FRET-based experiments

5.1.3 Specific objectives

1. To characterise the molecular weights and intracellular expression patterns of the plasmid constructs encoding for Epac1-camps and PLM-Epac1-camps in HEK293 cells.
2. To incorporate the genes of interest into an adenoviral vector to facilitate transfection into ARVMs.
3. To characterise the molecular weight of the gene products, and the expression patterns and functional characteristics of the recombinant adenoviruses in ARVMs.
4. To use these characterised sensors to probe the local intracellular cAMP concentration and signalling in the immediate vicinity of PLM.

5.2 Methods

5.2.1 Generation of cAMP sensors

The construction of Epac1-camps is outlined in detailed by Nikolaev and co-workers.[30] Briefly, the DNA construct encoding for the nucleotide binding sequence of Epac1-camps (E157-E316) was generated by PCR using human Epac1 (GenBank™ accession number AF103905) as a template. GFP variants were amplified with standard primers from pEYFP and pECFP (Clontech) and fused to the N-and C-termini of the gene construct. The construct was cloned into a pcDNA3 vector (Invitrogen) for transient expression in mammalian cells. PLM-Epac1-camps was constructed by fusing the full-length human PLM sequence (1-92 aa) to YFP on Epac1-camps.

All of the work detailed Section 5.2.1 was undertaken by our PhD project collaborator Dr George Baillie (University of Glasgow).

5.2.1.1 Generation of recombinant plasmids

5.2.1.1.1 Restriction enzyme digestion of plasmid DNA and shuttle vector

The pcDNA3 plasmid containing the GOI was digested with 5U each of *Hind*III and *Not*1 in 1x NEBuffer 2 and BSA to a final concentration of 100 μg/ml, for 2 hr at 37°C. 500 ng of the viral shuttle vector, pShuttle-CMV [Figure 5.3] was also digested with the same restriction enzymes.

5.2.1.1.2 DNA gel electrophoresis

DNA was visualised following restriction enzyme digestion (and other molecular biology techniques) by electrophoresis at 100 V on a 1% agarose TAE-gel. 1 g agarose dissolved in 100 ml 1 x TAE (50x TAE: 2 mol/L Tris base, 64 mmol/L EDTA, 17.5% acetic acid), by melting in a microwave, and then cooled, 10000x GelRed (Cambridge Biosciences) was added at a dilution of 1:10000. DNA was visualised by exposure to UV light (λ 365 nm) for 80 ms on a G:Box XT16 gel documentation and analysis system (Syngene).

5.2.1.1.3 Gel purification

The required insert and vector bonds were excised from the gel and purified using the Roche DNA purification kit according to the manufacturer's instructions. Briefly, 300 µl binding buffer was added to each 100 mg agarose and incubated for 10 min at 56°C until completely dissolved. 150 µl isopropanol was added for each 100 mg agarose. The sample was mixed, applied to the column and centrifuged for 1 min at 13,000 x *g*. Flow-through was discarded and the column washed twice with 500 µl and then 200 µl wash buffer before elution in 50 µl elution buffer by centrifugation into a fresh Eppendorf tube at 13,000 x *g* for 1 min. All centrifugation steps were carried out in an Eppendorf bench-top centrifuge (5417R) at room temperature.

5.2.1.2 Quantification of plasmid DNA

Eluted DNA concentration was determined by dilution of 1 µl purified plasmid DNA in 99 µl ddH_2O and measurement of absorbance at λ 260 nm using a spectrophotometer (Eppendorf BioPhotometer). Protein contamination of the purified DNA sample was assessed through measurement of absorbance at λ 280 nm, and was considered acceptable if the 260/280 ratio of absorbance was equal to or greater than 1.8.

5.2.1.2.1 Ligation of insert

The insert was ligated into the digested pShuttle-CMV shuttle vector using the Fermentas Rapid DNA Ligation Kit. The required volume of insert DNA for a 3:1 insert to vector molar ratio was calculated using the following formula (100 ng vector DNA was used):

[(ng vector) x (size of insert (kb) x molar ratio)]/(size of vector) = ng insert

The required volumes of vector and insert DNA were mixed, and ligation carried out using 5U T4 DNA ligase and 1x Rapid Ligation Buffer in a total volume of 20 µl at 22°C for 20 min.

5.2.1.2.2 Transformation of chemically competent E. coli DH5α cells

Chemically competent *E. coli* DH5α cells (Subcloning Efficiency, Invitrogen) were transformed with plasmid DNA. Competent cells stored at -80°C were gently thawed on ice and 50 µl aliquoted into pre-chilled 1.5 ml Eppendorf tubes on ice. Plasmid DNA (5 ng) was added to cells, gently mixed and incubated on ice for 30 min. Cells were heat-shocked at 42°C for 20s and incubated on ice for 2 min. Preheated (37°C) SOC medium (250 µl; 8.5 mmol/L NaCl, 2.5 mmol/L KCl, 20 g/L tryptone, 5 g/L yeast extract, 20 mmol/L glucose, pH 7.0) was added to each reaction and cells were incubated at 37°C for 1 hr, shaking at 250 rpm. All of the transformation reaction was spread out onto LB-agar (10 g/L NaCl, 10 g/L tryptone, 5 g/L yeast extract, 15 g/L agar) plates containing the appropriate antibiotic for the plasmid encoded resistance (50 µg/ml kanamycin) and incubated overnight at 37°C.

5.2.1.2.3 Isolation and purification of plasmid DNA

Well-isolated colonies of transformed cells were inoculated into 3 ml LB-Kan and grown at 37°C overnight, shaking at 250 rpm. Plasmid DNA was isolated using the QIAprep Spin Miniprep Kit (Qiagen). All centrifugation steps were carried out in an Eppendorf bench-top centrifuge (5417R) at room temperature.

1.5 ml of bacterial cells were pelleted by centrifugation at 5000 rpm for 5 min, the supernatant removed by aspiration, and a further 1.25 ml of bacterial cells added to the same Eppendorf tube and pelleted by centrifugation at 5000 rpm for 5 min. The supernatant was removed by aspiration and the cell pellet resuspended in 250 µl chilled buffer P1 by vortexing. 250 µ buffer P2 was added to lyse the cells, and tubes were inverted to mix. 350 µl buffer N3 was added to neutralise the cell lysates, and tubes were inverted to mix. Cell debris was pelleted by centrifugation at 13,000 rpm for 10 min. The supernatant was applied to a QIAprep column and centrifuged at 13,000 rpm for 1 min. The flow-through was discarded and the column washed with 500 µl buffer PB and centrifuged at 13,000 rpm for 1 min. The flow-through was discarded and the column washed with 750 µl buffer PE and centrifuged at 13,000 rpm for 1 min. To ensure removal of residual wash buffer, the flow-through was discarded and the empty column centrifuged for 13,000 rpm for 1 min. The column was transferred into a clean

Eppendorf tube and DNA was eluted by addition of 50 µl double distilled H_2O (ddH_2O, resistance 18.2 mΩ) to the column and centrifugation at 13,000 rpm for 1 min.

The remaining 0.25 ml bacterial cells that were not subjected to DNA isolation, were added to 0.25 ml 50% (v/v) glycerol and stored at -80^{o}C as glycerol stocks, and used in future experiments if large scale amplification of the DNA was required. 3 µl of plasmid DNA was digested with *Hind*III and *Not*I and the digestion products run on a 1% agarose gel to check that the GOI had been successfully cloned into the pShuttle-CMV shuttle vector, as previously.

5.2.2 Generation of recombinant adenoviruses

Recombinant adenoviruses are replication-deficient adenoviral vectors that are commonly used as a gene delivery tool. Adenoviruses contain a linear, dsDNA genome between 26 and 45 kbp in length that is able to replicate in the nucleus of mammalian cells using the host cell's DNA replication machinery. Generation of an adenoviral vector using the AdEasy system[301] involves subcloning the gene of interest (GOI) into a small shuttle plasmid, followed by the introduction of the linearised shuttle vector into a strain of BJ5183 cells that harbours the supercoiled backbone vector (AdEasier cells). BJ5183 bacterial cells are deficient in certain enzymes that mediate recombination in bacteria but still permit efficient generation of stable homologous recombinants. The PacI-digested recombinant adenoviral DNA is then transfected into HEK293 cells and viruses are harvested 14-20 days later. The individual steps will be outlined in more detail below.

All of the work detailed in Section 5.2.2 was undertaken by our 'in-house' virus technician Dr Elizabeth Kemp.

5.2.2.1 Cloning of GOI into pShuttle-CMV

The pShuttle-CMV plasmid (Stratagene) was used as a shuttle vector into which the GOI was subcloned, before homologous recombination was carried out between pShuttle-CMV-GOI and pAdEasy-1, to create recombinant viral DNA, rAd5-GOI. The plasmid contained the kanamycin (*Kan*^{R}) cassette, conferring resistance to the antibiotic,

kanamycin, in bacteria expressing the plasmid. A vector map of pShuttle-CMV is shown in Figure 5.3.

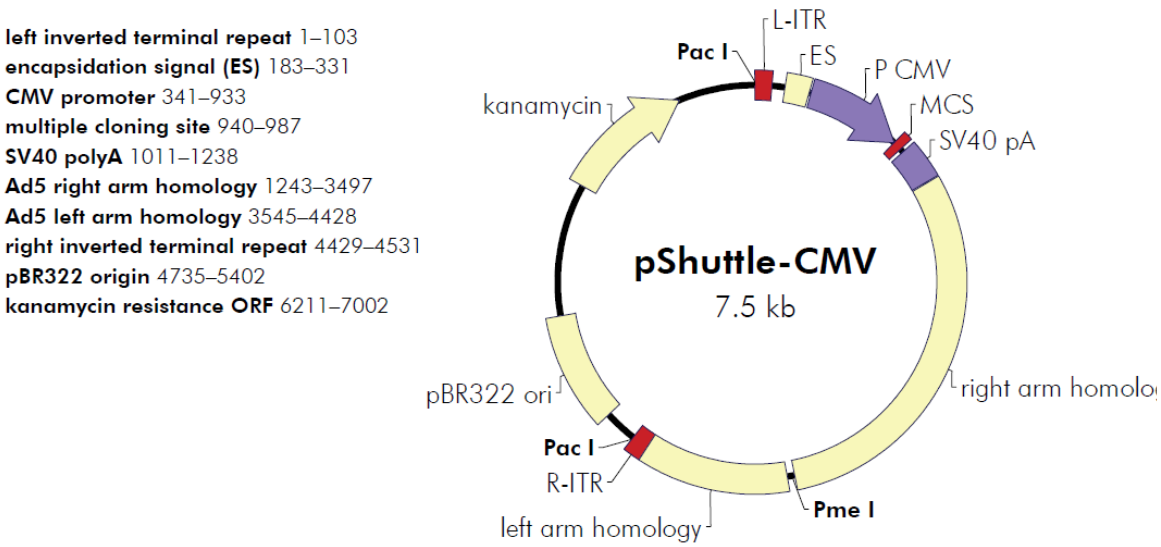

Figure 5.3 Vector map of pShuttle-CMV adenoviral shuttle vector utilised for the generation of recombinant viruses.

The GOI was cloned into the pShuttle-CMV at the MCS using the NotI and HindIII sites. The *Kan*^{R} confers resistance to the antibiotic, kanamycin, in bacteria expressing this plasmid. (taken from Agilent Technologies/Genomics/Vector Maps & Sequences/Adenoviral Vectors: http://www.genomics.agilent.com/GenericB.aspx?PageType=Vector&SubPageType=Vector&PageID=32.)

5.2.2.2 Homologous recombination between shuttle vector and the viral backbone DNA

Approximately 1 µl of the pShuttle-CMV shuttle vector containing the GOI was linearised using 3U *Pme*I in 1x NEBuffer 4 and BSA to a final concentration of 100 µg/ml in a total volume of 20 µl, for 2 hr at 37^{o}C. An aliquot of the digestion was checked by electrophoresis on a 1% agarose gel to ensure complete digestion of the plasmid, as previously.

5.2.2.3 Transformation of electrocompetent E. coli BJ5183 cells

BJ5183-AD-1 electroporation competent cells (Stratagene) containing the pAdEasy-1 viral DNA backbone were transformed with the linearised shuttle plasmid to produce recombinant rAd5-GOI by homologous recombination.

Electrocompetent BJ5183 cells stored at -80°C were gently thawed on ice and 40 µl aliquoted into pre-chilled 1.5 ml Eppendorf tubes on ice. Plasmid DNA (5 ng) was added to the cells, gently mixed and transferred to a pre-chilled 0.2 cm gap electroporation cuvette on ice. The sides of the electroporation cuvette were dried with a paper towel, and placed inside the electroporator (Eppendorf Electroporator 2510). Cells were electroporated at 25 µF, 200 Ω, 2.5 kV, and preheated (37°C) SOC medium (1 ml) added immediately after electroporation. Transformed cells were transferred to a 1.5 ml Eppendorf tube, and incubated at 37°C for 1 hr, shaking at 250 rpm. Different volumes (50, 100 and 850 µl) of transformed cells were spread onto LB-agar containing the appropriate antibiotic for the plasmid encoded resistance (50 µg/ml kanamycin) and incubated overnight at 37°C.

Small, well-isolated colonies (small colonies are more likely to contain successful recombinants than larger colonies) were inoculated into LB-*Kan*, and Miniprep isolation and purification of plasmid DNA carried out as previously. The size of the supercoiled DNA was checked on a 0.8% agarose gel to confirm recombination had occurred, and clones with a supercoiled band larger than the 12 kb marker on the 1 kb+ ladder were chosen for further restriction enzyme digestion.

Promising clones were digested separately with *Pac*I and *Hind*III, and digestion products resolved by electrophoresis on a 1% agarose gel, as previously. *Pac*I digestion yielded a band of either 4.5 or 3 kb, and a larger band at >30 kb where homologous recombination had occurred, and the stability of the genome was checked by *Hind*III digestion. Suitable clones (4 µl Miniprep DNA) were transformed into chemically competent *E. coli* DH5α cells, and Miniprep isolation and purification of the amplified DNA carried out, as previously.

5.2.2.4 Culture of the packaging cell line, HEK293 cells

HEK293 cells were maintained in T75 flasks in Dulbecco's modified Eagles medium (DMEM, Invitrogen) supplemented with 10% (v/v) FCS (Invitrogen), 50 U penicillin and 100 µg streptomycin (Penicillin-Streptomycin, Invitrogen). When confluent, the medium was removed and 1 ml Trypsin (0.5% (v/v00 in 5.3 mmol/L EDTA (Invitrogen) was used to detach cells from the surface of the flask. DMEM (10 ml) was

then added to the cell suspension, and 1.5 ml was transferred to each new T75 flask containing 13.5 ml fresh culture medium. Cells were passaged every 2-3 days. For experiments, cells were seeded onto 28 mm culture dishes (1 ml of detached cell suspension added to 1 ml of fresh medium) or larger T175 flasks for virus amplification (3 ml of detached cell suspension added to 22 ml of fresh medium).

5.2.2.5 Transfection of HEK293 cells with the adenoviral DNA

rAd5-GOI DNA (10 µg) was digested with 100 U *Pac*I in 1x NEBuffer 1 and BSA at a final concentration of 100 µg/ml in a total volume of 100 µl, overnight at 37^{o}C. An aliquot of the digestion was checked by electrophoresis on a 1% agarose gel to ensure complete digestion of the plasmid. Digested DNA was purified by isopropanol precipitation. 1 volume of isopropanol and 0.1 volumes of NaOAc were added to the digested DNA and mixed well. DNA was pelleted by centrifugation at 16,000 rpm for 15 min (4^{o}C), and the pellet washed with 0.5 ml 70% ethanol before a final centrifugation at 16,000 rpm for 5 min (4^{o}C). Centrifugation steps were carried out in an Eppendorf bench-top centrifuge (5417R). Ethanol was removed and the pellet allowed to air dry for 10-15 min, before resuspension of rAd5-GOI in 20 µl TE, pH 8.0 overnight at 4^{o}C.

HEK293 cells, cultured as described in the previous section (Section 5.2.2.11) were plated at 6 x 10^5 cells per well in a 6-well plate that had been incubated overnight at 37^{o}C, so cells were approximately 50-60% confluent (but not more than 70% confluent) prior to transfection. All of the linearised rAd5-GOI viral DNA was used to transfect HEK293 cells using the Polyfect transfection reagent (Qiagen). 20 µl linearised virus DNA was mixed with 80 µl OptiMEM and 20 µl Polyfect in an Eppendorf tube, flicked to mix (to minimise risk of shearing the DNA) and allowed to incubate at room temperature for 10 min. 600 µl DMEM was added to the transfection mix, 600 µl DMEM removed from the well of HEK293 cells to be transfected, and all of the transfection mix added to the well of cells, taking care not to disturb the cell monolayer. Transfected HEK293 cells were incubated at 37^{o}C/5% CO_2 for 14-20 days, until most cells exhibited cytopathic effects, and CFP/YFP expression monitored from 5-7 days.

5.2.2.6 Large scale amplification, purification and titration of recombinant adenovirus

HEK293 cells were plated at 6 x 10^5 cells per well in a 6-well plate and subsequently incubated overnight at 37^{o}C, so cells were approximately 50-60% confluent (but not more than 70% confluent) prior to adenoviral infection. The adenovirus was added directly to the well of cells in a careful manner so as not to disturb the monolayer. Infected HEK293 cells were incubated at 37^{o}C/5% CO_2 until cell lysis was observed (usually 2-3 days).

Virus replication within HEK293 cells results in cell lysis, which is observable through the 'rounding up' and detachment of cells from the surface of the culture plate. Following infection of HEK293 cells with adenovirus, CFP/YFP expression was monitored, and was seen to occur in localised areas or patches of cells, indicating the replication and release of adenoviruses and infection of nearby cells for further viral replication. When approximately 50% of HEK293 cells were either 'rounded up' or detached of the surface of the culture dishes (2-3 days after adenoviral infection), cells were scraped up into the medium (2 ml) using a cell scraper and transferred to a 15 ml Falcon tube. Cells were lysed by three cycles of freezing in liquid nitrogen, followed by thawing in a water bath at 37^{o}C and vortexing. The cell debris was pelleted by centrifugation at 800 x *g* for 10 min, and the supernatant gently added to the medium of HEK293 cells grown to 70-80% confluence in a T75 flask.

The next rounds of viral replication were generally more rapid, and the majority of HEK293 cells were detached 2-3 days after infection. Cells were scraped into the medium of the flask, pelleted by centrifugation at 800 x *g* for 10 min, and all but 2 ml of supernatant removed before the above process of freeze-thawing and re-infection was repeated, until finally ten T175 flasks of HEK293 cells had been infected with the adenovirus.

Cells from the ten T175 flasks were scraped into the media, cells pelleted at 800 x *g* for 10 min, and all of the supernatant removed. The cell pellet was resuspended in 2 ml PBS per adenovirus being amplified, subjected to three cycles of freeze-thawing, and cell debris pelleted by centrifugation at 800 x *g* for 10 min. The supernatant was transferred to a fresh tube for purification of the adenovirus.

5.2.2.7 Purification of adenovirus

A discontinuous CsCl gradient was set up in an ultracentrifuge tube, with 4 ml 1.4 g/ml CsCl (heavy) and 1.25 g/ml CsCl (light). The cleared virus suspension was gently overlaid onto the gradient, and centrifuged at 20,000 rpm for 2 hr (20^{o}C) with slow acceleration and no brake, in a Sw41 Ti swing-out rotor (Beckman. After centrifugation, two viral bands were visible on the gradient, the lower of which is close to the interface between the two phases and contains the intact adenovirus, which was removed with a needle and syringe in a volume of approximately 2 ml. The purified virus was transferred to dialysis tubing and dialysed against autoclaved virus dialysis buffer (10% (v/v) glycerol, 1 mmol/L $MgCl_2$, 10 mmol/L Tris, pH 7.4) over 24 hr at 4^{o}C with 3-4 buffer changes, to remove the CsCl. The virus was stored in aliquots at -80^{o}C.

5.2.2.8 Calculation of MOI

To determine the titre of the purified adenovirus, HEK293 cells were seeded into a 96-well plate and allowed to adhere for 24 hr, at which point they had reached approximately 70-80% confluence. The purified viral stock was subjected to serial dilution in DMEM culture medium, from 10^{-5} to 10^{-11}, and 10 µl of diluted viral stock added to the 90 µl medium in each well of a 96-well plate. Each serial dilution of adenovirus was added to a whole row of the plate, as shown below, and DMEM culture medium alone was added to the final row.

Cells were incubated at 37^{o}C/5% CO_2, the medium was replaced in wells that were not obviously infected after 5 days and the plate was scored for infection after 8 days, using CFP/YFP expression, by visualisation of the cells using a fluorescence microscope and UV lamp. Any well containing any infected CFP/YFP-expressing cells was scored positive, and any well containing exclusively uninfected cells was scored negative. The number of wells infected at each serial dilution of the adenovirus were tabulated as the percentage of cells infected and used to determine the virus titre using the equation described by Nicklin and Baker.[302]

Calculation of the PFU of an adenovirus:

Proportionate distance, PD = (A-50)/(A-B)

A = % response greater than 50%

B = % response less than 50%

$Log_{10}(TCID_{50})$(infectivity dose) = log of dilution giving a response > 50% - PD

Final virus titres:

Epac1-camps **1.85×10^{10} PFU/ml**

PLM-Epac1-camps **4.31×10^{10} PFU/ml**

5.2.3 Transfection of plasmid constructs in HEK293 cells

HEK293 cells, cultured as described in Section 5.2.2.11, were plated at 6×10^5 cells per well in a 6-well plate that had been incubated overnight at 37°C, so cells were approximately 50-60% confluent (but not more than 70% confluent) prior to transfection. 2 μg of plasmid DNA was used to transfect HEK293 cells using the Polyfect transfection reagent as described in Section 5.2.2.12. Transfected HEK293 cells were incubated at 37°C/5% CO_2 for 48 hr.

5.2.4 Isolation and culture of ARVMs

The experiments in this chapter were performed using ARVMs isolated from the hearts of adult (250 – 300 g body weight) male Wistar rats (B & K Universal), as described in Chapter 2 (Section 2.3.1). Cells were maintained in culture for biochemical analysis, as described in Section 2.3.3.2.

5.2.5 Adenoviral infection of ARVMs

ARVMs maintained in culture overnight were counted in three different fields (top, middle and bottom of well) of two wells of each 6-well culture plate, using an eye-piece graticule under 100x magnification, covering an area of 1 mm^2. ARVMs were counted if they crossed the top and right borders of the grid, but not if they crossed the bottom or

left borders, and cells were averaged to obtain the mean number of cells per mm^2, which was subsequently multiplied by 962 (to account for the area of each well of a 6-well culture plate) to calculate the number of cells per well.

This was used to calculate the volume of virus to add to each well to achieve the desired multiplicity of infection (MOI), using the following equation:

Volume added (µl) = (Required MOI x number of cells)/(PFU/µl)

ARVMs were infected with adenovirus after the culture medium was replaced, at varying MOIs (10, 30, 100, 300 and 1000). ARVMs were incubated with the adenovirus for 24, 48 or 72 hr at 37^oC/5% CO_2 without replacement of the culture medium.

5.2.6 Fluorescence confocal microscopy

All of the work described in Section 5.2.6 was undertaken with the assistance of our 'in-house' confocal microscopy technician Dr Peter Stevenson.

5.2.6.1 Principles

In laser scanning confocal microscopy, a point light source (laser) is projected through an objective onto a specific object plane of a fluorescent specimen. To generate an image of the whole object plane, the specimen is scanned point- by- point and line-by-line through the use of a computer-controlled x-y axis light deflection system. The resulting sequence of florescent light points are captured by the same objective lens and focused onto a photomultiplier (converting the optical signal into electrical signals) via a dichroic mirror. Any reflected excitation light captured by the objective is deflected away by this dichroic mirror, ensuring that only emitted light can reach the photomultiplier. The electrical output from the photomultiplier is relayed to the computer and is built into the image that is displayed on the monitor.

5.2.6.2 Preparation of ARVMS for confocal microscopy

The culture medium was aspirated from ARVMs maintained in culture and infected with adenoviruses, and cells were washed with 2 ml of PBS which was removed immediately by aspiration. For some experiments, live myocytes were directly imaged with confocal microscopy. In other cases, myocytes were fixed by incubation in 4% (v/v) paraformaldehyde (Agar Scientific; 1 ml per well) in PBS for 10 min, washed in 2 ml PBS (3 x 5 min washes) and stored at 4^{o}C in PBS. One drop of Lisbeth's medium (30 mmol/L Tris, pH 9.5, 70% (v/v) glycerol, 5% (w/v) n-propyl gallate) was applied to the cells and a cover slip put on top. The edges of the plate were removed and cells mounted onto a glass microscope slide using glue to attach the dish to the slide, and nail varnish to secure the cover slip. Slides were stored at 4^{o}C until examination under the confocal microscope.

5.2.6.3 Fluorescence cell imaging and FRET monitoring

Fluorescent images of specimens were acquired by confocal laser scanning on a Leica Sp5 II system equipped with Argon lasers (458, 476, 488 and 514 nm), Helium-Neon lasers (HeNe 543 and 633 nm) and a UV-diode (405 nm). Optical slices (~ 1 μm) of ARVMs were captured using a HCX L APO CS 63x/1.4 oil immersion lens, a frame size of 1024 x 1024 pixels at a pixel depth of 8 bit, a scan frequency of 400 Hz (4 frame average), and an exposure time of 30 ms. The excitation and emission/detection wavelengths for the fluorescent proteins used in confocal microscopy experiments are detailed in Table 5.1. Fluorescent images were background-corrected by subtracting autofluorescence intensities of untransfected cells (or background with no cells) from the emission intensities of fluorescent cells expressing the sensors. The ratios of cyan-to-yellow emissions were then calculated at different time points and normalised by dividing all ratios by the emission ratio just before stimulation, thereby setting the basal emission ratio to 1.0. Further image processing was carried out using LAS AF software (Leica).

Table 5.1 Excitation wavelengths and emission collection spectra for CFP and YFP used in confocal microscopy experiments.

Fluorophore	Excitation wavelength (nm)	Emission collection spectra (nm)
CFP	436	465-505
YFP	514	525-600

5.2.6.4 Acceptor photobleaching

FRET efficiency was determined by acceptor photobleaching; briefly, YFP was photobleached by intense illumination with a maximum laser output in the YFP channel (70x). CFP fluorescence intensities before and after YFP photobleaching was then calculated.

5.2.7 FRET monitoring using a dual photometer setup

ARVMs on coverslips were placed on an inverted NIKON microscope and excited at 436 nm. Emission of CFP and YFP was detected simultaneously through 470 ± 20 and 530 ± 25 nm band-pass filters placed inside two separate photo multipliter tubes. Data were digitised and FRET was expressed as a ratio of CFP to YFP signals, the value of which was set to 1.0 at the onset of experiments. Changes are expressed as percent deviation from this initial value of 1.0.

5.2.8 Pharmacological treatment of ARVMs

For assessment of agonist stimulation on FRET responses of the Epac1-camps and PLM-Epac1-camps, maximal concentrations of ISO or FRSK was added to ARVMs infected with the recombinant adenoviruses and the responses were measured using either fluorescence confocal imaging or the dual-photometer setup, as described in Chapter 3 (Section 3.2.2).

5.2.9 Sample preparation for SDS-PAGE

Adenovirally-infected myocytes in culture at 37^{o}C/5% CO_2 for 24, 48 or 72 hr were lysed with 2x SDS sample buffer and the proteins subsequently scraped off the wells as described in Section 2.5.2.

5.2.10 SDS-PAGE/Western blotting

SDS-PAGE/WB was used to detect the expression of Epac1-camps and PLM-Epac1-camps using antibodies against GFP, PLM-Ser63 and total PLM, as described in Chapter 2 (Section 2.5.5). The incubation times for each of the primary and secondary antibodies used are listed in Tables 2.5 and Table 2.6 respectively.

5.3 Results

5.3.1 Molecular structure of Epac1-camps and PLM-Epac1-camps

Epac1-camps consists of a single cAMP-binding domain of Epac1 (E157-E316) sandwiched between the GFP variants CFP and YFP. PLM-Epac1-camps comprises PLM at the N-terminus and Epac1-camps as a C-terminal tag. Figure 5.4 shows cartoons of the domain structure for each sensor.

Figure 5.4 Domain structure of FRET-based cAMP sensors used in confocal microscopy experiments.

(A) Epac1-camps, consisting of E157 – E316 of Epac1 sandwiched between CFP and YFP and (B) PLM-Epac1-camps, which has a full-length human PLM sequence (amino acids 1 – 92) attached to the YFP moiety of the original construct (adapted from 30).

5.3.2 Characterisation of Epac1-camps and PLM-Epac1-camps in HEK293 cells

5.3.2.1 Intracellular localisation pattern of plasmid constructs

The transfection efficiency of the plasmid constructs encoding for Epac1-camps and PLM-Epac1-camps in HEK293 cells was approximately 60% (data not shown). Epac1-camps showed a uniform distribution within the cell bodies while PLM-Epac1-camps was found to localise predominantly to membrane regions. Representative images are shown in Figure 5.5 [Panels A & B]. For both constructs, the CFP and YFP fluorescence signals were found to correspond to each other in both intensity and location, indicating that both the sensors were intact upon transfection, with the two fluorophores situated on the same protein [Figure 5.5; Panels A & B].

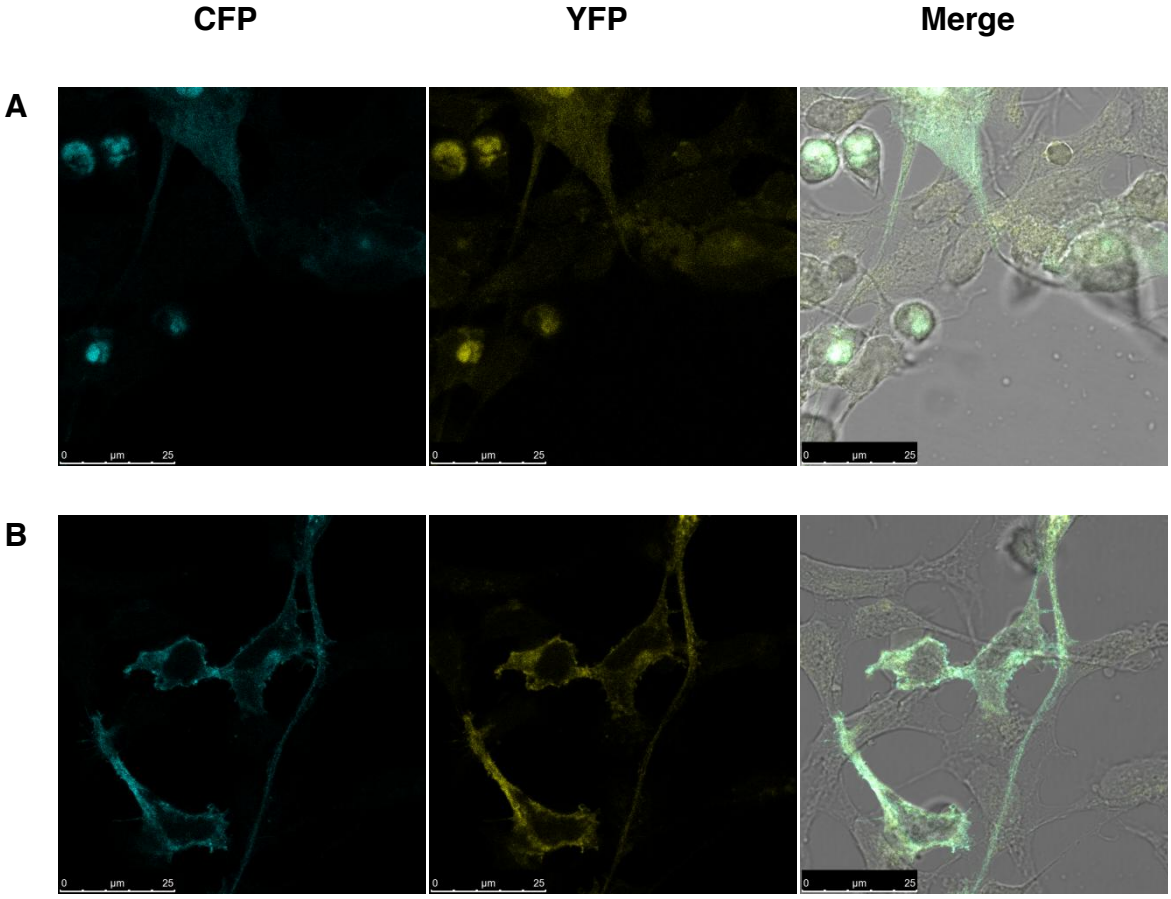

Figure 5.5 Intracellular localisation of FRET-based cAMP sensors in HEK293 cells.

Confocal microscopy images of HEK293 cells transfected with **(A)** Epac1-camps or **(B)** PLM-Epac1-camps. HEK293 cells that were approximately 50-60% confluent were transfected for 48 hr with Polyfect transfection reagent using 2 µg of plasmid DNA, and confocal microscopy was subsequently used to image the transfected cells. CFP and YFP fluorescence signals are displayed in separate channels, and a merged image of CFP and YFP is also shown. The CFP and YFP moieties were individually excited at wavelengths of 436 nm and 514 nm respectively.

5.3.2.2 Molecular weight of gene products

SDS-PAGE/Western blotting was carried out to check the size of the gene products being expressed. As deduced from the molecular weights of the individual components, Epac1-camps and PLM-Epac1 camps should have molecular weights of approximately 70 and 85 kDa respectively. Using both anti-GFP and anti-PLM antibodies, we observed bands corresponding to these theoretical weights for products expressed from both pcDNA constructs, and also from the pShuttle vector containing the GOI PLM-Epac1-camps. The recombinant virus expressing PLM-Epac1-camps could not be detected, likely due to the fact that it is a large plasmid and therefore is poorly

transfected in HEK293 cells. Our results indicated that the plasmid constructs were structurally intact upon transfection into HEK293 cells [Figure 5.6; Panels A & B].

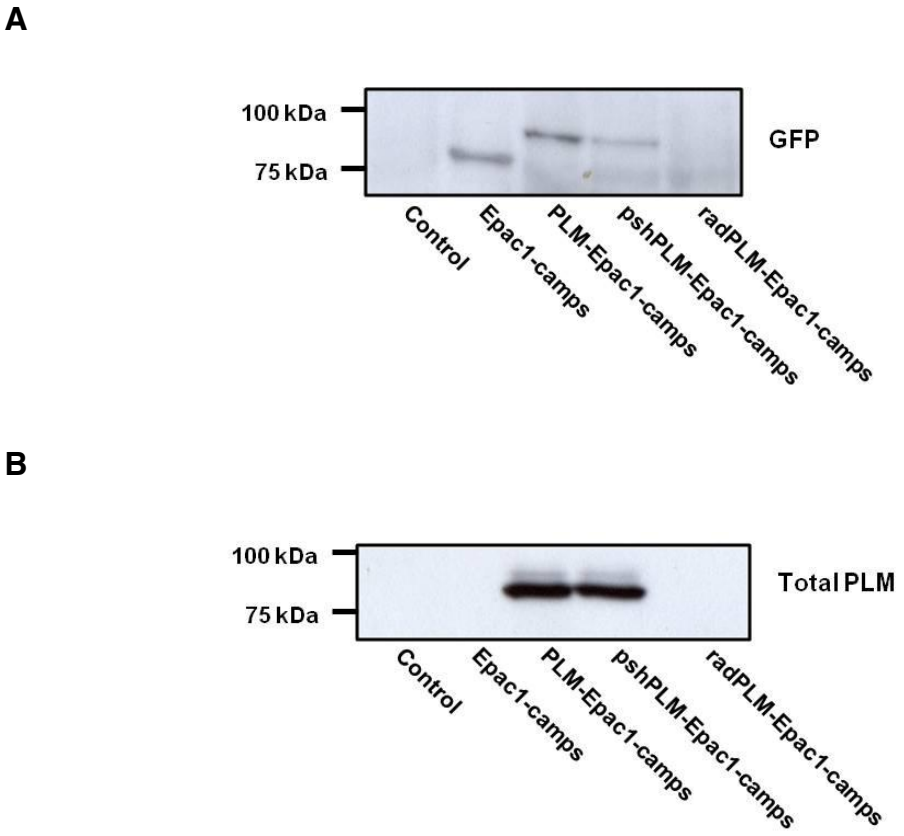

Figure 5.6 Molecular weight of plasmid gene products expressed in HEK293 cells.

Western blots of HEK cells transfected with pCDNA3 constructs encoding Epac1-camps and PLM-Epac1-camps, the pShuttle construct encoding PLM-Epac1-camps and the radPLM-Epac1-camps, a larger plasmid used in recombinant adenovirus generation.

For each construct, HEK293 cells were transfected with 2 µg of plasmid DNA using Polyfect transfection reagent. Cell lysates were subjected to SDS-PAGE (10% gel) and WB analysis using **(A)** anti-GFP or **(B)** anti-total PLM N1 antibodies. Blots are representative of at least three individual experiments.

5.3.3 Characterisation of Epac1-camps and PLM-Epac1-camps in ARVMs

In order to use these sensors as a tool in ARVMs, we incorporated the GOIs into adenoviral vectors. As in HEK293 cells, the intracellular expression patterns of the recombinant adenoviruses and molecular weights of the gene products in the infected

myocytes were investigated using confocal microscopy and SDS-PAGE/WB respectively.

5.3.3.1 Intracellular localisation pattern of recombinant adenoviruses

Figure 5.7 shows representative images of ARVMs that have been infected with the recombinant adenoviruses expressing Epac1-camps or PLM-Epac1-camps. The transfection efficiency of the recombinant viruses expressing the two sensors in ARVMs was approximately 40% at 300 MOI (data not shown). As observed in HEK293 cells, Epac1-camps was found to be distributed throughout the cytosol, but the fluorescence signals were determined to be more intense at the striations of the plasma membrane [Figure 5.7; Panel A]. In contrast, PLM-Epac1 was found to only minimally localise to the sarcolemmal membrane of ARVMs; rather, we observed a predominant localisation of the sensor to the perinuclear regions of the myocytes [Figure 5.7; Panel B], which is in direct contrast to confocal images previously generated by our laboratory showing an exclusive pattern of membrane staining by anti-PLM antibodies [Figure] For both cAMP sensors, the same pattern of expression was found across the different MOIs, although as expected, fluorescence intensities were greater with high MOIs. In all cases, CFP and YFP fluorescence signals obtained from infected ARVMs were found to correspond to each other in intensity and location, suggesting that the constructs remain intact upon adenoviral infection [Figure 5.7; Panels A & B].

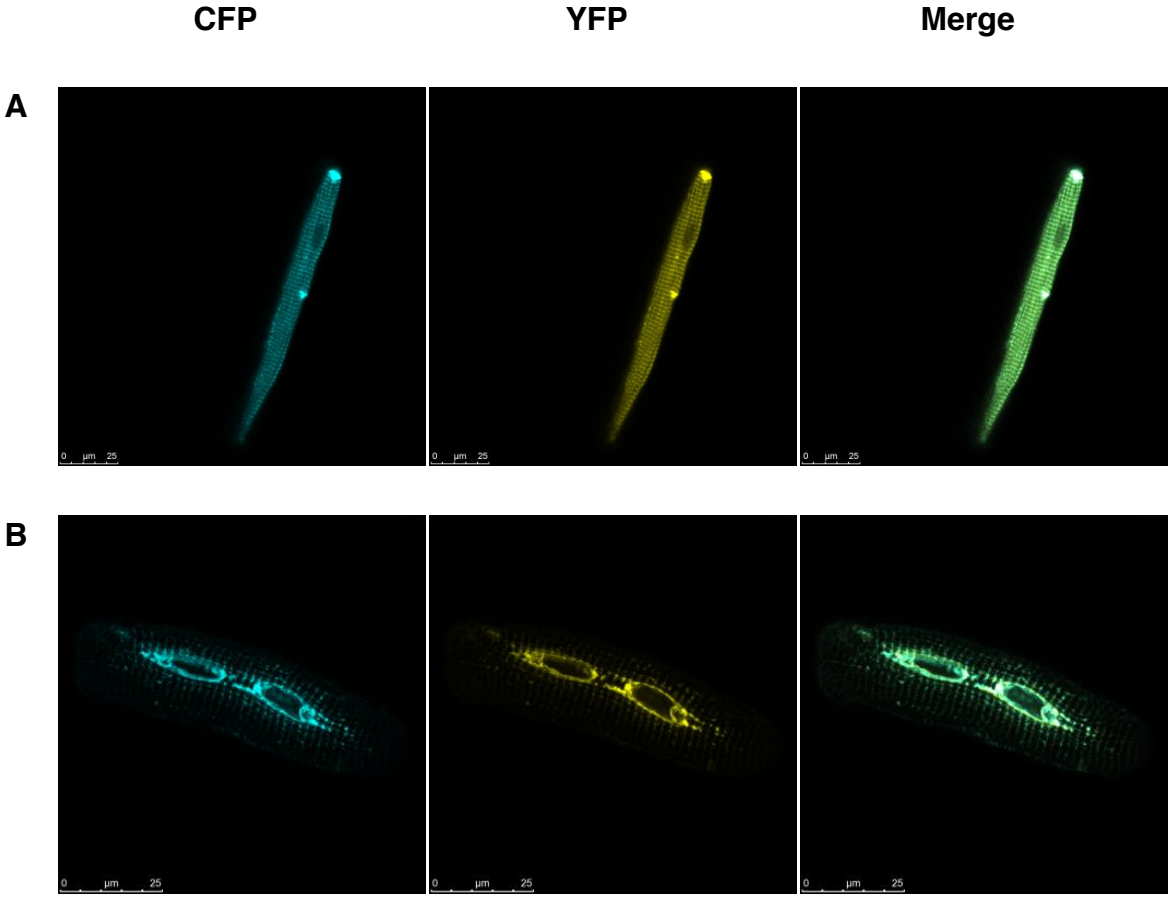

Figure 5.7 Intracellular localisation of FRET-based cAMP sensors in ARVMs.

Confocal microscopy images of ARVMs infected with **(A)** Epac1-camps or **(B)** PLM-Epac1-camps. ARVMs cultured overnight were infected for 48 hr with adenoviral vectors at 300 MOI and confocal microscopy was subsequently used to image the infected myocytes. CFP and YFP fluorescence signals are displayed in separate channels, and a merged image of CFP and YFP is also shown. The CFP and YFP moieties were individually excited at wavelengths of 436 nm and 514 nm respectively.

5.3.3.2 Molecular weight of gene products

To investigate the molecular weights of Epac1-camps and PLM-Epac1-camps in the recombinant adenoviruses, cell lysates from ARVMs that have been infected with adenoviral vectors expressing the constructs at a range of MOIs (10, 30, 100, 300 and 1000) for three different durations of infection (24, 48 or 72 hr) were subjected to SDS-PAGE/WB analysis using anti-GFP, anti-Ser63 and anti-total PLM antibodies.

To identify the molecular weight of Epac1-camps, we used an anti-GFP antibody to detect the CFP/YFP fluorophores (previous attempts at probing with an anti-Epac1 antibody produced no signals even after optimisation of the protocol) in ARVMs

infected with the recombinant adenovirus expressing Epac1-camps. Using the anti-GFP antibody, we observed a single band at approximately 37 kDa and a cluster of bands at 50 kDa region that seemed to be MOI-dependent, in contrast to the expected weight of 70 kDa [Figure 5.8; Panels A-C]. The number of bands was found to increase with a longer duration of infection [Figure 5.8; Panels A-C]. These observations were somewhat unexpected considering that the same antibody was used to pick up bands at approximately 70 kDa in HEK293 cells transfected with the plasmid construct [Figure 5.6; Panel A].

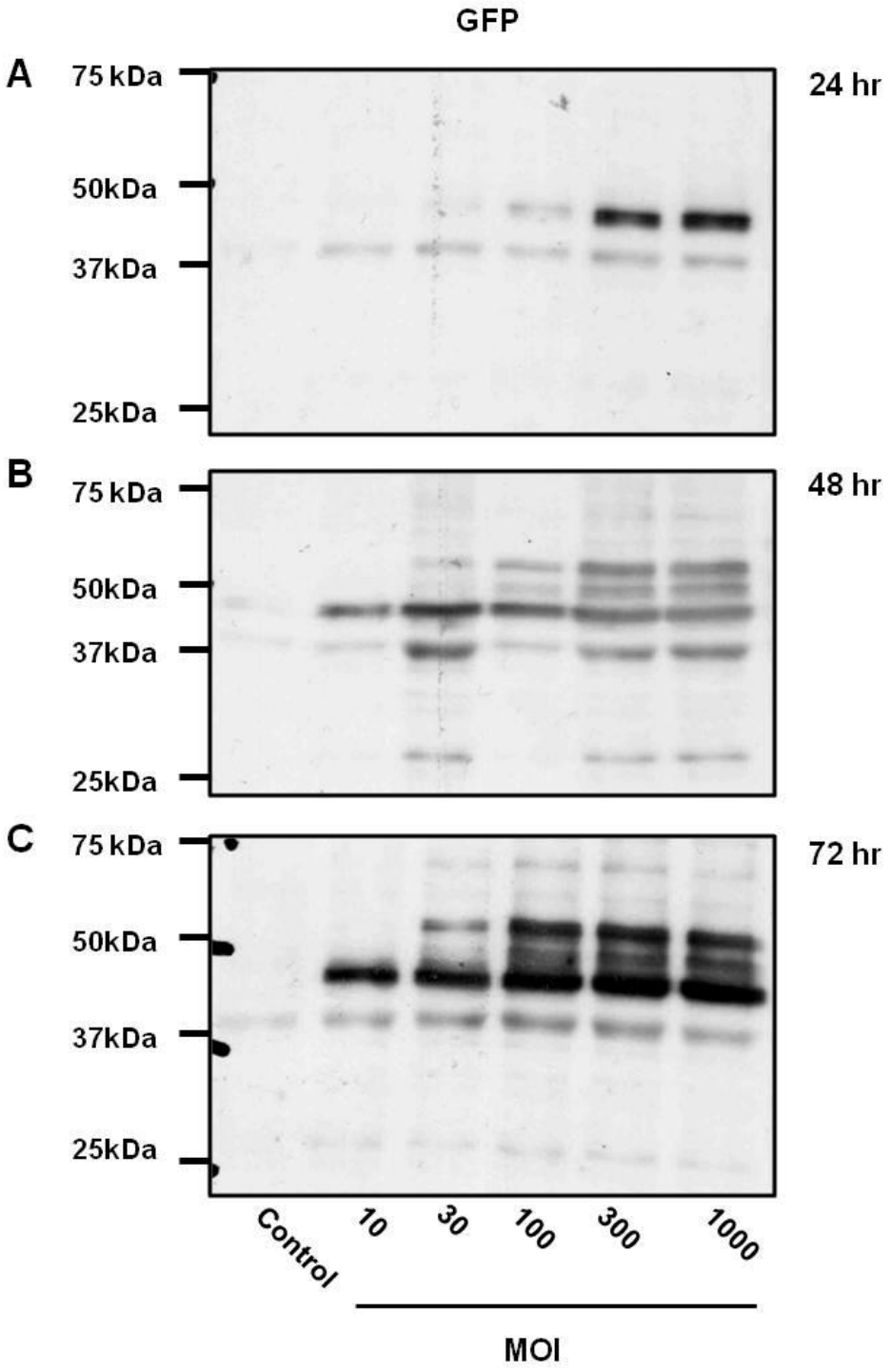

Figure 5.8 Molecular weight of Epac1-camps expressed in ARVMs.

Western blots of ARVMs infected with Epac1-camps. ARVMs cultured overnight were infected for **(A)** 24 hr; **(B)** 48 hr or **(C)** 72 hr with the adenoviral vector at 10, 30, 100, 300 or 1000 MOI. Cell lysates were subjected to SDS-PAGE (10% gel) and WB analysis using an anti-GFP antibody. Blots are representative of at least three individual experiments.

A similar pattern of expression was detected with this antibody for expression of PLM-Epac1-camps at a single time-point [Figure 5.9]. In an attempt to produce a 'cleaner' signal, we used the anti-Ser63 antibody to detect the PLM portion of the sensor. As with the anti-GFP antibody, multiple sets of bands were observed using the anti-Ser63 antibody that were seemingly dependent on both MOI and duration of infection; a dominant band and a 'shadow' band at between 75 kDa and 100 kDa [Figure 5.10; Panels A-C] and another set of bands at the 50 kDa region [Figure 5.10; Panels A-C]. An almost identical pattern of expression was observed with the anti-total PLM antibody, although the signals generated seemed to be more pronounced across the MOIs [Figure 5.10; Panels A-C].

On the whole, the signals observed with either antibody after 24 hr were quite weak, while in ARVMs infected with PLM-Epac1-camps for 48 hr at 300 or 1000 MOIs, the expression level of the recombinant adenovirus reached an easily detectable level, and was quantitatively similar to the expression level of basal PLM, indicating the presence of an adequate amount of the protein being expressed in the ARVMs. After 72 hr, similar levels of expression were reached with infection at lower MOIs; however, the extra 24 hr of culture was found to result in an increased level of apoptosis. Hence structural and functional characterisation of PLM-Epac1-camps was carried out in myocytes that have been infected with the recombinant adenovirus at either 300 or 1000 MOI for 48 hr.

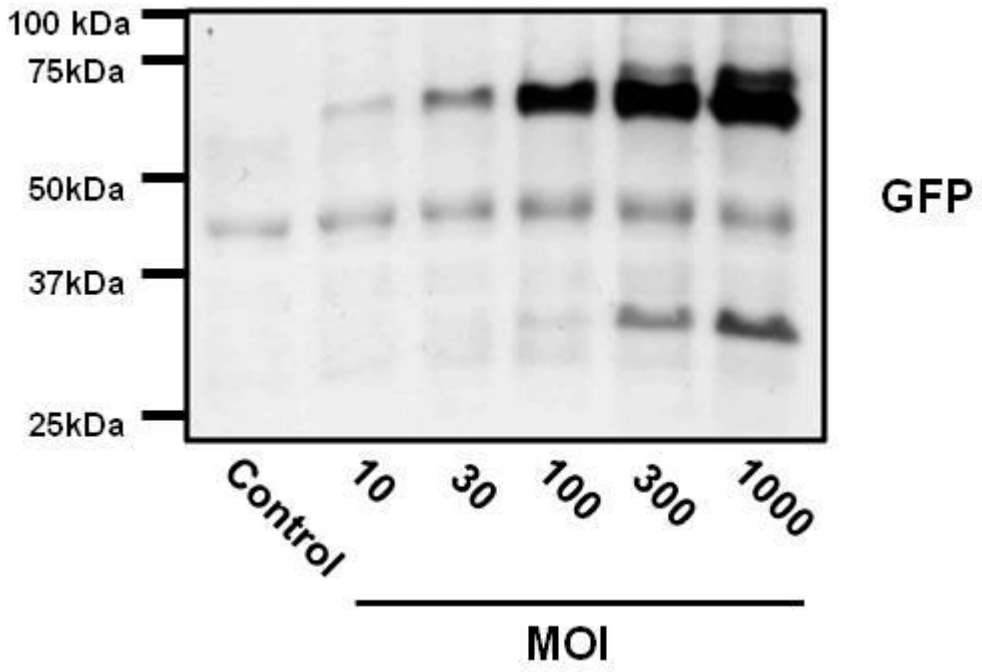

Figure 5.9 Molecular weight of PLM-Epac1-camps expressed in ARVMs.

Western blot of ARVMs infected with PLM-Epac1-camps. ARVMs cultured overnight were infected with the adenoviral vector at 10, 30, 100, 300 or 1000 MOI for 24 hr. Cell lysates were subjected to SDS-PAGE (10% gel) and WB analysis using an anti-GFP antibody. Blots are representative of at least three individual experiments.

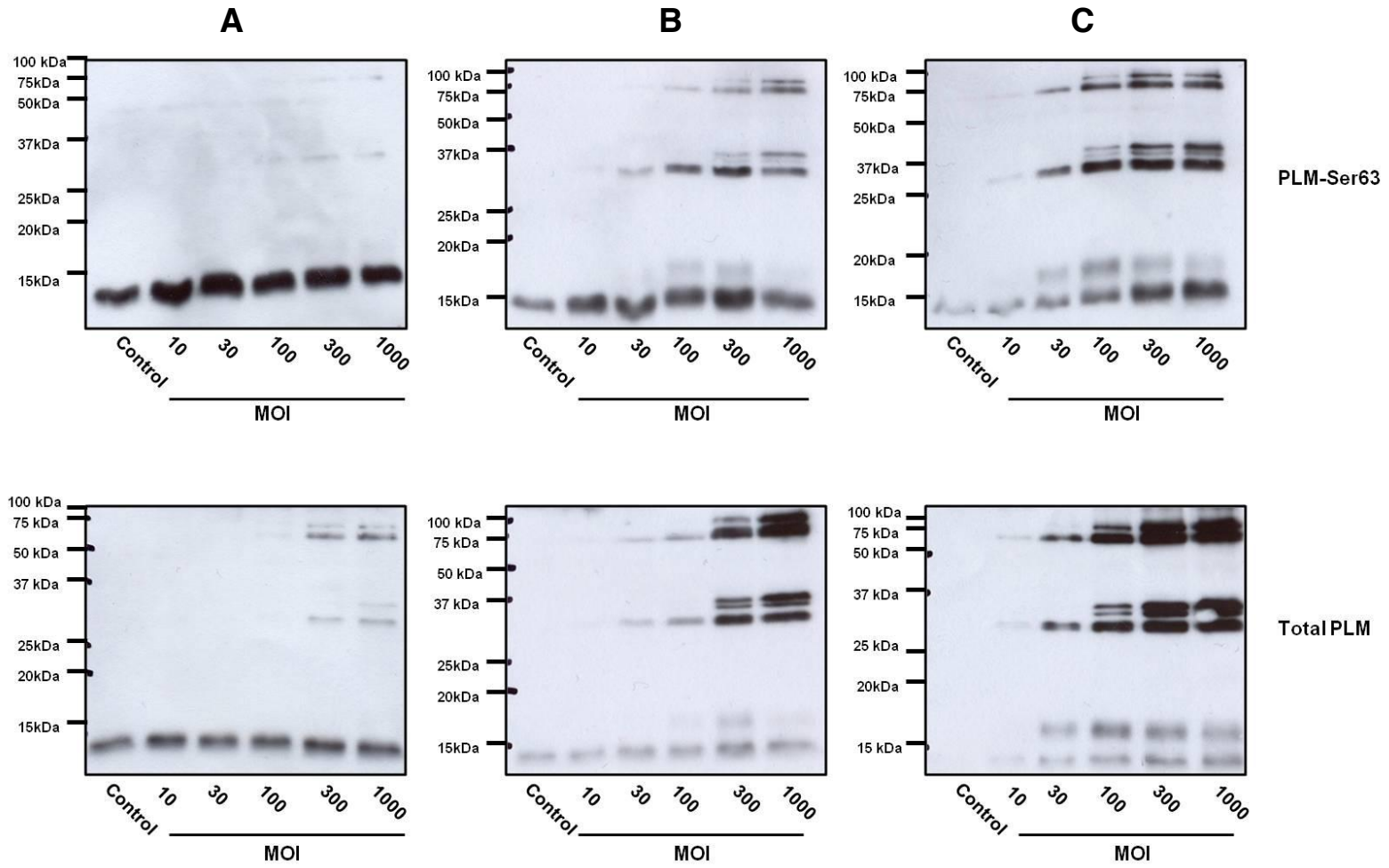

Figure 5.10 Molecular weight and relative expression level of PLM-Epac1-camps in ARVMs.

Western blot of ARVMs infected with PLM-Epac1-camps, in addition to native levels of PLM. ARVMs cultured overnight were infected with the adenoviral vector at 10, 30, 100, 300 or 1000 MOI for **(A)** 24 hr; **(B)** 48 hr or **(C)** 72 hr. Cell lysates were subjected to SDS-PAGE (10% gel) and WB analysis using either an anti-PLM-Ser63 antibody or anti-total PLM N1 antibody. Blots are representative of at least three individual experiments.

5.3.4 Functional characteristics of Epac1-camps and PLM-Epac1-camps

Following the structural characterisation of Epac1-camps and PLM-Epac1-camps in ARVMs, the functional characteristics of these sensors were assessed.

5.3.4.1 FRET monitoring in ARVMs

We previously made use of dual excitation of CFP and YFP to generate fluorescent signals; since FRET relies on transfer of energy between two fluorophores in proximity to each other – in this case, from CFP to YFP – we tested whether single excitation of CFP would result in both CFP and YFP emission and vice versa. For both Epac1-camps and PLM-Epac1-camps, CFP excitation at 436 nm was found to result in both CFP and YFP emissions [Figure 5.11; Panel B & Figure 5.12; Panel B], in an identical manner to the dual excitation of both fluorophores [Figure 5.12; Panel A & Figure 5.13; Panel A], while YFP excitation resulted in only YFP emission, with no CFP fluorescence detected [Figure 5.11; Panel C & Figure 5.12; Panel C]. This indicates the presence of FRET between the two fluorophores, thus implying that the sensors were functioning correctly.

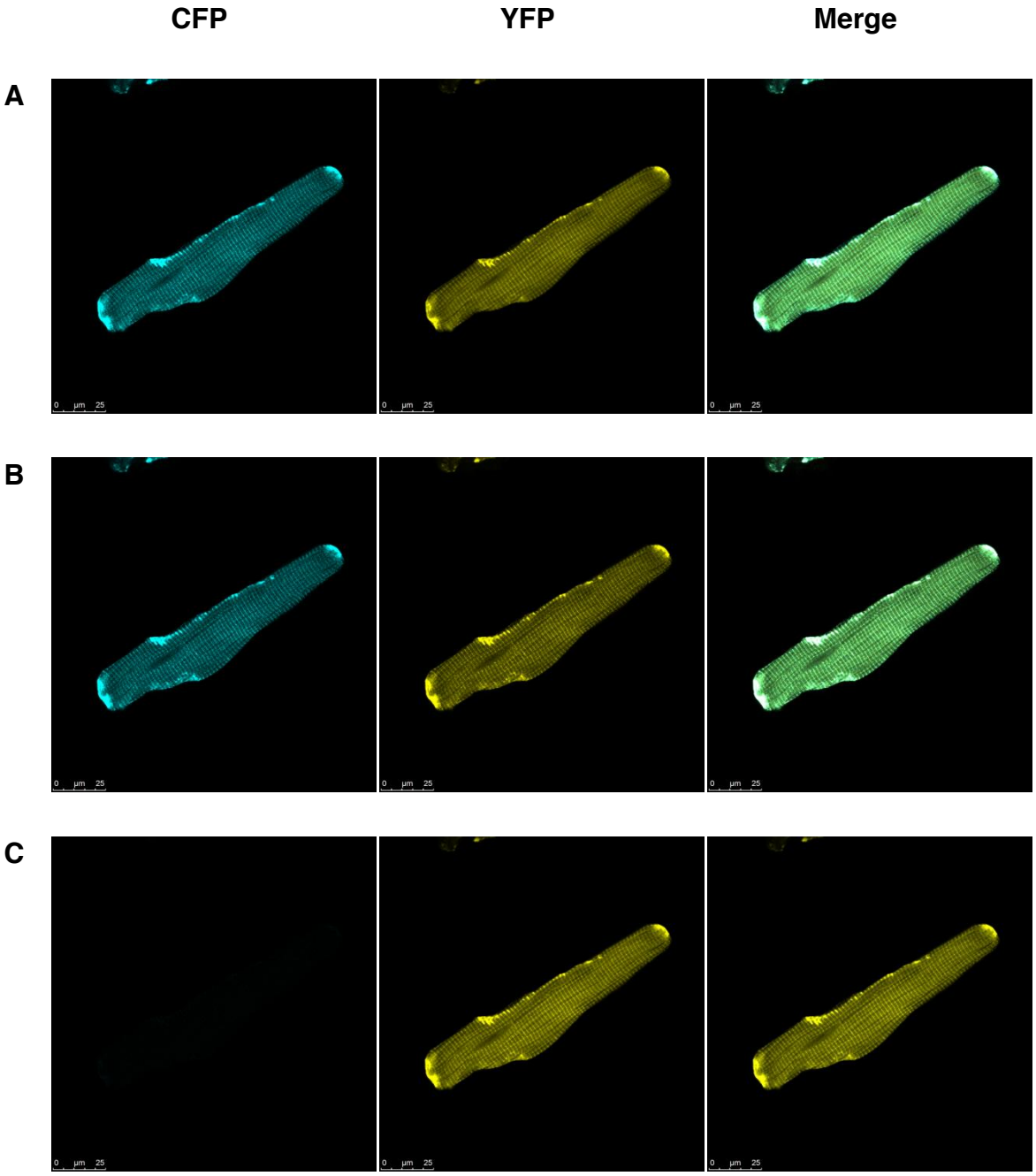

Figure 5.11 FRET monitoring of Epac1-camps in ARVMs.

Confocal microscopy images of Epac1-camps: **(A)** upon dual excitation of both CFP and YFP; **(B)** excitation of CFP only and **(C)** excitation of YFP only. ARVMs cultured overnight were infected for 48 hr with an adenoviral vector expressing Epac1-camps at 1000 MOI and confocal microscopy was subsequently used to image the infected myocytes. CFP and YFP fluorescence signals are displayed in separate channels, and a merged image of CFP and YFP is also shown. The CFP and YFP moieties were excited at wavelengths of 436 nm and 514 nm respectively.

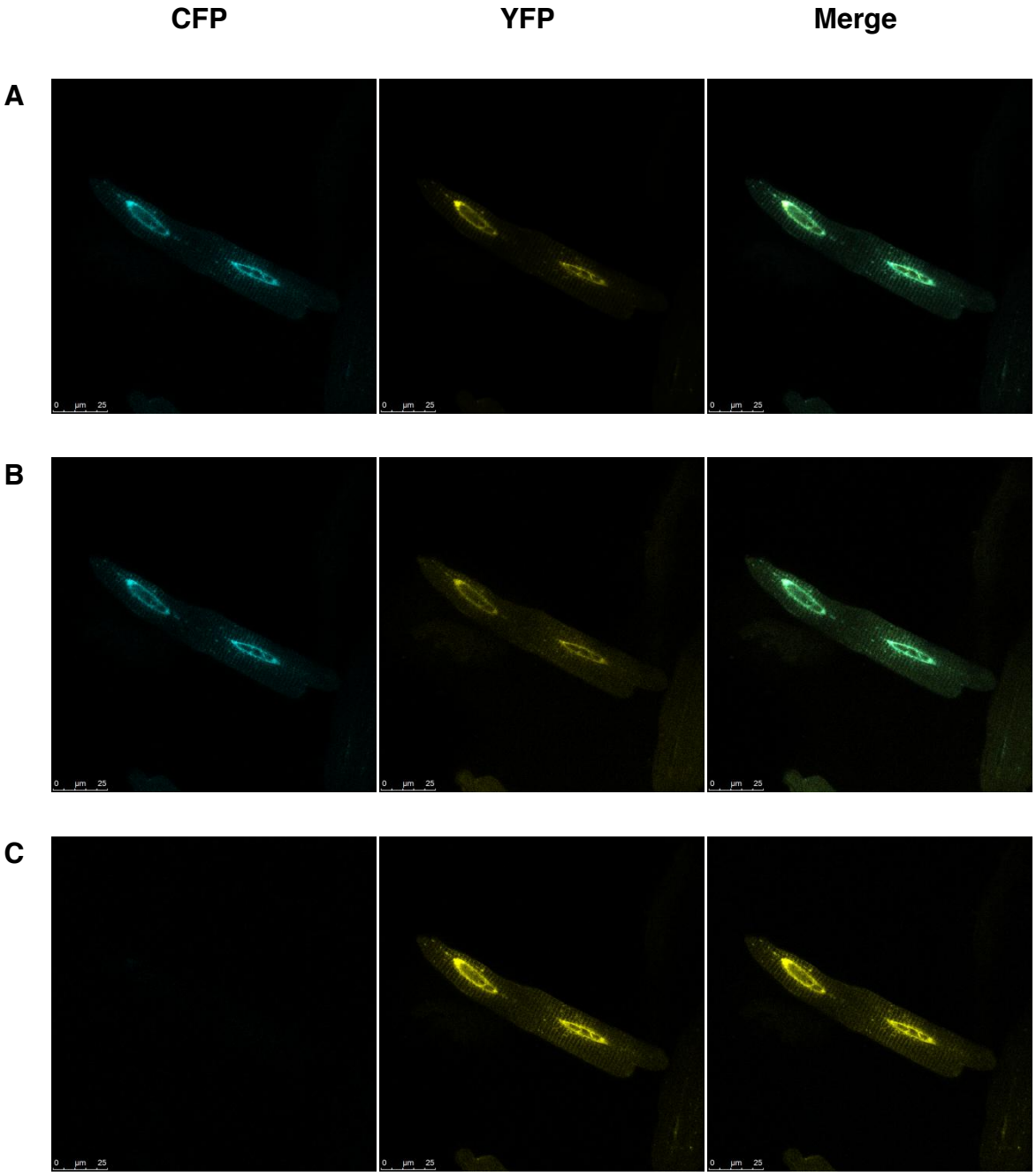

Figure 5.12 FRET monitoring of PLM-Epac1-camps in ARVMs.

Confocal microscopy images of PLM-Epac1-camps: **(A)** upon dual excitation of both CFP and YFP; **(B)** excitation of CFP only and **(C)** excitation of YFP only. ARVMs cultured overnight were infected for 48 hr with an adenoviral vector expressing PLM-Epac1-camps at 1000 MOI and confocal microscopy was subsequently used to image the infected myocytes. CFP and YFP fluorescence signals are displayed in separate channels, and a merged image of CFP and YFP is also shown. The CFP and YFP moieties were excited at wavelengths of 436 nm and 514 nm respectively.

5.3.4.2 FRET efficiency

The efficiency of FRET is defined as the proportion of donor molecules that transfer their excitation state energy to the acceptor molecules, and is a measure of the change in FRET signal in going from minimal to maximal cAMP levels. One way in which FRET efficiency can be determined is using acceptor photobleaching experiments. In this case, upon excitation of CFP, photobleaching of donor YFP molecules in selected regions of the myocyte using intense illumination for 60-120s was found to result in an increase in CFP fluorescence intensity (although not observable by eye, it was detected using computer software; see Figures 5.13 and 5.14; Panels A & B), suggesting that CFP and YFP are functionally sensitive to each other and capable of generating a FRET signal. Using this approach, FRET efficiency was determined to be approximately 20% for both constructs.

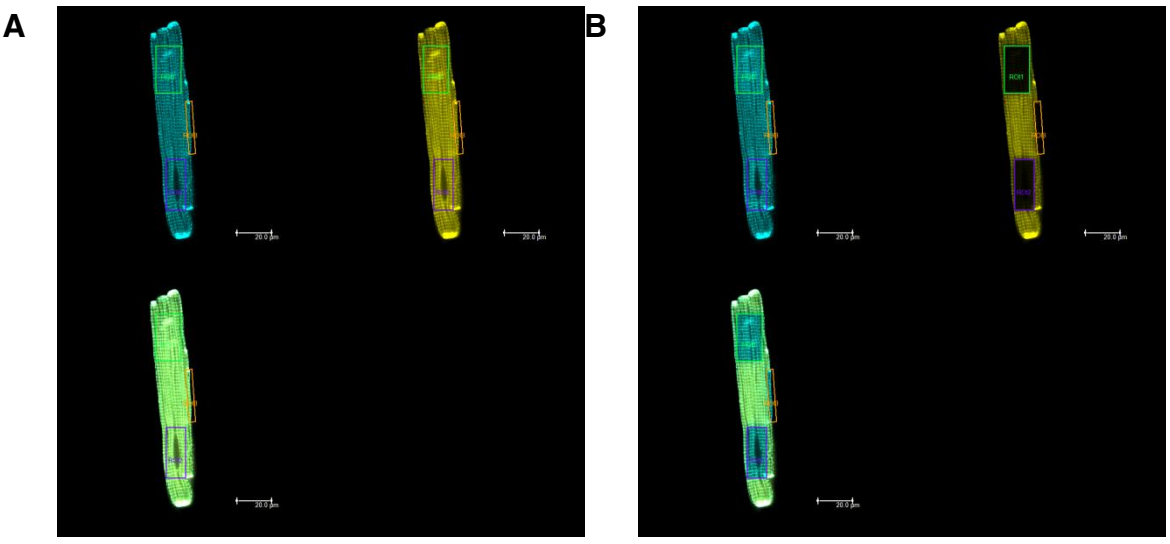

Figure 5.13 FRET efficiency of Epac1-camps in ARVMs.

Confocal microscopy images of Epac1-camps upon acceptor photobleaching. ARVMs cultured overnight were infected for 48 hr with an adenoviral vector expressing Epac1-camps at 1000 MOI and confocal microscopy was subsequently used to image the infected myocytes **(A)** before photobleaching of YFP and **(B)** after photobleaching of YFP moieties in selected regions of the myocyte with intense illumination. CFP and YFP fluorescence signals are displayed in separate channels, and a merged image of CFP and YFP is also shown. The CFP moiety was excited at a wavelength of 436 nm. FRET efficiency was determined to be ~20% (n=4).

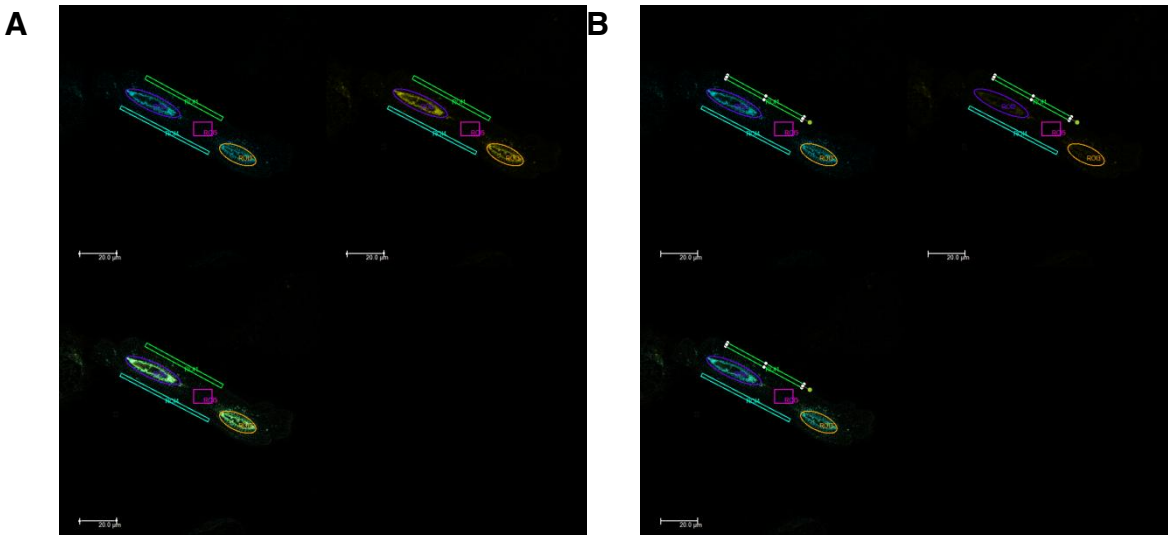

Figure 5.14 FRET efficiency of PLM-Epac1-camps in ARVMs.

Confocal microscopy images of PLM-Epac1-camps upon acceptor photobleaching. ARVMs cultured overnight were infected for 48 hr with an adenoviral vector expressing PLM-Epac1-camps at 1000 MOI and confocal microscopy was subsequently used to image the infected myocytes **(A)** before photobleaching of YFP and **(B)** after photobleaching of YFP moieties in selected regions of the myocyte with intense illumination. CFP and YFP fluorescence signals are displayed in separate channels, and a merged image of CFP and YFP is also shown. The CFP moiety was excited at a wavelength of 436 nm. FRET efficiency was determined to be ~20% (n=4).

5.3.4.3 FRET signal characteristics

Subsequent to our structural and functional characterisation of Epac1-camps and PLM-Epac1-camps, we attempted to characterise the amplitude and duration of the FRET signal in response to changes in $[cAMP]_i$ using fluorescence confocal microscopy and a dual-photometer setup.

5.3.4.3.1 Fluorescence confocal microscopy measurements

Using fluorescence cell imaging, a camp-dependent FRET change in response to the addition of a saturating concentration of ISO or FRSK was not observed for PLM-Epac1-camps, with no change in CFP or YFP fluorescence intensities after agonist treatment [Figure 5.15; Panels A & B].

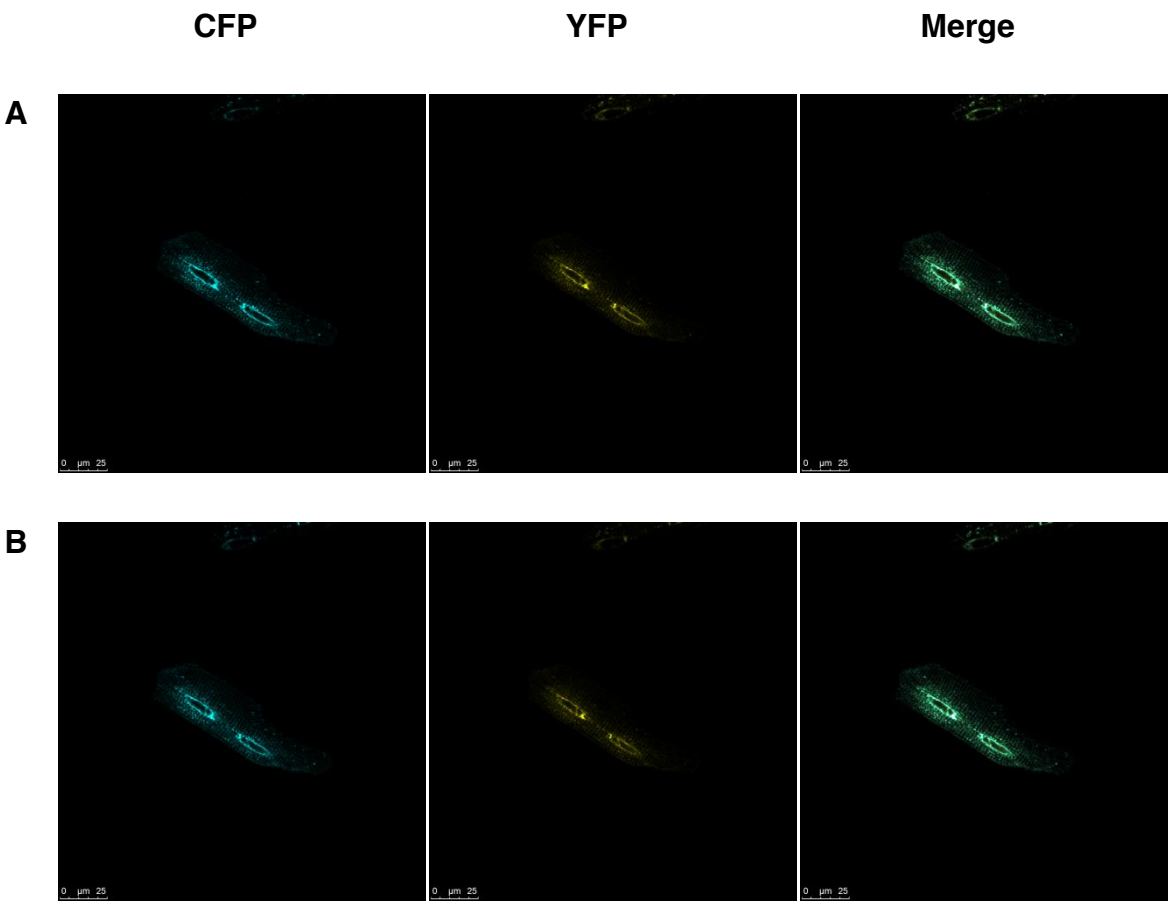

Figure 5.15 cAMP-induced FRET signal produced by PLM-Epac1-camps in ARVMs.

Confocal microscopy images of PLM-Epac1-camps (A) prior to treatment with ISO and (B) after treatment with 1 µmol/L ISO. ARVMs cultured overnight were infected for 48 hr with an adenoviral vector expressing PLM-Epac1-camps at 300 MOI and confocal microscopy was subsequently used to image the infected myocytes before and after addition of a saturating concentration of ISO to the myocytes. CFP and YFP fluorescence signals are displayed in separate channels, and a merged image of CFP and YFP is also shown. The CFP moiety was excited at a wavelength of 436 nm.

5.3.4.3.2 Dual photometer setup measurements

Figure 5.16 demonstrates the FRET response to an intracellular elevation of cAMP. Excitation of the CFP moiety in PLM-Epac1-camps at a wavelength of 436 nm led not only to CFP emission at ~480 nm but also to YFP emission at ~525 nm. Addition of a saturating concentration of FRSK resulted in a progressive reduction in YFP and increase in CFP fluorescence, demonstrating a loss in FRET (represented as the ratio of YFP to CFP emission).

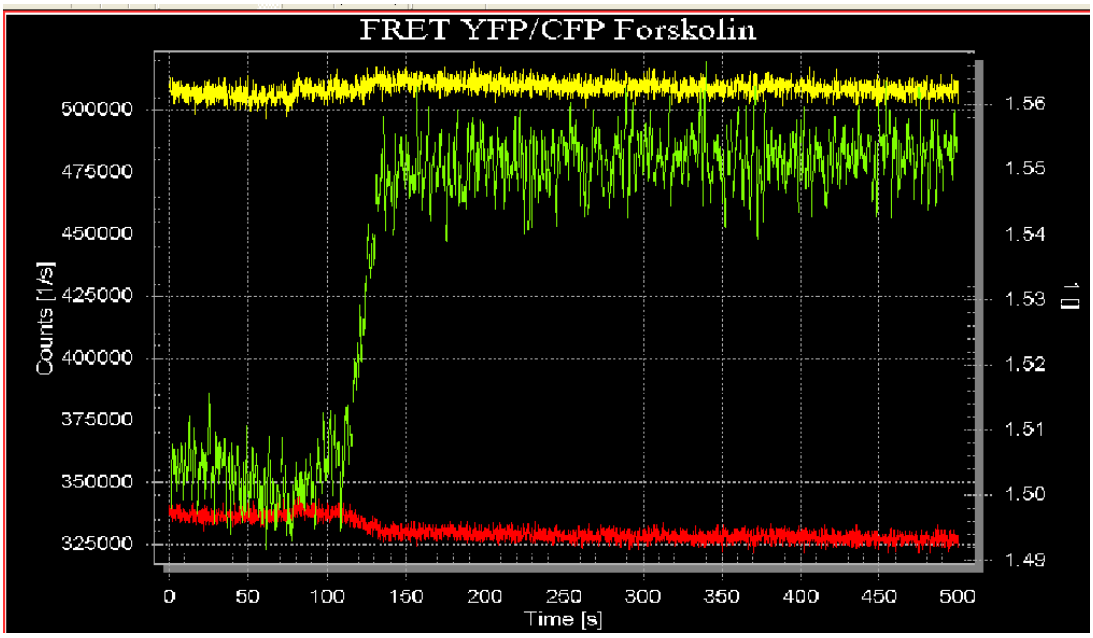

Figure 5.16 Quantitative assessment of cAMP-induced FRET signal produced by PLM-Epac1-camps in ARVMs.

Dual-photometer measurement of FRET signal generated by PLM-Epac1-camps in response to cAMP elevation with FRSK in ARVMs. ARVMs cultured overnight were infected for 48 hr with an adenoviral vector expressing PLM-Epac1-camps at 300 MOI and ratiometric measurements were made using a dual-photometer setup. A saturating concentration of FRSK was added directly to the myocytes during the experiment. CFP and YFP fluorescence signals are displayed in red and yellow respectively, while the green trace indicates the YFP/CFP ratio. The CFP moiety was excited at a wavelength of 436 nm. Trace is representative of three separate experiments.

5.4 Discussion

To develop a new generation of FRET-based cAMP reporters, several research groups have attempted to use the cAMP effector Epac as a backbone. It has been suggested that cAMP binding to Epac induces a conformational change that liberates the catalytic domain of Epac from intrasubunit allosteric inhibition.[299] In 2004, Ponsioen and co-workers generated a construct in which full-length Epac1was fused amino terminally to CFP and carboxyl terminally to YFP.[297] In the same year, DiPilato and co-workers generated a sensor based on Epac1 by sandwiching the full length protein between ECFP and citrine (an improved version of YFP) respectively, termed ICUE1.[296] Both of these sensors were shown to induce a cAMP-dependent FRET change in response to cAMP elevation. In contrast, Nikolaev and colleagues demonstrated that a single cAMP-binding domain is sufficient to generate a conformational change detectable by FRET, generating a construct based on the binding domain of Epac1 (E157-E316) sandwiched between CFP and YFP, termed Epac1-camps.[30] Based on structural data for cAMP binding to Epac1,[303] this implies that positioning of CFP and YFP directly on the cAMP-binding domain of these Epac proteins is sufficient to result in a change in the distance between the fluorophores in response to the cAMP-induced conformational switch. The fact that these sensors are catalytically active is all the more unexpected when considering that previous attempts at generating chimeric proteins based on various Epac truncations resulted in sensors that were either catalytically inactive and therefore unresponsive to cAMP elevation, or capable of only producing a weak FRET signal compared to the full-length construct.[297] This discrepancy could potentially be caused by use of different linkers connecting sequences of Epac and fluorescent proteins in individual constructs and the different cell types for testing these constructs.

In order to directly monitor cAMP dynamics at the membrane in the vicinity of PLM, PLM-Epac1-camps was generated (see Section 5.2.1), which we hypothesised to be specifically localised to the plasma membrane but otherwise possessing the same functional characteristics as Epac1-camps. As aforementioned, fusion of specific targeting motifs to the basic Epac1 sensor has been previously attempted. For instance, the attachment of ICUE1 to targeting motifs for the plasma membrane, nucleus and mitochondria has been shown to successfully localise the reporter to these particular regions of the cell.[296]

Our imaging experiments demonstrated that the expression pattern of the plasmid construct encoding for Epac1-camps in HEK293 cells was predominantly cytosolic (using both CFP and YFP fluorescence signals), which corresponds to initial observations by Nikolaev and colleagues, who found a uniform distribution of the sensor throughout the cytosol of CHO-A_{2B} cells.[30] They attributed this to the fact that the sensor contains only the cAMP-binding domain of Epac; on the other hand, the two aforementioned full-length Epac1 sensors were found not only to be localised to the cytosol, but also to the nuclear envelope and to perinuclear compartments, in addition to mitochondria.[296] In contrast, we observed using YFP fluorescence that approximately 60% of HEK293 cells transfected with the PLM-Epac1-camps construct displayed membrane localisation, consistent with the idea that under normal physiological conditions, PLM is selectively expressed in the sarcolemma of cardiac myocytes, and the inclusion of the PLM sequence in the construct should target the sensor exclusively to the membrane. We had initially expected a more predominant pattern of membrane localisation in these cells; the fact that we observed a cytosolic distribution of this reporter in some of the transfected HEK293 cells may reflect the possibility that the construct was being overexpressed in our experimental system, or the inherent differences between HEK293 cells (which do not normally express PLM) and ARVMs.

The use of monomolecular sensors records conformational changes that result in either the distance or the orientation of the probes (it is often difficult to experimentally distinguish between the two potential mechanisms) and has several advantages over sensors constituted of two separate proteins, such as PKA-based FRET sensors. One advantage is that unlike PKA probes, whereby the expression levels of the two fluorophore-labeled subunits have to be carefully matched to ensure reliable measurement, the two fluorophores on a monomolecular sensor are always expressed at a 1:1 stoichiometry if it remains intact. Furthermore, changes in the localisation and resultant artefact (such as fluorescence quenching) will affect both probes at the same time; as a result, intramolecular FRET will usually outweigh more complex interactions.

Importantly, for both Epac1-camps and PLM-Epac1-camps, we found equal expression levels of CFP and YFP upon individual excitation of the fluorophores at 436 and 514 nm respectively in virtually all of the transfected cells, with the localisation pattern and fluorescence intensities of the two fluorophores corresponding to each other in the vast

majority of cases. This suggests that the sensor was intact in these cell types and that the CFP and YFP moieties were attached to the same protein. These observations are consistent with our WB experiments using both the anti-total PLM N1 antibody and an anti-GFP antibody, with the bands observed corresponding to the respective molecular weights of the gene products, indicating that their structures remained unaltered after transfection of the plasmid constructs.

We subsequently incorporated the constructs into adenoviral vectors to allow their characterisation in ARVMs, and we investigated the pattern of expression in response to a range of MOIs. In imaging experiments, the uniform distribution of Epac1-camps in ARVMs observed across the different MOIs tested is generally consistent with its cytosolic localisation in HEK293 cells, although the fluorescence signal was observed to be greater at the striated junctions of the plasma membrane, suggesting that increased cAMP levels are present at the membrane regions surrounding the T-tubules, since one would not expect the sensor to be localised to these regions otherwise under normal circumstances. Interestingly, its localisation pattern is virtually identical to that of Epac2-camps in ARVMs, which we also investigated, suggesting that the cAMP binding domain of Epac proteins is preferentially targeted to sites with high [cAMP].

In contrast, we found that although there is some evidence for membrane localisation of PLM-Epac1-camps, the majority of the sensor population expressed was targeted exclusively to the perinuclear region in these cells, in sharp contrast to our hypothesised model of membrane localisation, based on previous observations of predominantly membrane staining of PLM in rat myocytes by our laboratory [Figure 5.17].

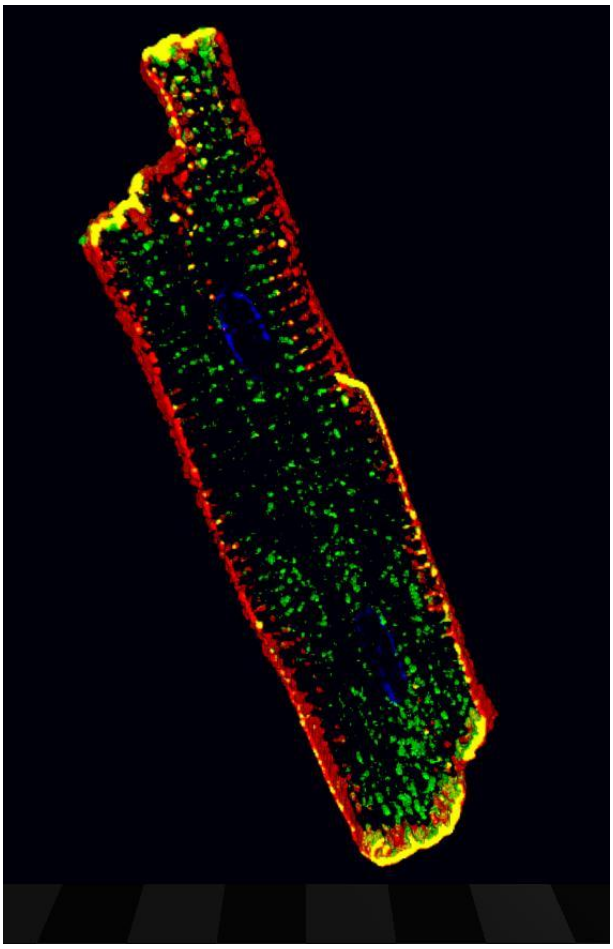

Figure 5.17 Membrane staining of PLM and NKA α1 subunit in ARVMs.

Confocal microscopy image of an ARVM immunolabelled with antibodies against PLM (red), the NKA α1 subunit (green), and co-localisation between PLM and the NKA (yellow). Nuclei were stained with DAPI (blue).

We initially proposed that this observation could be explained by the sensor being overexpressed, which led to incorrect intracellular trafficking of the sensor. Therefore, the relatively large fluorescence signal produced by the significant proportion of the protein that ended up in the perinuclear region would mask the significantly smaller signal generated by the sensor at the membrane. However, WB experiments demonstrated that even at 1000 MOI, the amount of PLM-Epac1-camps was not significantly higher than the amount of endogenous PLM normally present in ARVMs. Additionally, we found that the pattern of expression remained identical for both low and high MOIs, with little evidence of selective membrane localisation of PLM-Epac1-camps, suggesting that an inherent property of the sensor conferred incorrect trafficking and expression in this experimental system. This was surprising considering that the construct seemed to be expressed correctly in HEK293 cells, suggesting either an alteration of the molecular structure of PLM-Epac1-camps occurred in the process of

generating the recombinant adenovirus, or that the structure of the sensor was somehow incompatible with the trafficking system in cardiomyocytes.

As PLM-Epac1-camps was found to be not localised to the membrane, this suggested that PLM had been cleaved off either during the process of generating the recombinant adenovirus or after adenoviral infection in ARVMs. However, if this were the case, one would expect a uniform distribution of the truncated sensor within the cytosol, as PLM-Epac1-camps minus PLM would produce Epac1-camps. However, PLM-Epac1-camps was selectively targeted to the perinuclear region in our study. In WB experiments, probing with either the anti-Ser63 or anti-total PLM N1 antibody produced bands at approximately 75-85 kDa and 35-50 kDa for all MOIs investigated. The theoretical molecular weight of PLM-Epac1-camps is approximately 85 kDa. Additionally, we noticed that the gene product in the plasmid construct transfection experiments was also running at 75 kDa on our gels, suggesting that the structure of PLM-Epac1-camps in the adenoviral vector was intact but was running at 10 kDa below its theoretical weight.

This infers that one population of the sensor could have been structurally unaltered while the 35 kDa band suggested that in another population of PLM-Epac1-camps, approximately 40% of the gene product had been cleaved off, although at least a portion of the PLM sequence must have been intact as it could be detected by the relevant antibodies. Considering that PLM-Epac1 camps is constituted of PLM-YFP-Epac1-CFP (See Section 5.2.1 for further details), this population likely constituted the intact PLM sequence in addition to a portion of the YFP moiety. This implies that a third population of the sensor constituting the remaining portion of YFP, the cAMP binding site on Epac1, in addition to CFP, was present in the infected ARVMS, but could not be detected using the anti-PLM-Ser63 or the anti-total PLM N1 antibodies, as PLM was absent. Unfortunately, probing with an anti-GFP antibody revealed no further insights into the specificities of these truncated proteins as we detected a multiplicity of bands, most of them likely to be nonspecific for PLM-Epac1-camps or Epac1-camps. It remains unclear why the first population of PLM-Epac1-camps, which should have been relatively intact, was not targeted to the membrane, unless it too had undergone modification after adenoviral infection. We attempted to identify sites within the amino acid sequence of PLM-Epac1-camps that could be susceptible to degradation or alteration during intracellular trafficking, but the linker region between PLM and the

YFP moiety constituted approximately only three base pairs. It is possible that erroneous folding of the protein had occurred during incorporation of the GOI into the recombinant virus or after the adenoviral vector had been expressed in the myocytes.

Consistent with our observations in HEK293 cells, we found that the localisation patterns of CFP and YFP corresponded to each other upon individual excitation of the two fluorophores, with an equal level of intensity of the two fluorophores detected. On the whole, our findings suggest that the 75 kDa population of the sensor was primarily targeted to the perinuclear region and contributed to the CFP and YFP signals detected in the imaging experiments, while the 35 kDa population lacked intact YFP or CFP moieties, and therefore would not have contributed to the observed signals. What remains unclear is whether the third population contributed to the CFP signal, as it theoretically would have had an intact CFP moiety, although we found no discrepancy between the CFP and YFP channels in any of the infected myocytes that we investigated.

These findings, although unexpected, prompted us to investigate whether the intact population of PLM-Epac1-camps was catalytically active and capable of producing a cAMP-dependent FRET response upon cAMP elevation. FRET depends not only on the distance of the two fluorophores, but also on their spectral overlap and their relative orientation, and that the readouts can be affected by a number of parameters such as fluorescence quenching which require a number of careful controls.[304] One significant disadvantage of monomolecular cAMP reporters is that having two probes attached to a single protein generally produces less FRET, since the two probes will rarely move far away from each other to cause full loss of FRET. Particularly in the case of GFP variants such as CFP and YFP, the probes are large compared to the movements that they report, and they are quite flexibly attached to the proteins of interest, allowing for wide differences between the distances of the two probes and their attachment points. In most of the tested cells, significant FRET was observed, suggesting that CFP and YFP were in close proximity to each other. However, while FRET measurements indicate distances between the two probes, they do in general provide only relative information about distances between the attachment points in the proteins of interest. Therefore, these measurements, on their own without other structural information, are not really suited to elucidate molecular movements. However, they do indicate that

movements happen, and they reliably report when and where in a cell they happen. Indeed, in the course of designing new sensors, several constructs with fluorophores attached in different positions or with variable linkers between the GFP variant and effector molecule are often tested to maximise the efficiency of energy transfer, as is the case here.

The efficiency of FRET is defined as the proportion of donor molecules that transfer their excitation state energy to the acceptor molecules; this proportion depends on optimal (ideally parallel) orientation of the donor and acceptor dipoles. However, this is not often straightforward because while the molecular structures of the proteins to which the probes are attached are known, the structure of the overall sensor remains unclear, as is the case here. Relative FRET efficiency can be determined from the ratio of acceptor to donor fluorescence when the donor fluorophore is excited; in confocal imaging experiments, we found that upon single-channel excitation of CFP at 436 nm, fluorescent signals from both CFP and YFP were observed, suggesting energy transfer to YFP. However, care must be excised as the FRET signal might simply have resulted from the bleed-through of donor fluorescence into the acceptor detection channel, as we did not correct for the overlap between the closely matched excitation spectra of CFP and YFP.[305] We therefore proceeded to determine the FRET efficiency of these sensors by acceptor photobleaching and calculating the relative increase in donor emission.

Although precise intracellular environments may influence these values, the FRET efficiency of 20% for PLM-Epac1-camps was similar to that for Epac1-camps, and is highly consistent with the value obtained for Epac probes in general, suggesting that despite the unexpected pattern of localisation, PLM-Epac1 was capable of generating a FRET signal (although the increase in CFP emission was not discernible by eye). Likewise, we found that the change in the FRET response upon addition of saturating concentrations of ISO could not be detected using fluorescence confocal imaging; in this setting, the time taken to scan each image frame may limit the temporal resolution, and the higher intensity of the focused laser beam could result in greater photobleaching and loss of signal integrity over time. The most likely explanation for our observation is that our confocal microscope setup was not sensitive enough to detect the quantitatively small changes in the FRET signal.

In contrast, the relatively robust increase in YFP/CFP ratio as detected by the dual-photometer setup suggests that PLM-Epac1-camps is capable of generating a FRET signal in response to an elevation in intracellular cAMP concentration. The use of a saturating concentration of FRSK to directly activate AC-mediated production of cAMP meant that we could be sure a substantial rise in total intracellular cAMP levels had been induced, unlike ISO, which may increase cAMP concentration within specific intracellular compartments. *In vitro* studies have demonstrated that the affinity of the single cAMP-binding site on Epac is at least an order of magnitude lower than PKA;[303] as a result, many Epac-based sensors allow higher cAMP concentrations to be visualised at the expense of lower concentrations of the second messenger, since their K_D values generally lie between 14 and 50 μmol/L. This characteristic of PLM-Epac1-camps is particularly suited to investigating PDE function, since experiments involving the addition of a submaximal [ISO] followed by treatment with rolipram could lead to a significant degree of cAMP accumulation (akin to the PDE inhibition experiments described in Chapters 3 and 4), which could saturate probes with high sensitivity to cAMP. Indeed, awareness of the FRET efficiency and dynamic range for a given sensor is essential to appreciate the amplitude of any cAMP rise detected and to avoid misinterpretation of results, and further experiments are required to quantify the kinetic properties of PLM-Epac1-camps, including its dynamic range, sensitivity as well as its on- and off-rates.

In conclusion, our findings confirm that the binding domain of Epac, a protein that is highly expressed in many different tissues, provides an excellent backbone for fluorescent probes to monitor the dynamics of cAMP in ARVMs. PLM-Epac1-camps, the novel Epac-based cAMP reporter that we have generated, and whose structural and functional parameters have been partly characterised here, is potentially capable of measuring cAMP in the physiological range with high temporal and spatial resolution. Our finding that this particular sensor is displaying an 'incorrect' localisation pattern may reflect a particular structural defect that will need to be overcome. However, considering the encouraging functional characteristics observed to date, it is reasonable to propose that when used in conjunction with Epac1-camps, our novel sensor could be ubiquitously applied to study the regulation and biological functions of cAMP in cardiac myocytes in both the absence and presence of PDE inhibition.

6 FINAL CONCLUSIONS

PLM is the accessory protein to the cardiac NKA; it physically associates with the pump and is responsible for regulating its activity during sympathetic stimulation.

The primary objective of the project was to identify the possible roles that different PDE families within the heart may play in modulating cAMP-PKA dependent phosphorylation of PLM and how these translate into changes in NKA activity. As per this objective, the work described in this thesis has confirmed the involvement of individual PDE subtypes in the regulation of intracellular cAMP signalling to the cardiac PLM-NKA complex under neurohormonal stimulation, and provided some interesting insights into their roles which could be further explored in subsequent studies.

Our experimental model consisted of acute treatment of ARVMs with a number of family-selective PDE inhibitors in the absence and presence of ISO; changes in the biochemical and functional parameters of the PLM-NKA complex were subsequently assessed using biochemical and electrophysiological means. The consistently high basal phosphorylation level of PLM, including at the PLM-Ser68 site, could potentially compound investigation into PLM phosphorylation and/or NKA activity using pharmacological agents that raise intracellular cAMP and PKA levels. However, for each set of experiments, we were able to determine a suitable submaximal [ISO] that enabled the effects of the chosen PDE inhibitors to be accessed. Other practical considerations included the relative selectivity of each of the PDE inhibitors for the individual cardiac PDE subtypes of interest, in addition to the usage of ISO as a classical activator of the β-AR signalling pathway, and were experimentally justified based on comparison with the literature.

Collectively, our main findings consist of the identification of PDE4 as playing a predominant role in modulating PKA phosphorylation of PLM-Ser68, while both PDE2 and PDE4 seem to be important for regulating cAMP signalling to the NKA. The results have interesting implications as they suggest a scenario whereby intracellular cAMP signals to the NKA are modulated via the modulation of PKA-mediated PLM-Ser68 phosphorylation by PDE4, in addition to a yet identified mechanism involving

PDE2 activity that could potentially influence NKA function independent of PLM phosphorylation. The notion that PDE4 is involved in regulating cAMP signalling to the PLM-NKA complex is in accordance with the extensive body of both cell-based and *in vivo* findings underlining the predominant role of PDE4 in modulating cardiac function in the rodent heart upon β-AR stimulation. For example, it is known that PKA phosphorylation of a number of proteins and ion channels integral to the cardiac ECC process, such as PLB and the LTTC, are regulated to an extent by PDE4 activity. Our observation that PDE4-mediated changes in PLM-Ser68 status corresponds to a change in NKA activity is wholly consistent with the well-established role of PLM acting as a intermediate PKA target to functionally link the β-AR receptor with pump function during sympathetic activation.

Our series of biochemical experiments suggested potential differential roles of PDE4 in regulating PKA phosphorylation of ECC proteins, with the pattern of PLM phosphorylation subtly differing to those for PLB and cTnI. These data are consistent with the increasingly popular notion that individual isoforms within the PDE4 family may possess non-redundant functional roles, with the actions of the individual variants being localised to distinct intracellular compartments through physical coupling of the enzymes to the target proteins either directly or indirectly via intermediate protein scaffolds. Certainly, our finding that PDE2 may be responsible for modulating β-AR activation of NKA suggests the involvement of such compartmentalisation at play, considering the low relative activity of PDE2 in the rodent heart. What also remains unclear currently is the exact nature of the mechanism by which PDE2 modulates cAMP signalling to the pump. Since it seems to be able to modulate NKA activity without exerting a change in PLM phosphorylation status, it is possible that PDE2 activity may serve to indirectly influence pump function by regulating a component involved in other signalling pathways to PLM delineated to date, with glutathionylation or palmitoylation being possible mechanisms.

The conclusions that we have drawn serve to highlight some of the shortcomings of the pharmacological approach that was employed to investigate cardiac PDE function throughout this project. Firstly, selectivity of the inhibitors for the different PDE subtypes is by necessity relative and not absolute. This means that firstly, the idea of our results merely reflecting a product of 'dirty pharmacology', although unlikely,

cannot be completely ruled out. The other key disadvantage of these inhibitors is that they do not enable individual PDE isoforms to be studied, and different approaches are therefore required for investigating whether PDE2 and PDE4 modulate cAMP signals to the NKA in a compartmentalised manner.

The targeting of individual PDE isoforms to specific intracellular locations may require a physical association of the enzymes with a specific protein. Our efforts with the use of both a co-IP and peptide displacement approach to probe this possibility (see appendices) yielded little conclusive evidence of a physical interaction between cardiac PDE4 isoforms and PLM. Attempts to assess whether PDE2 isoforms are situated in proximity to the PLM-NKA complex remain ongoing, and could provide more concrete support of a compartmentalised model of PDE2 –mediated NKA function.

From a functional perspective, the generation and subsequent characterisation of two cAMP sensors should theoretically allow the intricate monitoring of cAMP dynamics within the myocyte in both the absence and presence of PDE inhibition. Such an approach relies on the correct targeting of the sensors, but the expression of PLM-Epac1-camps was found to be 'faulty' during our preliminary characterisation. Further work is clearly required in order to address the problems underlying this issue, although once resolved, the possibility of being able to measure subsarcolemmal gradients of cAMP in conjunction with real-time measurements of pump current using VPC in the presence of a PDE inhibitor (in the presence of ISO, FRSK or other membrane-permeable cAMP analogs) is highly encouraging. Such an approach could be further expanded to include the use of siRNAs and dominant-negative peptides, which would allow investigation into the contribution of selective PDE isoforms to regulation of cAMP signalling to the PLM, and using this potentially versatile experimental system would thus overcome any selectivity issues associated with the pharmacological inhibitors.

On the whole, considering the importance of the NKA in upholding normal cellular function – in particular its indirect control of the ECC process – it is only logical to suggest that the work described in this thesis has some physiological relevance central to our current understanding of PLM/NKA regulation. As aforementioned, it has recently been shown that PLM phosphorylation and cardiac NKA activity are negatively

regulated by PP-1, with this regulatory mechanism being counteracted by PP1-inhibitor 1.[237] Such a mechanism suggests a contribution of local kinase signalling to PLM and is markedly perturbed in failing hearts favouring PLM dephosphorylation and NKA deactivation and may therefore contribute to maladaptive hypertrophy and arrhythmogenesis via chronically elevated intracellular Na and Ca concentrations.[237] Thus termination of the cAMP/PKA signals to PLM is likely to be a crucial component of the regulation of NKA activity.

In the longer term, our observations of PDE-dependent modulation of PLM phosphorylation and cardiac NKA activity may serve not only as a foundation for further basic studies but may also support work with a more clinical orientation. Selective targeting of individual components of the Ca cycling process, such as PLB and SERCA, is increasingly viewed as a promising new therapeutic strategy for treating HF.[306] As such, it would be logical to propose that PDE2 and PDE4, being modulators of cAMP and thereby PKA signalling, could potentially be among the most important regulators of NKA activity during β-AR stimulation, and an undermining of their levels of expression and/or activity could potentially contribute to the progression of various pathologies, including cardiovascular diseases, as outlined in Chapter 1 (Sections 1.2.3 – 1.2.5). Indeed, selective PDE5A inhibition with sildenafil has been shown to rescue left ventricular dysfunction and cardiac remodelling in an *in vivo* HF model,[307] while it has been suggested the PLM-Ser69 phosphorylation could contribute to sildenafil-induced cardioprotection against reperfusion injury in the mouse via a NO/cGMP-dependent pathway.[308] Clearly, a greater understanding of how alterations in intracellular signalling related to individual PDE isozymes could potentially overcome some of the current difficulties encountered in the prevention and treatment of these diseases. Therefore, further investigation into the roles of several of the individual isoforms within the PDE and PDE4 families in both healthy and diseased hearts is likely to augment our current view of their roles in maintaining a balanced profile of NKA function under normal circumstances, and perhaps provide insights into novel therapeutic approaches in which the activity of individual PDE variants could be selectively targeted during cardiac dysfunction.

LIST OF REFERENCES

1. Fimia GM, Sassone-Corsi P. Cyclic AMP signalling. *J Cell Sci*. 2001;114(Pt 11):1971-1972.

2. Willoughby D, Cooper DM. Organization and Ca2+ regulation of adenylyl cyclases in cAMP microdomains. *Physiol Rev*. 2007;87(3):965-1010.

3. Bers DM. Cardiac excitation-contraction coupling. *Nature*. 2002;415(6868):198-205.

4. Petrashevskaya NN, Koch SE, Bodi I, Schwartz A. Calcium cycling, historic overview and perspectives. Role for autonomic nervous system regulation. *J Mol Cell Cardiol*. 2002;34(8):885-896.

5. Nikolaev VO, Moshkov A, Lyon AR, Miragoli M, Novak P, Paur H, Lohse MJ, Korchev YE, Harding SE, Gorelik J. Beta2-adrenergic receptor redistribution in heart failure changes cAMP compartmentation. *Science*.327(5973):1653-1657.

6. Hayes JS, Brunton LL, Brown JH, Reese JB, Mayer SE. Hormonally specific expression of cardiac protein kinase activity. *Proc Natl Acad Sci U S A*. 1979;76(4):1570-1574.

7. Corbin JD, Sugden PH, Lincoln TM, Keely SL. Compartmentalization of adenosine 3':5'-monophosphate and adenosine 3':5'-monophosphate-dependent protein kinase in heart tissue. *J Biol Chem*. 1977;252(11):3854-3861.

8. Keely SL. Prostaglandin E1 activation of heart cAMP-dependent protein kinase: apparent dissociation of protein kinase activation from increases in phosphorylase activity and contractile force. *Mol Pharmacol*. 1979;15(2):235-245.

9. Brunton LL, Hayes JS, Mayer SE. Hormonally specific phosphorylation of cardiac troponin I and activation of glycogen phosphorylase. *Nature*. 1979;280(5717):78-80.

10. Hayes JS, Brunton LL. Functional compartments in cyclic nucleotide action. *J Cyclic Nucleotide Res*. 1982;8(1):1-16.

11. Buxton IL, Brunton LL. Compartments of cyclic AMP and protein kinase in mammalian cardiomyocytes. *J Biol Chem*. 1983;258(17):10233-10239.

12. Farah AE. Glucagon and the circulation. *Pharmacol Rev*. 1983;35(3):181-217.

13. Juan-Fita MJ, Vargas ML, Kaumann AJ, Hernandez Cascales J. Rolipram reduces the inotropic tachyphylaxis of glucagon in rat ventricular myocardium. *Naunyn Schmiedebergs Arch Pharmacol*. 2004;370(4):324-329.

14. Vila Petroff MG, Egan JM, Wang X, Sollott SJ. Glucagon-like peptide-1 increases cAMP but fails to augment contraction in adult rat cardiac myocytes. *Circ Res*. 2001;89(5):445-452.

15. Bartel S, Krause EG, Wallukat G, Karczewski P. New insights into beta2-adrenoceptor signaling in the adult rat heart. *Cardiovasc Res*. 2003;57(3):694-703.

16. Xiao RP, Hohl C, Altschuld R, Jones L, Livingston B, Ziman B, Tantini B, Lakatta EG. Beta 2-adrenergic receptor-stimulated increase in cAMP in rat heart cells is not coupled to changes in Ca2+ dynamics, contractility, or phospholamban phosphorylation. *J Biol Chem*. 1994;269(29):19151-19156.

17. Kuschel M, Zhou YY, Spurgeon HA, Bartel S, Karczewski P, Zhang SJ, Krause EG, Lakatta EG, Xiao RP. beta2-adrenergic cAMP signaling is uncoupled from phosphorylation of cytoplasmic proteins in canine heart. *Circulation*. 1999;99(18):2458-2465.

18. Steinberg SF, Brunton LL. Compartmentation of G protein-coupled signaling pathways in cardiac myocytes. *Annu Rev Pharmacol Toxicol*. 2001;41:751-773.

19. Carr DW, Scott JD. Blotting and band-shifting: techniques for studying protein-protein interactions. *Trends Biochem Sci*. 1992;17(7):246-249.

20. Lohmann SM, Walter U, DeCamilli P. Interaction of the regulatory subunit (RII) of cAMP-dependent protein kinase with tissue-specific binding proteins including microtubule-associated proteins. *Ann N Y Acad Sci*. 1986;466:449-452.

21. Sarkar D, Erlichman J, Rubin CS. Identification of a calmodulin-binding protein that co-purifies with the regulatory subunit of brain protein kinase II. *J Biol Chem*. 1984;259(15):9840-9846.

22. Lohmann SM, DeCamilli P, Einig I, Walter U. High-affinity binding of the regulatory subunit (RII) of cAMP-dependent protein kinase to microtubule-associated and other cellular proteins. *Proc Natl Acad Sci U S A*. 1984;81(21):6723-6727.

23. Theurkauf WE, Vallee RB. Molecular characterization of the cAMP-dependent protein kinase bound to microtubule-associated protein 2. *J Biol Chem*. 1982;257(6):3284-3290.

24. Beene DL, Scott JD. A-kinase anchoring proteins take shape. *Curr Opin Cell Biol*. 2007;19(2):192-198.

25. McConnachie G, Langeberg LK, Scott JD. AKAP signaling complexes: getting to the heart of the matter. *Trends Mol Med*. 2006;12(7):317-323.

26. Wong W, Scott JD. AKAP signalling complexes: focal points in space and time. *Nat Rev Mol Cell Biol*. 2004;5(12):959-970.

27. Diviani D. Modulation of cardiac function by A-kinase anchoring proteins. *Curr Opin Pharmacol*. 2008;8(2):166-173.

28. Aass H, Skomedal T, Osnes JB. Increase of cyclic AMP in subcellular fractions of rat heart muscle after beta-adrenergic stimulation: prenalterol and isoprenaline caused different distribution of bound cyclic AMP. *J Mol Cell Cardiol*. 1988;20(9):847-860.

29. Hohl CM, Li QA. Compartmentation of cAMP in adult canine ventricular myocytes. Relation to single-cell free Ca2+ transients. *Circ Res*. 1991;69(5):1369-1379.

30. Nikolaev VO, Bunemann M, Hein L, Hannawacker A, Lohse MJ. Novel single chain cAMP sensors for receptor-induced signal propagation. *J Biol Chem*. 2004;279(36):37215-37218.

31. Bacskai BJ, Hochner B, Mahaut-Smith M, Adams SR, Kaang BK, Kandel ER, Tsien RY. Spatially resolved dynamics of cAMP and protein kinase A subunits in Aplysia sensory neurons. *Science*. 1993;260(5105):222-226.

32. Kasai H, Petersen OH. Spatial dynamics of second messengers: IP3 and cAMP as long-range and associative messengers. *Trends Neurosci*. 1994;17(3):95-101.

33. England PJ, Shahid M. Effects of forskolin on contractile responses and protein phosphorylation in the isolated perfused rat heart. *Biochem J*. 1987;246(3):687-695.

34. Jurevicius J, Fischmeister R. cAMP compartmentation is responsible for a local activation of cardiac Ca2+ channels by beta-adrenergic agonists. *Proc Natl Acad Sci U S A*. 1996;93(1):295-299.

35. Rochais F, Vandecasteele G, Lefebvre F, Lugnier C, Lum H, Mazet JL, Cooper DM, Fischmeister R. Negative feedback exerted by cAMP-dependent protein kinase and cAMP phosphodiesterase on subsarcolemmal cAMP signals in intact cardiac myocytes: an in vivo study using adenovirus-mediated expression of CNG channels. *J Biol Chem*. 2004;279(50):52095-52105.

36. Berrera M, Dodoni G, Monterisi S, Pertegato V, Zamparo I, Zaccolo M. A toolkit for real-time detection of cAMP: insights into compartmentalized signaling. *Handb Exp Pharmacol*. 2008(186):285-298.

37. Gesellchen F, Stangherlin A, Surdo N, Terrin A, Zoccarato A, Zaccolo M. Measuring spatiotemporal dynamics of cyclic AMP signaling in real-time using FRET-based biosensors. *Methods Mol Biol*.746:297-316.

38. Lohse MJ, Bunemann M, Hoffmann C, Vilardaga JP, Nikolaev VO. Monitoring receptor signaling by intramolecular FRET. *Curr Opin Pharmacol*. 2007;7(5):547-553.

39. Zaccolo M, De Giorgi F, Cho CY, Feng L, Knapp T, Negulescu PA, Taylor SS, Tsien RY, Pozzan T. A genetically encoded, fluorescent indicator for cyclic AMP in living cells. *Nat Cell Biol*. 2000;2(1):25-29.

40. Zaccolo M, Pozzan T. Discrete microdomains with high concentration of cAMP in stimulated rat neonatal cardiac myocytes. *Science*. 2002;295(5560):1711-1715.

41. Nikolaev VO, Lohse MJ. Monitoring of cAMP synthesis and degradation in living cells. *Physiology (Bethesda)*. 2006;21:86-92.

42. Di Benedetto G, Zoccarato A, Lissandron V, Terrin A, Li X, Houslay MD, Baillie GS, Zaccolo M. Protein kinase A type I and type II define distinct intracellular signaling compartments. *Circ Res*. 2008;103(8):836-844.

43. Nikolaev VO, Bunemann M, Schmitteckert E, Lohse MJ, Engelhardt S. Cyclic AMP imaging in adult cardiac myocytes reveals far-reaching beta1-adrenergic but locally confined beta2-adrenergic receptor-mediated signaling. *Circ Res*. 2006;99(10):1084-1091.

44. Soto D, De Arcangelis V, Zhang J, Xiang Y. Dynamic protein kinase a activities induced by beta-adrenoceptors dictate signaling propagation for substrate phosphorylation and myocyte contraction. *Circ Res*. 2009;104(6):770-779.

45. Zaccolo M, Magalhaes P, Pozzan T. Compartmentalisation of cAMP and Ca(2+) signals. *Curr Opin Cell Biol*. 2002;14(2):160-166.

46. Rich TC, Fagan KA, Tse TE, Schaack J, Cooper DM, Karpen JW. A uniform extracellular stimulus triggers distinct cAMP signals in different compartments of a simple cell. *Proc Natl Acad Sci U S A*. 2001;98(23):13049-13054.

47. Fischmeister R, Castro LR, Abi-Gerges A, Rochais F, Jurevicius J, Leroy J, Vandecasteele G. Compartmentation of cyclic nucleotide signaling in the heart: the role of cyclic nucleotide phosphodiesterases. *Circ Res*. 2006;99(8):816-828.

48. Omori K, Kotera J. Overview of PDEs and their regulation. *Circ Res*. 2007;100(3):309-327.

49. Mika D, Leroy J, Vandecasteele G, Fischmeister R. PDEs create local domains of cAMP signaling. *J Mol Cell Cardiol*.52(2):323-329.

50. Stangherlin A, Zaccolo M. Phosphodiesterases and subcellular compartmentalized cAMP signaling in the cardiovascular system. *Am J Physiol Heart Circ Physiol*.302(2):H379-390.

51. Francis SH, Blount MA, Corbin JD. Mammalian cyclic nucleotide phosphodiesterases: molecular mechanisms and physiological functions. *Physiol Rev*.91(2):651-690.

52. Lugnier C. Cyclic nucleotide phosphodiesterase (PDE) superfamily: a new target for the development of specific therapeutic agents. *Pharmacol Ther*. 2006;109(3):366-398.

53. Sonnenburg WK, Mullaney PJ, Beavo JA. Molecular cloning of a cyclic GMP-stimulated cyclic nucleotide phosphodiesterase cDNA. Identification and distribution of isozyme variants. *J Biol Chem*. 1991;266(26):17655-17661.

54. Wechsler J, Choi YH, Krall J, Ahmad F, Manganiello VC, Movsesian MA. Isoforms of cyclic nucleotide phosphodiesterase PDE3A in cardiac myocytes. *J Biol Chem*. 2002;277(41):38072-38078.

55. Abi-Gerges A, Richter W, Lefebvre F, Mateo P, Varin A, Heymes C, Samuel JL, Lugnier C, Conti M, Fischmeister R, Vandecasteele G. Decreased expression and activity of cAMP phosphodiesterases in cardiac hypertrophy and its impact on beta-adrenergic cAMP signals. *Circ Res*. 2009;105(8):784-792.

56. Kostic MM, Erdogan S, Rena G, Borchert G, Hoch B, Bartel S, Scotland G, Huston E, Houslay MD, Krause EG. Altered expression of PDE1 and PDE4 cyclic nucleotide phosphodiesterase isoforms in 7-oxo-prostacyclin-preconditioned rat heart. *J Mol Cell Cardiol*. 1997;29(11):3135-3146.

57. Richter W, Jin SL, Conti M. Splice variants of the cyclic nucleotide phosphodiesterase PDE4D are differentially expressed and regulated in rat tissue. *Biochem J*. 2005;388(Pt 3):803-811.

58. Bode DC, Kanter JR, Brunton LL. Cellular distribution of phosphodiesterase isoforms in rat cardiac tissue. *Circ Res*. 1991;68(4):1070-1079.

59. Verde I, Vandecasteele G, Lezoualc'h F, Fischmeister R. Characterization of the cyclic nucleotide phosphodiesterase subtypes involved in the regulation of the L-type Ca2+ current in rat ventricular myocytes. *Br J Pharmacol*. 1999;127(1):65-74.

60. Taira M, Hockman SC, Calvo JC, Belfrage P, Manganiello VC. Molecular cloning of the rat adipocyte hormone-sensitive cyclic GMP-inhibited cyclic nucleotide phosphodiesterase. *J Biol Chem*. 1993;268(25):18573-18579.

61. Engels P, Fichtel K, Lubbert H. Expression and regulation of human and rat phosphodiesterase type IV isogenes. *FEBS Lett*. 1994;350(2-3):291-295.

62. Anant JS, Ong OC, Xie HY, Clarke S, O'Brien PJ, Fung BK. In vivo differential prenylation of retinal cyclic GMP phosphodiesterase catalytic subunits. *J Biol Chem*. 1992;267(2):687-690.

63. Baillie GS, MacKenzie SJ, McPhee I, Houslay MD. Sub-family selective actions in the ability of Erk2 MAP kinase to phosphorylate and regulate the activity of PDE4 cyclic AMP-specific phosphodiesterases. *Br J Pharmacol*. 2000;131(4):811-819.

64. Rapundalo ST, Solaro RJ, Kranias EG. Inotropic responses to isoproterenol and phosphodiesterase inhibitors in intact guinea pig hearts: comparison of cyclic AMP levels and phosphorylation of sarcoplasmic reticulum and myofibrillar proteins. *Circ Res*. 1989;64(1):104-111.

65. Leroy J, Abi-Gerges A, Nikolaev VO, Richter W, Lechene P, Mazet JL, Conti M, Fischmeister R, Vandecasteele G. Spatiotemporal dynamics of beta-adrenergic cAMP signals and L-type Ca2+ channel regulation in adult rat ventricular myocytes: role of phosphodiesterases. *Circ Res*. 2008;102(9):1091-1100.

66. Willoughby D, Cooper DM. Live-cell imaging of cAMP dynamics. *Nat Methods*. 2008;5(1):29-36.

67. Georget M, Mateo P, Vandecasteele G, Lipskaia L, Defer N, Hanoune J, Hoerter J, Lugnier C, Fischmeister R. Cyclic AMP compartmentation due to increased cAMP-phosphodiesterase activity in transgenic mice with a cardiac-directed expression of the human adenylyl cyclase type 8 (AC8). *FASEB J*. 2003;17(11):1380-1391.

68. Xiang Y, Naro F, Zoudilova M, Jin SL, Conti M, Kobilka B. Phosphodiesterase 4D is required for beta2 adrenoceptor subtype-specific signaling in cardiac myocytes. *Proc Natl Acad Sci U S A*. 2005;102(3):909-914.

69. Richter W, Xie M, Scheitrum C, Krall J, Movsesian MA, Conti M. Conserved expression and functions of PDE4 in rodent and human heart. *Basic Res Cardiol*.106(2):249-262.

70. Shahid M, Nicholson CD. Comparison of cyclic nucleotide phosphodiesterase isoenzymes in rat and rabbit ventricular myocardium: positive inotropic and phosphodiesterase inhibitory effects of Org 30029, milrinone and rolipram. *Naunyn Schmiedebergs Arch Pharmacol*. 1990;342(6):698-705.

71. Reeves ML, Leigh BK, England PJ. The identification of a new cyclic nucleotide phosphodiesterase activity in human and guinea-pig cardiac ventricle. Implications for the mechanism of action of selective phosphodiesterase inhibitors. *Biochem J*. 1987;241(2):535-541.

72. Masunaga R, Nagasaka A, Sawai Y, Hayakawa N, Nakai A, Hotta K, Kato Y, Hishida H, Takahashi H, Naka M, Shimada Y, Tanaka T, Hidaka H, Itoh M. Changes in cyclic nucleotide phosphodiesterase activity and calmodulin concentration in heart muscle of cardiomyopathic hamsters. *J Mol Cell Cardiol*. 2004;37(3):767-774.

73. Vandeput F, Wolda SL, Krall J, Hambleton R, Uher L, McCaw KN, Radwanski PB, Florio V, Movsesian MA. Cyclic nucleotide phosphodiesterase PDE1C1 in human cardiac myocytes. *J Biol Chem*. 2007;282(45):32749-32757.

74. Hambleton R, Krall J, Tikishvili E, Honeggar M, Ahmad F, Manganiello VC, Movsesian MA. Isoforms of cyclic nucleotide phosphodiesterase PDE3 and their

contribution to cAMP hydrolytic activity in subcellular fractions of human myocardium. *J Biol Chem*. 2005;280(47):39168-39174.

75. Mongillo M, Tocchetti CG, Terrin A, Lissandron V, Cheung YF, Dostmann WR, Pozzan T, Kass DA, Paolocci N, Houslay MD, Zaccolo M. Compartmentalized phosphodiesterase-2 activity blunts beta-adrenergic cardiac inotropy via an NO/cGMP-dependent pathway. *Circ Res*. 2006;98(2):226-234.

76. Nikolaev VO, Gambaryan S, Engelhardt S, Walter U, Lohse MJ. Real-time monitoring of the PDE2 activity of live cells: hormone-stimulated cAMP hydrolysis is faster than hormone-stimulated cAMP synthesis. *J Biol Chem*. 2005;280(3):1716-1719.

77. Dittrich M, Jurevicius J, Georget M, Rochais F, Fleischmann B, Hescheler J, Fischmeister R. Local response of L-type Ca(2+) current to nitric oxide in frog ventricular myocytes. *J Physiol*. 2001;534(Pt 1):109-121.

78. Hartzell HC, Fischmeister R. Opposite effects of cyclic GMP and cyclic AMP on Ca2+ current in single heart cells. *Nature*. 1986;323(6085):273-275.

79. Mery PF, Pavoine C, Pecker F, Fischmeister R. Erythro-9-(2-hydroxy-3-nonyl)adenine inhibits cyclic GMP-stimulated phosphodiesterase in isolated cardiac myocytes. *Mol Pharmacol*. 1995;48(1):121-130.

80. Vandecasteele G, Verde I, Rucker-Martin C, Donzeau-Gouge P, Fischmeister R. Cyclic GMP regulation of the L-type Ca(2+) channel current in human atrial myocytes. *J Physiol*. 2001;533(Pt 2):329-340.

81. Simmons MA, Hartzell HC. Role of phosphodiesterase in regulation of calcium current in isolated cardiac myocytes. *Mol Pharmacol*. 1988;33(6):664-671.

82. Rivet-Bastide M, Vandecasteele G, Hatem S, Verde I, Benardeau A, Mercadier JJ, Fischmeister R. cGMP-stimulated cyclic nucleotide phosphodiesterase regulates the basal calcium current in human atrial myocytes. *J Clin Invest*. 1997;99(11):2710-2718.

83. Mongillo M, McSorley T, Evellin S, Sood A, Lissandron V, Terrin A, Huston E, Hannawacker A, Lohse MJ, Pozzan T, Houslay MD, Zaccolo M. Fluorescence resonance energy transfer-based analysis of cAMP dynamics in live neonatal rat cardiac myocytes reveals distinct functions of compartmentalized phosphodiesterases. *Circ Res*. 2004;95(1):67-75.

84. Lehnart SE, Wehrens XH, Reiken S, Warrier S, Belevych AE, Harvey RD, Richter W, Jin SL, Conti M, Marks AR. Phosphodiesterase 4D deficiency in the ryanodine-receptor complex promotes heart failure and arrhythmias. *Cell*. 2005;123(1):25-35.

85. De Arcangelis V, Soto D, Xiang Y. Phosphodiesterase 4 and phosphatase 2A differentially regulate cAMP/protein kinase a signaling for cardiac myocyte contraction under stimulation of beta1 adrenergic receptor. *Mol Pharmacol*. 2008;74(5):1453-1462.

86. Kerfant BG, Zhao D, Lorenzen-Schmidt I, Wilson LS, Cai S, Chen SR, Maurice DH, Backx PH. PI3Kgamma is required for PDE4, not PDE3, activity in subcellular microdomains containing the sarcoplasmic reticular calcium ATPase in cardiomyocytes. *Circ Res*. 2007;101(4):400-408.

87. Beca S, Helli PB, Simpson JA, Zhao D, Farman GP, Jones PP, Tian X, Wilson LS, Ahmad F, Chen SR, Movsesian MA, Manganiello V, Maurice DH, Conti M, Backx PH. Phosphodiesterase 4D regulates baseline sarcoplasmic reticulum Ca2+ release and cardiac contractility, independently of L-type Ca2+ current. *Circ Res*.109(9):1024-1030.

88. Katano Y, Endoh M. Differential effects of Ro 20-1724 and isobutylmethylxanthine on the basal force of contraction and beta-adrenoceptor-mediated response in the rat ventricular myocardium. *Biochem Biophys Res Commun*. 1990;167(1):123-129.

89. Katano Y, Endoh M. Effects of a cardiotonic quinolinone derivative Y-20487 on the isoproterenol-induced positive inotropic action and cyclic AMP accumulation in rat ventricular myocardium: comparison with rolipram, Ro 20-1724, milrinone, and isobutylmethylxanthine. *J Cardiovasc Pharmacol*. 1992;20(5):715-722.

90. Galindo-Tovar A, Kaumann AJ. Phosphodiesterase-4 blunts inotropism and arrhythmias but not sinoatrial tachycardia of (-)-adrenaline mediated through mouse cardiac beta(1)-adrenoceptors. *Br J Pharmacol*. 2008;153(4):710-720.

91. Vargas ML, Hernandez J, Kaumann AJ. Phosphodiesterase PDE3 blunts the positive inotropic and cyclic AMP enhancing effects of CGP12177 but not of noradrenaline in rat ventricle. *Br J Pharmacol*. 2006;147(2):158-163.

92. Rochais F, Abi-Gerges A, Horner K, Lefebvre F, Cooper DM, Conti M, Fischmeister R, Vandecasteele G. A specific pattern of phosphodiesterases controls the cAMP signals generated by different Gs-coupled receptors in adult rat ventricular myocytes. *Circ Res*. 2006;98(8):1081-1088.

93. Fischmeister R, Hartzell HC. Regulation of calcium current by low-Km cyclic AMP phosphodiesterases in cardiac cells. *Mol Pharmacol*. 1990;38(3):426-433.

94. Movsesian MA, Smith CJ, Krall J, Bristow MR, Manganiello VC. Sarcoplasmic reticulum-associated cyclic adenosine 5'-monophosphate phosphodiesterase activity in normal and failing human hearts. *J Clin Invest*. 1991;88(1):15-19.

95. Martins TJ, Mumby MC, Beavo JA. Purification and characterization of a cyclic GMP-stimulated cyclic nucleotide phosphodiesterase from bovine tissues. *J Biol Chem*. 1982;257(4):1973-1979.

96. Rosman GJ, Martins TJ, Sonnenburg WK, Beavo JA, Ferguson K, Loughney K. Isolation and characterization of human cDNAs encoding a cGMP-stimulated 3',5'-cyclic nucleotide phosphodiesterase. *Gene*. 1997;191(1):89-95.

97. Martinez SE, Beavo JA, Hol WG. GAF domains: two-billion-year-old molecular switches that bind cyclic nucleotides. *Mol Interv*. 2002;2(5):317-323.

98. Han X, Kobzik L, Balligand JL, Kelly RA, Smith TW. Nitric oxide synthase (NOS3)-mediated cholinergic modulation of Ca2+ current in adult rabbit atrioventricular nodal cells. *Circ Res*. 1996;78(6):998-1008.

99. Zaccolo M, Movsesian MA. cAMP and cGMP signaling cross-talk: role of phosphodiesterases and implications for cardiac pathophysiology. *Circ Res*. 2007;100(11):1569-1578.

100. Muller B, Stoclet JC, Lugnier C. Cytosolic and membrane-bound cyclic nucleotide phosphodiesterases from guinea pig cardiac ventricles. *Eur J Pharmacol*. 1992;225(3):263-272.

101. Weishaar RE, Kobylarz-Singer DC, Steffen RP, Kaplan HR. Subclasses of cyclic AMP-specific phosphodiesterase in left ventricular muscle and their involvement in regulating myocardial contractility. *Circ Res*. 1987;61(4):539-547.

102. Okruhlicova L, Tribulova N, Eckly A, Lugnier C, Slezak J. Cytochemical distribution of cyclic AMP-dependent 3',5'-nucleotide phosphodiesterase in the rat myocardium. *Histochem J*. 1996;28(3):165-172.

103. Okruhlicova L, Tribulova N, Styk J, Eckly A, Lugnier C, Slezk J. Species differences in localization of cardiac cAMP-phosphodiesterase activity: a cytochemical study. *Mol Cell Biochem*. 1997;173(1-2):183-188.

104. Lugnier C, Muller B, Le Bec A, Beaudry C, Rousseau E. Characterization of indolidan- and rolipram-sensitive cyclic nucleotide phosphodiesterases in canine and human cardiac microsomal fractions. *J Pharmacol Exp Ther*. 1993;265(3):1142-1151.

105. Kauffman RF, Crowe VG, Utterback BG, Robertson DW. LY195115: a potent, selective inhibitor of cyclic nucleotide phosphodiesterase located in the sarcoplasmic reticulum. *Mol Pharmacol*. 1986;30(6):609-616.

106. Conti M, Beavo J. Biochemistry and physiology of cyclic nucleotide phosphodiesterases: essential components in cyclic nucleotide signaling. *Annu Rev Biochem*. 2007;76:481-511.

107. Martinez SE, Wu AY, Glavas NA, Tang XB, Turley S, Hol WG, Beavo JA. The two GAF domains in phosphodiesterase 2A have distinct roles in dimerization and in cGMP binding. *Proc Natl Acad Sci U S A*. 2002;99(20):13260-13265.

108. Rahn T, Ronnstrand L, Leroy MJ, Wernstedt C, Tornqvist H, Manganiello VC, Belfrage P, Degerman E. Identification of the site in the cGMP-inhibited phosphodiesterase phosphorylated in adipocytes in response to insulin and isoproterenol. *J Biol Chem*. 1996;271(19):11575-11580.

109. MacKenzie SJ, Baillie GS, McPhee I, MacKenzie C, Seamons R, McSorley T, Millen J, Beard MB, van Heeke G, Houslay MD. Long PDE4 cAMP specific phosphodiesterases are activated by protein kinase A-mediated phosphorylation of a single serine residue in Upstream Conserved Region 1 (UCR1). *Br J Pharmacol*. 2002;136(3):421-433.

110. Conti M, Richter W, Mehats C, Livera G, Park JY, Jin C. Cyclic AMP-specific PDE4 phosphodiesterases as critical components of cyclic AMP signaling. *J Biol Chem*. 2003;278(8):5493-5496.

111. Houslay MD, Adams DR. PDE4 cAMP phosphodiesterases: modular enzymes that orchestrate signalling cross-talk, desensitization and compartmentalization. *Biochem J*. 2003;370(Pt 1):1-18.

112. Houslay MD, Baillie GS, Maurice DH. cAMP-Specific phosphodiesterase-4 enzymes in the cardiovascular system: a molecular toolbox for generating compartmentalized cAMP signaling. *Circ Res*. 2007;100(7):950-966.

113. Houslay MD. The long and short of vascular smooth muscle phosphodiesterase-4 as a putative therapeutic target. *Mol Pharmacol*. 2005;68(3):563-567.

114. Dodge KL, Khouangsathiene S, Kapiloff MS, Mouton R, Hill EV, Houslay MD, Langeberg LK, Scott JD. mAKAP assembles a protein kinase A/PDE4 phosphodiesterase cAMP signaling module. *EMBO J*. 2001;20(8):1921-1930.

115. Richter W, Conti M. The oligomerization state determines regulatory properties and inhibitor sensitivity of type 4 cAMP-specific phosphodiesterases. *J Biol Chem*. 2004;279(29):30338-30348.

116. Baillie GS, Sood A, McPhee I, Gall I, Perry SJ, Lefkowitz RJ, Houslay MD. beta-Arrestin-mediated PDE4 cAMP phosphodiesterase recruitment regulates beta-adrenoceptor switching from Gs to Gi. *Proc Natl Acad Sci U S A*. 2003;100(3):940-945.

117. McCahill A, McSorley T, Huston E, Hill EV, Lynch MJ, Gall I, Keryer G, Lygren B, Tasken K, van Heeke G, Houslay MD. In resting COS1 cells a dominant negative approach shows that specific, anchored PDE4 cAMP phosphodiesterase isoforms gate the activation, by basal cyclic AMP production, of AKAP-tethered protein kinase A type II located in the centrosomal region. *Cell Signal*. 2005;17(9):1158-1173.

118. Lynch MJ, Baillie GS, Mohamed A, Li X, Maisonneuve C, Klussmann E, van Heeke G, Houslay MD. RNA silencing identifies PDE4D5 as the functionally relevant cAMP phosphodiesterase interacting with beta arrestin to control the protein kinase A/AKAP79-mediated switching of the beta2-adrenergic receptor to activation of ERK in HEK293B2 cells. *J Biol Chem*. 2005;280(39):33178-33189.

119. Leroy J, Richter W, Mika D, Castro LR, Abi-Gerges A, Xie M, Scheitrum C, Lefebvre F, Schittl J, Mateo P, Westenbroek R, Catterall WA, Charpentier F, Conti M, Fischmeister R, Vandecasteele G. Phosphodiesterase 4B in the cardiac

L-type Ca(2)(+) channel complex regulates Ca(2)(+) current and protects against ventricular arrhythmias in mice. *J Clin Invest*.121(7):2651-2661.

120. De Arcangelis V, Liu R, Soto D, Xiang Y. Differential association of phosphodiesterase 4D isoforms with beta2-adrenoceptor in cardiac myocytes. *J Biol Chem*. 2009;284(49):33824-33832.

121. Richter W, Day P, Agrawal R, Bruss MD, Granier S, Wang YL, Rasmussen SG, Horner K, Wang P, Lei T, Patterson AJ, Kobilka B, Conti M. Signaling from beta1- and beta2-adrenergic receptors is defined by differential interactions with PDE4. *EMBO J*. 2008;27(2):384-393.

122. Dessauer CW. Adenylyl cyclase--A-kinase anchoring protein complexes: the next dimension in cAMP signaling. *Mol Pharmacol*. 2009;76(5):935-941.

123. Bauman AL, Soughayer J, Nguyen BT, Willoughby D, Carnegie GK, Wong W, Hoshi N, Langeberg LK, Cooper DM, Dessauer CW, Scott JD. Dynamic regulation of cAMP synthesis through anchored PKA-adenylyl cyclase V/VI complexes. *Mol Cell*. 2006;23(6):925-931.

124. Baillie GS, Scott JD, Houslay MD. Compartmentalisation of phosphodiesterases and protein kinase A: opposites attract. *FEBS Lett*. 2005;579(15):3264-3270.

125. Stangherlin A, Zaccolo M. Local termination of 3'-5'-cyclic adenosine monophosphate signals: the role of a kinase anchoring protein-tethered phosphodiesterases. *J Cardiovasc Pharmacol*.58(4):345-353.

126. Redden JM, Dodge-Kafka KL. AKAP phosphatase complexes in the heart. *J Cardiovasc Pharmacol*.58(4):354-362.

127. Sette C, Conti M. Phosphorylation and activation of a cAMP-specific phosphodiesterase by the cAMP-dependent protein kinase. Involvement of serine 54 in the enzyme activation. *J Biol Chem*. 1996;271(28):16526-16534.

128. Carlisle Michel JJ, Dodge KL, Wong W, Mayer NC, Langeberg LK, Scott JD. PKA-phosphorylation of PDE4D3 facilitates recruitment of the mAKAP signalling complex. *Biochem J*. 2004;381(Pt 3):587-592.

129. Hoffmann R, Baillie GS, MacKenzie SJ, Yarwood SJ, Houslay MD. The MAP kinase ERK2 inhibits the cyclic AMP-specific phosphodiesterase HSPDE4D3 by phosphorylating it at Ser579. *EMBO J*. 1999;18(4):893-903.

130. Dodge-Kafka KL, Soughayer J, Pare GC, Carlisle Michel JJ, Langeberg LK, Kapiloff MS, Scott JD. The protein kinase A anchoring protein mAKAP coordinates two integrated cAMP effector pathways. *Nature*. 2005;437(7058):574-578.

131. Marx SO, Reiken S, Hisamatsu Y, Jayaraman T, Burkhoff D, Rosemblit N, Marks AR. PKA phosphorylation dissociates FKBP12.6 from the calcium release channel (ryanodine receptor): defective regulation in failing hearts. *Cell*. 2000;101(4):365-376.

132. Terrin A, Di Benedetto G, Pertegato V, Cheung YF, Baillie G, Lynch MJ, Elvassore N, Prinz A, Herberg FW, Houslay MD, Zaccolo M. PGE(1) stimulation of HEK293 cells generates multiple contiguous domains with different [cAMP]: role of compartmentalized phosphodiesterases. *J Cell Biol*. 2006;175(3):441-451.

133. Iancu RV, Ramamurthy G, Warrier S, Nikolaev VO, Lohse MJ, Jones SW, Harvey RD. Cytoplasmic cAMP concentrations in intact cardiac myocytes. *Am J Physiol Cell Physiol*. 2008;295(2):C414-422.

134. Herget S, Lohse MJ, Nikolaev VO. Real-time monitoring of phosphodiesterase inhibition in intact cells. *Cell Signal*. 2008;20(8):1423-1431.

135. Iancu RV, Jones SW, Harvey RD. Compartmentation of cAMP signaling in cardiac myocytes: a computational study. *Biophys J*. 2007;92(9):3317-3331.

136. Castro LR, Verde I, Cooper DM, Fischmeister R. Cyclic guanosine monophosphate compartmentation in rat cardiac myocytes. *Circulation*. 2006;113(18):2221-2228.

137. Stangherlin A, Gesellchen F, Zoccarato A, Terrin A, Fields LA, Berrera M, Surdo NC, Craig MA, Smith G, Hamilton G, Zaccolo M. cGMP signals modulate cAMP levels in a compartment-specific manner to regulate catecholamine-dependent signaling in cardiac myocytes. *Circ Res*.108(8):929-939.

138. Dyachok O, Isakov Y, Sagetorp J, Tengholm A. Oscillations of cyclic AMP in hormone-stimulated insulin-secreting beta-cells. *Nature*. 2006;439(7074):349-352.

139. Ostrom RS, Violin JD, Coleman S, Insel PA. Selective enhancement of beta-adrenergic receptor signaling by overexpression of adenylyl cyclase type 6: colocalization of receptor and adenylyl cyclase in caveolae of cardiac myocytes. *Mol Pharmacol*. 2000;57(5):1075-1079.

140. Patel HH, Murray F, Insel PA. G-protein-coupled receptor-signaling components in membrane raft and caveolae microdomains. *Handb Exp Pharmacol*. 2008(186):167-184.

141. Calaghan S, Kozera L, White E. Compartmentalisation of cAMP-dependent signalling by caveolae in the adult cardiac myocyte. *J Mol Cell Cardiol*. 2008;45(1):88-92.

142. Carr AN, Schmidt AG, Suzuki Y, del Monte F, Sato Y, Lanner C, Breeden K, Jing SL, Allen PB, Greengard P, Yatani A, Hoit BD, Grupp IL, Hajjar RJ, DePaoli-Roach AA, Kranias EG. Type 1 phosphatase, a negative regulator of cardiac function. *Mol Cell Biol*. 2002;22(12):4124-4135.

143. Nicolaou P, Hajjar RJ, Kranias EG. Role of protein phosphatase-1 inhibitor-1 in cardiac physiology and pathophysiology. *J Mol Cell Cardiol*. 2009;47(3):365-371.

144. Oliver CJ, Shenolikar S. Physiologic importance of protein phosphatase inhibitors. *Front Biosci*. 1998;3:D961-972.

145. Dodge-Kafka KL, Bauman A, Mayer N, Henson E, Heredia L, Ahn J, McAvoy T, Nairn AC, Kapiloff MS. cAMP-stimulated protein phosphatase 2A activity associated with muscle A kinase-anchoring protein (mAKAP) signaling complexes inhibits the phosphorylation and activity of the cAMP-specific phosphodiesterase PDE4D3. *J Biol Chem*.285(15):11078-11086.

146. Silverman BZ, Fuller W, Eaton P, Deng J, Moorman JR, Cheung JY, James AF, Shattock MJ. Serine 68 phosphorylation of phospholemman: acute isoform-specific activation of cardiac Na/K ATPase. *Cardiovasc Res*. 2005;65(1):93-103.

147. Bossuyt J, Ai X, Moorman JR, Pogwizd SM, Bers DM. Expression and phosphorylation of the na-pump regulatory subunit phospholemman in heart failure. *Circ Res*. 2005;97(6):558-565.

148. Fuller W, Eaton P, Bell JR, Shattock MJ. Ischemia-induced phosphorylation of phospholemman directly activates rat cardiac Na/K-ATPase. *FASEB J*. 2004;18(1):197-199.

149. Reis J, Zhang L, Cala S, Jew KN, Mace LC, Chung L, Moore RL, Ng YC. Expression of phospholemman and its association with Na+-K+-ATPase in skeletal muscle: effects of aging and exercise training. *J Appl Physiol*. 2005;99(4):1508-1515.

150. Feschenko MS, Donnet C, Wetzel RK, Asinovski NK, Jones LR, Sweadner KJ. Phospholemman, a single-span membrane protein, is an accessory protein of Na,K-ATPase in cerebellum and choroid plexus. *J Neurosci*. 2003;23(6):2161-2169.

151. Wetzel RK, Sweadner KJ. Phospholemman expression in extraglomerular mesangium and afferent arteriole of the juxtaglomerular apparatus. *Am J Physiol Renal Physiol*. 2003;285(1):F121-129.

152. Rembold CM, Ripley ML, Meeks MK, Geddis LM, Kutchai HC, Marassi FM, Cheung JY, Moorman JR. Serine 68 phospholemman phosphorylation during forskolin-induced swine carotid artery relaxation. *J Vasc Res*. 2005;42(6):483-491.

153. Palmer CJ, Scott BT, Jones LR. Purification and complete sequence determination of the major plasma membrane substrate for cAMP-dependent protein kinase and protein kinase C in myocardium. *J Biol Chem*. 1991;266(17):11126-11130.

154. Chen Z, Jones LR, O'Brian JJ, Moorman JR, Cala SE. Structural domains in phospholemman: a possible role for the carboxyl terminus in channel inactivation. *Circ Res*. 1998;82(3):367-374.

155. Zhang XQ, Moore RL, Tillotson DL, Cheung JY. Calcium currents in postinfarction rat cardiac myocytes. *Am J Physiol*. 1995;269(6 Pt 1):C1464-1473.

156. Moorman JR, Ackerman SJ, Kowdley GC, Griffin MP, Mounsey JP, Chen Z, Cala SE, O'Brian JJ, Szabo G, Jones LR. Unitary anion currents through phospholemman channel molecules. *Nature*. 1995;377(6551):737-740.

157. Cornelius F, Mahmmoud YA. Functional modulation of the sodium pump: the regulatory proteins "Fixit". *News Physiol Sci*. 2003;18:119-124.

158. Beevers AJ, Kukol A. Secondary structure, orientation, and oligomerization of phospholemman, a cardiac transmembrane protein. *Protein Sci*. 2006;15(5):1127-1132.

159. Franzin CM, Gong XM, Thai K, Yu J, Marassi FM. NMR of membrane proteins in micelles and bilayers: the FXYD family proteins. *Methods*. 2007;41(4):398-408.

160. Franzin CM, Choi J, Zhai D, Reed JC, Marassi FM. Structural studies of apoptosis and ion transport regulatory proteins in membranes. *Magn Reson Chem*. 2004;42(2):172-179.

161. Bogaev RC, Jia LG, Kobayashi YM, Palmer CJ, Mounsey JP, Moorman JR, Jones LR, Tucker AL. Gene structure and expression of phospholemman in mouse. *Gene*. 2001;271(1):69-79.

162. Chen LS, Lo CF, Numann R, Cuddy M. Characterization of the human and rat phospholemman (PLM) cDNAs and localization of the human PLM gene to chromosome 19q13.1. *Genomics*. 1997;41(3):435-443.

163. Presti CF, Jones LR, Lindemann JP. Isoproterenol-induced phosphorylation of a 15-kilodalton sarcolemmal protein in intact myocardium. *J Biol Chem*. 1985;260(6):3860-3867.

164. Presti CF, Scott BT, Jones LR. Identification of an endogenous protein kinase C activity and its intrinsic 15-kilodalton substrate in purified canine cardiac sarcolemmal vesicles. *J Biol Chem*. 1985;260(25):13879-13889.

165. Chu G, Lester JW, Young KB, Luo W, Zhai J, Kranias EG. A single site (Ser16) phosphorylation in phospholamban is sufficient in mediating its maximal cardiac responses to beta -agonists. *J Biol Chem*. 2000;275(49):38938-38943.

166. Lu KP, Kemp BE, Means AR. Identification of substrate specificity determinants for the cell cycle-regulated NIMA protein kinase. *J Biol Chem*. 1994;269(9):6603-6607.

167. Walaas SI, Czernik AJ, Olstad OK, Sletten K, Walaas O. Protein kinase C and cyclic AMP-dependent protein kinase phosphorylate phospholemman, an insulin and adrenaline-regulated membrane phosphoprotein, at specific sites in the carboxy terminal domain. *Biochem J*. 1994;304 (Pt 2):635-640.

168. Bibert S, Roy S, Schaer D, Horisberger JD, Geering K. Phosphorylation of phospholemman (FXYD1) by protein kinases A and C modulates distinct Na,K-ATPase isozymes. *J Biol Chem*. 2008;283(1):476-486.

169. Despa S, Bossuyt J, Han F, Ginsburg KS, Jia LG, Kutchai H, Tucker AL, Bers DM. Phospholemman-phosphorylation mediates the beta-adrenergic effects on Na/K pump function in cardiac myocytes. *Circ Res*. 2005;97(3):252-259.

170. Han F, Bossuyt J, Despa S, Tucker AL, Bers DM. Phospholemman phosphorylation mediates the protein kinase C-dependent effects on Na+/K+ pump function in cardiac myocytes. *Circ Res*. 2006;99(12):1376-1383.

171. Fuller W, Howie J, McLatchie LM, Weber RJ, Hastie CJ, Burness K, Pavlovic D, Shattock MJ. FXYD1 phosphorylation in vitro and in adult rat cardiac myocytes: threonine 69 is a novel substrate for protein kinase C. *Am J Physiol Cell Physiol*. 2009;296(6):C1346-1355.

172. Song J, Zhang XQ, Ahlers BA, Carl LL, Wang J, Rothblum LI, Stahl RC, Mounsey JP, Tucker AL, Moorman JR, Cheung JY. Serine 68 of phospholemman is critical in modulation of contractility, [Ca2+]i transients, and Na+/Ca2+ exchange in adult rat cardiac myocytes. *Am J Physiol Heart Circ Physiol*. 2005;288(5):H2342-2354.

173. Zhang XQ, Moorman JR, Ahlers BA, Carl LL, Lake DE, Song J, Mounsey JP, Tucker AL, Chan YM, Rothblum LI, Stahl RC, Carey DJ, Cheung JY. Phospholemman overexpression inhibits Na+-K+-ATPase in adult rat cardiac myocytes: relevance to decreased Na+ pump activity in postinfarction myocytes. *J Appl Physiol*. 2006;100(1):212-220.

174. Fuller W, Shattock MJ. Phospholemman and the cardiac sodium pump: protein kinase C, take a bow. *Circ Res*. 2006;99(12):1290-1292.

175. Davis CE, Patel MK, Miller JR, John JE, 3rd, Jones LR, Tucker AL, Mounsey JP, Moorman JR. Effects of phospholemman expression on swelling-activated ion currents and volume regulation in embryonic kidney cells. *Neurochem Res*. 2004;29(1):177-187.

176. Morales-Mulia M, Pasantes-Morales H, Moran J. Volume sensitive efflux of taurine in HEK293 cells overexpressing phospholemman. *Biochim Biophys Acta*. 2000;1496(2-3):252-260.

177. Sweadner KJ, Rael E. The FXYD gene family of small ion transport regulators or channels: cDNA sequence, protein signature sequence, and expression. *Genomics*. 2000;68(1):41-56.

178. Crambert G, Geering K. FXYD proteins: new tissue-specific regulators of the ubiquitous Na,K-ATPase. *Sci STKE*. 2003;2003(166):RE1.

179. Skou JC. The influence of some cations on an adenosine triphosphatase from peripheral nerves. *Biochim Biophys Acta*. 1957;23(2):394-401.

180. Gadsby DC, Takeuchi A, Artigas P, Reyes N. Review. Peering into an ATPase ion pump with single-channel recordings. *Philos Trans R Soc Lond B Biol Sci*. 2009;364(1514):229-238.

181. Thomas RC. Electrogenic sodium pump in nerve and muscle cells. *Physiol Rev*. 1972;52(3):563-594.

182. Morth JP, Pedersen BP, Toustrup-Jensen MS, Sorensen TL, Petersen J, Andersen JP, Vilsen B, Nissen P. Crystal structure of the sodium-potassium pump. *Nature*. 2007;450(7172):1043-1049.

183. Lingrel JB, Kuntzweiler T. Na+,K(+)-ATPase. *J Biol Chem*. 1994;269(31):19659-19662.

184. Hu YK, Kaplan JH. Site-directed chemical labeling of extracellular loops in a membrane protein. The topology of the Na,K-ATPase alpha-subunit. *J Biol Chem*. 2000;275(25):19185-19191.

185. Kaplan JH. Biochemistry of Na,K-ATPase. *Annu Rev Biochem*. 2002;71:511-535.

186. James PF, Grupp IL, Grupp G, Woo AL, Askew GR, Croyle ML, Walsh RA, Lingrel JB. Identification of a specific role for the Na,K-ATPase alpha 2 isoform as a regulator of calcium in the heart. *Mol Cell*. 1999;3(5):555-563.

187. Gao J, Wymore R, Wymore RT, Wang Y, McKinnon D, Dixon JE, Mathias RT, Cohen IS, Baldo GJ. Isoform-specific regulation of the sodium pump by alpha- and beta-adrenergic agonists in the guinea-pig ventricle. *J Physiol*. 1999;516 (Pt 2):377-383.

188. Shamraj OI, Melvin D, Lingrel JB. Expression of Na,K-ATPase isoforms in human heart. *Biochem Biophys Res Commun*. 1991;179(3):1434-1440.

189. Dostanic I, Schultz Jel J, Lorenz JN, Lingrel JB. The alpha 1 isoform of Na,K-ATPase regulates cardiac contractility and functionally interacts and co-localizes with the Na/Ca exchanger in heart. *J Biol Chem*. 2004;279(52):54053-54061.

190. Berry RG, Despa S, Fuller W, Bers DM, Shattock MJ. Differential distribution and regulation of mouse cardiac Na+/K+-ATPase alpha1 and alpha2 subunits in T-tubule and surface sarcolemmal membranes. *Cardiovasc Res*. 2007;73(1):92-100.

191. Juhaszova M, Blaustein MP. Na+ pump low and high ouabain affinity alpha subunit isoforms are differently distributed in cells. *Proc Natl Acad Sci U S A*. 1997;94(5):1800-1805.

192. Despa S, Lingrel JB, Bers DM. Na+/K+-ATPase alpha2-isoform preferentially modulates Ca2+ transients and sarcoplasmic reticulum Ca2+ release in cardiac myocytes. *Cardiovasc Res*.95(4):480-486.

193. Martin-Vasallo P, Dackowski W, Emanuel JR, Levenson R. Identification of a putative isoform of the Na,K-ATPase beta subunit. Primary structure and tissue-specific expression. *J Biol Chem*. 1989;264(8):4613-4618.

194. Sweadner KJ. Isozymes of the Na+/K+-ATPase. *Biochim Biophys Acta*. 1989;988(2):185-220.

195. Lemas MV, Hamrick M, Takeyasu K, Fambrough DM. 26 amino acids of an extracellular domain of the Na,K-ATPase alpha-subunit are sufficient for assembly with the Na,K-ATPase beta-subunit. *J Biol Chem*. 1994;269(11):8255-8259.

196. Geering K, Beggah A, Good P, Girardet S, Roy S, Schaer D, Jaunin P. Oligomerization and maturation of Na,K-ATPase: functional interaction of the cytoplasmic NH2 terminus of the beta subunit with the alpha subunit. *J Cell Biol*. 1996;133(6):1193-1204.

197. Horisberger JD, Jaunin P, Good PJ, Rossier BC, Geering K. Coexpression of alpha 1 with putative beta 3 subunits results in functional Na+/K+ pumps in Xenopus oocytes. *Proc Natl Acad Sci U S A*. 1991;88(19):8397-8400.

198. Geering K. The functional role of the beta-subunit in the maturation and intracellular transport of Na,K-ATPase. *FEBS Lett*. 1991;285(2):189-193.

199. Horisberger JD, Jaunin P, Reuben MA, Lasater LS, Chow DC, Forte JG, Sachs G, Rossier BC, Geering K. The H,K-ATPase beta-subunit can act as a surrogate for the beta-subunit of Na,K-pumps. *J Biol Chem*. 1991;266(29):19131-19134.

200. Crambert G, Hasler U, Beggah AT, Yu C, Modyanov NN, Horisberger JD, Lelievre L, Geering K. Transport and pharmacological properties of nine different human Na, K-ATPase isozymes. *J Biol Chem*. 2000;275(3):1976-1986.

201. Kirley TL. Inactivation of (Na+,K+)-ATPase by beta-mercaptoethanol. Differential sensitivity to reduction of the three beta subunit disulfide bonds. *J Biol Chem*. 1990;265(8):4227-4232.

202. Gloor S, Antonicek H, Sweadner KJ, Pagliusi S, Frank R, Moos M, Schachner M. The adhesion molecule on glia (AMOG) is a homologue of the beta subunit of the Na,K-ATPase. *J Cell Biol*. 1990;110(1):165-174.

203. Shattock MJ. Phospholemman: its role in normal cardiac physiology and potential as a druggable target in disease. *Curr Opin Pharmacol*. 2009;9(2):160-166.

204. Ismail-Beigi F, Edelman IS. The mechanism of the calorigenic action of thyroid hormone. Stimulation of Na plus + K plus-activated adenosinetriphosphatase activity. *J Gen Physiol*. 1971;57(6):710-722.

205. Blaustein MP. Sodium ions, calcium ions, blood pressure regulation, and hypertension: a reassessment and a hypothesis. *Am J Physiol*. 1977;232(5):C165-173.

206. Bers DM, Despa S. Na/K-ATPase--an integral player in the adrenergic fight-or-flight response. *Trends Cardiovasc Med*. 2009;19(4):111-118.

207. Fuller W, Tulloch LB, Shattock MJ, Calaghan SC, Howie J, Wypijewski KJ. Regulation of the cardiac sodium pump. *Cell Mol Life Sci*.

208. Crambert G, Fuzesi M, Garty H, Karlish S, Geering K. Phospholemman (FXYD1) associates with Na,K-ATPase and regulates its transport properties. *Proc Natl Acad Sci U S A*. 2002;99(17):11476-11481.

209. Lindzen M, Gottschalk KE, Fuzesi M, Garty H, Karlish SJ. Structural interactions between FXYD proteins and Na+,K+-ATPase: alpha/beta/FXYD subunit stoichiometry and cross-linking. *J Biol Chem*. 2006;281(9):5947-5955.

210. Bossuyt J, Despa S, Han F, Hou Z, Robia SL, Lingrel JB, Bers DM. Isoform specificity of the Na/K-ATPase association and regulation by phospholemman. *J Biol Chem*. 2009;284(39):26749-26757.

211. Franzin CM, Gong XM, Teriete P, Marassi FM. Structures of the FXYD regulatory proteins in lipid micelles and membranes. *J Bioenerg Biomembr*. 2007;39(5-6):379-383.

212. Beevers AJ, Kukol A. Phospholemman transmembrane structure reveals potential interactions with Na+/K+-ATPase. *J Biol Chem*. 2007;282(45):32742-32748.

213. Bertorello AM, Aperia A, Walaas SI, Nairn AC, Greengard P. Phosphorylation of the catalytic subunit of Na+,K(+)-ATPase inhibits the activity of the enzyme. *Proc Natl Acad Sci U S A*. 1991;88(24):11359-11362.

214. Fisone G, Cheng SX, Nairn AC, Czernik AJ, Hemmings HC, Jr., Hoog JO, Bertorello AM, Kaiser R, Bergman T, Jornvall H, et al. Identification of the phosphorylation site for cAMP-dependent protein kinase on Na+,K(+)-ATPase and effects of site-directed mutagenesis. *J Biol Chem*. 1994;269(12):9368-9373.

215. Beguin P, Beggah AT, Chibalin AV, Burgener-Kairuz P, Jaisser F, Mathews PM, Rossier BC, Cotecchia S, Geering K. Phosphorylation of the Na,K-ATPase alpha-subunit by protein kinase A and C in vitro and in intact cells. Identification of a novel motif for PKC-mediated phosphorylation. *J Biol Chem*. 1994;269(39):24437-24445.

216. Feschenko MS, Sweadner KJ. Conformation-dependent phosphorylation of Na,K-ATPase by protein kinase A and protein kinase C. *J Biol Chem*. 1994;269(48):30436-30444.

217. Pavlovic D, Fuller W, Shattock MJ. The intracellular region of FXYD1 is sufficient to regulate cardiac Na/K ATPase. *FASEB J*. 2007;21(7):1539-1546.

218. Bell JR, Kennington E, Fuller W, Dighe K, Donoghue P, Clark JE, Jia LG, Tucker AL, Moorman JR, Marber MS, Eaton P, Dunn MJ, Shattock MJ. Characterization of the phospholemman knockout mouse heart: depressed left

ventricular function with increased Na-K-ATPase activity. *Am J Physiol Heart Circ Physiol*. 2008;294(2):H613-621.

219. Berry RG. Regulation of Na/K pump current in isolated cardiac myocytes: studies in the phospholemman knockout mouse. 2007.

220. Jia LG, Donnet C, Bogaev RC, Blatt RJ, McKinney CE, Day KH, Berr SS, Jones LR, Moorman JR, Sweadner KJ, Tucker AL. Hypertrophy, increased ejection fraction, and reduced Na-K-ATPase activity in phospholemman-deficient mice. *Am J Physiol Heart Circ Physiol*. 2005;288(4):H1982-1988.

221. Wang J, Gao E, Song J, Zhang XQ, Li J, Koch WJ, Tucker AL, Philipson KD, Chan TO, Feldman AM, Cheung JY. Phospholemman and beta-adrenergic stimulation in the heart. *Am J Physiol Heart Circ Physiol*.298(3):H807-815.

222. Bossuyt J, Despa S, Martin JL, Bers DM. Phospholemman phosphorylation alters its fluorescence resonance energy transfer with the Na/K-ATPase pump. *J Biol Chem*. 2006;281(43):32765-32773.

223. Asahi M, McKenna E, Kurzydlowski K, Tada M, MacLennan DH. Physical interactions between phospholamban and sarco(endo)plasmic reticulum Ca2+-ATPases are dissociated by elevated Ca2+, but not by phospholamban phosphorylation, vanadate, or thapsigargin, and are enhanced by ATP. *J Biol Chem*. 2000;275(20):15034-15038.

224. Pavlovic D, Fuller W, Shattock MJ. Novel regulation of cardiac Na pump via phospholemman. *J Mol Cell Cardiol*.

225. Bailey BA, Houser SR. Sarcoplasmic reticulum-related changes in cytosolic calcium in pressure-overload-induced feline LV hypertrophy. *Am J Physiol*. 1993;265(6 Pt 2):H2009-2016.

226. Bers DM, Despa S. Cardiac myocytes Ca2+ and Na+ regulation in normal and failing hearts. *J Pharmacol Sci*. 2006;100(5):315-322.

227. Desilets M, Baumgarten CM. Isoproterenol directly stimulates the Na+-K+ pump in isolated cardiac myocytes. *Am J Physiol*. 1986;251(1 Pt 2):H218-225.

228. Glitsch HG. Electrophysiology of the sodium-potassium-ATPase in cardiac cells. *Physiol Rev*. 2001;81(4):1791-1826.

229. Glitsch HG, Krahn T, Pusch H, Suleymanian M. Effect of isoprenaline on active Na transport in sheep cardiac Purkinje fibres. *Pflugers Arch*. 1989;415(1):88-94.

230. Teriete P, Franzin CM, Choi J, Marassi FM. Structure of the Na,K-ATPase regulatory protein FXYD1 in micelles. *Biochemistry*. 2007;46(23):6774-6783.

231. Song J, Zhang XQ, Wang J, Cheskis E, Chan TO, Feldman AM, Tucker AL, Cheung JY. Regulation of cardiac myocyte contractility by phospholemman: Na+/Ca2+ exchange versus Na+ -K+ -ATPase. *Am J Physiol Heart Circ Physiol*. 2008;295(4):H1615-1625.

232. Zhang XQ, Ahlers BA, Tucker AL, Song J, Wang J, Moorman JR, Mounsey JP, Carl LL, Rothblum LI, Cheung JY. Phospholemman inhibition of the cardiac Na+/Ca2+ exchanger. Role of phosphorylation. *J Biol Chem*. 2006;281(12):7784-7792.

233. Wang X, Gao G, Guo K, Yarotskyy V, Huang C, Elmslie KS, Peterson BZ. Phospholemman modulates the gating of cardiac L-type calcium channels. *Biophys J*.98(7):1149-1159.

234. Cheung JY, Zhang XQ, Song J, Gao E, Rabinowitz JE, Chan TO, Wang J. Phospholemman: a novel cardiac stress protein. *Clin Transl Sci*.3(4):189-196.

235. Despa S, Tucker AL, Bers DM. Phospholemman-mediated activation of Na/K-ATPase limits [Na]i and inotropic state during beta-adrenergic stimulation in mouse ventricular myocytes. *Circulation*. 2008;117(14):1849-1855.

236. Despa S, Islam MA, Weber CR, Pogwizd SM, Bers DM. Intracellular Na(+) concentration is elevated in heart failure but Na/K pump function is unchanged. *Circulation*. 2002;105(21):2543-2548.

237. El-Armouche A, Wittkopper K, Fuller W, Howie J, Shattock MJ, Pavlovic D. Phospholemman-dependent regulation of the cardiac Na/K-ATPase activity is modulated by inhibitor-1 sensitive type-1 phosphatase. *FASEB J*.25(12):4467-4475.

238. Butcher RW, Sutherland EW. Adenosine 3',5'-phosphate in biological materials. I. Purification and properties of cyclic 3',5'-nucleotide phosphodiesterase and use of this enzyme to characterize adenosine 3',5'-phosphate in human urine. *J Biol Chem*. 1962;237:1244-1250.

239. Chasin M HD. Inhibitors and activators of cyclic nucleotide phosphodiesterase. In: Greengard P RG, ed. *Advances in Cyclic Nucleotide Research*. New York: Raven press; 1976:225-264.

240. Lugnier C KN. Modulation of vascular cyclic nucleotide phosphodiesterases by cyclic GMP: role in vasodilation *Eur*. *Heart J*. 1993;14 (Suppl. I):141-148.

241. Lugnier C, Gauthier C, Le Bec A, Soustre H. Cyclic nucleotide phosphodiesterases from frog atrial fibers: isolation and drug sensitivities. *Am J Physiol*. 1992;262(3 Pt 2):H654-660.

242. Duncan GS, Wolberg G, Schmitges CJ, Deeprose RD, Zimmerman TP. Inhibition of lymphocyte-mediated cytolysis and cyclic AMP phosphodiesterase by erythro-9-(2-hydroxy-3-nonyl)adenine. *J Immunopharmacol*. 1982;4(1-2):79-100.

243. Podzuweit T, Nennstiel P, Muller A. Isozyme selective inhibition of cGMP-stimulated cyclic nucleotide phosphodiesterases by erythro-9-(2-hydroxy-3-nonyl) adenine. *Cell Signal*. 1995;7(7):733-738.

244. Keravis T SA, Favot L, Lugnier C. Role of PDEs in vascular health and disease: endothelial PDEs and angiogenesis. . In: Beavo JA FS, houslay MD, ed. *Cyclic Nucleotide Phosphodiesterases in Health and Disease* Boca Raton: CRC Press; 2006:417-439

245. Schaeffer HJ, Schwender CF. Enzyme inhibitors. 26. Bridging hydrophobic and hydrophilic regions on adenosine deaminase with some 9-(2-hydroxy-3-alkyl)adenines. *J Med Chem*. 1974;17(1):6-8.

246. Hidaka H, Hayashi H, Kohri H, Kimura Y, Hosokawa T, Igawa T, Saitoh Y. Selective inhibitor of platelet cyclic adenosine monophosphate phosphodiesterase, cilostamide, inhibits platelet aggregation. *J Pharmacol Exp Ther*. 1979;211(1):26-30.

247. Schwabe U, Miyake M, Ohga Y, Daly JW. 4-(3-Cyclopentyloxy-4-methoxyphenyl)-2-pyrrolidone (ZK 62711): a potent inhibitor of adenosine cyclic 3',5'-monophosphate phosphodiesterases in homogenates and tissue slices from rat brain. *Mol Pharmacol*. 1976;12(6):900-910.

248. Schneider HH, Schmiechen R, Brezinski M, Seidler J. Stereospecific binding of the antidepressant rolipram to brain protein structures. *Eur J Pharmacol*. 1986;127(1-2):105-115.

249. Marivet MC, Bourguignon JJ, Lugnier C, Mann A, Stoclet JC, Wermuth CG. Inhibition of cyclic adenosine-3',5'-monophosphate phosphodiesterase from vascular smooth muscle by rolipram analogues. *J Med Chem*. 1989;32(7):1450-1457.

250. Lugnier C, Stierle A, Beretz A, Schoeffter P, Lebec A, Wermuth CG, Cazenave JP, Stoclet JC. Tissue and substrate specificity of inhibition by alkoxy-aryl-lactams of platelet and arterial smooth muscle cyclic nucleotide phosphodiesterases relationship to pharmacological activity. *Biochem Biophys Res Commun*. 1983;113(3):954-959.

251. Lugnier C, Schoeffter P, Le Bec A, Strouthou E, Stoclet JC. Selective inhibition of cyclic nucleotide phosphodiesterases of human, bovine and rat aorta. *Biochem Pharmacol*. 1986;35(10):1743-1751.

252. Thomas AJ, DaSilva JN, Lortie M, Renaud JM, Kenk M, Beanlands RS, deKemp RA. PET of (R)-11C-rolipram binding to phosphodiesterase-4 is reproducible and sensitive to increased norepinephrine in the rat heart. *J Nucl Med*.52(2):263-269.

253. Kenk M, Greene M, Thackeray J, deKemp RA, Lortie M, Thorn S, Beanlands RS, DaSilva JN. In vivo selective binding of (R)-[11C]rolipram to phosphodiesterase-4 provides the basis for studying intracellular cAMP signaling in the myocardium and other peripheral tissues. *Nucl Med Biol*. 2007;34(1):71-77.

254. Komas N, Lugnier C, Le Bec A, Serradeil-Le Gal C, Barthelemy G, Stoclet JC. Differential sensitivity to cardiotonic drugs of cyclic AMP phosphodiesterases

isolated from canine ventricular and sinoatrial-enriched tissues. *J Cardiovasc Pharmacol*. 1989;14(2):213-220.

255. Jacobitz S, McLaughlin MM, Livi GP, Burman M, Torphy TJ. Mapping the functional domains of human recombinant phosphodiesterase 4A: structural requirements for catalytic activity and rolipram binding. *Mol Pharmacol*. 1996;50(4):891-899.

256. Solaro RJ, Rarick HM. Troponin and tropomyosin: proteins that switch on and tune in the activity of cardiac myofilaments. *Circ Res*. 1998;83(5):471-480.

257. Metzger JM, Westfall MV. Covalent and noncovalent modification of thin filament action: the essential role of troponin in cardiac muscle regulation. *Circ Res*. 2004;94(2):146-158.

258. Haworth RS, Cuello F, Avkiran M. Regulation by phosphodiesterase isoforms of protein kinase A-mediated attenuation of myocardial protein kinase D activation. *Basic Res Cardiol*.106(1):51-63.

259. Perino A, Ghigo A, Ferrero E, Morello F, Santulli G, Baillie GS, Damilano F, Dunlop AJ, Pawson C, Walser R, Levi R, Altruda F, Silengo L, Langeberg LK, Neubauer G, Heymans S, Lembo G, Wymann MP, Wetzker R, Houslay MD, Iaccarino G, Scott JD, Hirsch E. Integrating cardiac PIP3 and cAMP signaling through a PKA anchoring function of p110gamma. *Mol Cell*.42(1):84-95.

260. Hodgkin AL, Huxley AF. The components of membrane conductance in the giant axon of Loligo. *J Physiol*. 1952;116(4):473-496.

261. Hodgkin AL, Huxley AF. Currents carried by sodium and potassium ions through the membrane of the giant axon of Loligo. *J Physiol*. 1952;116(4):449-472.

262. Hodgkin AL, Huxley AF, Katz B. Measurement of current-voltage relations in the membrane of the giant axon of Loligo. *J Physiol*. 1952;116(4):424-448.

263. Cole KS. Some physical aspects of bioelectric phenomena. *Proc Natl Acad Sci U S A*. 1949;35(10):558-566.

264. Meech RW, Standen NB. Potassium activation in Helix aspersa neurones under voltage clamp: a component mediated by calcium influx. *J Physiol*. 1975;249(2):211-239.

265. Wilson WA, Goldner MM. Voltage clamping with a single microelectrode. *J Neurobiol*. 1975;6(4):411-422.

266. Neher E, Sakmann B. Single-channel currents recorded from membrane of denervated frog muscle fibres. *Nature*. 1976;260(5554):799-802.

267. Shattock MJ, Matsuura H. Measurement of Na(+)-K+ pump current in isolated rabbit ventricular myocytes using the whole-cell voltage-clamp technique. Inhibition of the pump by oxidant stress. *Circ Res*. 1993;72(1):91-101.

268. Gadsby DC, Kimura J, Noma A. Voltage dependence of Na/K pump current in isolated heart cells. *Nature*. 1985;315(6014):63-65.

269. Ehara T, Matsuoka S, Noma A. Measurement of reversal potential of Na+-Ca2+ exchange current in single guinea-pig ventricular cells. *J Physiol*. 1989;410:227-249.

270. Su Z, Bridge JH, Philipson KD, Spitzer KW, Barry WH. Quantitation of Na/Ca exchanger function in single ventricular myocytes. *J Mol Cell Cardiol*. 1999;31(5):1125-1135.

271. Ammala C, Eliasson L, Bokvist K, Larsson O, Ashcroft FM, Rorsman P. Exocytosis elicited by action potentials and voltage-clamp calcium currents in individual mouse pancreatic B-cells. *J Physiol*. 1993;472:665-688.

272. Neher E, Marty A. Discrete changes of cell membrane capacitance observed under conditions of enhanced secretion in bovine adrenal chromaffin cells. *Proc Natl Acad Sci U S A*. 1982;79(21):6712-6716.

273. Smith CB, Betz WJ. Simultaneous independent measurement of endocytosis and exocytosis. *Nature*. 1996;380(6574):531-534.

274. Shattock MJ, Matsuura H, Ward JP. Sodium pump current measured in cardiac ventricular myocytes isolated from control and potassium depleted rabbits. *Cardiovasc Res*. 1994;28(12):1854-1862.

275. Stimers JR, Dobretsov M. Adrenergic stimulation of Na/K pump current in adult rat cardiac myocytes in short-term culture. *J Membr Biol*. 1998;163(3):205-216.

276. Gao J, Cohen IS, Mathias RT, Baldo GJ. Regulation of the beta-stimulation of the Na(+)-K+ pump current in guinea-pig ventricular myocytes by a cAMP-dependent PKA pathway. *J Physiol*. 1994;477 (Pt 3):373-380.

277. Gao J, Mathias RT, Cohen IS, Baldo GJ. Isoprenaline, Ca2+ and the Na(+)-K+ pump in guinea-pig ventricular myocytes. *J Physiol*. 1992;449:689-704.

278. Gao J, Mathias RT, Cohen IS, Shi J, Baldo GJ. The effects of beta-stimulation on the Na(+)-K+ pump current-voltage relationship in guinea-pig ventricular myocytes. *J Physiol*. 1996;494 (Pt 3):697-708.

279. Gao J, Cohen IS, Mathias RT, Baldo GJ. The inhibitory effect of beta-stimulation on the Na/K pump current in guinea pig ventricular myocytes is mediated by a cAMP-dependent PKA pathway. *Pflugers Arch*. 1998;435(4):479-484.

280. White CN, Liu CC, Garcia A, Hamilton EJ, Chia KK, Figtree GA, Rasmussen HH. Activation of cAMP-dependent signaling induces oxidative modification of the cardiac Na+-K+ pump and inhibits its activity. *J Biol Chem*.285(18):13712-13720.

281. Ishizuka N, Berlin JR. Beta-adrenergic stimulation does not regulate Na pump function in voltage-clamped ventricular myocytes of the rat heart. *Pflugers Arch*. 1993;424(3-4):361-363.

282. McLatchie LM BR, Shattock MJ. The phospholemman-induced modulation of Na/K ATPase Na affinity is dependnet on intracellular calcium. *J Mol Cell Cardiol*. 2007;42: S21.

283. Cheng SX, Aizman O, Nairn AC, Greengard P, Aperia A. [Ca2+]i determines the effects of protein kinases A and C on activity of rat renal Na+,K+-ATPase. *J Physiol*. 1999;518 (Pt 1):37-46.

284. Mitchell DA, Vasudevan A, Linder ME, Deschenes RJ. Protein palmitoylation by a family of DHHC protein S-acyltransferases. *J Lipid Res*. 2006;47(6):1118-1127.

285. Linder ME, Deschenes RJ. Palmitoylation: policing protein stability and traffic. *Nat Rev Mol Cell Biol*. 2007;8(1):74-84.

286. Shipston MJ. Ion channel regulation by protein palmitoylation. *J Biol Chem*.286(11):8709-8716.

287. Tulloch LB, Howie J, Wypijewski KJ, Wilson CR, Bernard WG, Shattock MJ, Fuller W. The inhibitory effect of phospholemman on the sodium pump requires its palmitoylation. *J Biol Chem*.286(41):36020-36031.

288. Petrushanko IY, Yakushev S, Mitkevich VA, Kamanina YV, Ziganshin RH, Meng X, Anashkina AA, Makhro A, Lopina OD, Gassmann M, Makarov AA, Bogdanova A. S-Glutathionylation of the Na,K-ATPase Catalytic alpha Subunit Is a Determinant of the Enzyme Redox Sensitivity. *J Biol Chem*.287(38):32195-32205.

289. Brunton LL, Hayes JS, Mayer SE. Functional compartmentation of cyclic AMP and protein kinase in heart. *Adv Cyclic Nucleotide Res*. 1981;14:391-397.

290. Gilman AG. A protein binding assay for adenosine 3':5'-cyclic monophosphate. *Proc Natl Acad Sci U S A*. 1970;67(1):305-312.

291. Brooker G, Terasaki WL, Price MG. Gammaflow: a completely automated radioimmunoassay system. *Science*. 1976;194(4262):270-276.

292. Adams SR, Harootunian AT, Buechler YJ, Taylor SS, Tsien RY. Fluorescence ratio imaging of cyclic AMP in single cells. *Nature*. 1991;349(6311):694-697.

293. Zhang J, Ma Y, Taylor SS, Tsien RY. Genetically encoded reporters of protein kinase A activity reveal impact of substrate tethering. *Proc Natl Acad Sci U S A*. 2001;98(26):14997-15002.

294. Rich TC, Tse TE, Rohan JG, Schaack J, Karpen JW. In vivo assessment of local phosphodiesterase activity using tailored cyclic nucleotide-gated channels as cAMP sensors. *J Gen Physiol*. 2001;118(1):63-78.

295. Fagan KA, Schaack J, Zweifach A, Cooper DM. Adenovirus encoded cyclic nucleotide-gated channels: a new methodology for monitoring cAMP in living cells. *FEBS Lett*. 2001;500(1-2):85-90.

296. DiPilato LM, Cheng X, Zhang J. Fluorescent indicators of cAMP and Epac activation reveal differential dynamics of cAMP signaling within discrete subcellular compartments. *Proc Natl Acad Sci U S A*. 2004;101(47):16513-16518.

297. Ponsioen B, Zhao J, Riedl J, Zwartkruis F, van der Krogt G, Zaccolo M, Moolenaar WH, Bos JL, Jalink K. Detecting cAMP-induced Epac activation by fluorescence resonance energy transfer: Epac as a novel cAMP indicator. *EMBO Rep*. 2004;5(12):1176-1180.

298. Forster T. Energy migration and fluorescence. 1946. *J Biomed Opt*.17(1):011002.

299. Bos JL. Epac: a new cAMP target and new avenues in cAMP research. *Nat Rev Mol Cell Biol*. 2003;4(9):733-738.

300. de Rooij J, Zwartkruis FJ, Verheijen MH, Cool RH, Nijman SM, Wittinghofer A, Bos JL. Epac is a Rap1 guanine-nucleotide-exchange factor directly activated by cyclic AMP. *Nature*. 1998;396(6710):474-477.

301. Luo J, Deng ZL, Luo X, Tang N, Song WX, Chen J, Sharff KA, Luu HH, Haydon RC, Kinzler KW, Vogelstein B, He TC. A protocol for rapid generation of recombinant adenoviruses using the AdEasy system. *Nat Protoc*. 2007;2(5):1236-1247.

302. Nicklin SA BA. Simple methods for preparing recombinant adenoviruses for high efficiency transduction of vascular cells. In: AH B, ed. *Vascular disease: molecular biology and gene transfer protocols (methods in molecular medicine)*. New York: Humana Press; 1999.

303. de Rooij J, Rehmann H, van Triest M, Cool RH, Wittinghofer A, Bos JL. Mechanism of regulation of the Epac family of cAMP-dependent RapGEFs. *J Biol Chem*. 2000;275(27):20829-20836.

304. Borner S, Schwede F, Schlipp A, Berisha F, Calebiro D, Lohse MJ, Nikolaev VO. FRET measurements of intracellular cAMP concentrations and cAMP analog permeability in intact cells. *Nat Protoc*.6(4):427-438.

305. Hou BH, Takanaga H, Grossmann G, Chen LQ, Qu XQ, Jones AM, Lalonde S, Schweissgut O, Wiechert W, Frommer WB. Optical sensors for monitoring dynamic changes of intracellular metabolite levels in mammalian cells. *Nat Protoc*.6(11):1818-1833.

306. Lompre AM, Hajjar RJ, Harding SE, Kranias EG, Lohse MJ, Marks AR. Ca2+ cycling and new therapeutic approaches for heart failure. *Circulation*.121(6):822-830.

307. Westermann D, Becher PM, Lindner D, Savvatis K, Xia Y, Frohlich M, Hoffmann S, Schultheiss HP, Tschope C. Selective PDE5A inhibition with sildenafil rescues left ventricular dysfunction, inflammatory immune response and cardiac remodeling in angiotensin II-induced heart failure in vivo. *Basic Res Cardiol*.107(6):308.

308. Madhani M, Hall AR, Cuello F, Charles RL, Burgoyne JR, Fuller W, Hobbs AJ, Shattock MJ, Eaton P. Phospholemman Ser69 phosphorylation contributes to sildenafil-induced cardioprotection against reperfusion injury. *Am J Physiol Heart Circ Physiol*.299(3):H827-836.

APPENDIX I

Another of our hypotheses was that PLM may directly bind individual PDE4 isoforms. To further investigate any direct physical interaction between PLM and such isoforms, preliminary co-IP experiments were undertaken. All the work described in Appendix I was undertaken by our project collaborator Dr William Fuller, University of Dundee.

PLM was shown to be successfully 'pulled-down' with the NKA antibody [Figure 1; Panel A] but collectively, the data obtained from this series of experiments were inconclusive. Despite the presence of bands at 75 kDa, which corresponded to the molecular weights of PDE4B [Figure 1; Panel C], and at 100 kDa, which corresponded to PDE4A [Figure 1; Panel B] and PDE4D [Figure 1; Panel D] respectively, the quality of the data set was compromised by a multitude of non-specific bands across the samples. Specifically, multiple bands were observed in the unfractionated cardiac homogenate for all of the PDE4 antibodies tested, with PDE4B additionally binding to a component of the molecular ladder. Furthermore, the bands at 25 kDa and 100 kDa could likely be attributed to binding of the primary antibody to IgGs present in the samples, which may be overcome in future experiments by pre-boiling the samples prior to carrying out the co-IP procedure.

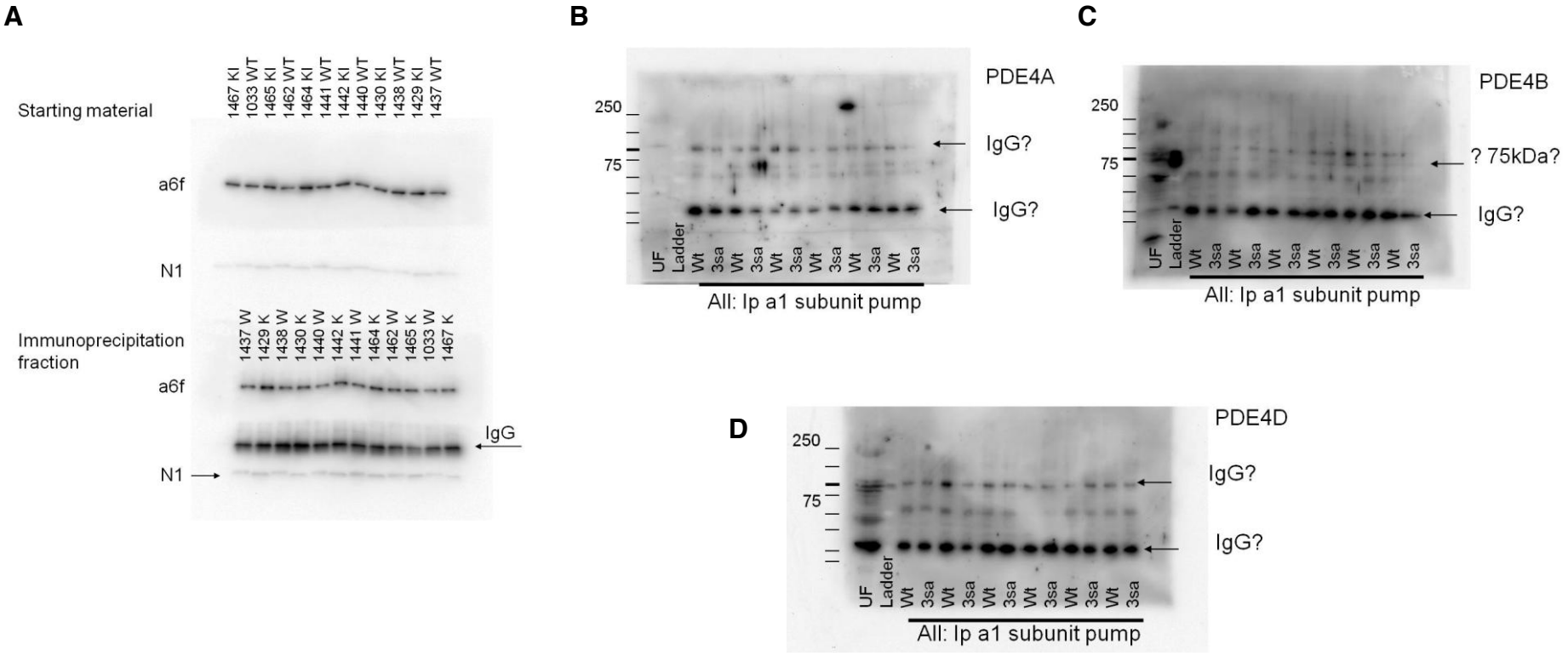

Figure A1 Potential physical interaction between PLM and PDE4 in PLM-WT and PLM-KI hearts.

Western blots of PLM-NKA co-IP probed with PDE4A, B and D antibodies. **(A)** A NKA-α1 antibody was first used to pull down PLM in both PLM-WT and PLM-KI (3sa) heart homogenate samples. For co-IP of FXYD1 and the NKA α_1-subunit, samples were lysed in PBS supplemented with 6 mg/ml octaethylene glycol monododecyl ether (C12E8, Sigma), plus protease and phosphatase inhibitors. Samples were agitated gently for 30 min at 4°C and diluted 1:1 with PBS (plus protease and phosphatase inhibitors), and insoluble material was removed by centrifugation (15,000 *g*, 5 min). Supernatants were agitated overnight at 4°C with anti-NKA α_1-subunit monoclonal C464.6 (Santa Cruz Biotechnology), immune complexes were harvested with protein G Sepharose for 2 hr at 4°C, and beads were washed 5 times with 0.5 mg/ml C12E8 in PBS supplemented with protease and phosphatase inhibitors. To avoid the confounding presence of mouse IgG in immunoprecipitated samples, successful co-IP of PLM was confirmed using an antibody raised in chickens (Chemicon). The membranes were then probed with antibodies against **(B)** PDE4A, **(C)** B and **(D)** D (generated by our project collaborator, Dr. George Baillie, University of Glasgow). The darkened marker on the left of each blot indicates the theoretical molecular weight of the individual PDE4 subfamilies.

APPENDIX II

To further investigate the manner in which PLM binds PDE4, ARVMs were treated with a specially designed PDE4-PLM disruptor peptide (generated by our project collaborator, Dr George Baillie, University of Glasgow). PDE4 isoforms are thought to bind directly to their signalling partners (or to AKAPs) via their unique N-terminal region, which is distinct to each isoform, and the notion of displacing PDE4s using peptides is relatively well established. This particular disruptor peptide, rather than based on the PDE4 binding sequence, is instead based on the last 16 amino acids of PLM and the sequence is virtually identical to that belonging to a peptide representing the 19 C-terminal residues of PLM (54-72) used in a previous study in our laboratory.[217] This particular sequence of PLM has been determined to directly bind purified PDE4 using peptide array technology developed by Dr George Baillie (unpublished data).

The control peptide, on the other hand, consists of another sequence of PLM that does not bind PDE4. Dr George Baillie had hypothesised that this peptide would induce a similar functional response to Rol; that is, increase cAMP levels and thus PKA phosphorylation of PLM by displacing PDE4 away from the immediate vicinity of PLM.

Disruptor peptide: {Ste}-EGTFRSSIRRLSTRRR
Control peptide: {Ste}-QRTGEPDEEEGTFR

Both the disruptor and the control peptides consist of an identical stearate group to enable penetration through the plasma membrane. The treatment of ARVMs with this peptide was largely similar to the protocol outlined in Chapter 3 (Section 3.2.2), with the exception that the disruptor and control peptides were incubated with the cells at 10 μmol/L for 2 hr rather than 10 min to facilitate entry into the cell. All treatment groups were exposed to an equal amount of DMSO (0.1%). PLM-Ser68 phosphorylation levels were subsequently analysed as outlined in Chapter 2 (Sections 2.5.5 and 2.5.6).

The inhibitor peptide markedly reduced PLM-Ser68 phosphorylation in both the absence and presence of ISO, in contrary to initial expectations that the peptide behaves in an analogous manner to Rol [Figure 1; Panel A]. Incidentally, the 19 aa peptide

aforementioned was shown to inhibit the NKA in VPC experiments, which we always assumed that this was because it displaced phosphorylated PLM off the pump. Since the addition of this peptide did not seem to enhance PLM-Ser68 phosphorylation under both basal conditions and β-AR stimulation, this implies that PLM does not bind a local pool of PDE4 directly under normal circumstances, at least not involving this particular PLM domain. On the other hand, if PDE4 is targeted to the proximity to the protein, our results may reflect a displacing of endogenous PLM and/or an augmentation of the basal activity of the PDE4 enzymes induced by the peptide. An alternative explanation for our findings is that an AKAP in the vicinity of PLM normally functions as an intermediate complex for binding of PLM to PDE4, and the peptide served to displace the AKAP from its normal location, thereby reducing cAMP-PKA signalling to PLM. This possibility is consistent with the notion that PLM may not be binding PDE4 in a direct manner, and the requirement of an intermediate protein could be investigated using AKAP-specific antibodies in co-IP experiments in the future.

A definitive conclusion remains elusive; one obstacle is the lack of understanding of the manner in which the disruptor peptide displaces PDE4 from PLM. Since this putative binding sequence on PLM is also the region that contains all three phosphorylatable residues, PDE4 might sterically hinder the access of PKA to PLM-Ser68. Whether our results are merely reflecting the actions of an incorrectly designed pharmacological agent must be considered, and delineation of the peptide's mechanism of action may shed further light onto this issue. For instance, it would be useful to determine whether the peptide activates PDE4 or a phosphatase (identity not yet known) in proximity to PLM and/or inhibits PKA or AC.

Furthermore, it is possible that our observations are merely a result of cell apoptosis induced by the presence of the peptide (and/or the stearate groups) for 2 hr, a relatively extensive treatment time. Supporting this possibility is the observation that the control peptide also led to a reduction in PLM-Ser68 phosphorylation level, although the effect was not statistically significant [Figure 1; Panel B]. Despite this, analysis of the total actin levels across the treatment groups did not show a marked reduction in the peptides-treated wells. Importantly, the pattern of PLM-Ser68 phosphorylation was found to be completely consistent with that of PLB-Ser16, giving rise to the possibility that the peptide-mediated actions on PLM were non-specific [Figure 1; Panel C].

In conclusion, the disruptor peptide tested is unlikely to be displacing PDE4 binding to PLM, either due to the peptide not functioning correctly or the fact that PDE4 does not directly interact with PLM under normal circumstances. Further work is required to fully distinguish the effects of this peptide on PLM-Ser68 phosphorylation.

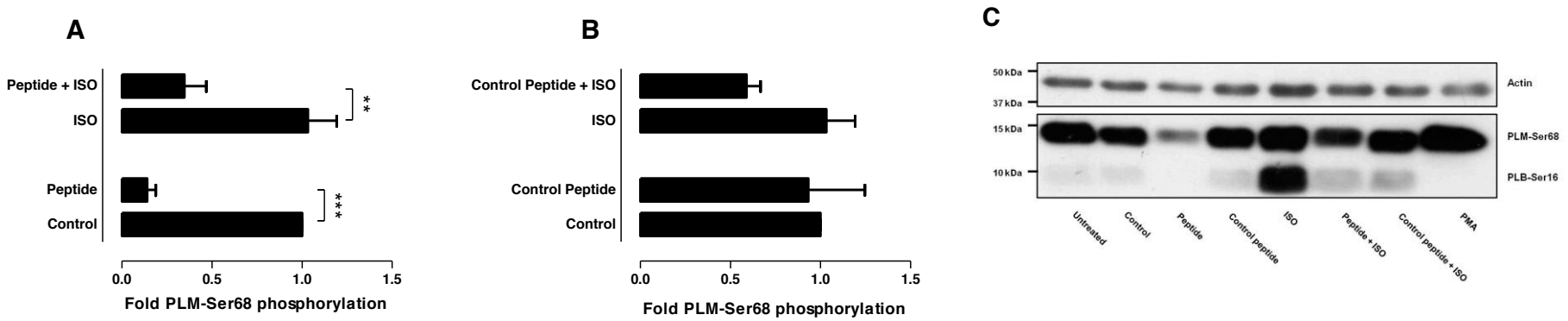

Figure A2 PLM-Ser68 phosphorylation levels in response to treatment with a PDE4-PLM disruptor peptide in the absence and presence of a submaximal [ISO].

ARVMs were treated with a PDE4-PLM disruptor peptide or a control peptide **(A)** alone or **(B)** in combination with 10 nmol/L ISO. Negative and positive controls comprised of ARVMS challenged with 0.1% DMSO and 300 nmol/L PMA (not shown) respectively. ARVMs in all treatment groups were exposed to 0.1% DMSO. SDS-PAGE (15% gel) and WB analysis was used to analyse PLM-Ser68 and PLB-Ser16 phosphorylation levels using an anti-phospho PLM-Ser68 antibody. All samples were subjected to complementary WB analysis using an anti-total actin antibody, to demonstrate equal protein loading between samples. Membranes were subsequently stained with Coomassie Blue to demonstrate equal protein loading and transfer. Densitometry values for PLM-Ser68 were normalised to those for total actin and subsequently normalised to the DMSO control to generate fold values. Data are expressed as means ± SEM (n=6). **(C)** Representative blot of PLM-Ser68 phosphorylation levels in response to pharmacological treatment.